CHROMATIN DYNAMICS IN HOMOLOGY DIRECTED REPAIR

INAUGURALDISSERTATION

zur

Erlangung der Würde eines Doktors der Philosophie

vorgelegt der

Philosophisch-Naturwissenschaftlichen Fakultät

der Universität Basel

von

Anaïs Thiziri Cheblal

Basel, 2021

Genehmigt von der Philosophisch-Naturwissenschaftlichen Fakultät
auf Antrag von

Prof. Dr. Susan M. Gasser
Prof. Dr. Primo Leo Schär
Prof. Dr. Kerstin Bystricky

Basel, den 13 Oktober 2020

Prof. Dr. Martin Spiess
Dekan

In memory of Michael Hermann Hauer,

"Live as if you were to die tomorrow. Learn as if you were to live forever".

Mahatma Gandhi.

Table of Contents

Thesis overview

This thesis consist of six chapters and the appendices. Each chapter starts with a brief summary page. If parts or the whole of the chapter has been published, that sheet indicates the title, author list and the date of the publication as well as my personal contribution to the papers.

Chapter I is an overview of chromatin organization and dynamics in the context of DNA double-strand break (DSB) repair.

Chapter II is a specific published guideline for DNA recombination and repair studies. This chapter is an extracted section of my contribution to a published review. It describes the method I used to visualize and quantify chromosomal dynamics upon DNA double strand breaks in yeast *S. cerevisiae.*

Chapter III describes my main thesis research question, results, discussion and experimental procedures. This study show that DNA damage induced histone depletion enhances homology search through the induced chromatin expansion and ectopic locus mobility, independently of local DSB movement. Moreover, we show that local DSB dynamics is cell cycle dependent and is regulated by Cohesin turnover. Finally, we find that centromeres do not detach upon DNA damage.

Chapter IV in an overview of the roles of two post-translational modifications (PTMs) in the regulation of DNA repair pathway choice in budding yeast: Ubiquitination and the small ubiquitin-related modifier protein (SUMO). This chapter introduces the research context to Chapter V.

Chapter V contains a study to which I had contributed in which we reported that the presence of telomeric repeat sequences on one side of a double-strand break alters the outcome of repair. We show that the two sides of the break show uncoordinated movement and are repaired asymmetrically leading to translocation. We observed that the repair outcome is tightly controlled by SUMO targeted ubiquitin ligases.

Chapter VI summarizes the main conclusion of this thesis and discusses the results stemming from Chapter III together with relevant future directions.

Finally, the appendices contain a list of abbreviations, my curriculum vitae and acknowledgments.

This thesis include the following publications:

Peer-reviewed publications

Anaïs Cheblal, Kiran Challa, Andrew Seeber, Kenji Shimada, Haruka Yoshida, Helder C. Ferreira, Assaf Amitai, and Susan M. Gasser.

DNA damage-induced nucleosome depletion enhances homology search independently of local break movement. Molecular Cell, 2020. DOI: 10.1016/j.molcel.2020.09.002

Kiran Challa, Christoph Schmid, Saho Kitagawa, **Anaïs Cheblal**, Vytautas Iesmantavicius, Andrew Seeber, Assaf Amitai, Jan Seebacher, Michael H. Hauer, Kenji Shimada and Susan M Gasser

Damage-induced chromatome dynamics link Ubiquitin ligase and proteasome recruitment to histone loss and efficient DNA repair. Molecular Cell, 2021. DOI:10.1016/j.molcel.2020.12.021

Isabella Marcomini, Kenji Shimada, Neda Delgoshaie, Io Yamamoto, Andrew Seeber, **Anaïs Cheblal**, Chihiro Horigome, Ulrike Naumann, and Susan M. Gasser

Asymmetric Processing of DNA Ends at a Double-Strand Break Leads to Unconstrained Dynamics and Ectopic Translocation. Cell Reports, 2018. DOI: 10.1016/j.celrep.2018.07.102

Review article

Hannah L. Klein1, Giedrė Bačinskaja, Jun Che, **Anais Cheblal**, Rajula Elango, Anastasiya Epshtein, Devon M. Fitzgerald, Belén Gómez-González, Sharik R. Khan, Sandeep Kumar, Bryan A. Leland, Léa Marie, Qian Mei, Judith Miné-Hattab, Alicja Piotrowska, Erica J. Polleys, Christopher D Putnam, Elina A. Radchenko, Anissia Ait Saada, Cynthia J. Sakofsky, Eun Yong Shim, Mathew Stracy, Jun Xia, Zhenxin Yan, Yi Yin, Andrés Aguilera, Juan Lucas Argueso, Catherine H. Freudenreich. Susan M. Gasser, Dmitry A. Gordenin, James E. Haber, Grzegorz Ira, Sue Jinks-Robertson, Megan C. King, Richard D. Kolodner, Andrei Kuzminov, Sarah AE Lambert, Sang Eun Lee, Kyle M. Miller, Sergei M. Mirkin, Thomas D. Petes, Susan M. Rosenberg, Rodney Rothstein, Lorraine S. Symington, Pawel Zawadzki, Nayun Kim, Michael Lisby, and Anna Malkova

Guidelines for DNA recombination and repair studies: Cellular assays of DNA repair pathways. Microbial Cell, 2019. DOI: 10.15698/mic2019.01.664

CHAPTER I: INTRODUCTION TO CHROMATIN ORGANIZATION AND DYNAMICS DURING DNA REPAIR

Summary

Nuclear and chromatin organization can influence all aspects of the genome's life cycle. Indeed, it has been shown that chromatin dynamics and nuclear organization are not only important for gene regulation, but also for the maintenance of genome stability.

In this first Chapter, I first summarize current knowledge on chromatin organization and how chromatin dynamics is regulated in both mammalian cells and *S. cerevisiae*.

In a second part, I discuss how chromatin responds to DNA damage and the role of chromatin movement in DNA double-strand break (DSB) repair.

Chromatin organization

Chromatin organization in higher eukaryotes

In the nineteenth century, Friedrich Miescher discovered nucleic acid when he isolated and characterized a phosphorus rich substance from human leukocyte nuclei, which he called 'nuclein' (Miescher, 1871). 130 years later, it was shown that the complete genetic information of a eukaryotic human cell resides in about three billion base pairs of deoxyribonucleic acid (DNA) sequence. These sequences need to be both continuously protected against potential damage and accessible for gene regulation and expression in a very controlled manner. To enable this, the genome of all eukaryotic cells is organized in a dynamic protein-DNA structure called chromatin. The basic unit of chromatin is called nucleosome, consisting of about 146 bp of DNA wrapped around an octameric core of histone proteins H2A, H2B, H3 and H4 **(Figure 1**).

The level of chromatin compaction and hence of DNA accessibility, which limits the activity of many cellular processes, is regulated by specific post-translational modifications of the core histones and of the linker histone, H1. The most common histone modifications are methylation, acetylation, phosphorylation, ubiquitination and sumoylation. In higher eukaryotes, chromatin is organized in subnuclear compartments with an active open euchromatin enriched centrally and silent heterochromatin at the nuclear periphery and surrounding nucleoli (Riddle et al., 2011) **(Figure 1).** Euchromatic regions are enriched for active histone modifications such as Histone H3 methylation on lysines 4 and 36 (H3K4me3 and H3K36me3); while peripheral heterochromatin regions exhibit gene silencing histone modifications such as histone H3 di-methylation on lysines 9 and 27 (H3K9me2/me3 and H3K27me3) and the binding of Heterochromatic Protein 1 (HP1) (Bannister and Kouzarides, 2011; Grewal and Jia, 2007; Lachner et al., 2001).

This global chromatin organization is highly conserved among multicellular eukaryotic organisms, although notable differences can be found, particularly within heterochromatin (Ho et al., 2014; Riddle et al., 2011). Within active regions, the interaction between regulatory sequences, such as enhancers, and gene promotors is necessary to ensure precise control of gene expression. To enable these interactions, eukaryotic chromosomes are organized in so called Topologically Associated Domains (TADs), that represent genomics regions within chromatin that preferentially associate, and which are generally open or transcribed chromatin domains (Dixon et al., 2012; Pombo and Dillon, 2015).

Although open domains are prone to transcription, this does not mean that in contrast heterochromatin is static and never transcribed. Indeed, it has been shown that low levels of transcription can occur in facultative heterochromatin in *C. elegans*, and these transcripts are then used to reinforce its silencing (Mattout et al., 2020). Similar events occur at centromeric satellite repeats in fission yeast and in mammals (Smurova and De Wulf, 2018). In the former the repeat transcripts are targeted by an Argonaut Ago1 and associated machinery (RITS) to nucleate silencing (Buhler and Gasser, 2009; Grewal and Jia, 2007), and in the latter, CEN transcripts both help load CENP-A, the kinetochore specific H3 variant, and associate with SUMOylated HP1, which is stabilized by H3K9me3, connecting pericentromere transcription with heterochromatin formation (Maison et al., 2011).

Structure of the budding yeast nucleus and chromatin organization

The budding yeast *Saccharomyces cerevisiae* is a unicellular eukaryote, with distinct aspects of nuclear organization that distinguish it from higher eukaryotes. Imaging studies have shown that the yeast nucleus is highly organized, with centromeres tethered to the Spindle Pole Body (SPB) through a kinetochore complex and telomeres clustered to the nuclear envelope (reviewed in (Fabre and Zimmer, 2018; Taddei et al., 2010)). This organization is similar to that described by Carl Rabl in salamander cells, with a polar arrangement of centromeres and telomeres (Rabl, 1885) **(Figure 1)**. Although the Rabl configuration is generally detected in metazoan cells at telophase, the presence of short intranuclear microtubules that anchor the kinetochores throughout interphase is unique to budding yeasts.

Another distinguishing feature is that budding yeast chromosomes have little repetitive DNA, apart from the rDNA, and no centromeric heterochromatin. Consistently budding yeast lacks repressive histone marks such as H3K9 methylation and its ligand HP1, although fission yeast has both. Instead, budding yeast has a heterochromatic silencing complex composed of Sir2, Sir3 and Sir4 proteins that recognizes unmodified nucleosomes to reduce chromatin accessibility and repress transcription. The Sir complex silences subtelomeric genes and the homologous mating type loci in yeast (reviewed in (Kueng et al., 2013)), and these are, like heterochromatin in higher eukaryotes, usually enriched at the nuclear periphery (Palladino et al., 1993; Taddei et al., 2004). Thanks to these similarities, yeast has

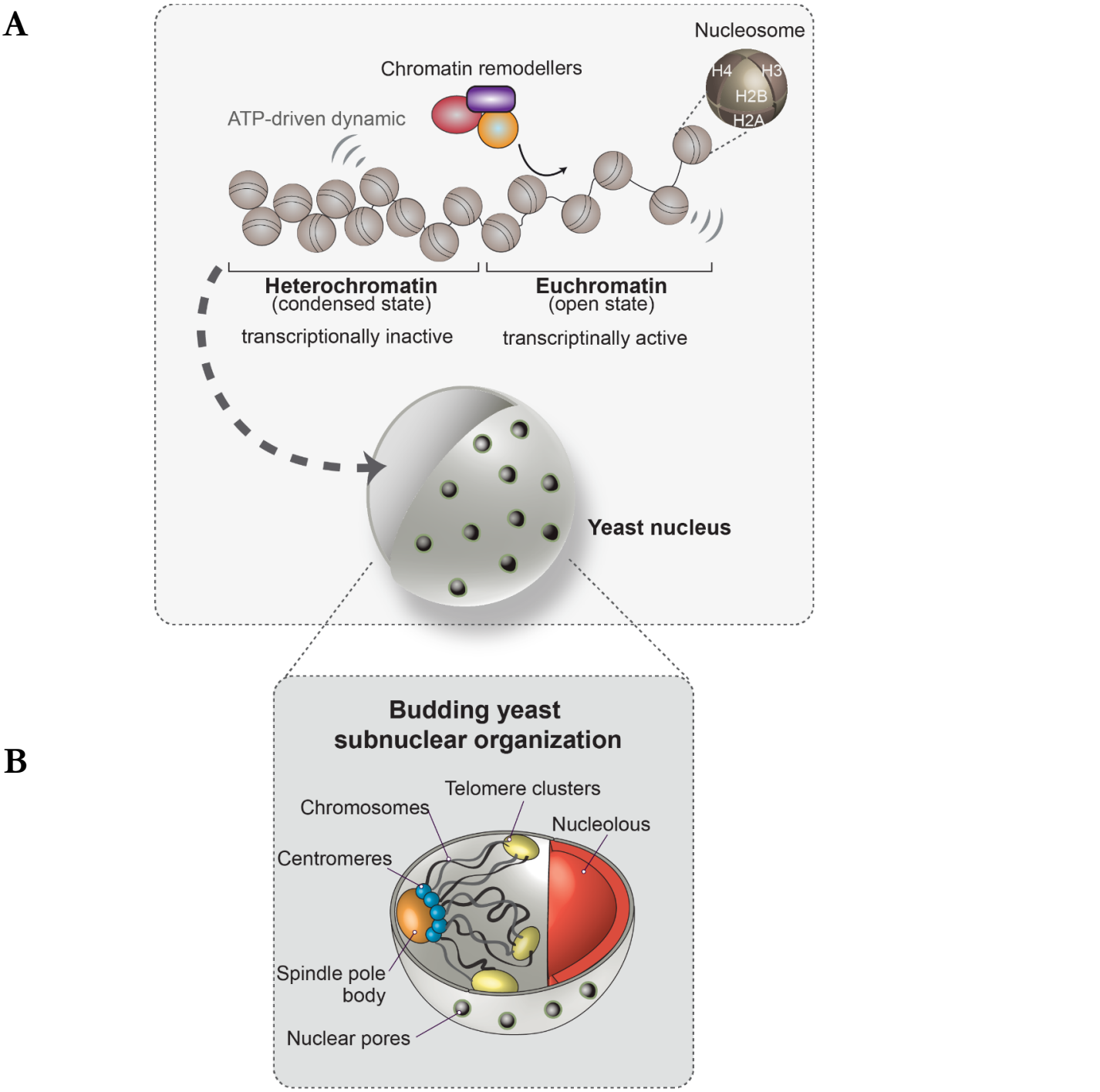

<u>Figure 1:</u> Chromatin organization in eukaryotes

(A) Overview of the nucleosome structure and chromatin compaction state in heterochromatin and euchromatin. **(B)** Chromatin organization and subnuclear organization in budding yeast.

been useful for testing the functional impact of chromatin sequestration at the nuclear envelope on gene regulation and genome stability.

It has been questioned whether the notion of chromosome "territories" is appropriate for yeast due to the relatively large volume explored by the random movement of an individual locus (Radius of constraint, or Rc (Rc ~ 0.6 μm) and the small size of the yeast nucleus (nuclear radius = 1 μm). Bystricky et al. have analyzed the relative positions of right and left telomeres of several yeast chromosomes and showed that the two telomeres of the same chromosome move in a partially coordinated manner. This work suggested that the tendency of a chromosome to move as one body could reflect the formation of a "chromosomal territory". (Bystricky et al. 2005).

However, yeast chromosomal position is controlled and defined by several structural parameters: the compaction of the chromosomal fiber, the sites of anchorage (centromeres to the SPB and telomeres to the NE) and, the loose interactions between right and left telomeres, when arms are of similar length (Schober et al., 2008)

Using chromosome conformation capture and fluorescently tagged genomic loci, other studies have attempted to show the presence of chromosomal territories in yeast. Duan et al. reported an extensive regional and higher order folding of the individual chromosomes, and constructed a three-dimensional model of the yeast genome (Duan et al, 2010). Although this study confirmed the previously reported Rabl like conformation of the yeast genome, the presence of "chromosomal territories" as suggested in mammalian cells is unclear. Therizols et al. rather suggested that the yeast genome organization is governed by physical constraints, including chromosome structure and the attachment to SPB and the nuclear envelope (Therizols et al. 2010).

Using chromosome modelling, Rosa et al. showed that the fast equilibration of yeast chromosomes explains the lack of a clear territorial organization in yeast nuclei (Rosa and Everaers 2008). Indeed, most chromosomes in yeast have a size smaller than 1 Mbp, this study suggested that the yeast chromosome disentanglement time is comparable to the time duration of the relative interphase (~1 hour). The evidence that chromosomes are self-interacting compartments is more pronounced in mammalian cells given the size of the chromosomes and nucleus (Cremer and Cremer, 2001).

Chromatin movement

History and definition

The concept of discrete chromosomal territories in interphase nuclei led to an image of the nucleus as a static structure with apparently immobile chromosomes. Nonetheless, it was proposed that these various levels of chromatin organization contribute to the control of gene expression and to the maintenance of genomic integrity. Functional studies of chromosome behavior suggested that chromatin has to be flexible and mobile to allow for homologous pairing during DNA repair, the formation of DNA replication and repair foci, and in particular, gene activation through promotor-enhancer interaction. the notion that all genomic loci have assigned, static positions in the interphase nucleus changed in 1997, when John Sedat's laboratory first reported high resolution time-lapse imaging of a GFP-tagged chromatin locus in interphase nuclei in *S. cerevisiae* and in *Drosophila melanogaster* (Marshall et al., 1997).

The development of a GFP-*LacI* fusion that can bind *lacO* repeats integrated in the yeast genome enabled the tracking of the position occupied by a single genomic locus over time. The development of multi-color imaging has allowed the coupling with nuclear pore tagging in budding yeast. This considerably improved the accuracy of genomic loci tracking by correcting for instrumental or nuclear drift, and allowing one to track single loci (Sage et al., 2005), rather than the relative movement of two homologous loci (Marshall et al., 1997). Using mean-square displacement (MSD) analysis (Berg, 1993), one was able to generate quantitative movement parameters such as the Rc and the Diffusion coefficient (see technical details in Chapter 2). Since then, time-lapse microscopy has been used to track various genomic loci and many studies have analyzed the character of chromatin movement from yeast and other species based on log MSD curves (Dion and Gasser, 2013).

The type of motion observed under various conditions was analyzed as either directed, random or subdiffusive (reviewed in (Seeber et al., 2018)). Because the motion of any chromosomal locus is constrained within the nucleus, the MSD curve must reach a plateau eventually, with the Rc = the radius of the nucleus. However, it was observed that only excised rings of chromatin moved throughout the entire nucleoplasm (Adam et al., 2016; Gartenberg et al., 2004). Other loci in the yeast genome showed different degrees of constraint depending on the stage of the cell cycle, their proximity to a site attached to a structural element (nuclear pore or SPB), and the metabolic state of the cell the

radii of constraint range from 0.2 μm to 0.6 μm (reviewed in (Fabre and Zimmer, 2018; Seeber et al., 2018)). In addition the rate of diffusion of chromatin is proposed to be limited by viscoelastic environment and nuclear crowding (Weber et al., 2010). In any case, it is now well accepted that chromatin is in constant motion. More recent work has investigated whether chromatin movement has a biological function and how it is regulated.

Intrinsic regulation of chromatin dynamics

The effect of cell cycle

Intuitively, one can imagine that the different cellular and nuclear processes of the cell cycle influence chromatin dynamics. For example, in S-phase cells, chromatin needs to be locally accessible for the initiation of replication, pulled through replication foci and replicated sister chromatids have to be held together. Each event could in itself alter chromatin mobility. One of the first observations made while analyzing chromatin dynamics in yeast was that genomic locus movement and radii of constraint change significantly with the phase of the cell cycle (Heun et al., 2001). In this study, the Gasser laboratory reported that the rapid subdiffusive movement observed in G1 phase becomes reduced in S-phase cells through a mechanism that is dependent on active DNA replication. It appeared not to be the initiation of replication that imposed constraints, but rather Cohesin-mediated sister chromatid cohesion. As confirmation, they showed that the inactivation of the Cohesin complex led to a significant loss of constraint on the movement of a locus in S phase (Dion et al., 2013).

As the mobility of a chromosomal locus can vary significantly with stages of the cell cycle, it is crucial to determine precisely, and in a standardized manner, what stage in the cell cycle each imaged cell occupies. Although identifying the cell cycle stage of mammalian cell nuclei by microscopy is non-trivial, it is rather easy in budding yeast. This is done by monitoring bud presence and bud size, together with the shape and the position of the nucleus in relation to the bud neck (described in (Neumann, 2005)). Finding major differences in chromatin dynamics among cell cycle stages argued for pathways that control constraint. We discuss what directly or indirectly influences chromatin movement and constraint in the paragraphs below.

Chromatin movement: an active process

It has been observed by many laboratories that chromatin movement could be significantly attenuated upon treatments that reduce intracellular ATP levels or following glucose starvation (Gartenberg et

al., 2004; Heun et al., 2001; Joyner et al., 2016; Levi and Gratton, 2008; Seeber et al., 2013; Weber et al., 2012). Moreover, a collapse or compaction of chromatin has been observed upon ATP depletion (Gartenberg et al., 2004; Heun et al., 2001; Martin et al., 2007). These observations suggest that chromatin movement is regulated by ATP-dependent factors. One of the main group of factors that regulate chromatin structure are chromatin remodelers. Indeed, nucleosome remodeling complexes generally contain a Swi/Snf2 family ATPase domain as their catalytic subunit and use the energy of ATP hydrolysis to exchange histone variants or slide nucleosomes along DNA. The role of chromatin remodeler complex INO80 on chromatin movement has been extensively studied. The direct targeting of INO80 to a genomic locus significantly increased its dynamics (Neumann et al., 2012; Spichal et al., 2016), and the deletion of one subunit of the INO80 complex, Arp8, which is essential for remodeling activity, led to reduced movement of a chromosomal locus (Cheblal *et al.* in press). Given the significant effect of the INO80 chromatin remodeler on chromatin dynamics, we and others have used the *arp8* deletion, which is viable in most backgrounds, to examine the physiological role of locus movement. In Chapter 3, we will discuss its implication in the DNA damage response.

The effect of subnuclear localization and tethering

As discussed above, chromatin is highly organized both in mammalian cells and in budding yeast. Several studies have investigated whether subnuclear positioning and/or locus tethering influence chromatin movement. In mammalian cells, it was reported that chromatin associated with active genes (replicated in early S phase) is significantly more dynamic than inactive chromatin (replicated in mid and late S phase) (Pliss et al., 2009). Despite being less mobile, heterochromatic regions were nonetheless accessible to transcription factors and polymerase, suggesting that other factors restrict silent chromatin movement. One obvious source of constraint is the intramolecular tethering of heterochromatic DNA to the nuclear periphery – either to nuclear pores, the nuclear lamina or to other integral inner nuclear membrane proteins. It has been described in mammalian cells, that a loss of chromosomal anchoring to the nuclear lamina increases movement of telomeres (Bronshtein et al., 2015). In budding yeast, it has also been shown that telomere or centromere release from the periphery increases chromatin dynamics (Gartenberg et al., 2004; Hediger et al., 2002) as does treatment with Nocodazole, which depolymerizes microtubules and releases kinetochore attachment to the SPB, an integral inner nuclear envelope structure (Gartenberg et al., 2004; Lawrimore et al., 2017; Strecker et al., 2016).

In line with this, centromeric or telomeric chromosomal loci have more constrained movement than loci found distant from these landmarks, and the artificial tethering of a chromosomal locus to the nuclear envelope indeed restricts movement (Bystricky et al., 2005b; Hediger et al., 2002; Jin et al., 2000).

Chromatin dynamic during transcription

How chromatin dynamics are regulated by transcription is a persistent question that has not been conclusively answered. However, the Gasser laboratory showed that in yeast the inhibition of RNA polymerase II, which is required for transcription elongation, does not affect chromatin movement in yeast (Neumann et al., 2012). On the other hand, targeting the transcription activator VP16 to a chromosomal locus was shown to increase its movement. Given that the targeting of Gal4, a transcription factor that also activates transcription, did not increase mobility, it was proposed that VP16 may recruit something other than RNA Pol II that enhances movement. VP16 is known to recruit nucleosome remodelers, including Swi/Snf and INO80C. Since the targeting of INO80C to a tagged locus led to increased mobility, it was proposed that nucleosome remodeling and not transcription itself enhances locus mobility (Neumann et al., 2012). In a recent study in mouse stem cells Gu *et al.* developed a strategy to deliver multiple RNAs to guide an inactive Cas9 complex to specific promoters and enhancers (Gu et al., 2018). Quantitative measurement of their movement during mouse stem cell differentiation revealed that increased DNA locus mobility correlated with transcriptional activation. In contrast, a study from the Bystricky laboratory reported that transcription initiation in mammalian cells correlated with increased locus confinement (Germier et al., 2017). Taken together, these reports paint a contradictory picture that fails to fully address whether the observed fluctuations in confinement or mobility are critical for gene regulation.

Recently work in *Drosophila* embryos tackled this question and showed that sustained proximity of the enhancer to its target is required for gene activation (Chen et al., 2018). This latter observation appears to favor the hypothesis that locus confinement is needed to allow a stabilized enhancer – promoter interactions and trigger fruitful transcriptional initiation. However, further studies are needed to investigate more systematically the changes in chromatin dynamics that occur during transcriptional initiation and test whether they actually regulate gene expression.

Regulation of chromatin dynamic by cellular architecture

The actin cytoskeleton

Chromatin exhibits movements that are qualitatively consistent with confined diffusion or subdiffusion (Cabal et al., 2006; Marshall et al., 1997). Nonetheless, as discussed above, evidence for active, ATP-dependent chromatin movement has also been reported in yeast, worms and mammals (Conrad et al., 2008; Heun et al., 2001; Koszul et al., 2008; Weber et al., 2012; Zidovska et al., 2013).

The control of cell shape and locomotion is largely controlled by the actin cytoskeleton. Actin is the most abundant intracellular protein in a eukaryotic cell, and in yeast it is encoded by a single essential gene *ACT1*. In its monomeric G form, yeast actin in found in the nucleus as part of the histone acetyl transferase complex NuA4, as well as chromatin remodeling complexes SWR1 and INO80, in which it forms a heterodimer with the actin-related protein Arp4 (Kapoor et al., 2013).

Several studies have investigated the impact of actin on chromosome dynamics. The LINC complex (Linker of Nucleoskeleton and Cytoskeleton) is a protein complex associated with both inner and outer membranes of the nucleus. It is composed of SUN-domain proteins (chromatin-associated) and KASH-domain proteins (actin and microtubule associated). In a recent study the Fabre laboratory have suggested that both the cytoskeletal and the nuclear forms of actin drive chromatin movement independently of the LINC complex. Moreover, they showed that an inhibition of actin polymerization reduces subtelomere dynamics (Spichal et al., 2016). This may be attributed to remodeler complexes or to an attenuation of nuclear rocking motion which is mediated by cytoplasmic actin.

The Gasser laboratory showed that the drug Latrunculin A, which depolymerizes cytoplasmic actin filaments, decreases nuclear rotation and indirectly internal reduces chromatin locus movement, suggesting that in untreated cells actin filaments bind the external surface of the nuclear envelope and contribute to nuclear rotation (Amitai et al., 2017; Spichal et al., 2016). This may be mediated by the LINC complex, but other scenarios are possible. These data suggest that actin polymerization indirectly influences the underlying nature of chromatin movement (Amitai et al., 2017; Spichal et al., 2016). To date evidence suggests that both actin-containing remodeling complexes and cytosplasmic actin filaments affect chromatin movement, either directly, or indirectly through nuclear rotation.

Microtubule dynamics

In the earliest study on fine chromosomal locus movement, the Sedat laboratory observed an increase in chromatin movement upon microtubule depolymerization by Nocodazole in yeast (Marshall et al., 1997). They monitored, however, only a centromere-proximal locus, and it was unclear whether microtubules would also affect the movement of other loci. As discussed above, the yeast chromosomes assume a Rabl like conformation, whereby centromeres are tethered to the SPB by microtubules that also attach to the kinetochore. The disruption of kinetochore bound microtubules will release the centromeres and can in turn increase chromosome dynamics (Amitai et al., 2017; Bystricky et al., 2005b; Lawrimore et al., 2017; Strecker et al., 2016).

In contrast, in mammalian cells the de Lange laboratory have shown that Nocodazole treatment decreases chromosome dynamics in a LINC- and kinesin-dependent manner, more akin to the effect of actin depolymerization in yeast (Lottersberger et al., 2015). This suggests that changes in the cytoplasm are transduced to the nucleus in mammalian cells through microtubules, kinesins and the LINC complex, in contrast to yeast where microtubules are located in the nucleus and directly tether centromeres, throughout the cell cycle. In yeast, actin cytoskeletal filaments may fulfil the role played by microtubules in mammals with respect to chromatin movement influenced by the cytoskeleton (Amitai et al., 2017; Spichal et al., 2016).

DNA double- strand break response

DNA double-strand break checkpoint activation and DNA repair pathways

Our genome is continuously challenged by DNA damage from both exogenous environmental sources and from endogenous cellular mechanisms such as metabolism and replication errors. A single double strand break (DSB) is lethal in a haploid organism if unrepaired, and can lead to loss of genetic information or mutations in diploid or haploid cells. These genetic alterations are the main cause of cancer and genetic diseases. Therefore, eukaryotic cells have developed very conserved and efficient DNA damage checkpoint (DDC) response and repair mechanisms (reviewed in (Lisby and Rothstein, 2009)). The main aim of the DDC is to stall the cell cycle to allow time for repair.

In budding yeast, the induction of a single DSB lead to the recruitment of Ku (yKu70 and yKu80) and the MRX (Mre11-Rad50-Xrs2) complexes at the site of damage in order to hold together the two

broken ends. This first step is very critical as it will determine the repair outcome of this lesion: the recruitment of Ku complex delays 5' DNA end resection while MRX recruitment promotes early

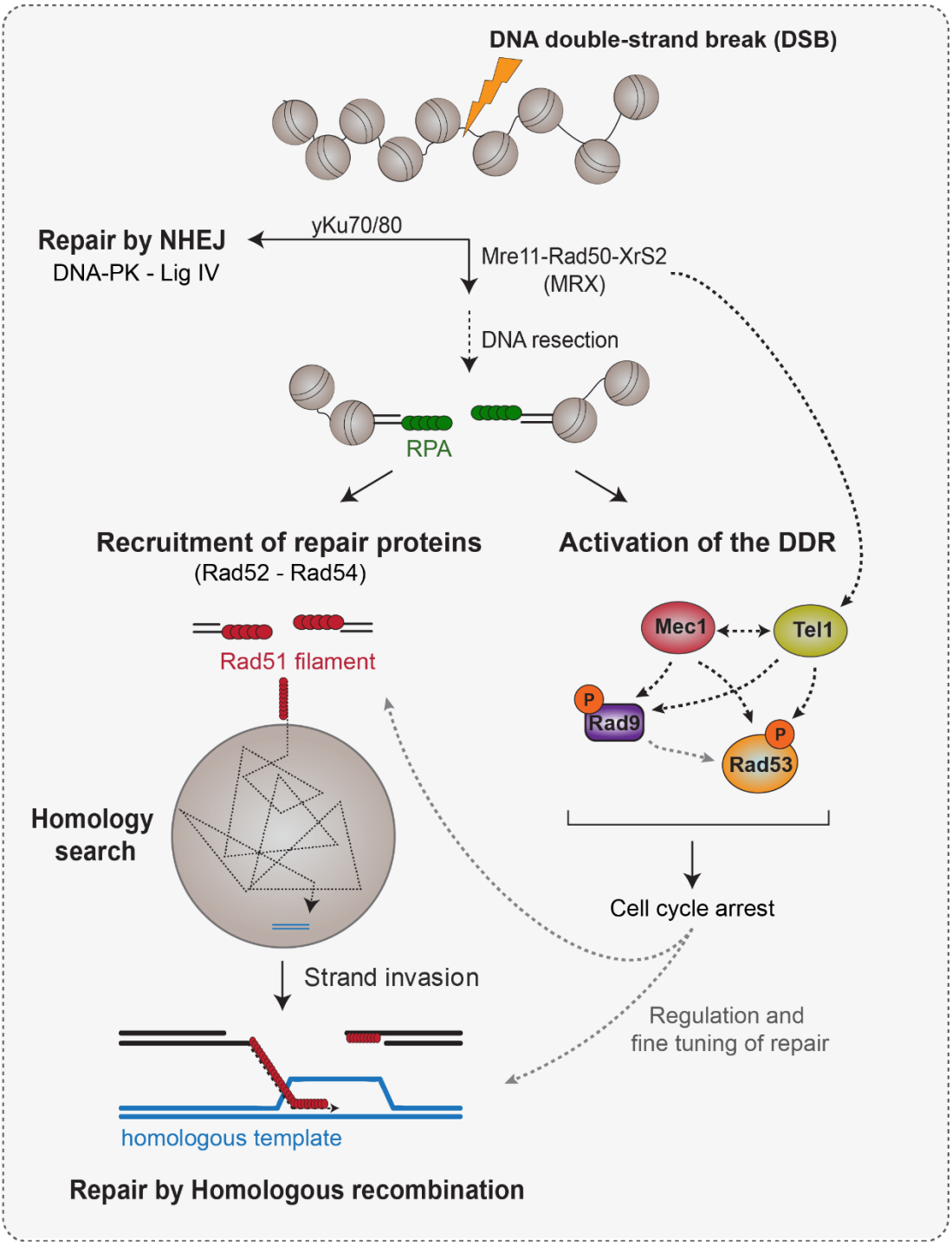

Figure 2: DNA damage checkpoint activation and DSB repair

Overview of the DNA damage checkpoint activation through Mec1 and Tel1 kinases. The two major DNA DSB repair pathways are NHEJ (mediated by yKu70/80, DNA-PK and Ligase IV) and Homologous recombination (mediated by MRX-Rad52-Rad54 and Rad51).

DNA end resection by creating a nick and generating a short 3' overhang . A second more processive DNA end resection is performed either by Exo1 or by Sgs1/Dna2 (Zhu et al., 2008). In parallel, MRX binding activates the checkpoint kinase Tel1(Nakada et al., 2003) which phosphorylates histone H2A. Phosphorylated H2A (γH2A) facilitates Rad9 binding to methylated H3K79 and the subsequent Rad53 activation (Lisby et al., 2004; Toh et al., 2006). DNA end resection leads to the formation of 3' DNA overhangs, the dissociation of the MRX complex and the binding of RPA to the resulting single stranded DNA (ssDNA). RPA binding will allow both checkpoint protein activation (Mec1 and subsequently Rad53) and the recruitment of homologous recombination (HR) proteins such as Rad52, which loads Rad51 to form a Rad51-ssDNA filament. This is the basis of homology search and subsequent repair of the DSB by HR **(Figure 2).**

Efficient DNA end-resection at a DSB favors repair by HR. However, a second, more error-prone mechanism called Non-Homologous End Joining (NHEJ) is the dominant pathway in G1-phase cells. **(Figure 2).** NHEJ is considered as an error prone repair mechanism as the two broken ends are simply religated. If the ends do not annealed in frame or have modified bases, insertions or deletions can occur. When the sister chromatid is available for homology-based repair, then recombination from the sister is the preferred mechanism of DSB repair. If neither NHEJ nor sister recombination are possible, then there will be a search for an ectopic sequence with homology. HR is the repair pathway of choice in budding yeast, and is active even in G1 in yeast, although resection is far less efficient in G1 phase. Several lines of evidence suggest that homology search in the nucleus is rate limiting for HR (Wilson et al., 1994), which led to the suggestion that DSB movement might enhance recombination rates. In the following sections, we will discuss how chromatin movement is regulated during DSB induction and its role in DNA repair.

Damage induced chromatin movement

Using time-lapse microscopy several studies have addressed the question of how chromatin dynamics respond to DNA damage either locally at a DSB, or ectopically – i.e., elsewhere in the genome. This has been monitored following global DNA damage (radiomimetic genotoxic drugs such as Zeocin, or γ-irradiation (γIR) or with a single, targeted DSB, mediated by I-SCE1 or HO endonuclease.

Local double-strand break dynamics

In budding yeast endonuclease-induced DSBs have increased dynamics when compared to the same locus uncleaved, and Rc increases, such that the volume accessed is roughly 3 to 4-fold larger (Dion et al., 2012; Hauer et al., 2017; Mine-Hattab et al., 2017; Mine-Hattab and Rothstein, 2012; Strecker et al., 2016). We also note that the Bystricky laboratory observed a decrease of local DSB movement upon damage at very short times-scales (<10ms) (Saad et al., 2014), which may enable early steps in DSB recognition and the stabilization of end tethering to occur. The reduced movement is later followed by an increase in mobility. Thise widely confirmed increase in DSB dynamics has been shown to depend on the activation of the DNA damage checkpoint: in yeast by activation of Mec1-Ddc2 and its target Rad9 (Dion et al., 2012; Strecker et al., 2016). Importantly, an artificial activation of the DDC by targeting Ddc1/Ddc2, known Mec1 activators, is sufficient to increase local chromatin mobility at the site of Mec1 binding, in S-phase cells that have not been exposed to DNA damage (Seeber et al., 2013). While the increase was not equivalent to that scored at a real DSB, this result strengthens the hypothesis that DDC activation triggers the observed DNA damage-induced chromatin mobility.

There are discrepancies in the literature concerning the roles of different kinases in the DDC cascade. The increase in DSB dynamics appeared to be independent of the key kinase downstream of Mec1, Rad53, in S phase (Dion et al., 2012), while another study reported that Rad53 activation was required for DSB increase in movement (Strecker et al., 2016). Hauer et al. (2017) found that ectopic movement in response to Zeocin, and the histone eviction that drives this, was Rad53-dependent (Hauer et al., 2017). It is likely therefore that Strecker et al., were monitoring a general ectopic increase in mobility and not that of the DSB.

In addition to the checkpoint activation, the local increase in DSB movement was shown to be highly dependent on chromatin remodeler function, namely the INO80 and the SWR1 remodeling complexes (Neumann et al., 2012; Seeber et al., 2013), with elements of the HR machinery, Rad51 and Rad52, to play modulatory roles (Smith et al., 2018)(Smith . The mechanisms behind this dependency are discussed below.

Global (ectopic) movement of undamaged sites

The Rothstein laboratory was the first to report an increase in chromatin mobility of an uncut locus upon DNA damage in diploid yeast cells (Mine-Hattab and Rothstein, 2012). This was confirmed by

several studies that have now shown that Zeocin increases general chromatin decompaction and enhanced movement even at sites that apparently have no damage, as does a single DSB (Amitai et al., 2017; Cheblal, in press; Hauer et al., 2017; Herbert et al., 2017; Seeber et al., 2013). Similar to the local DSB dynamics, this DNA damage enhanced global chromatin movement was shown to be dependent on the activation of the DDC (Hauer et al., 2017; Seeber et al., 2013; Smith et al., 2018). Moreover, increased global DNA damage was also dependent on the chromatin remodeler complex INO80. In contrast, the SWR1 complex that was shown to be required for local DSB dynamics appeared not to be required for the increase in ectopic mobility (Seeber et al., 2013), suggesting that local DSB mobility and the ectopic mobility at undamaged sites are regulated at least in part by distinct mechanisms. This will be addressed in the second Chapter of this dissertation.

Mechanisms that controls damage-induced chromatin movement

Investigations into the mechanisms that control heightened chromatin movement following DNA damage have led to multiple nonexclusive models for how this might occur (reviewed in (Seeber et al., 2018)). In this section, we will discuss the key mechanisms proposed to control DSB induced chromatin movement in budding yeast.

DNA damage induced loss of chromosomal tethering

A recent study from the Durocher laboratory reported that treatment of yeast cells with the radiomimetic drug Zeocin induced a general kinetochore declustering that led to centromere detachment from the SPB (Strecker et al., 2016). This phenomenon was suggested to be dependent on the phosphorylation by the DDC kinase Rad53 of the essential spindle checkpoint protein Cep3 on Serine 575, and these events were proposed to be the mechanism that underlies the increase in chromosomal dynamics upon DNA damage. Indeed, they reported that there was no DSB-induced increase in dynamics in a Cep3 phosphomutant (*cep3-S575A*). Other studies have failed to observe this dependency (Lawrimore et al., 2017) (Cheblal et al., in press), and no significant changes in the distances between SPB and yeast centromeres were observed upon DNA damage (Strecker et al., 2016) Cheblal et al., in press). Although, a loss of chromosomal tethering is able to increase chromosomal dynamics (Gartenberg et al., 2004; Lawrimore et al., 2017; Strecker et al., 2016; Verdaasdonk et al., 2013), recent observations render it unlikely to be the underlying mechanism that controls DNA damage-induced chromatin movement. We note that the measurement of chromatin

dynamics in Strecker et *al.* was performed automatically on an asynchronous population of yeast cells, with no monitoring of cut efficiency (in the case of an HO-induced cut) and with no distinction made between G1, S and G2 phase cells. Since the quantification in each mutant was averaged over a population, any treatment or condition that changes the cell cycle distribution could alter the movement as well, indirectly. Finally, another study reported Rad52 foci dynamics at DSB was dependent on a kinesin (Chung et al., 2015). The study attempted to determine whether DSB-induced chromatin dynamics have directed motion along microtubule filaments. Kinesin dependence was not correlated with directed motion, although the correlation was reported in other studies that were performed on damage in heterochromatin in flies (Ryu et al., 2015) (Janssen et al., 2016). It is important to note that the imaging time-scale used for DSB movement in flies and in yeast are different and that the time-scale used in yeast is probably not appropriate to measure directed motion (reviewed in (Oshidari et al., 2019)). Depending on the temporal resolution of the imaging used, one can reach different conclusions about whether movement is directed or subdiffusive. The same movement can be subdiffusive and random at shorter time scales and directed at longer time scales (e.g. lipid movement on microtubules). It is plausible that in comparison to other eukaryotes, the small size of the budding yeast nucleus renders directed motion unnecessary for DNA repair by HR, since random movement already allows a sufficient homology search to occur. Nonetheless, a study of DSB movement in yeast over longer time scales remains to be carried out.

Chromatin remodeling

Rather than changes in chromosome tethering, other laboratories have demonstrated that intrinsic changes in chromatin structure regulate DSB induced chromatin movement. The Gasser laboratory first reported local histone H3 eviction at the site of DSB dependent on the chromatin remodeler INO80C (van Attikum et al., 2007). Consistent with that observation, later they showed that targeting INO80C to a chromosomal locus significantly increases its motion (Neumann et al., 2012). A recent study from the Gasser laboratory reconciled these two observations by showing that treatment of yeast cells with the radiomimetic drug Zeocin triggers a global 20-40% loss of core histones from chromatin, that could be observed by mass spectrometry, Western blotting of the core histones and live microscopy (Hauer et al., 2017) **(Figure 3).** This histone depletion was shown to be dependent on the proteasome, suggesting a ubiquitination-triggered histone degradation process. Consistent with the previous observations, this DNA damage induced histone depletion was dependent on the INO80

chromatin remodeler and on the activation of the DNA damage checkpoint. Interestingly, either the artificial histone depletion by transcriptional shutdown, or a natural depletion that occurs in a mutant that lacks the two HMGB1 homologs in yeast, led to a significant increase in chromatin mobility. The HMGB1 double knockout (*nhp6*Δ Δ) was shown to reduce histone levels by 20% (Celona et al., 2011). Taken together, the Gasser laboratory proposed that DNA damage-induced global histone depletion and chromatin expansion contributes to enhanced ectopic chromatin movement (Hauer et al., 2017). Interestingly, and in line with Hauer et al., it has been observed that in mammalian cells, parental histone redistribution appeared to allow chromatin expansion upon DNA damage (Adam et al., 2016).

In parallel, another study suggested that DNA damage-induced global chromatin dynamics can be explained by an increase in chromatin rigidity and stiffening instead of chromatin decondensation (Herbert et al., 2017). Changes in chromatin structure might regulate DNA repair, either by increasing local accessibility to repair factors or by changing the stiffness of the resected end. Indeed, consistent with the observation that DNA damage-induced chromatin movement is dependent on Rad51 repair protein (Dion et al., 2012; Mine-Hattab et al., 2017; Smith et al., 2018), Mine-Hattab et al. suggested a model in which stiffening of the damaged ends by the repair complex, combined with a global increase in stiffness, act like a "needle in a ball of yarn". This enhanced stiffness might allow reptation through the dense nucleoplasm (Herbert et al., 2017; Mine-Hattab et al., 2017), promoting an efficient homology search during HR. Whether the observed chromatin decompaction in Hauer et al. and the increase in global stiffness described in Mine-Hattab et al. reflect the same underlying biological processes is unclear, although these two phenomenon appear rather to be contradictory. Further studies are needed to investigate whether the observed chromatin stiffening is controlled by chromatin remodelers and histone degradation.

In the next section, we will discuss recent observations on how chromatin organization states regulate DNA repair.

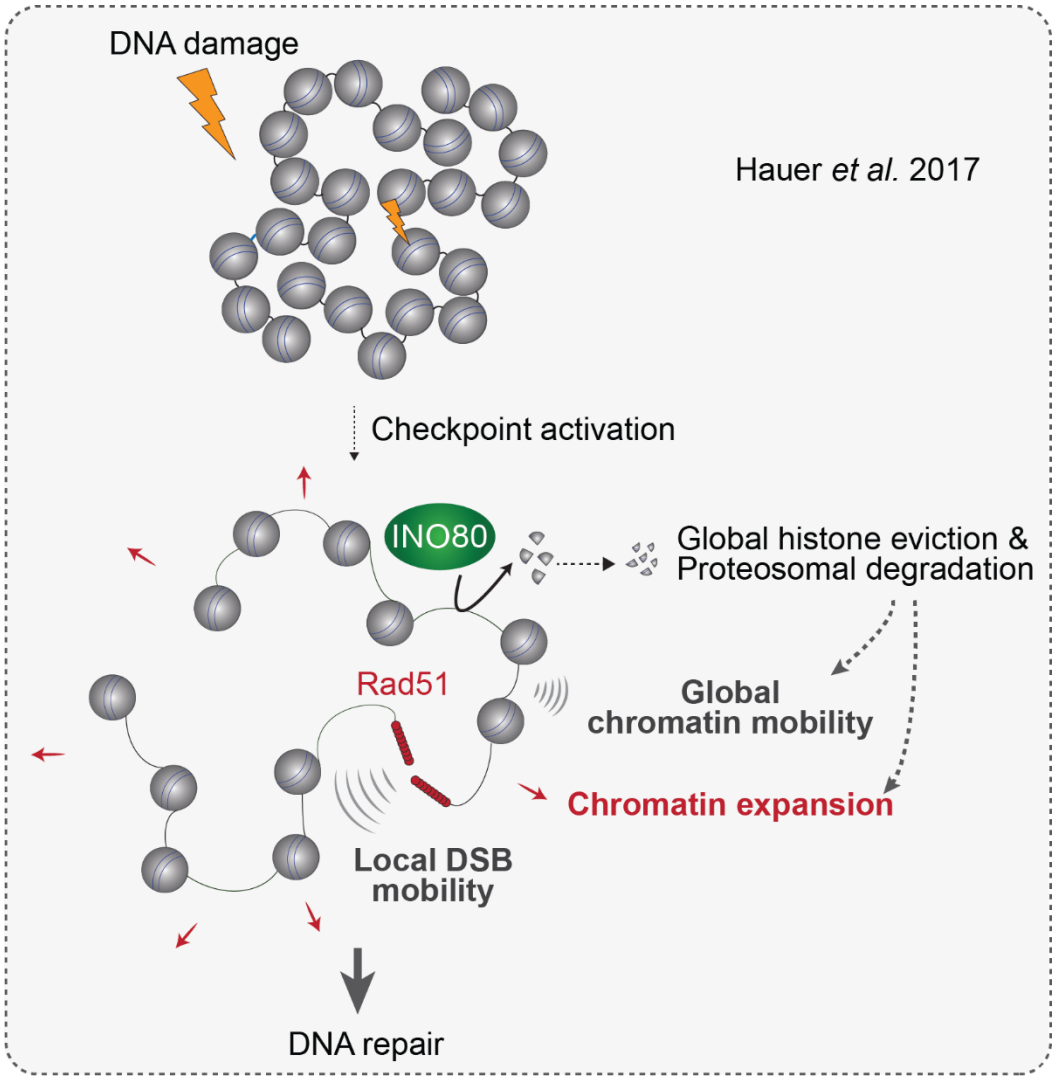

<u>Figure 3:</u> DNA damage-induced histone degradation enhances chromatin mobility

DNA damage-induced checkpoint activation triggers global nucleosome remodeling by INO80-C and proteosomal histone degradation. This general nucleosome loss increases chromatin mobility and expansion (Hauer et al., 2017).

The role of chromatin organization in DNA DSB repair

As discussed above, DNA repair mechanisms are made possible through a choreography of DNA repair proteins that are sequentially recruited at the DSB site (reviewed in (Lisby and Rothstein, 2009)). The opening of the chromatin structure, either through histone removal (Hauer et al., 2017) or histone redistribution (Adam et al., 2016) is critical to allow a proper access of the lesion to DNA repair proteins. On the other hand, chromatin expansion might also be of critical relevance during the homology search step of HR, allowing the Rad51 filament to access potential ectopic homologous sequence in the genome efficiently (Renkawitz et al., 2014). Here I review the multiple studies that have addressed the question how chromatin accessibility influences DNA repair pathway choice (HR vs NHEJ) and repair efficiency.

Chromatin remodeling

The deletion of a subunit of the chromatin remodeler INO80 complex, Arp8, renders cells sensitive to DNA damaging agents such as Zeocin, γIR or hydroxyurea (Adam et al., 2016; Seeber et al., 2013; Shen et al., 2000; van Attikum et al., 2007) (Cheblal et al., in press). It has been shown that the INO80 complex slightly delays DNA end resection upon DSB induction (Lademann et al., 2017; van Attikum et al., 2007). As mentioned above, the INO80C chromatin remodeler is required for Zeocin induced histone depletion and the subsequent increase in chromatin expansion, as well as mobility (Hauer et al., 2017). Moreover, using a mutant that has lower levels of histones and therefore has higher levels of chromatin decompaction, Hauer *et al.,* observed an increase in the integration rate of a *URA3* cassette in yeast cells. These observations suggest that chromatin accessibility and/or movement might facilitate homology directed repair (HDR). My thesis directly addressed the effect of chromatin accessibility on strand invasion kinetics during homology based DNA repair, which will be discussed in Chapter 3.

DNA repair in heterochromatin vs euchromatin

One way to address whether DNA repair efficiency is dependent on the chromatin context in higher eukaryotes is to understand how DNA damage is repaired in heterochromatin (compacted) *vs* euchromatin (open state) (reviewed in (Marnef and Legube, 2017). Many laboratories have analyzed DNA repair behavior in pericentric and centromeric repeats, which in most cell types form heterochromatin. They have shown that DSBs relocate away from heterochromatic domains to the

nuclear periphery prior to repair by HR (Chiolo et al., 2011; Ryu et al., 2015). Moreover, in mouse cells, DSBs are repaired by NHEJ in G1, and remain heterochromatic, whereas in S phase, heterochromatic DSBs shift to the nuclear periphery to enable repair by HR (Tsouroula et al., 2016). Similarly, it was shown that DSBs in ribosomal DNA (rDNA) in yeast relocate out of the nucleolus to be processed for HR (Torres-Rosell et al., 2007). This relocation was also confirmed in mammalian cells where persistent DSB shift away from the nucleolus and the repetitive DNA (Harding et al., 2015; van Sluis and McStay, 2015). What is common in all these studies, is the need to avoid the repair of breaks in a repeat, whether heterochromatin or rDNA, in an environment that contains many copies of the same sequences, as this is prone to illegitimate recombination and either sequence excision or translocation.

Some studies have also observed heterochromatin expansion after DNA damage in mammalian cells and flies (Chiolo et al., 2011; Ryu et al., 2015). However, in these conditions, repair protein accessibility seemed to be unchanged, although one cannot exclude that some regions within heterochromatin behave differently from the bulk. The expansion within heterochromatin, however, might facilitate DSB relocation to the periphery away from heterochromatin, rather than accessibility of repair components.

Chromosomal positioning

As mentioned above, subnuclear positioning influences DSB repair and this does not only apply to repetitive regions such as heterochromatin. Several studies have demonstrated that the nuclear pore complex (NPC) is a key player in DNA repair pathway choice. Indeed, the Gasser laboratory have observed that persistent DSBs relocate to nuclear pores 1-2 hours after HO induction (Nagai et al., 2008). This recruitment was shown to be critical for persistent DSBs where either template switching based repair or break induced replication (BIR) repair would have to be initiated (Horigome et al., 2016; Horigome and Gasser, 2016). The relocation to the NPC was shown to be controlled by the conserved SUMO-dependent E3 ligase Slx5/Slx8 (Horigome et al., 2016; Nagai et al., 2008).

Another key platform for DSB binding *in S. cerevisiae* is the SUN domain protein Mps3, which spans the inner nuclear membrane. In contrast to NPC, relocation to Mps3 was shown to be dependent on the INO80C chromatin remodeler and DNA end resection (Horigome et al., 2014). Consistent with that, the binding of DSBs to Mps3 favors homology based repair in S/G2 phases of the cell cycle (Horigome et al., 2016).

We note, however, that any perturbation of nuclear actin will inevitably affect the function of the most abundant chromatin remodelers, including INO80C, which is an important factor in DSB repair (reviewed in (Hurst et al., 2019)). Additional studies are needed to determine if actin filaments or an altered G/F actin pool alter the efficiency of DSB repair. Only more detailed studies can clarify whether there is a direct effect of nuclear actin on the dynamics of a damaged locus, or if it has an indirect effect through INO80C or other remodelers. Most likely only a a distinct subset of damaged sites will show sensitivity to actin depolymerization.

In the mammalian system, the Soutoglou laboratory have demonstrated that DSBs induced at the nuclear membrane (but not at nuclear pores or nuclear interior) fail to rapidly activate the DNA damage response (DDR) and repair by HR. Moreover, instead of relocating to an HR permissive subcompartent, these DSBs are repaired in situ by alternative end-joining. This observation suggested that nuclear positioning is able to dictate DNA repair pathway choice (Lemaitre et al., 2014). Consistent with this hypothesis, it has been shown that telomeric DSB are preferentially repaired by BIR (Batte et al., 2017) or homology-driven non reciprocal translocation compared to non-telomeric DSBs in yeast (Marcomini et al., 2018).

Other studies have addressed whether genomic proximity would facilitate repair by HR. The Kupiec and the Haber laboratories have demonstrated that in yeast genomic regions that are spatially juxtaposed recombine more efficiently than sequences located in spatially distant territories (Agmon et al., 2013; Lee et al., 2016). This study reinforced early evidence that homology search throughout the nucleus was rate limiting for HR (Wilson et al., 1994), and that differences in repair efficiencies can be predicted in silico thanks to a locus position. Nevertheless, it remained unproven whether chromatin mobility enhances the homology search during HR or not.

Does DSB-induced chromatin movement enhance DNA repair efficiency?

In this section, I will examine whether DNA damage-induced chromatin mobility per se, either locally at the DSB site or ectopically at undamaged sites, contributes to efficient DNA repair by HR.

On the hypothesis of Homology search (and chromatin movement)

During HR, the resected DSB ends coated by a Rad51 filament, need to undergo a search within the nucleus in order to find a homologous partner among a wide range of imperfect ones. The most obvious donor after replication is the sister chromatid, but in our test system both sisters are cleaved by HO endonuclease, and there is no intact sister available for repair by HR. Therefore, the broken ends need to undergo a critical long-range search for a homologous template from which to repair the resected end. As mentioned above, homology search is thought to be rate limiting for HR (Agmon et al., 2013; Wilson et al., 1994), and the increase in local DSB movement has been suggested to be the driver of homology search (Mine-Hattab and Rothstein, 2012). In support of this, it was shown that the targeting the chromatin remodeler INO80C to a break increases both local dynamics and HR repair rates (Neumann et al., 2012). Similarly, the observed increase in chromatin dynamics in *nhp6ΔΔ* cells, which have a 20% reduction in histone levels, correlated with an increase in integration rates (Hauer et al., 2017). Finally it was shown that the deletion of an important protein for DNA damage checkpoint amplification, Rad9, abolished the increase in DSB mobility, and significantly reduced HR repair kinetics (Dion et al., 2012). In contrast to this, the Durocher laboratory argued that in the Cep3 phospho-mutant, local DSB movement seemed to abolished but repair by HDR was unchanged. They suggested that the local increase in DSB dynamics was dispensable for DNA repair (Strecker et al., 2016).

In other studies the hypothesis that movement would enhance HR was extended to mammalian cells. For instance, several studies showed that an increase in motion at uncapped telomeres facilitated the search required for repair (Cho et al., 2014; Dimitrova et al., 2008). However, none of the yeast nor the mammalian work to date had directly investigated the role of DSB-induced chromatin mobility on the kinetics of strand invasion during HR. Moreover, it remained unclear whether general chromatin accessibility or the DNA damage induced ectopic movement was critical for DNA repair. Indeed, as an alternative, either the access of DNA repair proteins to DSBs or to the template for recognition, might limit repair efficiency. In yeast, a general expansion of undamaged chromatin in response to Zeocin, as reported in Hauer et al., also increased homology-based fragment integration (Hauer et al., 2017). In Chapter 3, we address the question whether such global chromatin expansion is critical for strand invasion kinetics during homology-directed repair.

REFERENCES

Adam, S., Dabin, J., Chevallier, O., Leroy, O., Baldeyron, C., Corpet, A., Lomonte, P., Renaud, O., Almouzni, G., and Polo, S.E. (2016). Real-Time Tracking of Parental Histones Reveals Their Contribution to Chromatin Integrity Following DNA Damage. Mol Cell *64*, 65-78.

Agmon, N., Liefshitz, B., Zimmer, C., Fabre, E., and Kupiec, M. (2013). Effect of nuclear architecture on the efficiency of double-strand break repair. Nature cell biology *15*, 694-699.

Amitai, A., Seeber, A., Gasser, S.M., and Holcman, D. (2017). Visualization of Chromatin Decompaction and Break Site Extrusion as Predicted by Statistical Polymer Modeling of Single-Locus Trajectories. Cell reports *18*, 1200-1214.

Bannister, A.J., and Kouzarides, T. (2011). Regulation of chromatin by histone modifications. Cell Res *21*, 381-395.

Batte, A., Brocas, C., Bordelet, H., Hocher, A., Ruault, M., Adjiri, A., Taddei, A., and Dubrana, K. (2017). Recombination at subtelomeres is regulated by physical distance, double-strand break resection and chromatin status. The EMBO journal *36*, 2609-2625.

Berg, H.C. (1993). Random Walks in Biology. Princeton University Press, Princeton, New Jersey.

Bronshtein, I., Kepten, E., Kanter, I., Berezin, S., Lindner, M., Redwood, A.B., Mai, S., Gonzalo, S., Foisner, R., Shav-Tal, Y.*, et al.* (2015). Loss of lamin A function increases chromatin dynamics in the nuclear interior. Nat Commun *6*, 8044.

Bruhl, J., Trautwein, J., Schafer, A., Linne, U., and Bouazoune, K. (2019). The DNA repair protein SHPRH is a nucleosome-stimulated ATPase and a nucleosome-E3 ubiquitin ligase. Epigenetics Chromatin *12*, 52.

Buhler, M., and Gasser, S.M. (2009). Silent chromatin at the middle and ends: lessons from yeasts. The EMBO journal *28*, 2149-2161.

Bystricky, K., Laroche, T., van Houwe, G., Blaszczyk, M., and Gasser, S.M. (2005). Chromosome looping in yeast: telomere pairing and coordinated movement reflect anchoring efficiency and territorial organization. J Cell Biol *168*, 375-387.

Cabal, G.G., Genovesio, A., Rodriguez-Navarro, S., Zimmer, C., Gadal, O., Lesne, A., Buc, H., Feuerbach-Fournier, F., Olivo-Marin, J.C., Hurt, E.C.*, et al.* (2006). SAGA interacting factors confine sub-diffusion of transcribed genes to the nuclear envelope. Nature *441*, 770-773.

Caridi, P.C., Delabaere, L., Zapotoczny, G., and Chiolo, I. (2017). And yet, it moves: nuclear and chromatin dynamics of a heterochromatic double-strand break. Philos Trans R Soc Lond B Biol Sci *372*.

Celona, B., Weiner, A., Di Felice, F., Mancuso, F.M., Cesarini, E., Rossi, R.L., Gregory, L., Baban, D., Rossetti, G., Grianti, P.*, et al.* (2011). Substantial histone reduction modulates genomewide nucleosomal occupancy and global transcriptional output. PLoS Biol *9*, e1001086.

Chen, H., Levo, M., Barinov, L., Fujioka, M., Jaynes, J.B., and Gregor, T. (2018). Dynamic interplay between enhancer-promoter topology and gene activity. Nat Genet *50*, 1296-1303.

Chen, Y.J., Chuang, Y.C., Chuang, C.N., Cheng, Y.H., Chang, C.R., Leng, C.H., and Wang, T.F. (2016). S. cerevisiae Mre11 recruits conjugated SUMO moieties to facilitate the assembly and function of the Mre11-Rad50-Xrs2 complex. Nucleic Acids Res *44*, 2199-2213.

Chiolo, I., Minoda, A., Colmenares, S.U., Polyzos, A., Costes, S.V., and Karpen, G.H. (2011). Double-strand breaks in heterochromatin move outside of a dynamic HP1a domain to complete recombinational repair. Cell *144*, 732-744.

Cho, N.W., Dilley, R.L., Lampson, M.A., and Greenberg, R.A. (2014). Interchromosomal homology searches drive directional ALT telomere movement and synapsis. Cell *159*, 108-121.

Chung, D.K., Chan, J.N., Strecker, J., Zhang, W., Ebrahimi-Ardebili, S., Lu, T., Abraham, K.J., Durocher, D., and Mekhail, K. (2015). Perinuclear tethers license telomeric DSBs for a broad kinesin- and NPC-dependent DNA repair process. Nat Commun *6*, 7742.

Churikov, D., Charifi, F., Eckert-Boulet, N., Silva, S., Simon, M.N., Lisby, M., and Geli, V. (2016). SUMO-Dependent Relocalization of Eroded Telomeres to Nuclear Pore Complexes Controls Telomere Recombination. Cell reports *15*, 1242-1253.
Conrad, M.N., Lee, C.Y., Chao, G., Shinohara, M., Kosaka, H., Shinohara, A., Conchello, J.A., and Dresser, M.E. (2008). Rapid telomere movement in meiotic prophase is promoted by NDJ1, MPS3, and CSM4 and is modulated by recombination. Cell *133*, 1175-1187.
Cremer, T., and Cremer, C. (2001). Chromosome territories, nuclear architecture and gene regulation in mammalian cells. Nat Rev Genet *2*, 292-301.
Cremona, C.A., Sarangi, P., Yang, Y., Hang, L.E., Rahman, S., and Zhao, X. (2012). Extensive DNA damage-induced sumoylation contributes to replication and repair and acts in addition to the mec1 checkpoint. Mol Cell *45*, 422-432.
Dimitrova, N., Chen, Y.C., Spector, D.L., and de Lange, T. (2008). 53BP1 promotes non-homologous end joining of telomeres by increasing chromatin mobility. Nature *456*, 524-528.
Dion, V., and Gasser, S.M. (2013). Chromatin movement in the maintenance of genome stability. Cell *152*, 1355-1364.
Dion, V., Kalck, V., Horigome, C., Towbin, B.D., and Gasser, S.M. (2012). Increased mobility of double-strand breaks requires Mec1, Rad9 and the homologous recombination machinery. Nature cell biology *14*, 502-509.
Dion, V., Kalck, V., Seeber, A., Schleker, T., and Gasser, S.M. (2013). Cohesin and the nucleolus constrain the mobility of spontaneous repair foci. EMBO reports *14*, 984-991.
Dixon, J.R., Selvaraj, S., Yue, F., Kim, A., Li, Y., Shen, Y., Hu, M., Liu, J.S., and Ren, B. (2012). Topological domains in mammalian genomes identified by analysis of chromatin interactions. Nature *485*, 376-380.
Downs, J.A., Kosmidou, E., Morgan, A., and Jackson, S.P. (2003). Suppression of homologous recombination by the Saccharomyces cerevisiae linker histone. Mol Cell *11*, 1685-1692.
Fabre, E., and Zimmer, C. (2018). From dynamic chromatin architecture to DNA damage repair and back. Nucleus *9*, 161-170.
Fyodorov, D.V., Zhou, B.R., Skoultchi, A.I., and Bai, Y. (2018). Emerging roles of linker histones in regulating chromatin structure and function. Nat Rev Mol Cell Biol *19*, 192-206.
Gartenberg, M.R., Neumann, F.R., Laroche, T., Blaszczyk, M., and Gasser, S.M. (2004). Sir-mediated repression can occur independently of chromosomal and subnuclear contexts. Cell *119*, 955-967.
Germier, T., Kocanova, S., Walther, N., Bancaud, A., Shaban, H.A., Sellou, H., Politi, A.Z., Ellenberg, J., Gallardo, F., and Bystricky, K. (2017). Real-Time Imaging of a Single Gene Reveals Transcription-Initiated Local Confinement. Biophys J *113*, 1383-1394.
Grewal, S.I., and Jia, S. (2007). Heterochromatin revisited. Nat Rev Genet *8*, 35-46.
Gu, B., Swigut, T., Spencley, A., Bauer, M.R., Chung, M., Meyer, T., and Wysocka, J. (2018). Transcription-coupled changes in nuclear mobility of mammalian cis-regulatory elements. Science *359*, 1050-1055.
Harding, S.M., Boiarsky, J.A., and Greenberg, R.A. (2015). ATM Dependent Silencing Links Nucleolar Chromatin Reorganization to DNA Damage Recognition. Cell reports *13*, 251-259.
Hauer, M.H., Seeber, A., Singh, V., Thierry, R., Sack, R., Amitai, A., Kryzhanovska, M., Eglinger, J., Holcman, D., Owen-Hughes, T*., et al.* (2017). Histone degradation in response to DNA damage enhances chromatin dynamics and recombination rates. Nat Struct Mol Biol *24*, 99-107.
Hediger, F., Neumann, F.R., Van Houwe, G., Dubrana, K., and Gasser, S.M. (2002). Live imaging of telomeres: yKu and Sir proteins define redundant telomere-anchoring pathways in yeast. Curr Biol *12*, 2076-2089.
Herbert, S., Brion, A., Arbona, J.M., Lelek, M., Veillet, A., Lelandais, B., Parmar, J., Fernandez, F.G., Almayrac, E., Khalil, Y*., et al.* (2017). Chromatin stiffening underlies enhanced locus mobility after DNA damage in budding yeast. The EMBO journal *36*, 2595-2608.

Heun, P., Laroche, T., Shimada, K., Furrer, P., and Gasser, S.M. (2001). Chromosome dynamics in the yeast interphase nucleus. Science *294*, 2181-2186.
Ho, J.W., Jung, Y.L., Liu, T., Alver, B.H., Lee, S., Ikegami, K., Sohn, K.A., Minoda, A., Tolstorukov, M.Y., Appert, A.*, et al.* (2014). Comparative analysis of metazoan chromatin organization. Nature *512*, 449-452.
Horigome, C., Bustard, D.E., Marcomini, I., Delgoshaie, N., Tsai-Pflugfelder, M., Cobb, J.A., and Gasser, S.M. (2016). PolySUMOylation by Siz2 and Mms21 triggers relocation of DNA breaks to nuclear pores through the Slx5/Slx8 STUbL. Genes Dev *30*, 931-945.
Horigome, C., and Gasser, S.M. (2016). SUMO wrestles breaks to the nuclear ring's edge. Cell Cycle *15*, 3011-3013.
Horigome, C., Oma, Y., Konishi, T., Schmid, R., Marcomini, I., Hauer, M.H., Dion, V., Harata, M., and Gasser, S.M. (2014). SWR1 and INO80 chromatin remodelers contribute to DNA double-strand break perinuclear anchorage site choice. Mol Cell *55*, 626-639.
Horigome, C., Unozawa, E., Ooki, T., and Kobayashi, T. (2019). Ribosomal RNA gene repeats associate with the nuclear pore complex for maintenance after DNA damage. PLoS Genet *15*, e1008103.
Hurst, V., Shimada, K., and Gasser, S.M. (2019). Nuclear Actin and Actin-Binding Proteins in DNA Repair. Trends in cell biology *29*, 462-476.
Janssen, A., Breuer, G.A., Brinkman, E.K., van der Meulen, A.I., Borden, S.V., van Steensel, B., Bindra, R.S., LaRocque, J.R., and Karpen, G.H. (2016). A single double-strand break system reveals repair dynamics and mechanisms in heterochromatin and euchromatin. Genes Dev *30*, 1645-1657.
Jin, Q.W., Fuchs, J., and Loidl, J. (2000). Centromere clustering is a major determinant of yeast interphase nuclear organization. Journal of cell science *113 (Pt 11)*, 1903-1912.
Joyner, R.P., Tang, J.H., Helenius, J., Dultz, E., Brune, C., Holt, L.J., Huet, S., Muller, D.J., and Weis, K. (2016). A glucose-starvation response regulates the diffusion of macromolecules. Elife *5*.
Kapoor, P., Chen, M., Winkler, D.D., Luger, K., and Shen, X. (2013). Evidence for monomeric actin function in INO80 chromatin remodeling. Nat Struct Mol Biol *20*, 426-432.
Koszul, R., Kim, K.P., Prentiss, M., Kleckner, N., and Kameoka, S. (2008). Meiotic chromosomes move by linkage to dynamic actin cables with transduction of force through the nuclear envelope. Cell *133*, 1188-1201.
Kueng, S., Oppikofer, M., and Gasser, S.M. (2013). SIR proteins and the assembly of silent chromatin in budding yeast. Annu Rev Genet *47*, 275-306.
Lachner, M., O'Carroll, D., Rea, S., Mechtler, K., and Jenuwein, T. (2001). Methylation of histone H3 lysine 9 creates a binding site for HP1 proteins. Nature *410*, 116-120.
Lademann, C.A., Renkawitz, J., Pfander, B., and Jentsch, S. (2017). The INO80 Complex Removes H2A.Z to Promote Presynaptic Filament Formation during Homologous Recombination. Cell reports *19*, 1294-1303.
Lawrimore, J., Barry, T.M., Barry, R.M., York, A.C., Friedman, B., Cook, D.M., Akialis, K., Tyler, J., Vasquez, P., Yeh, E.*, et al.* (2017). Microtubule dynamics drive enhanced chromatin motion and mobilize telomeres in response to DNA damage. Molecular biology of the cell *28*, 1701-1711.
Lee, C.S., Wang, R.W., Chang, H.H., Capurso, D., Segal, M.R., and Haber, J.E. (2016). Chromosome position determines the success of double-strand break repair. Proceedings of the National Academy of Sciences of the United States of America *113*, E146-154.
Lemaitre, C., Grabarz, A., Tsouroula, K., Andronov, L., Furst, A., Pankotai, T., Heyer, V., Rogier, M., Attwood, K.M., Kessler, P.*, et al.* (2014). Nuclear position dictates DNA repair pathway choice. Genes Dev *28*, 2450-2463.
Lescasse, R., Pobiega, S., Callebaut, I., and Marcand, S. (2013). End-joining inhibition at telomeres requires the translocase and polySUMO-dependent ubiquitin ligase Uls1. The EMBO journal *32*, 805-815.
Levi, V., and Gratton, E. (2008). Chromatin dynamics during interphase explored by single-particle tracking. Chromosome Res *16*, 439-449.

Lisby, M., and Rothstein, R. (2009). Choreography of recombination proteins during the DNA damage response. DNA Repair (Amst) *8*, 1068-1076.
Lottersberger, F., Karssemeijer, R.A., Dimitrova, N., and de Lange, T. (2015). 53BP1 and the LINC Complex Promote Microtubule-Dependent DSB Mobility and DNA Repair. Cell *163*, 880-893.
Maison, C., Bailly, D., Roche, D., Montes de Oca, R., Probst, A.V., Vassias, I., Dingli, F., Lombard, B., Loew, D., Quivy, J.P.*, et al.* (2011). SUMOylation promotes de novo targeting of HP1alpha to pericentric heterochromatin. Nat Genet *43*, 220-227.
Marcomini, I., Shimada, K., Delgoshaie, N., Yamamoto, I., Seeber, A., Cheblal, A., Horigome, C., Naumann, U., and Gasser, S.M. (2018). Asymmetric Processing of DNA Ends at a Double-Strand Break Leads to Unconstrained Dynamics and Ectopic Translocation. Cell reports *24*, 2614-2628 e2614.
Marnef, A., and Legube, G. (2017). Organizing DNA repair in the nucleus: DSBs hit the road. Curr Opin Cell Biol *46*, 1-8.
Marshall, W.F., Straight, A., Marko, J.F., Swedlow, J., Dernburg, A., Belmont, A., Murray, A.W., Agard, D.A., and Sedat, J.W. (1997). Interphase chromosomes undergo constrained diffusional motion in living cells. Curr Biol *7*, 930-939.
Martin, R.M., Gorisch, S.M., Leonhardt, H., and Cardoso, M.C. (2007). An unexpected link between energy metabolism, calcium, chromatin condensation and cell cycle. Cell Cycle *6*, 2422-2424.
Mattout, A., Gaidatzis, D., Padeken, J., Schmid, C.D., Aeschimann, F., Kalck, V., and Gasser, S.M. (2020). LSM2-8 and XRN-2 contribute to the silencing of H3K27me3-marked genes through targeted RNA decay. Nature cell biology *22*, 579-590.
Miescher, F. (1871). Ueber die chemische Zusammensetzung der Eiterzellen. Hoppe-Seyler's Medicinisch-Chemische Untersuchungen, 441-460.
Mine-Hattab, J., Recamier, V., Izeddin, I., Rothstein, R., and Darzacq, X. (2017). Multi-scale tracking reveals scale-dependent chromatin dynamics after DNA damage. Molecular biology of the cell.
Mine-Hattab, J., and Rothstein, R. (2012). Increased chromosome mobility facilitates homology search during recombination. Nature cell biology *14*, 510-517.
Mukherjee, K., English, N., Meers, C., Kim, H., Jonke, A., Storici, F., and Torres, M. (2020). Systematic analysis of linker histone PTM hotspots reveals phosphorylation sites that modulate homologous recombination and DSB repair. DNA Repair (Amst) *86*, 102763.
Mullen, J.R., and Brill, S.J. (2008). Activation of the Slx5-Slx8 ubiquitin ligase by poly-small ubiquitin-like modifier conjugates. J Biol Chem *283*, 19912-19921.
Nagai, S., Dubrana, K., Tsai-Pflugfelder, M., Davidson, M.B., Roberts, T.M., Brown, G.W., Varela, E., Hediger, F., Gasser, S.M., and Krogan, N.J. (2008). Functional targeting of DNA damage to a nuclear pore-associated SUMO-dependent ubiquitin ligase. Science *322*, 597-602.
Neumann, F.R., Dion, V., Gehlen, L.R., Tsai-Pflugfelder, M., Schmid, R., Taddei, A., and Gasser, S.M. (2012). Targeted INO80 enhances subnuclear chromatin movement and ectopic homologous recombination. Genes Dev *26*, 369-383.
Neumann, F.R.H., F. ; Taddei, A. and Gasser, S.M. (2005). Tracking Individual Chromosomes with Integrated lacO sites and GFP-lacI repressor: Analysing Position and Dynamics of Chromosomal loci in S. cerevisiae. Cell Biology A Laboratory Handbook *2*, 359-367
Oshidari, R., Mekhail, K., and Seeber, A. (2019). Mobility and Repair of Damaged DNA: Random or Directed? Trends in cell biology.
Palladino, F., Laroche, T., Gilson, E., Axelrod, A., Pillus, L., and Gasser, S.M. (1993). SIR3 and SIR4 proteins are required for the positioning and integrity of yeast telomeres. Cell *75*, 543-555.
Pliss, A., Malyavantham, K., Bhattacharya, S., Zeitz, M., and Berezney, R. (2009). Chromatin dynamics is correlated with replication timing. Chromosoma *118*, 459-470.

Pombo, A., and Dillon, N. (2015). Three-dimensional genome architecture: players and mechanisms. Nat Rev Mol Cell Biol *16*, 245-257.
Qu, Y., Gharbi, N., Yuan, X., Olsen, J.R., Blicher, P., Dalhus, B., Brokstad, K.A., Lin, B., Oyan, A.M., Zhang, W.*, et al.* (2016). Axitinib blocks Wnt/beta-catenin signaling and directs asymmetric cell division in cancer. Proceedings of the National Academy of Sciences of the United States of America *113*, 9339-9344.
Rabl, C. (1885). Über zelltheilung. Morphologisches Jahrbuch *10*, 214-330.
Renkawitz, J., Lademann, C.A., and Jentsch, S. (2014). Mechanisms and principles of homology search during recombination. Nat Rev Mol Cell Biol *15*, 369-383.
Riddle, N.C., Minoda, A., Kharchenko, P.V., Alekseyenko, A.A., Schwartz, Y.B., Tolstorukov, M.Y., Gorchakov, A.A., Jaffe, J.D., Kennedy, C., Linder-Basso, D.*, et al.* (2011). Plasticity in patterns of histone modifications and chromosomal proteins in Drosophila heterochromatin. Genome Res *21*, 147-163.
Ryu, T., Spatola, B., Delabaere, L., Bowlin, K., Hopp, H., Kunitake, R., Karpen, G.H., and Chiolo, I. (2015). Heterochromatic breaks move to the nuclear periphery to continue recombinational repair. Nature cell biology *17*, 1401-1411.
Saad, H., Gallardo, F., Dalvai, M., Tanguy-le-Gac, N., Lane, D., and Bystricky, K. (2014). DNA dynamics during early double-strand break processing revealed by non-intrusive imaging of living cells. PLoS Genet *10*, e1004187.
Sage, D., Neumann, F.R., Hediger, F., Gasser, S.M., and Unser, M. (2005). Automatic tracking of individual fluorescence particles: application to the study of chromosome dynamics. IEEE transactions on image processing : a publication of the IEEE Signal Processing Society *14*, 1372-1383.
Seeber, A., Dion, V., and Gasser, S.M. (2013). Checkpoint kinases and the INO80 nucleosome remodeling complex enhance global chromatin mobility in response to DNA damage. Genes Dev *27*, 1999-2008.
Seeber, A., Hauer, M.H., and Gasser, S.M. (2018). Chromosome Dynamics in Response to DNA Damage. Annu Rev Genet *52*, 295-319.
Seeber, A., Hegnauer, A.M., Hustedt, N., Deshpande, I., Poli, J., Eglinger, J., Pasero, P., Gut, H., Shinohara, M., Hopfner, K.P.*, et al.* (2016). RPA Mediates Recruitment of MRX to Forks and Double-Strand Breaks to Hold Sister Chromatids Together. Mol Cell *64*, 951-966.
Shen, X., Mizuguchi, G., Hamiche, A., and Wu, C. (2000). A chromatin remodelling complex involved in transcription and DNA processing. Nature *406*, 541-544.
Shukron, O., Seeber, A., Amitai, A., and Holcman, D. (2019). Advances Using Single-Particle Trajectories to Reconstruct Chromatin Organization and Dynamics. Trends Genet *35*, 685-705.
Smith, M.J., Bryant, E.E., and Rothstein, R. (2018). Increased chromosomal mobility after DNA damage is controlled by interactions between the recombination machinery and the checkpoint. Genes Dev *32*, 1242-1251.
Smurova, K., and De Wulf, P. (2018). Centromere and Pericentromere Transcription: Roles and Regulation ... in Sickness and in Health. Front Genet *9*, 674.
Spichal, M., Brion, A., Herbert, S., Cournac, A., Marbouty, M., Zimmer, C., Koszul, R., and Fabre, E. (2016). Evidence for a dual role of actin in regulating chromosome organization and dynamics in yeast. Journal of cell science *129*, 681-692.
Strecker, J., Gupta, G.D., Zhang, W., Bashkurov, M., Landry, M.C., Pelletier, L., and Durocher, D. (2016). DNA damage signalling targets the kinetochore to promote chromatin mobility. Nature cell biology *18*, 281-290.
Su, X.A., Dion, V., Gasser, S.M., and Freudenreich, C.H. (2015). Regulation of recombination at yeast nuclear pores controls repair and triplet repeat stability. Genes Dev *29*, 1006-1017.
Taddei, A., Hediger, F., Neumann, F.R., and Gasser, S.M. (2004). The function of nuclear architecture: a genetic approach. Annu Rev Genet *38*, 305-345.

Taddei, A., Schober, H., and Gasser, S.M. (2010). The budding yeast nucleus. Cold Spring Harb Perspect Biol *2*, a000612.
Thomas, J.O. (1999). Histone H1: location and role. Curr Opin Cell Biol *11*, 312-317.
Torres-Rosell, J., Sunjevaric, I., De Piccoli, G., Sacher, M., Eckert-Boulet, N., Reid, R., Jentsch, S., Rothstein, R., Aragon, L., and Lisby, M. (2007). The Smc5-Smc6 complex and SUMO modification of Rad52 regulates recombinational repair at the ribosomal gene locus. Nature cell biology *9*, 923-931.
Tsouroula, K., Furst, A., Rogier, M., Heyer, V., Maglott-Roth, A., Ferrand, A., Reina-San-Martin, B., and Soutoglou, E. (2016). Temporal and Spatial Uncoupling of DNA Double Strand Break Repair Pathways within Mammalian Heterochromatin. Mol Cell *63*, 293-305.
Unal, E., Heidinger-Pauli, J.M., and Koshland, D. (2007). DNA double-strand breaks trigger genome-wide sister-chromatid cohesion through Eco1 (Ctf7). Science *317*, 245-248.
Unk, I., Hajdu, I., Blastyak, A., and Haracska, L. (2010). Role of yeast Rad5 and its human orthologs, HLTF and SHPRH in DNA damage tolerance. DNA Repair (Amst) *9*, 257-267.
van Attikum, H., Fritsch, O., and Gasser, S.M. (2007). Distinct roles for SWR1 and INO80 chromatin remodeling complexes at chromosomal double-strand breaks. The EMBO journal *26*, 4113-4125.
van Sluis, M., and McStay, B. (2015). A localized nucleolar DNA damage response facilitates recruitment of the homology-directed repair machinery independent of cell cycle stage. Genes Dev *29*, 1151-1163.
Verdaasdonk, J.S., Vasquez, P.A., Barry, R.M., Barry, T., Goodwin, S., Forest, M.G., and Bloom, K. (2013). Centromere tethering confines chromosome domains. Mol Cell *52*, 819-831.
Vignali, M., and Workman, J.L. (1998). Location and function of linker histones. Nat Struct Biol *5*, 1025-1028.
Weber, S.C., Spakowitz, A.J., and Theriot, J.A. (2010). Bacterial chromosomal loci move subdiffusively through a viscoelastic cytoplasm. Phys Rev Lett *104*, 238102.
Weber, S.C., Spakowitz, A.J., and Theriot, J.A. (2012). Nonthermal ATP-dependent fluctuations contribute to the in vivo motion of chromosomal loci. Proceedings of the National Academy of Sciences of the United States of America *109*, 7338-7343.
Whalen, J.M., and Freudenreich, C.H. (2020). Location, Location, Location: The Role of Nuclear Positioning in the Repair of Collapsed Forks and Protection of Genome Stability. Genes (Basel) *11*.
Wilson, J.H., Leung, W.Y., Bosco, G., Dieu, D., and Haber, J.E. (1994). The frequency of gene targeting in yeast depends on the number of target copies. Proceedings of the National Academy of Sciences of the United States of America *91*, 177-181.
Zidovska, A., Weitz, D.A., and Mitchison, T.J. (2013). Micron-scale coherence in interphase chromatin dynamics. Proceedings of the National Academy of Sciences of the United States of America *110*, 15555-15560.

CHAPTER II: VISUALIZING CHROMOSOMAL DYNAMICS UPON DNA DAMAGE IN BUDDING YEAST

Based on:

Hannah L. Klein1, Giedrė Bačinskaja, Jun Che, **Anais Cheblal**, Rajula Elango, Anastasiya Epshtein, Devon M. Fitzgerald, Belén Gómez-González, Sharik R. Khan, Sandeep Kumar, Bryan A. Leland, Léa Marie, Qian Mei, Judith Miné-Hattab, Alicja Piotrowska, Erica J. Polleys, Christopher D Putnam, Elina A. Radchenko, Anissia Ait Saada, Cynthia J. Sakofsky, Eun Yong Shim, Mathew Stracy, Jun Xia, Zhenxin Yan, Yi Yin, Andrés Aguilera, Juan Lucas Argueso, Catherine H. Freudenreich. Susan M. Gasser, Dmitry A. Gordenin, James E. Haber, Grzegorz Ira, Sue Jinks-Robertson, Megan C. King, Richard D. Kolodner, Andrei Kuzminov, Sarah AE Lambert, Sang Eun Lee, Kyle M. Miller, Sergei M. Mirkin, Thomas D. Petes, Susan M. Rosenberg, Rodney Rothstein, Lorraine S. Symington, Pawel Zawadzki, Nayun Kim, Michael Lisby, and Anna Malkova

Guidelines for DNA recombination and repair studies: Cellular assays of DNA repair pathways. Microbial Cell, 2019. DOI: 10.15698/mic2019.01.664

Summary

Understanding the plasticity of genomes has been greatly aided by assays for recombination, repair and mutagenesis. These assays have been developed in microbial systems that provide the advantages of genetic and molecular reporters that can readily be manipulated. Cellular assays comprise genetic, molecular, and cytological reporters. The assays are powerful tools but each comes with its particular advantages and limitations. In Klein et al., the most commonly used assays are reviewed, discussed, and presented as the guidelines for future studies.

This **Chapter II** is based on my contribution to Klein et al. and describes the microscopy techniques we use in the laboratory to visualize the subnuclear localization of DSBs and examine how changes in position can influence the pathway of repair and/or repair efficiency. It also describes how to perform three-dimensional tracking of a single DSB to enables an in-depth characterization of the motion and its modeling as a polymer fiber. I wrote my part, which is inserted here, independently.

microbial cell

Review

www.microbialcell.com

Guidelines for DNA recombination and repair studies: Cellular assays of DNA repair pathways

Hannah L. Klein[1,*], Giedrė Bačinskaja[2], Jun Che[3], Anais Cheblal[4], Rajula Elango[5], Anastasiya Epshtein[1], Devon M. Fitzgerald[6-9], Belén Gómez-González[10], Sharik R. Khan[11], Sandeep Kumar[7], Bryan A. Leland[12], Léa Marie[13], Qian Mei[14], Judith Miné-Hattab[16,17], Alicja Piotrowska[18], Erica J. Polleys[19], Christopher D. Putnam[20,21], Elina A. Radchenko[19], Anissia Ait Saada[22,23], Cynthia J. Sakofsky[24], Eun Yong Shim[3], Mathew Stracy[25], Jun Xia[6-9], Zhenxin Yan[7], Yi Yin[26], Andrés Aguilera[10], Juan Lucas Argueso[27], Catherine H. Freudenreich[19,28], Susan M. Gasser[4], Dmitry A. Gordenin[24], James E. Haber[29], Grzegorz Ira[7], Sue Jinks-Robertson[30], Megan C. King[12], Richard D. Kolodner[20, 31-33], Andrei Kuzminov[11], Sarah AE Lambert[22,23], Sang Eun Lee[3], Kyle M. Miller[6,15], Sergei M. Mirkin[19], Thomas D. Petes[26], Susan M. Rosenberg[6-9,14], Rodney Rothstein[34], Lorraine S. Symington[13], Pawel Zawadzki[18], Nayun Kim[35,*], Michael Lisby[2,*] and Anna Malkova[5,*]

[1] Department of Biochemistry and Molecular Pharmacology, New York University School of Medicine, New York, NY, USA. [2] Department of Biology, University of Copenhagen, DK-2200 Copenhagen N, Denmark. [3] Department of Radiation Oncology, University of Texas Health Science Center at San Antonio, 7703 Floyd Curl Drive, San Antonio, TX, USA. [4] Friedrich Miescher Institute for Biomedical Research (FMI), 4058 Basel, Switzerland. [5] Department of Biology, University of Iowa, Iowa City, IA, USA. [6] Dan L Duncan Comprehensive Cancer Center, Baylor College of Medicine, Houston, TX, USA. [7] Department of Molecular and Human Genetics, Baylor College of Medicine, Houston, TX, USA. [8] Department of Biochemistry and Molecular Biology, Baylor College of Medicine, Houston, TX, USA. [9] Department of Molecular Virology and Microbiology, Baylor College of Medicine, Houston, TX, USA. [10] Centro Andaluz de BIología Molecular y Medicina Regenerativa-CABIMER, Universidad de Sevilla, Seville, Spain. [11] Department of Microbiology, University of Illinois at Urbana-Champaign, Urbana, IL, USA. [12] Yale School of Medicine, New Haven, CT, USA. [13] Department of Microbiology and Immunology, Columbia University Medical Center, New York, NY, USA. [14] Systems, Synthetic and Physical Biology Graduate Program, Rice University, Houston, TX, USA. [15] Department of Molecular Biosciences, University of Texas at Austin, Austin, TX, USA. [16] Institut Curie, PSL Research University, CNRS, UMR3664, F-75005 Paris, France. [17] Sorbonne Université, Institut Curie, CNRS, UMR3664, F-75005 Paris, France. [18] NanoBioMedical Centre, Faculty of Physics, Adam Mickiewicz University, Umultowska 85, 61-614 Poznan, Poland. [19] Department of Biology, Tufts University, Medford, MA USA. [20] Ludwig Institute for Cancer Research, University of California School of Medicine, San Diego, La Jolla, CA, USA. [21] Department of Medicine, University of California School of Medicine, San Diego, La Jolla, CA, USA. [22] Institut Curie, PSL Research University, CNRS, UMR3348 F-91405, Orsay, France. [23] University Paris Sud, Paris-Saclay University, CNRS, UMR3348, F-91405, Orsay, France. [24] Genome Integrity and Structural Biology Laboratory, National Institute of Environmental Health Sciences, Durham, NC, USA. [25] Department of Biochemistry, University of Oxford, South Parks Road, Oxford, OX1 3QU, UK. [26] Department of Molecular Genetics and Microbiology and University Program in Genetics and Genomics, Duke University Medical Center, Durham, NC USA. [27] Department of Environmental and Radiological Health Sciences, Colorado State University, Fort Collins, CO, USA. [28] Program in Genetics, Tufts University, Boston, MA, USA. [29] Department of Biology and Rosenstiel Basic Medical Sciences Research Center Brandeis University, Waltham, MA, USA. [30] Department of Molecular Genetics and Microbiology, Duke University Medical Center, Durham, NC USA. [31] Department of Cellular and Molecular Medicine, University of California School of Medicine, San Diego, La Jolla, CA, USA. [32] Moores-UCSD Cancer Center, University of California School of Medicine, San Diego, La Jolla, CA, USA. [33] Institute of Genomic Medicine, University of California School of Medicine, San Diego, La Jolla, CA, USA. [34] Department of Genetics & Development, Columbia University Irving Medical Center, New York, NY, USA. [35] Department of Microbiology and Molecular Genetics, The University of Texas Health Science Center at Houston, Houston, TX, USA..

* Corresponding Authors:
Hannah Klein, New York University School of Medicine, New York, NY USA; E-mail: hannah.klein@nyumc.org;
Nayun Kim, The University of Texas Health Science Center, Houston, TX, USA; Email: Nayun.Kim@uth.tmc.edu;
Michael Lisby, University of Copenhagen, Copenhagen, Denmark; Email: mlisby@bio.ku.dk;
Anna Malkova, University of Iowa, Iowa City, IA, USA; Email: anna-malkova@uiowa.edu

Extracted from: Klein et al., 2019 Microbial Cell

Visualizing chromosomal dynamics upon DNA double strand breaks in yeast *S. cerevisiae.*

Anais Cheblal, Susan M Gasser.

DNA double strand breaks (DSB) are the most deleterious type of DNA damage, thus understanding their behavior in living cells is of major importance. Using *S. cerevisiae* as model organism, where most of the DNA repair proteins are similar to those in humans, allows us to use genetic tools to characterize the properties of DNA DSBs. Using live microscopy one can visualize the subnuclear localization of DSBs and examine how changes in position can influence the pathway of repair and/or repair efficiency. Three-dimensional tracking of a single DSB enables an in-depth characterization of the motion and its modeling as a polymer fiber.

Determining chromosomal locus subnuclear position following DNA damage

It has been shown in budding yeast that when a DSB cannot be immediately repaired by recombination from its sister chromatid, it relocates to the nuclear periphery where it binds either Nup84 nuclear pore subcomplex or an inner nuclear membrane SUN-domain protein, Mps3. The relocation and interaction with these two distinct sites has different effects on repair outcome, given that pore mutants and Mps3 mutants influence the lesion repair outcome very differently. The three-zone technique for determining the position of damaged or undamaged loci (Horigome et al., 2015; Meister et al., 2010) has been a useful tool to determine precise positioning relative to the nuclear envelope. The imaging technique takes advantage of the bacterial Lac operator (*lacO*) sequence that binds the LacI repressor fused to a green fluorescent protein (LacI-GFP). One can then exploit a site-specific budding yeast endonuclease to create a single HO endonuclease cut at the mating type locus (*MAT* locus) that is tagged by a *lacO* array. This permits a highly accurate determination of the subnuclear position of the induced DSB. The nuclear periphery is generally identified with a fluorescent tag (e.g., RFP) on the pore protein Nup49 (Figure 1A).

Method and data analysis

By putting HO endonuclease under control of the GAL1 promoter, cleavage can be induced with 2% galactose for up to 2h. Cut efficiency is quantified by qPCR. Immediately, multi-stack images are

acquired, usually with a spinning disk confocal microscope. Spherical nuclei are needed for a proper statistical analysis of relative nuclear localization, thus G1 or early S-phase cells are usually analyzed, using the imageJ plugin *Point Picker* (Horigome et al., 2015). Briefly, the positions of the DSB and diameter of the nuclear pore-defined circle in the same plane of focus are determined. Using a pre-designed excel sheet, one can calculate the size of the nucleus, sets this to one, and then determines a relative value for the distance between the periphery and the spot (Figure 1B). To confirm cleavage it is often helpful to express a Rad52-YFP fusion, which will colocalize with the DSB.

Using a nuclear pore mutant *nup133⊿N*, which forces the main pore structure to form a large, single cluster at the nuclear periphery, allows one to accurately score the co- localization of the DSB with pore. DSB binding to Mps3 is best scored by Mps3 Chromatin Immunoprecipitation, because Mps3 gives only a weak fluorescence at the nuclear rim, apart from the spindle pole body. There may be other anchorage sites that remain to be characterized.

Cautionary notes

This technique relies on an accurate dual-color imaging, thus it is crucial to take into account and correct the emission wavelengths phase shift. To score accurate distances, it is important to only score nuclei if the fluorescent spot is within the middle 50 % of the Z-stack (not at the N or S pole), due to a lower resolution in Z. One should not use DNA fluorescence as the boundary of the nucleus because the edge is not easy to detect and thus depends on thresholding, which is often subjective. Therefore, a nuclear pore marker is essential for proper three-zone scoring. For a theoretical discussion of why the three-zone measurement is appropriate for such analyses, and the error inherent in the method, see Cavalieri's principle discussed in Meister *et al.* 2010.

Analyzing chromosomal locus mobility upon DNA damage

It has been shown that chromatin dynamics increase upon DNA DSB induction, probably favoring repair efficiency through homology search or relocation to a repair center. Using a similar cellular system for cut induction, as for the three-zone method (Figure 1A), a live cell tracking strategy has been developed to monitor DSB mobility over time.

Method and analysis

High speed timelapse fluorescence microscopy allows one to track the LacI-GFP tagged locus over time by live cell imaging. Here the center of the nucleus is used as a reference to correct for nuclear oscillations or translational movement of the entire field of imaging. Different imaging scales (i.e variation in time between image capture and length of capture) can be used. One system that has been useful has been the acquisition of single cell images every 80 ms taking Z-stacks of 200nm for 1 min total. Alternatively, longer times between stack can be introduced and capture can be extended to 5 or 7 min. One must always monitor for laser- or light-induced cellular damage as the response may bias subsequent measurements.

After deconvolution and Z projection, the ImageJ plugin *Spot Tracker 2D* can track the LacI-GFP fluorescent locus and the Nup49-RFP nuclear periphery (Figure 1C). Nuclear alignment is achieved by aligning the centers of an idealized circle (the nuclear perimeter) frame by frame, and then determining the movement of the tracked locus. To quantify locus mobility, the mean square displacement of the fluorescent locus is calculated over time using a pre-designed excel sheet (Sage et al., 2005). Biophysical parameters derived from polymer model analysis can be applied to the spot trajectories to further characterize its motion. Briefly, the length of constraint Lc measures the locus confinement in distance traveled, the effective diffusion coefficient Dc reflects its velocity, the effective spring coefficient Kc estimate the forces acting on this specific locus and the anomalous exponent α describe the nature of the motion (Amitai et al., 2017).

Cautionary notes

The quantification of the trajectories directly relies on the imaging scale used. Recently, a study show that changes in chromatin dynamics upon DNA damage depend on the tracking scale used (Mine-Hattab et al., 2017). It is therefore crucial to take into account this variation when choosing the time intervals used for imaging. Basal levels of chromatin mobility (i.e without damage) vary during the cell cycle, and chromatin in G1-phase cells, is more mobile than in S/G2. This has been assigned to the presence of cohesin in S/G2, which holds sister chromatids together after replication. Its removal and/or degradation allows an increase in the chromatin mobility (Dion et al., 2013). Thus, to eliminate any cell cycle variation, it is essential to compare mobility changes within the same cell cycle stage. For determining cell cycle stage accurately see Neumann *et al.* 2006.

Using *S. cerevisiae* as model organism allow us to accurately characterize chromatin dynamics upon DNA damage. The use LacO/LacI arrays for chromatin tagging enable us to specifically determine the position of chromatin loci in response to DSBs. We and others, have shown that chromatin dynamics and re-localization plays a central role in response to DNA damage, but how this impacts DNA repair efficiencies remains unclear.

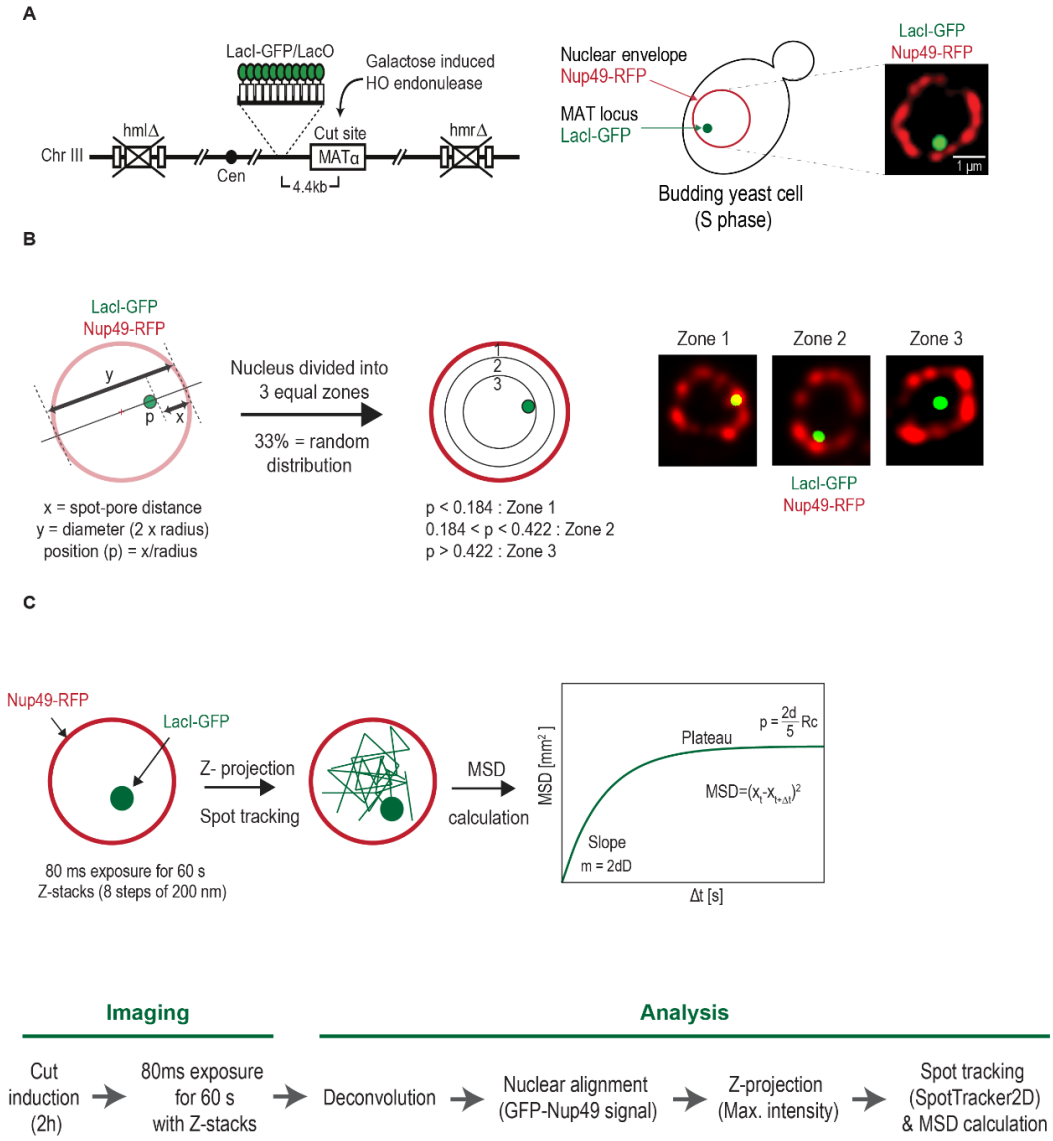

<u>Figure 17:</u> Visualizing chromosomal dynamics upon DNA double strand breaks in yeast *S. cerevisiae*. (Published in Klein et al., 2019, Microbial Cell).

A) Schematic representation of the chromosomal locus tagging system. HO endonuclease is used to create a single double-strand break at the mating type locus (MAT locus) that is tagged with a lacO array. The LacO array binds the LacI repressor fused to a green fluorescent protein (LacI-GFP). The nuclear envelope is visualized using a fluorescently tagged nuclear pore protein (Nup49-RFP). **B)** Analyzing chromosomal locus position. Relative locus position (p) is calculated by normalizing the distance pore-locus (x) by the nuclear radius (y/2). The radial distances are then classified into three groups - Zone 1 (peripheral width=0.184 x nuclear radius(*r*)), 2 (middle width between 0.185*r* and 0.422*r*) and 3 (central width=0.578*r*) - of equal surface. **C)** Analyzing chromosomal locus mobility. Overview of the imaging procedure. Single cell, multi-stack images are acquired every 80 ms for 60 s. After deconvolution and nuclear alignment, the 3D images are converted to 2D using a maximum z-projection. The tagged locus is tracked using SpotTracker2D and an absolute MSD calculation is applied.

Amitai A, Seeber A, Gasser SM, Holcman D. 2017. Visualization of Chromatin Decompaction and Break Site Extrusion as Predicted by Statistical Polymer Modeling of Single-Locus Trajectories. Cell reports 18(5): 1200-1214.

Dion V, Kalck V, Seeber A, Schleker T, Gasser SM. 2013. Cohesin and the nucleolus constrain the mobility of spontaneous repair foci. EMBO reports 14(11): 984-991.

Horigome C, Dion V, Seeber A, Gehlen LR, Gasser SM. 2015. Visualizing the spatiotemporal dynamics of DNA damage in budding yeast. Methods in molecular biology 1292: 77-96.

Meister P, Gehlen LR, Varela E, Kalck V, Gasser SM. 2010. Visualizing yeast chromosomes and nuclear architecture. Methods in enzymology 470: 535-567.

Mine-Hattab J, Recamier V, Izeddin I, Rothstein R, Darzacq X. 2017. Multi-scale tracking reveals scale-dependent chromatin dynamics after DNA damage. Molecular biology of the cell.

Sage D, Neumann FR, Hediger F, Gasser SM, Unser M. 2005. Automatic tracking of individual fluorescence particles: application to the study of chromosome dynamics. IEEE transactions on image processing : a publication of the IEEE Signal Processing Society 14(9): 1372-1383.

Neumann FR., Hediger F, Taddei A, Gasser SM. 2006. Tracking Individual Chromosomes with Intergrated Arrays of lacop Sites and GFP-laci Repressor: Analyzing Position and Dynamics of Chromosomal Loci in Saccharomyces cerevisiae. Cell Biology (Third Edition) – Chapter 46 Pages 359–367; Vol2.

CHAPTER III: DNA DAMAGE-INDUCED NUCLEOSOME DEPLETION ENHANCES HOMOLOGY SEARCH INDEPENDENTLY OF LOCAL BREAK MOVEMENT

Based on:

DNA damage-induced nucleosome depletion enhances homology search independently of local break movement. I contributed to all Figures except 5 D, E.

Cheblal *et al.* Molecular Cell, 2020. DOI: 10.1016/j.molcel.2020.09.002

Graphical Abstract

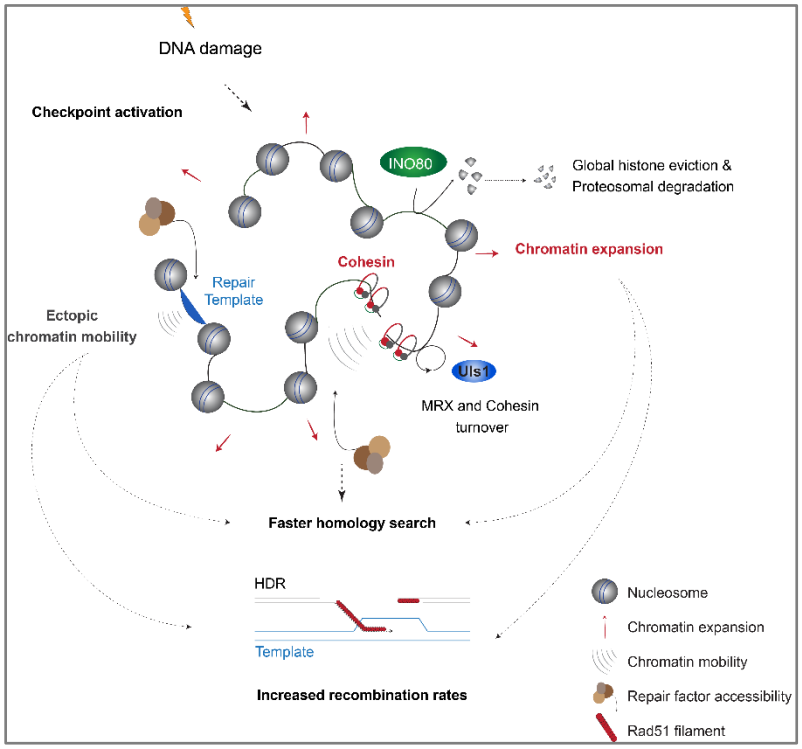

Authors

Anaïs Cheblal, Kiran Challa, Andrew Seeber, Kenji Shimada, Haruka Yoshida, Helder C. Ferreira, Assaf Amitai, and Susan M. Gasser.

In Brief

Cheblal et al. show that DNA damage induced histone depletion enhances homology search through the induced chromatin expansion and ectopic locus mobility, independently of local DSB movement. Local DSB dynamics is cell cycle dependent and is regulated by Cohesin turnover. They find that centromeres do not detach upon DNA damage.

Highlights

- Intrinsic and DSB-induced chromatin dynamic is cell cycle dependent
- Loss of centromere tethering is not a major DNA damage response
- Uls1 STUbL regulates local DSB dynamics through MRX and Cohesin turnover
- Chromatin expansion and ectopic movement are critical for DSB repair by HR

DNA damage-induced nucleosome depletion enhances homology search independently of local break movement

Anaïs Cheblal[1,2], Kiran Challa[1], Andrew Seeber[1,3], Kenji Shimada[1], Haruka Yoshida[1], Helder C. Ferreira[1,4], Assaf Amitai[5], and Susan M. Gasser[1,2*]

1) Friedrich Miescher Institute for Biomedical Research, Maulbeerstrasse 66, CH-4058 Basel, Switzerland
2) University of Basel, Faculty of Natural Sciences, CH-4056 Basel, Switzerland
3) Current address: Center for Advanced Imaging, Northwest Building, 52 Oxford St, Suite 147, Harvard University, Cambridge, MA, 02138, USA.
4) Biomedical Sciences Research Complex, School of Biology, University of St Andrews, St Andrews KY16 9ST, UK.
5) Department of Chemical Engineering, Institute for Medical Engineering and Science, Massachusetts Institute of Technology, Cambridge, MA, USA; The Ragon Institute of MGH, MIT, and Harvard, Cambridge, MA, USA.

*Lead author and contact S.M.G.: susan.gasser@fmi.ch, +41 61 697 7025

Key words: chromatin movement, DNA damage, histone eviction, Uls1, Cohesin, Cep3, kinetochore, homologous recombination

Short title: Histone eviction facilitates ectopic homology search

SUMMARY

To test whether double-strand break (DSB) mobility enhances the physical search for an ectopic template during homology-directed repair (HDR), we tested the effects of factors that control chromatin dynamics, including Cohesin loading and kinetochore anchoring. The former but not the latter is altered in response to DSBs. Loss of the nonhistone high mobility group protein Nhp6 reduces histone occupancy, and increases chromatin movement, decompaction and ectopic HDR. Loss of nucleosome remodeler INO80-C did the opposite. To see if enhanced HDR depends on DSB mobility or the global chromatin response, we tested the Ubiquitin ligase mutant, *uls1*Δ*,* which selectively impairs local, but not global movement, in response to Zeocin or a DSB. Strand-invasion occurs in *uls1*Δ cells with wild-type kinetics, arguing that global histone depletion rather than DSB movement is rate-limiting for HDR. Impaired break movement in *uls1*Δ correlates with elevated MRX and Cohesin loading, despite normal resection and checkpoint activation.

INTRODUCTION

In *S. cerevisiae* nuclei, resected DNA double-strand breaks (DSBs) show increased random, subdiffusive movement (Dion et al., 2012; Mine-Hattab and Rothstein, 2012) This observation has been confirmed by many laboratories (Agmon et al., 2013; Amitai et al., 2017; Batte et al., 2017; Herbert et al., 2017; Krawczyk et al., 2012; Lawrimore et al., 2017; Mine-Hattab and Rothstein, 2013; Neumann et al., 2012; Saad et al., 2014; Strecker et al., 2016) and was extended to vertebrate species as well (Dimitrova et al., 2008; Krawczyk et al., 2012; Lottersberger et al., 2015; Schrank et al., 2018). However, the mechanisms that trigger heightened movement and, above all, its physiological role in repair, remained unclear.

A recent study suggested that damage-induced chromatin movement in budding yeast might stem from the declustering of centromeres regulated by the phosphorylation of the essential kinetochore protein Cep3 at Serine-575 (Strecker et al., 2016). Other studies have invoked microtubule-based motors in chromatin movement (Chung et al., 2015; Lottersberger et al., 2015; Oshidari et al., 2019). Our work and that of others suggested that chromatin dynamics increase upon damage due to decompaction of the chromatin fibre and a 20-30% drop in core histone levels (Adam et al., 2016; Amitai et al., 2017; Hauer et al., 2017; Neumann et al., 2012). In budding yeast this depends on the DNA damage checkpoint and the INO80 chromatin remodelling complex (Amitai et al., 2017; Hauer et al., 2017; Neumann et al., 2012). It remains possible that multiple mechanisms contribute to enhanced chromatin mobility following DNA damage (reviewed in (Seeber et al., 2018).

Less clear is whether or not enhanced break movement facilitates the search for a homologous template during homology-directed repair (HDR) (Barzel and Kupiec, 2008; Gehlen et al., 2011; Haber, 2018). To undergo repair by homologous recombination, DSBs are resected, allowing the single-strand binding protein RPA to load Rad51, creating a filament that can detect and anneal to homologous dsDNA (reviewed in (Renkawitz et al., 2014). In haploid budding yeast, the processing of the break and the search for sequence homology can take 3-5 hours, particularly when an intact sister

chromatid is unavailable (Agmon et al., 2013; Haber, 2018; Haber et al., 1991; Mine-Hattab and Rothstein, 2012; Piazza et al., 2019) . This search is thought to be rate-limiting for DSB repair by HR, and hence it was proposed that increased local movement of the DSB would facilitate the search (Barzel and Kupiec, 2008; Haber, 2018; Mine-Hattab and Rothstein, 2012; Seeber et al., 2018). On the other hand, excessive movement of a Rad51-coated ssDNA filament is harmful, as a repeat-proximal break that explores the genome too efficiently might anneal with repeats elsewhere in the genome, resulting in chromosomal translocations (Marcomini et al., 2018; Roukos et al., 2013).

Previous work from our laboratory showed that damage induced chromatin movement stems at least in part from genome-wide changes in the density of nucleosome packing (Hauer et al., 2017). Thus HDR might be facilitated either by local movement of the DSB, or by the global increase in DNA accessibility that arises from histone degradation (discussed in (Seeber et al., 2018)). A recent study in *S. cerevisiae* tried to address this by showing that a single point mutation of Serine 575 to Alanine in the essential kinetochore protein Cep3 (*cep3-S575A*) abolished the increase in DSB movement (Strecker et al., 2016). They presented evidence that DNA damage induced by the radiomimetic drug Zeocin led to centromere declustering, an event dependent on Cep3 Ser575 phosphorylation by the checkpoint kinase Rad53. The authors argued that increased DSB movement does not contribute significantly to repair, because there was no effect of the *cep3* phospho-site mutant on cell survival after DSB induction (Strecker et al., 2016). Unfortunately, in most studies to date repair was monitored as colony growth after several days, and the kinetics of homology search was not monitored.

Here we tested whether enhanced DSB movement enhances the rate of homologous strand invasion during HDR. We used a system in which both the DSB and the template for repair are distant from telomeres and centromeres, because one of the factors thought to influence homology search is the spatial juxtaposition of relevant sequences in the nucleus, particularly for subtelomeric DSB repair (Agmon et al., 2013; Batte et al., 2017; Donnianni and Symington, 2013; Jain et al., 2016; Lee et al., 2016; Lichten and Haber, 1989; Wang et al., 2017). Yeast chromosomes have a polarized Rabl arrangement, whereby telomeres and centromeres form distinct clusters, on opposite sides of the

nucleus (Bystricky et al., 2005a; Duan et al., 2010). This organization is maintained throughout interphase thanks to short microtubules that link centromeres to the spindle pole body (SPB), and telomere tethering to the nuclear periphery by Sir4 and telomerase co-factors (Bystricky et al., 2005a; Duan et al., 2010; Taddei and Gasser, 2012).The artificial detachment of the centromeres from the SPB and the depolymerisation of interphase microtubules both seemed to increase chromatin movement (Amitai et al., 2017; Lawrimore et al., 2017; Strecker et al., 2016), yet neither the release of telomeres nor of centromeres enhanced recombination efficiency at internal breaks (Batte et al., 2017). Other constraints on chromatin movement stem from Cohesin-mediated sister cohesion (Dion et al., 2013), which is even more pronounced near centromeres (Stephens et al., 2011; Verdaasdonk et al., 2013; Weber et al., 2004). Finally, the density of nucleosomal packing can limit chromatin movement (Hauer et al., 2017).

Here we tested whether alterations in constraint on chromatin locus mobility changes the rate at which homologous strand invasion occurs. We have carefully analysed both local and global chromatin mobility, as well as changes in compaction, following the induction of a HO endonuclease-induced DSB. We have performed a quantitative assay for strand invasion during homology-driven DSB repair using a template placed on another chromosome. Our paper presents the first evidence that a global reduction in nucleosome density, and not a local increase in DSB movement, is rate-limiting for ectopic strand invasion during HDR in yeast.

RESULTS

Intrinsic and DSB-induced chromatin mobility is cell-cycle stage dependent.

As discussed above, there are conflicting conclusions about the effect of break mobility on HDR in yeast reviewed in (Seeber et al., 2018). We noticed that cell cycle phase is rarely taken into account in the relevant studies, although in haploid yeast, DSB repair by NHEJ is clearly favored in G1 phase, while HDR is favored in S phase (Lieber, 2010). Moreover, the intrinsic mobility of intact chromosomal loci is higher in G1 than in S phase (Dion et al., 2013; Heun et al., 2001). To see if intrinsic cell-cycle linked differences in chromatin organisation influence the physical mobility of DSBs, we used single particle

tracking of a fluorescently tagged genomic locus, quantifying its mobility *in vivo* at different stages of the cell cycle. We standardly track the yeast *MAT* locus tagged by a *lac* operator array (*lacO*x256), which binds a Lac repressor-GFP fusion protein (LacI-GFP; Fig. 1A). An updated imaging protocol in which high resolution stacks acquired at 80 ms intervals for 1min, provides datasets sufficiently rich for the extraction of biophysical parameters of movement (Amitai et al., 2017). We determined the effect of the cell cycle on chromatin movement by comparing movement in G1-, S- and G2-phase cells, triaged by cell and nuclear morphology (Meister et al., 2010; Sage et al., 2005). By tracking the movement of the interpolated center of the nuclear sphere (based on the pore marker, Nup49-RFP), together with the LacI-GFP, we correct for nuclear or instrumental drift (Fig. 1A; see STAR Methods).

In the absence of an HO-induced DSB, *MAT* locus movement was lower in G2- and S-phase cells, than in G1-phase cells (Fig. 1B). By Mean square displacement analysis (MSD) the relative radii of constraint (Rc) are 0.25 μm (G2) 0.28 μm (S) and 0.38 μm (G1). The extraction of biophysical parameters from the single particle tracking data allows further characterization of the movement (Amitai et al., 2017; Shukron et al., 2019): length of constraint Lc defines locus confinement, effective spring coefficient Kc reflects tethering interactions that constrain movement, and the anomalous exponent α, indicates directed ($\alpha>1$), random-walk (normal diffusion; $\alpha= 1$) or subdiffusive (constrained; $\alpha<1$) movement (Amitai et al., 2017). In agreement with the MSD plots, the volume explored by the tracked locus Lc is higher, and the spring constant Kc is lower in G1-phase cells (Fig. 1B). The anomalous exponent α showed a significant drop in S and G2 phases, indicating enhanced constraint (α in G1, 0.61±0.11; S, 0.53±0.12; G2, 0.35±0.13). Clearly, cell-cycle distribution influences the degree and nature of chromatin movement measured.

One key difference in chromatin structure between G1- and S-phase cells is the replication-dependent loading of Cohesin, which establishes sister-sister cohesion in S phase (Onn et al., 2008). Earlier work suggested that Cohesin degradation alters chromatin movement of the *PES4* locus (Dion et al., 2013). Indeed, we found that even under high resolution imaging conditions, auxin-inducible degradation of the Scc1-degron

subunit, which opens the Cohesin ring that holds sister chromatids together, leads to increased chromatin movement at *MAT* locus in S-phase cells (Fig. 1C; see Fig. S1A,B for degradation protocol and efficiency). Following Scc1 degradation, an uncleaved *MAT* locus in S phase moves as it would in G1-phase cells, with similar Rc, Lc and Kc values (Fig. 1C). We conclude that the cohesion of sister chromatids, similar to the Cohesin-dependent compaction of pericentric chromatin (Stephens et al., 2011), constrains chromatin mobility in S phase.

We next monitored the effect of inducing a DSB in either S- or G1-phase cells (Fig. 1D-E). Consistent with previous studies that tracked Rad52 at a resected cut (Dion et al., 2012), we found a striking increase in the mobility of the cleaved *MAT* locus in S-phase cells (uncut Rc=0.28 μm to cut Rc=0.37 μm), to roughly the same value as the intact *MAT* locus after Scc1-degradation (Rc=0.37 μm). We were unable to detect an additional increase in Rc in G1-phase cells (uncut Rc=0.38 μm vs cut Rc=0.38 μm), even though cut efficiency was equivalent (Table S1). The extracted parameters Kc and Lc confirm these observations (Fig. 1D,E). Thus, both in the presence and absence of damage, it is essential to triage cells with respect to their cell cycle stage in order to accurately monitor mobility change.

Resection does not correlate strictly with mobility increase at DSBs

Because DNA end resection is very limited in G1 phase, but efficient in S-phase cells (Aylon et al., 2004; Ira et al., 2004; Zierhut and Diffley, 2008), we next examined if the rate of end-resection alters DSB mobility. We quantified ssDNA at an HO cut site (Fig. S2A; Zierhut and Diffley, 2008) in two mutants known to affect resection differentially, namely *rad50Δ* and *ku70Δ.* The Rad50-containing MRX complex is a Cohesin-like complex that is recruited rapidly to DSBs, where it holds the broken ends together and initiates resection to facilitate repair by HDR (Garcia et al., 2011; Lengsfeld et al., 2007; Lisby et al., 2004; Seeber et al., 2016). As expected, in *rad50Δ* cells DNA end resection dropped sharply in comparison to WT cells (Fig. S2B,C). In contrast, the elimination of yKu70, an end-binding factor that inhibits resection and favors NHEJ, showed increased resection (Fig. S2D). Importantly, despite a reduced 3’ overhang, loss of MRX (*rad50*Δ)

accentuated *MAT* mobility in S phase after cut induction (Fig. S2E,F). Conversely, despite extensive end resection in *ku70*Δ cells, we scored less mobility increase of the break than in WT cells (Fig. S2F). MSD values were all consistent with the Lc and Kc values (Fig. S2G,H). While we do not have a simple explanation why a DSB does not increase mobility in the *ku70*Δ mutant, it is clear that DSB movement does not correlate with the efficiency of end resection. Given that both resection and checkpoint activation drop in the *rad50Δ* strain, it is likely that the heightened DSB movement in *rad50Δ* arises from a loss of end-to-end tethering by MRX, and/or from reduced Cohesin loading (Seeber et al., 2016; Unal et al., 2004; Unal et al., 2007).

Centromere attachment to SPB is preserved upon DNA damage.

Having ruled out end-resection, but implicated cell cycle, as a factor altering DSB mobility, we next examined whether the declustering or release of centromeres, a process thought to be regulated by the phosphorylation of the essential kinetochore protein Cep3 at Ser575 (Strecker et al., 2016), governs break mobility. Previous work on asynchronous populations of cells, argued that Cep3 phosphorylation by Rad53 kinase was needed for centromere release, and that this enhanced locus mobility following DSB induction. The authors reported that DSBs did not increase mobility in the *cep3-S575A* mutant, and argued on this basis that chromatin mobility does not contribute to homology search, since repair efficiency in a *cep3-S575A* strain was like wild-type (Strecker et al., 2016).

We first examined whether DNA damage indeed induces robust centromere detachment from the SPB, as previously reported (45%; (Strecker et al., 2016)). Using a GFP-tagged kinetochore protein Mtw1-GFP that localizes to a cluster of centromeres near the Nup49-RFP marked nuclear envelope (Fig. 2A), we monitored kinetochore declustering upon treatment with Zeocin (250 or 500 µg/ml; Fig. 2A), as in the previous study. Although we detected centromere declustering in the previously described kinetochore mutant, *ndc80-1* (Pinsky et al., 2006), we scored no release or declustering of centromeres in WT cells (in either G1 or S/G2 cells; Fig. S3A);. Furthermore, there was no significant change provoked by ablating the Rad53-sensitive Cep3 phophorylation site (WT vs *cep3-S575A*,

Fig. 2A), although the mutant was slightly more sensitive to10 µg/ml Zeocin in a serial dilution growth assay (Fig. 2D).

We next asked if the kinetochores were released as a cluster from the nuclear envelope (NE) in response to DNA damage by scoring spot distance from the NE (Fig. 2B). However, we did not detect centromere release on Zeocin in either wild-type (WT) or *cep3-575A* cells (Fig. 2C). As a control we used the microtubule depolymerizing agent nocodazole, which gave the expected release of the Mtw1-GFP cluster (Fig. 2C). This result confirms two other reports that found no change in SPB-centromere distances following DNA damage (Herbert et al., 2017; Lawrimore et al., 2017). In conclusion, we find neither declustering nor detachment of centromeres from the NE in response to DNA damage, despite the induction of a robust checkpoint kinase response (Fig. S2B).

Cep3 phosphorylation does not regulate DSB induced chromatin movement.

Although centromere release was not detected, we nonetheless monitored whether the phosphosite mutant in Cep3, *cep3-S575A*, would compromise the increase in DSB dynamics, as previously reported. Using validated and isogenic wild-type and *cep3-S575A* strains (Strecker et al., 2016), we carried out MSD analysis of the HO cut at *MAT.* In the *cep3-S575A* mutant we found a robust increase in DSB mobility in S phase, over the uncut *MAT* locus (Fig. 2E; Rc=0.30 µm uncut, increased to Rc=0.38 µm upon cleavage). This is reflected in Lc as well as Kc values. We conclude that the absence Cep3 phosphorylation does not significantly impair increased DSB mobility (Fig. 2A-C), even though the starting chromatin mobility level is slightly higher in this mutant (Fig. 2E). Given that DSB-induced mobility is affected by cell cycle and that the earlier study did not triage by cell-cycle phase, we analysed the cell cycle distribution in *cep3-S575A* before and after cleavage. Distributions were very similar to WT cells (Fig. S2C). Thus, the *cep3-S575A* mutation has no effect on centromere clustering, position nor chromatin mobility, consistent with the reported WT levels of repair (Strecker et al., 2016).

Reduced nucleosome occupancy and chromatin remodelling facilitate homology-based repair

Having ruled out checkpoint-induced centromere detachment and resection as drivers of break-induced chromatin mobility, we examined the observations of Hauer et al. (2017), who showed a genome-wide histone eviction and chromatin expansion following Zeocin treatment. Previous studies had shown that local histone depletion following DSB induction at *MAT*, was dependent on the INO80 remodeler and on activation of the checkpoint, as was the increase in DSB mobility (Neumann et al., 2012; van Attikum et al., 2007; Zheng et al., 2018). This global, Zeocin-induced chromatin decompaction and chromatin dynamics was also *arp8-* and *mec1-*dependent (Amitai et al., 2017; Hauer et al., 2017). Confirming that *arp8*Δ cells are sensitive to break-inducing DNA damage in a serial dilution drop assay (Fig. 2D), we then monitored the baseline mobility of the intact *MAT* locus and its increase upon cleavage in WT *vs. arp8*Δ strains, using our improved imaging protocol. Basal level movement was slightly lower in *arp8Δ* cells, suggesting that constraining forces are higher in the absence of INO80-C than in WT cells, which is reflected in a higher Kc. (Fig. 3A,B). More importantly, following DSB induction at *MAT* in the *arp8Δ* strain, there was no significant increase in Rc (MSD plots, Fig. 3B) and no change in the extracted biophysical parameters (Table S1), even though cleavage was 75% as efficient as WT. The attenuated increase in mobility correlates with reduced histone eviction and compromised checkpoint activation in *arp8Δ* cells. In contrast, the loss of the high mobility group protein, Nhp6 (encoded by two loci, *NHP6a, NHP6b, nhp6ΔΔ*), generated a higher baseline of movement compared to WT, and correspondingly higher Lc values and lower Kc (Hauer et al., 2017) (Fig. 3A,C). We monitored the mobility of an undamaged locus*, MET10*, after exposure to Zeocin, and were able to score a slight increase in Rc and in the anomalous exponent α in *nhp6ΔΔ* cells (Fig. 3C). This is in line with recent mass spectrometry data from our laboratory which confirm an attenuated response to damage (Challa et al., in preparation), because the steady-state histone levels are lower by 20% in *nhp6ΔΔ* cells (Amitai et al., 2017; Hauer et al., 2017).

Given that we see no histone eviction and reduced DSB movement in the *arp8Δ* mutant, and the opposite in *nhp6ΔΔ*, we used these two mutants to examine the impact of histone eviction on the rate of homology search. We made use of a well-characterized assay for

Break Induced Replication repair (BIR) (Donnianni and Symington, 2013), in which the repair of an induced HO cut depends on the search for and invasion of homology on an unrelated chromosome (Fig. 3D). After HO cut induction, the BIR efficiency was scored using PCR primers unique to ChrV and ChrXI to detect the strand invasion product. Successful BIR also restores a functional *LYS2* gene, which can be scored by colony growth on synthetic medium lacking lysine (SC-Lys; Fig. 3E). In the WT background roughly 60% of cells generated Lys+ colonies after HO cut induction, while *pol32Δ* BIR deficient cells failed to form colonies altogether, confirming earlier reports that Pol32 is needed for efficient BIR (Fig. 3E; (Donnianni and Symington, 2013)). We compared this with the effects of *arp8Δ*, and *nhp6ΔΔ*, and found that the rate of Lys+ colony formation was strongly compromised in *arp8Δ* and significantly increased in *nhp6ΔΔ* (Fig. 3E). We used PCR to see if these trends are reflected in the time of appearance of the strand invasion product after HO induction. We first detected the BIR-enabled PCR product around 2h after DSB induction and it further increased to 25% in WT cells by 6h (Fig. 3F,G). The appearance of the strand invasion product was greatly reduced in *arp8Δ*, while in *nhp6ΔΔ* cells it appeared after 1h and increased more rapidly than in WT, reaching 40% by 6h (Fig. 3F,G). These data establish a correlation between increased and decreased histone loss with enhanced and reduced HDR efficiency, respectively. We confirmed this reduced strand invasion efficiency for *arp8Δ* using an alternative HDR-driven repair system based on cleavage at *MAT* (Fig. S4A,B).

Uls1 regulates local DSB movement and Cohesin levels at DSBs

Previous work identified the SUMO-targeted ubiquitin ligase (STUbL) Uls1 as a factor that modulates the dynamics of an HO cut site at *MAT,* when it was flanked by an array of telomeric repeats (Marcomini et al., 2018). One of the few known roles for this combined STUbL/ATPase enzyme (Fig. 4A) is that it is recruited by SUMO chains to telomeres, where it ubiquitinates and targets Rap1 for degradation (Lescasse et al., 2013). However, *uls1Δ* does not show sensitivity to Zeocin or other commonly used DNA damaging agents. At the TG-flanked break, we found that *uls1*Δ blocked movement of the TG-rich side of a DSB (Marcomini et al., 2018), but it was unclear whether Uls1 would be recruited to and/or

alter the mobility of a canonical DSB. Performing Chromatin immunoprecipitation (ChIP) before and after induction of a DSB at *MAT*, we found that Uls1 is indeed recruited and enriched at the HO-induced DSB at *MAT* (Fig. 4A). We then monitored the impact of Uls1 ablation on local movement after DSB induction. Both MSD analysis and the derived biophysical parameters showed complete attenuation of heightened DSB movement (Fig. 4B). This was surprising given that end resection (Fig. S5A) and checkpoint activation (Fig. S6A) occurred in this mutant as in WT cells.

Based on data showing that Cohesin constrains locus mobility (Fig. 1), we next tested whether Uls1 modulates Cohesin levels at the HO-induced DSB. We first we showed that in WT cells, Scc1-HA levels indeed increased, reaching 10-fold enrichment over a background control, during the first 180min after cleavage at *MAT* (Fig. 4C). In the *uls1*Δ cells, however, Scc-HA levels increased 2.5-fold more efficiently than in WT cells (Fig. 4C). This argues that Uls1 helps limit Cohesin loading at breaks. To see if the elevated levels of Cohesin in *uls1*Δ might constrain DSB movement, we triggered the degradation of Scc1 after the induction of a DSB (Fig. S1D). We found that the loss of Scc1 at a DSB indeed led to an even greater increase in DSB movement than in WT cells (Fig. 4D), even though Scc1 degradation did not alter DNA end-resection (Fig. S4A, right panel). The increased MSD values upon Scc1 degradation correlated well with increased Lc and reduced Kc (Fig. 4D). We propose that Cohesin loading and the establishment of sister-sister cohesion at a DSB is kept in check by Uls1. In its absence, Cohesin loading appears to proceed unchecked, restricting chromatin movement after DSB induction (Figs. 1E, 4D).

It has been proposed that Cohesin loading at a DSB is MRX-dependent (Seeber et al., 2016; Unal et al., 2004; Unal et al., 2007), and indeed we find that Scc1-HA loading at the break drops significantly in the absence of MRX (*rad50*Δ, Fig. S5B). We then scored for MRX accumulation at the HO-induced DSB in WT *vs uls1*Δ cells. Break-dependent MRX recruitment is also enhanced in *uls1Δ* over WT, albeit slightly less enhanced than Scc1 (Fig. S4C). Nonetheless, even in the presence of Uls1, sufficient MRX binds to initiate resection, hold ends together, and activate the checkpoint cascade. It is likely that

the control over MRX and Cohesin levels by Uls1 depends on sumoylation, given that multiple MRX and Cohesin subunits are SUMOylated (Cremona et al., 2012), and Uls1 recognizes its substrates through SUMO-interacting motifs (SIM) (Bermudez-Lopez and Aragon, 2017; Chen et al., 2016). Mre11 also has SIMs, thus multiple interactions may enable Uls1 to control Cohesin levels, either by targeting it directly, or indirectly through MRX.

Zeocin-induced ectopic locus mobility and checkpoint-triggered histone loss occur in uls1Δ cells.

It was unclear whether *uls1Δ* would lead to reduced chromatin mobility only at the DSB, or genome-wide. After treatment with the radiomimetic drug Zeocin, we found that chromatin movement increases globally, even at undamaged sites, due to a generalized reduction in nucleosome occupancy (Hauer et al., 2017). The global increase in chromatin movement correlated with chromatin expansion and required activation of the DNA damage checkpoint. To monitor the effect of *uls1Δ* on non-damaged sites, we exposed WT and *uls1Δ* strains carrying a tagged *MAT* locus and Rad52-Ruby for identifying damage, to Zeocin. We then tracked the mobility of the undamaged *MAT* locus (LacI-GFP without colocalizing Rad52-Ruby; Fig. 5A-C). Importantly, both checkpoint activation and colony survival on Zeocin were unaffected by *uls1Δ* (Fig. S6A,B), and unlike the behavior of the tagged DSB, the increase in general chromatin mobility induced by Zeocin was not compromised in *uls1Δ* cells (Fig. 5B,C). This suggested that the global histone degradation that occurs in WT strains, also occurs in *uls1Δ*. This was confirmed through a quantitative HiBit assay that monitors H2B levels before and after Zeocin treatment (Fig. 5D). Zeocin-induced H2B degradation was equivalent in *uls1Δ* and WT cells (Fig. 5D).

The loss of nucleosomes has been correlated with an expansion or opening of chromatin structure, that can be measured with structured illumination microscopy. We therefore monitored the volume of the *lacO* array near *MAT* locus following exposure to Zeocin and find an equivalent expansion in WT and *uls1Δ* strains (Fig. 5E). This expansion has been shown to require INO80-C and checkpoint activation, and occurs at undamaged loci (i.e., no Rad52 bound) as shown here. In conclusion, the loss of Uls1 compromises local DSB

mobility, coincident with increased Cohesin and MRX loading (Fig. 4C, Fig. S5C), but does not restrict the damage-induced increase in DNA dynamics and undamaged locus decompaction (Hauer et al., 2017).

A single DSB at MAT triggers ectopic locus movement, enabling efficient HDR in uls1∆ cells.

The differential effect of *uls1Δ* on DSB mobility *vs*. the global chromatin response on Zeocin was highly suggestive, but it remained to be seen whether a single DSB at *MAT* would also trigger a genome-wide increase in mobility, at least in WT cells (Fig. 6A). This is crucial for any model testing the importance of general movement in homology search, since HDR occurs in response to a single DSB. To test this, we monitored the mobility of an undamaged (ectopic) locus in WT cells by tracking LacI-GFP at the *MET10* locus 4h after induction of a single DSB at the *MAT* locus. This time point coincides with full checkpoint kinase activation (Fig. S6C). We observed a significant increase in ectopic movement at *MET10* locus after induction of a single DSB, based on MSD analysis (Fig. 6B), which was confirmed by the derived biophysical parameters Lc and Kc (Fig. 6B). This is the first evidence that full checkpoint activation arising from a single irreparable DSB can trigger ectopic changes in chromatin. Importantly, this increase in ectopic mobility was preserved in *uls1*Δ cells (Fig. 6C), with effects even more pronounced than those detected in WT cells (Fig. 6B,C). This suggests that in the absence of Uls1, cells somehow overcompensate for a lack of local DSB movement by elevating ectopic locus mobility.

We next asked whether a single, localized DSB was also sufficient to trigger ectopic chromatin expansion. Indeed, we monitored a GFP-tagged locus at the *MET10* locus in WT cells after inducing HO-dependent cleavage at *MAT*, and detected significant locus expansion by SIM (Fig. 6D, WT). Very similar *MET10* locus expansion occurred in *uls1∆* cells (Fig. 6D). In summary, both WT and *uls1*Δ cells respond to a single irreparable DSB by increasing chromatin mobility and generally decompacting chromatin, which correlates with partial nucleosome depletion (Hauer et al., 2017). The *uls1* mutant thus provided us

a unique opportunity to test whether the loss of local DSB movement affects the rate of homology-driven strand exchange.

We monitored the efficiency of HDR in isogenic *uls1*Δ and WT cells using the ectopic BIR assay introduced above (Fig. 3D,F). We first found that the rates of Lys+ colony formation were indistinguishable between WT and *uls1*Δ strains (Fig. 6E). If anything, *uls1*Δ was slightly more efficient. Second, by monitoring the accumulation of the strand invasion product by qPCR, we found that the rates were identical in *uls1Δ* and WT cells (Fig. 6F). Thus, consistent with the lack of sensitivity to Zeocin (Fig. S6C), neither BIR-mediated survival nor homology-mediated strand invasion (Fig. 6E,F) were altered in *uls1*Δ, despite the drop in local DSB movement. The fact that HDR is equally efficient suggests that DSB mobility *per se* is not rate-limiting for homology-directed BIR, as long as sufficient resection takes place to load Rad51. This result, coupled with the observation that *nhp6ΔΔ* increases and *arp8Δ* decreases strand invasion, suggests that histone degradation and enhanced movement genome-wide are more critical for homology search than a local increase in DSB mobility (Fig. 7).

DISCUSSION

The bimolecular recognition of two partners among a vast number of imperfect matches, is fundamental to the biochemistry of life. Nothing exemplifies this challenge better than the homology search that is needed for DSB repair by HR. For homology-based repair to occur, a unique stretch of DNA must search for an identical template amongst millions of base pairs. In the absence of an intact sister chromatid, productive recombination requires a search throughout the nucleus, a process that takes between 3 – 5 hours for completion in budding yeast (Haber, 2018; Mine-Hattab and Rothstein, 2012; Piazza et al., 2019). Although the spatial juxtaposition of chromosomes may contribute to recombination efficiency in some cases (Agmon et al., 2013; Batte et al., 2017; Donnianni and Symington, 2013; Jain et al., 2016; Lee et al., 2016; Lichten and Haber, 1989; Wang et al., 2017), donor sequences can still be found and productive recombination can still occur in yeast without spatial juxtaposition of the cleavage site and its repair template. The larger the nucleus and genome, the more complex this becomes. Factors that

facilitate homology search are thus not only of theoretical interest, but are actively sought in order to render human gene therapy through CRISPR targeted recombination more efficient.

Here we show that a reduction in nucleosome density, manifest as a lower steady-state pool of histones and decompacted chromatin, occurs in yeast not only in response to Zeocin (Hauer et al., 2017), but also in response to a single localized DSB (Fig. 6B,D). This leads to increased movement not only of the DSB, but of undamaged sequences, including a potential template for HDR. Building on earlier work which showed that a single DSB becomes more dynamic in a checkpoint and INO80-C dependent manner (Dion et al., 2012), we show here that potential donor sequences also become more accessible and explore larger nuclear volumes through random subdiffusive movement triggered by checkpoint activation in response to a single DSB.

Using a yeast strain deficient for a SUMO-binding Ubiquitin ligase called Uls1, we found that one can compromise local DSB movement, but maintain break resection, checkpoint activation, histone degradation and chromatin decompaction more generally, in response to a single break. Importantly, we show that under these conditions, homology-directed strand invasion is not compromised, even though we scored no increase in DSB movement. This argues that local DSB mobility is not rate-limiting for repair, as long as ectopic chromatin mobility is ensured (Fig. 7). The observation that INO80-C deficient (*arp8*Δ) cells reduce strand invasion efficiency, coincident with a drop in both DSB and ectopic mobility, suggests that histone mobilization is important for HDR. Similarly, the enhanced rates of recombination observed in *nhp6ΔΔ* cells indicate that reduced nucleosome density *per se* can facilitate the homology search during repair. It remains unclear whether the accessibility of the ectopic sequence, or its dynamic movement, is more important, given that the two phenomena are inextricably linked through histone loss (Hauer et al., 2017).

We show here that the movement of the chromatin fiber is lower in S/G2 than in G1, due to the loading of Cohesin which tethers replicated sister chromatids to each other (Fig. 1; (Dion et al., 2013)). At DSBs, movement is further restricted by the local loading of

Cohesin in an MRX-dependent manner (Seeber et al., 2016; Unal et al., 2007). We propose that Uls1, which mediates a SUMO-dependent protein ubiquitination, controls the levels of Cohesin (Scc1) and MRX (Rad50) at processed breaks, possibly by regulating their turnover. The removal of these tethering molecules may enable access for the recombination machinery, and/or release the damage from local constraining forces (Fig. 7).

Although we argue that break mobility is not rate-limiting under the conditions employed here, there may be other sites of damage for which local movement is rate-limiting. We do not exclude that at some sites, for example centromere-proximal breaks, the removal of MRX and Cohesin from sequences surrounding the damage might be crucial to facilitate repair. We note that Mre11 is a key target of sumoylation, as are subunits of Cohesin following DNA damage (Cremona et al., 2012). It has been shown that MRX helps recruit SUMO ligases, and sumoylation would, in turn, recruit Uls1 through its SIM domains (Chen et al., 2016; Cremona et al., 2012). Uls1 could then trigger a dynamic turnover of Cohesin and MRX, given that the loss of Uls1 led to a steady-state increase of Cohesin and Rad50 at a persistent DSB (Fig. 4).

Other mechanisms have been proposed to regulate chromatin dynamics upon DNA damage, including the loss of a tether to the NE (Hauer et al., 2017; Lottersberger et al., 2015; Strecker et al., 2016). While chromatin domain release may occur at some loci,, it is important to stress that we and others (Lawrimore et al., 2017) failed to detect centromere release or declustering in response to DNA damage (Fig. 2). Moreover, the loss of the regulatory Cep3 phosphoacceptor site, which was thought to regulate this release, did not compromise the damage-enhanced mobility of a DSB at *MAT*. We have highlighted various conditions that obscure accurate mobility measurements, including the distribution of cells in the cell cycle and the efficiency of cut induction. It is also important to note that capturing time-lapse imaging at a significantly lower frequency (1.5s ms vs 80 ms intervals) or resolution, can mask one's ability to detect an increase in DSB mobility (Shukron et al., 2019; Strecker et al., 2016).

Uls1 is an unusual member of the STUbL family, in that besides ubiquitin ligase activity, it contains a SNF2-like helicase domain related to nucleosome remodelers and multiple SIM motifs (Fig. 5A). A very close homologue to Uls1, the human E3 Ub ligase SHPRH, was identified as a tumor suppressor that helps prevent genome instability (Bruhl et al., 2019; Qu et al., 2016). It is thought that SHPRH increases DNA damage tolerance or post-replication repair, which depends on the ubiquitination of PCNA (Unk et al., 2010). We do not know all the relevant targets of Uls1 and cannot rule out that PCNA is a target in yeast. The strong effect of Uls1 loss on break mobility correlates with Cohesin and MRX accumulation, but could also reflect a SIM-mediated crosslinking of break-associated sumoylated proteins.

The expansion or increased mobility of chromatin in response to DSBs or UV irradiation has been described in flies (Chiolo et al., 2011; Janssen et al., 2016; Ryu et al., 2015) and humans (Adam et al., 2016; Tsouroula et al., 2016). Moreover, DSBs in repetitive satellite heterochromatin in mammals and flies appear to move away from heterochromatin prior to resection (Chiolo et al., 2011; Janssen et al., 2016; Ryu et al., 2015; Tsouroula et al., 2016). This is thought to reduce the likelihood of inappropriate recombination and an undesirable loss of sequence (Caridi et al., 2017). Although it was reported in flies that lesions move for limited periods of time with directed motion towards the NE, we have not observed directed motion of yeast DSBs on the time scales that enable accurate biophysical analysis. The importance of directed movement for strand invasion has never been demonstrated, and here we show that break movement is less important than chromatin decompaction for HDR in yeast. Indeed, the size of the yeast nucleus may render directed motion unnecessary (reviewed in (Marnef and Legube, 2017)).

One practical outcome of our study is to reinforce the model that a transient reduction in nucleosome density could enhance repair by HR over NHEJ. This will be crucial for CRISPR-mediated gene therapies, which are currently too inefficient to be used clinically. Preliminary evidence suggests that a transient reduction in nucleosome levels in human cultured cells, can increase recombination 2-3 fold (Koren, S., Hauer, M.H., and S.M.G.,

personal communication). Combining this with appropriately upregulated chromatin remodelers may increase the efficiency of cleavage, processing, and resection, as well. The data presented here shows the impact of a global chromatin response to a DSB, triggering changes in chromatin compaction at ectopic sites and implicating checkpoint kinases in a signalling pathway that regulates histones genome-wide. It is easy to imagine that this pathway could be used to facilitate DNA-based reactions in other situations of stress.

Limitations

The major limitation of the study stems from the fact that the conclusions one can draw from the imaging of locus dynamics are influenced by the parameters used for image capture (Amitai et al., 2017; Mine-Hattab et al., 2017; Shukron et al., 2019). We use an optimized time-lapse capture interval of 80ms for 1min, in order to be able to extract precise biophysical parameters of locus movement relevant to chromatin compaction. It cannot be assumed that this is robustly scalable to larger time intervals. In our case, if 3D stacks are acquired at either 80ms or 300ms intervals, very similar results are obtained, but at 1.5s intervals over 7.5min, finer aspects of the dynamics are lost (Amitai et al., 2016). At 80ms intervals we image for 1min to avoid inflicting damage to the DNA through the activating light. We are rigorously consistent in our study, which is based on previous optimization (Amitai et al., 2016; Hauer et al., 2017). We do not however exclude that other movements might be detected at much longer time intervals. Given that the character of the chromatin fiber is conserved from yeast to human cells, we predict that our findings on chromatin mobility changes are also relevant to HDR in mammalian cells. With respect to the role of chromatin decompaction in mammalian DSB repair, we can only point to one study that addressed this directly by observing chromatin decompaction during the repair of UV lesions (Adam et al., 2016).

Acknowledgements

We thank J. Haber, D. Durocher, J. Strecker, L. Symington and S. Biggins for yeast strains. We thank L. Gelman, S. Bourke and J. Eglinger for technical imaging assistance (FMI FAIM)) and H. Kohler (FMI FACS). We thank all members of the Gasser laboratory for valuable discussions and technical support, and S.M.G. thanks the HFSP, SNSF and the Novartis Research Foundation for support. We dedicate this manuscript to our dearly missed friend and colleague, Michael Hauer.

Author contributions

A.C. and S.M.G. wrote the paper. A.C., A.S., K.C and K.S designed experiments, performed and analyzed data. A.A performed biophysical analysis of high-speed tracking data. H.C.F. performed the Uls1-Myc chromatin immunoprecipitation experiment, and H.Y. contributed to the BIR assay data.

Competing financial interests

The authors declare no competing financial interests.

MAIN FIGURES

Figure 1: Basal and DSB induced chromatin mobility is cell-cycle stage dependent.
A) Sketch of the experimental set-up for high-speed time-lapse imaging of a GFP-tagged chromosomal locus near an inducible DSB (see STAR Methods).
B) Mean Square Displacement (MSD) analysis (Δt= 80ms) of the *MAT* locus in the haploid strain GA-9764 at different cell-cycle stages of G1, S and G2 sorted by cell and nuclear morphology (n^{G1}=26, n^{S}=25, n^{G2}=19). The right panel presents box plots of biophysical parameters derived from imaging in G1, S, G2 phase cells, of length of constraint (Lc) and mean spring force coefficient (Kc) acting on this specific locus ((Shukron et al., 2019)).
C) MSD analysis (Δt= 80ms) of the *MAT* locus in GA-8862 (WT) (n^{noDSB}=16) and GA-10231 (*scc1-degron)* (n^{noDSB}=18) cells in S phase. Right hand panels show box plots of biophysical parameters as panel b. Scc1 degradation is induced for 2h together with HO cleavage by galactose. For efficiency of degradation see Supp Fig. S1b.
D and E) MSD analysis (Δt= 80ms) of the *MAT* locus in GA-9764 +/- DSB in S-phase (d) and G1-phase (e) cells. The right panel shows box plots of biophysical parameters as in b.
Statistical analyses testing the significance of the all biophysical parameters derived from the imaging data were performed with Matlab using the Kolmogorov–Smirnov test ($p<0.05$ *; $p<0.01$ **; $p<0.001$ ***), see Tables S1 and S3 for significance values.

Cheblal et al. Figure 1: Basal and DSB-induced chromatin mobility is cell cycle-stage dependent.

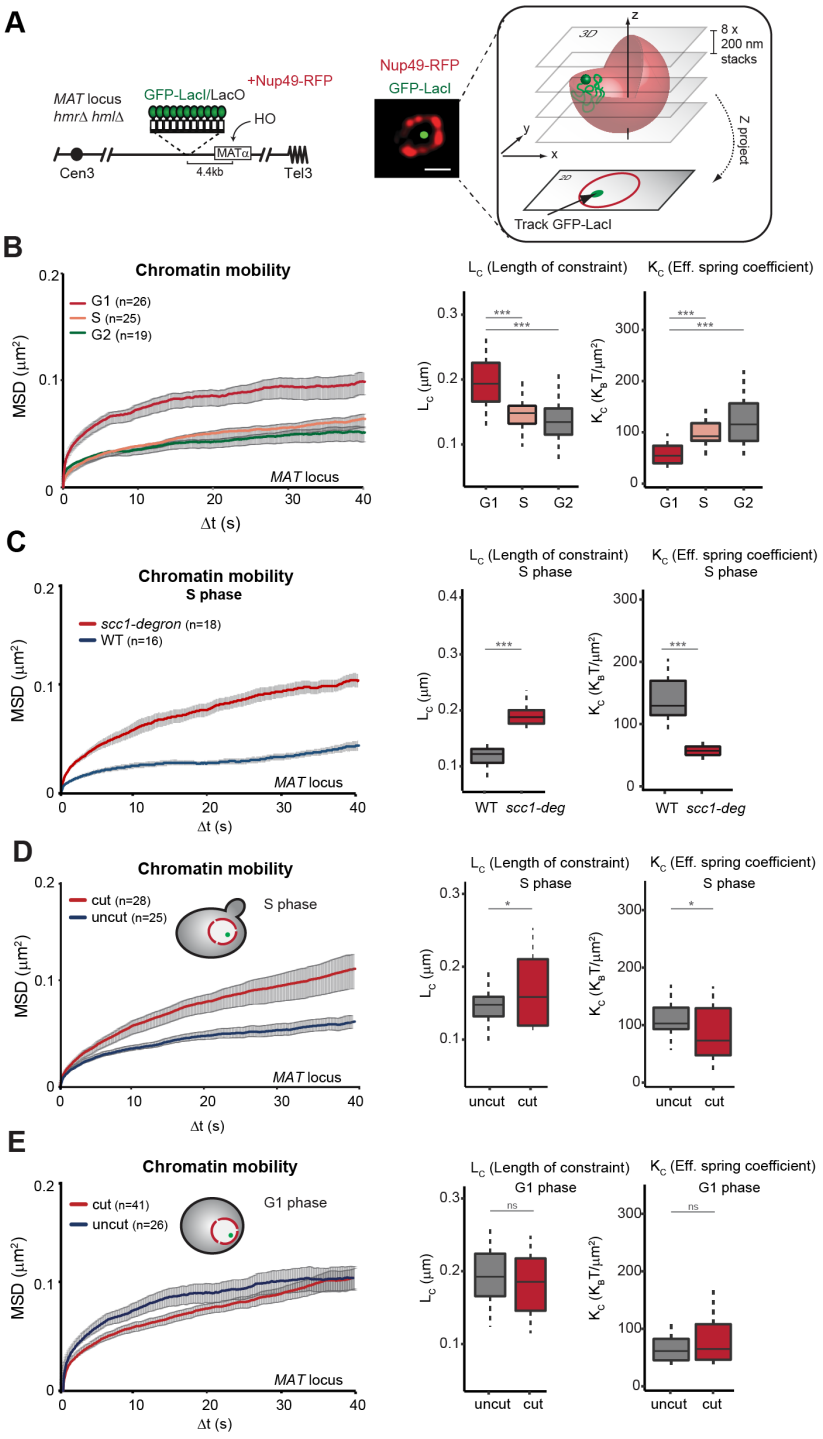

<u>Figure 2:</u> Neither centromere release nor CEP3 phosphorylation controls DSB mobility.

A) Scheme of the imaging a centromere Mtw1-ECFP and pore Nup49-RFP marker in GA-9905 (WT) and GA-9906 (*cep3-S575A)* cells. Shown is a representative G2/M yeast cell. Images shown are images of G1 or G2 phase nuclei. Plots to the right show the percentage of cells with kinetochore declustering (≥2 Mtw1-GFP foci per cell) after 1h Zeocin treatment (250 or 500 µg/ml) of GA-9905 (WT) and GA-9906 (*cep3-S575A)*, in G2/M and G1. N= 3 independent experiments; n= number of nuclei scored. Valid for panels a-c.

B) Scheme of measurement to determine pore-Mtw1-GFP spot distances in G1 cells and illustration of attached vs detached centromeres.

C) Box and Whisker plots showing effect of DNA damage induced by indicated amounts of Zeocin (1h) for WT and GA-9906 (*cep3-S575A)* cells. Right panel: Box and Whisker plot shows release before and after 2h treatment with Nocodazole (50 µM) in GA-9905 (WT) cells.

D) Drop assay (10-fold dilution series) to measure survival during DNA damage in GA-9764 (WT), GA-9767 (*cep3-S575A)* and GA-8921 *(arp8Δ)* cells. Serial dilutions of the indicated yeast strains grew on YPAD at 30ºC for 3 days (control) or on YPAD containing the indicated concentrations of Zeocin.

E) MSD analysis (Δt= 80ms) of the *MAT* locus in WT and *cep3-S575A* (n^{DSB}= 154, n^{noDSB}=86) S-phase cells. Right-hand panels show box plots of biophysical parameters as in Fig. 1B. Statistical analysis were performed as Fig.1B. Kinetochore events were analysed by the Student T-test. $p<0.05$ *; $p<0.01$ **; $p<0.001$ ***.

Cheblal et al. Figure 2: Neither centromere release nor CEP3 phosphorylation control DSB mobility

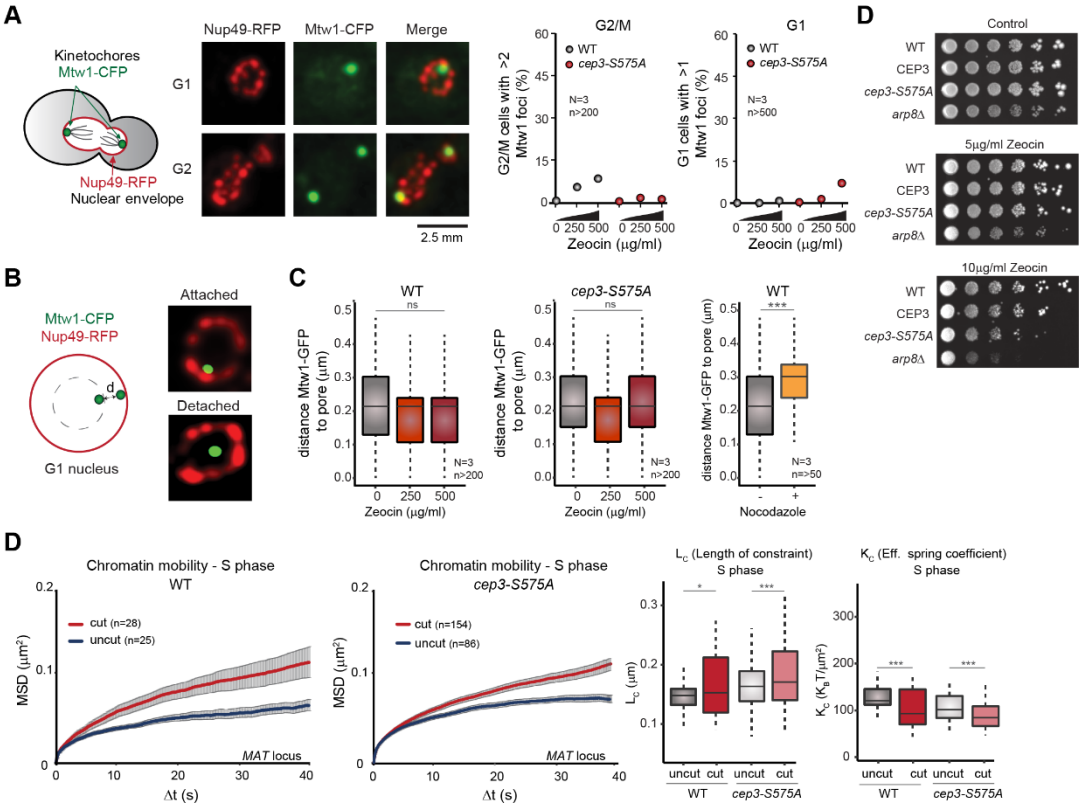

<u>Figure 3:</u> Reduced nucleosome occupancy and chromatin remodeling facilitate strand annealing during BIR.

Chromatin reorganization upon DSB induction in WT, *arp8Δ* and *nhp6ΔΔ* cells is sketched to the left in panels A-C), based on expansion states monitored by SIM in (Hauer et al., 2017).

A) MSD analysis (Δt= 80ms) of the *MAT* locus in GA-9764 (WT) (n^{DSB}=28 , n^{noDSB}=25) and **B)** GA-8921 (*arp8Δ*) (n^{DSB}=19 , n^{noDSB}=19) cells in S phase. The right panels show box plots of biophysical parameters derived as Fig. 1B.

C**)** MSD analysis (Δt= 80ms) of the *MET10* locus in GA-9813 (*nhp6a/b*ΔΔ) cells in S phase, after 1h 300µg/ml Zeocin treatment (n^{nozeo}=15, n^{zeo300}=30). Dotted grey lines in the MSD plot indicate maximal Rc after similar Zeocin treatment in WT cells. Statistical analysis were performed as in Fig.1B.

D) Experimental set-up for the BIR assay with recipient and donor cassettes indicated on ChrV and ChrXI, respectively. The PCR primer pairs used to amplify BIR products (P1, P2) are shown. See STAR methods.

E) BIR efficiency determined by CFU Lys+ YPGal/CFU YPGlu in GA-8990 (WT, N=7), GA-9070 (*pol32Δ*, N=5), GA-10455 (*arp8Δ*, N=4) and GA-10316 (*nhp6 Δ Δ*, N=7). Bar represents mean of biological replica and error bar represents SEM. Welch's t-test scores WT vs *pol32* P<0.0001(***), WT vs *arp8 Δ* P=0.004(***), and WT vs *nhp6 Δ Δ* P=0.023(*). n number of scored colonies per plate is greater than 100.

F) Representative PCR to detect DSB and BIR product from G2-M arrested cells after HO induction in GA-8990 (WT), GA-9070 (*pol32 Δ*), GA-10455 (*arp8*Δ), and GA-10316 (*nhp6ΔΔ*)

G) Kinetics of BIR product formation in WT, *pol32Δ*, *arp8*Δ, and *nhp6ΔΔ*cells. The signal intensity of BIR (P1-P2) product was normalized by control (C1-C2) PCR product, then percentage of BIR recombination was plotted as the value of Lys+ colony from WT as 100. (N=4, error bar represents SEM).

Cheblal et al. Figure 3: Reduced nucleosome occupancy and chromatin remodeling facilitate strand annealing during BIR

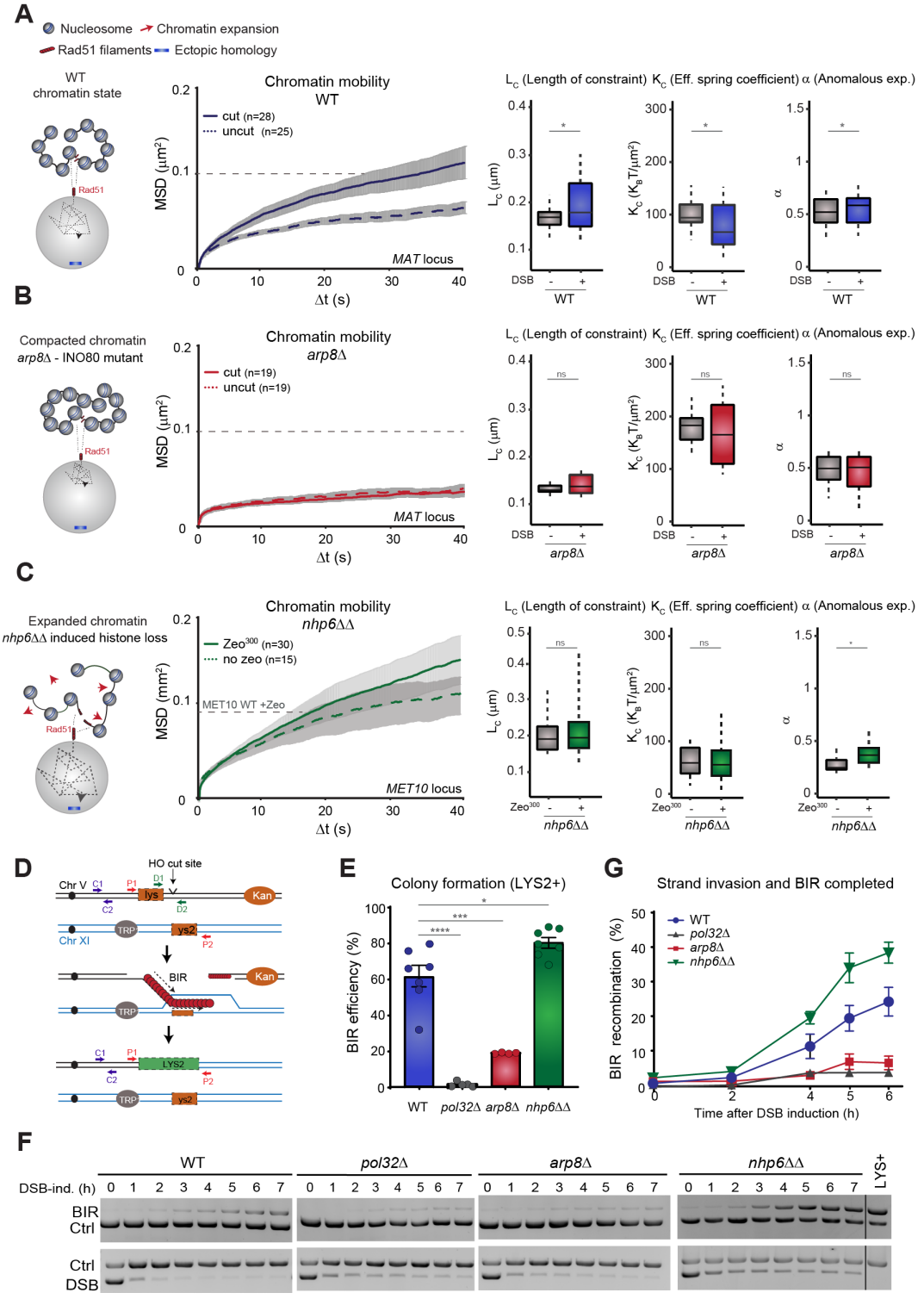

<u>Figure 4:</u> STUBL-ATPase Uls1 regulates local DSB movement and Cohesin levels at the break.

A) Left panel: Structures and annotated domains of major *S. cerevisiae* STUBLs (Uls1 and Slx5/8) and potential homologs in *H. sapiens* (SHPRH, RNF4 and RNF111). Right panel: Uls1-3Myc ChIP before (0min) or after (90min, 180min) DSB induction using the indicated probes at 0.6, 1.8 or 4.5kb of the HO cut site in GA-4467 (WT) cells. ChIP signals are normalized to a fragment in the *SMC2* gene (see STAR Methods).
B) MSD analysis (Δt= 80ms) of the *MAT* locus in GA-9948 (WT) (n^{DSB}= 28, n^{noDSB}=25) and GA-10436 (*uls1Δ)* (n^{DSB}=17 , n^{noDSB}=15) cells in S phase. Panels to right show box plots of biophysical parameters. Statistical analysis were performed as Fig.1B.
C) Scc1-3HA ChIP before (0min) or after (90, 180min) DSB induction using the indicated probes at 0.6kb and 4.5kb of the HO cut site in GA-9194 (WT) and GA-10677 (*uls1Δ*) cells.
D) MSD analysis (Δt= 80ms) of the *MAT* locus in GA-8862 (WT) (nDSB= 18) and GA-10231 (*scc1-degron*) (nDSB= 18) cells in S phase. To the right, box plots of biophysical parameters as in Fig. 1B. Scc1 degradation is induced for 2h together with HO cleavage by galactose. Efficiency of degradation is shown in Fig. S1. Dotted red and blue lines in the second MSD plot indicate maximal Rc without cleavage.

Cheblal et al., Figure 4: STUBL-ATPase Uls1 regulates local DSB movement and cohesin levels at DSBs

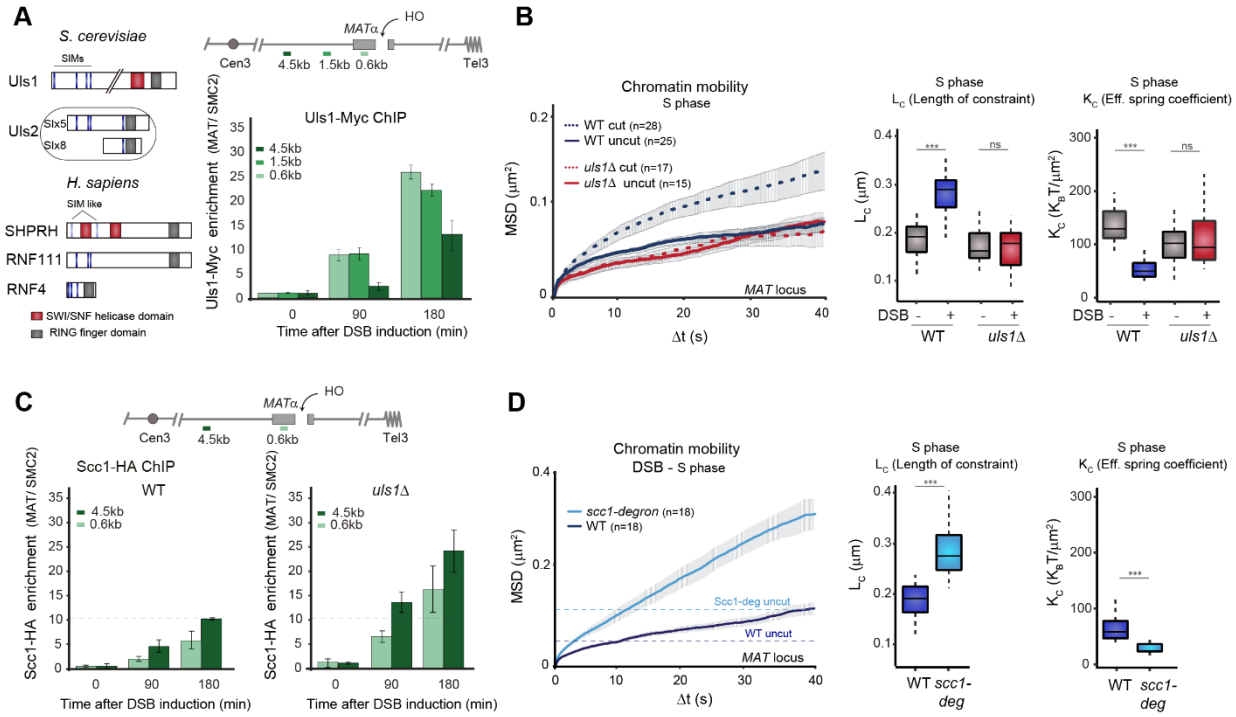

Figure 5: Zeocin-induced ectopic locus movement and checkpoint-triggered histone loss in *uls1Δ* cells.

A) Experimental set-up for high-speed imaging of an undamaged site through LacI-GFP at *MAT* locus and Rad52-Ruby2. GFP foci that do not have colocalizing Rad52 are scored.

B) MSD analysis (Δt= 80ms) showing enhanced chromatin mobility at the *MAT* locus after 1h of 250μg/ml Zeocin in GA-9948 (WT) (n^{ctrl}=25, n^{zeo250}=11) and **C)** in GA-10436 (*uls1Δ)* (n^{ctrl}=15 , n^{zeo250}=17) cells in S phase. To the right, box plots of biophysical parameters as Fig. 1B. Statistical analysis were performed as Fig. 1B.

D) Representative Western blots of HiBit Tagged H2B, Mcm4 (loading control) and Rad53, to monitor checkpoint induction, after cells are exposed for 1h to 250 μg/ml Zeocin. Cells used are GA-10173 (WT) and GA-10676 (*uls1Δ*) cells. P* indicates phosphorylation dependent upshift of Rad53. To the right is the quantitation of histone H2B levels normalized to the Mcm4 control and the 0 h time point.

E) Quantitation of expansion of the undamaged *lacO* array at the *MAT* locus in response to Zeocin treatment (STAR methods). The significance of compaction change is calculated using a t-test ($p<0.05$ *; $p<0.01$ **; $p<0.001$ ***).

Cheblal et al., Figure 5: Zeocin-induced ectopic locus movement and checkpoint-triggered histone loss is preserved in *uls1*Δ cells

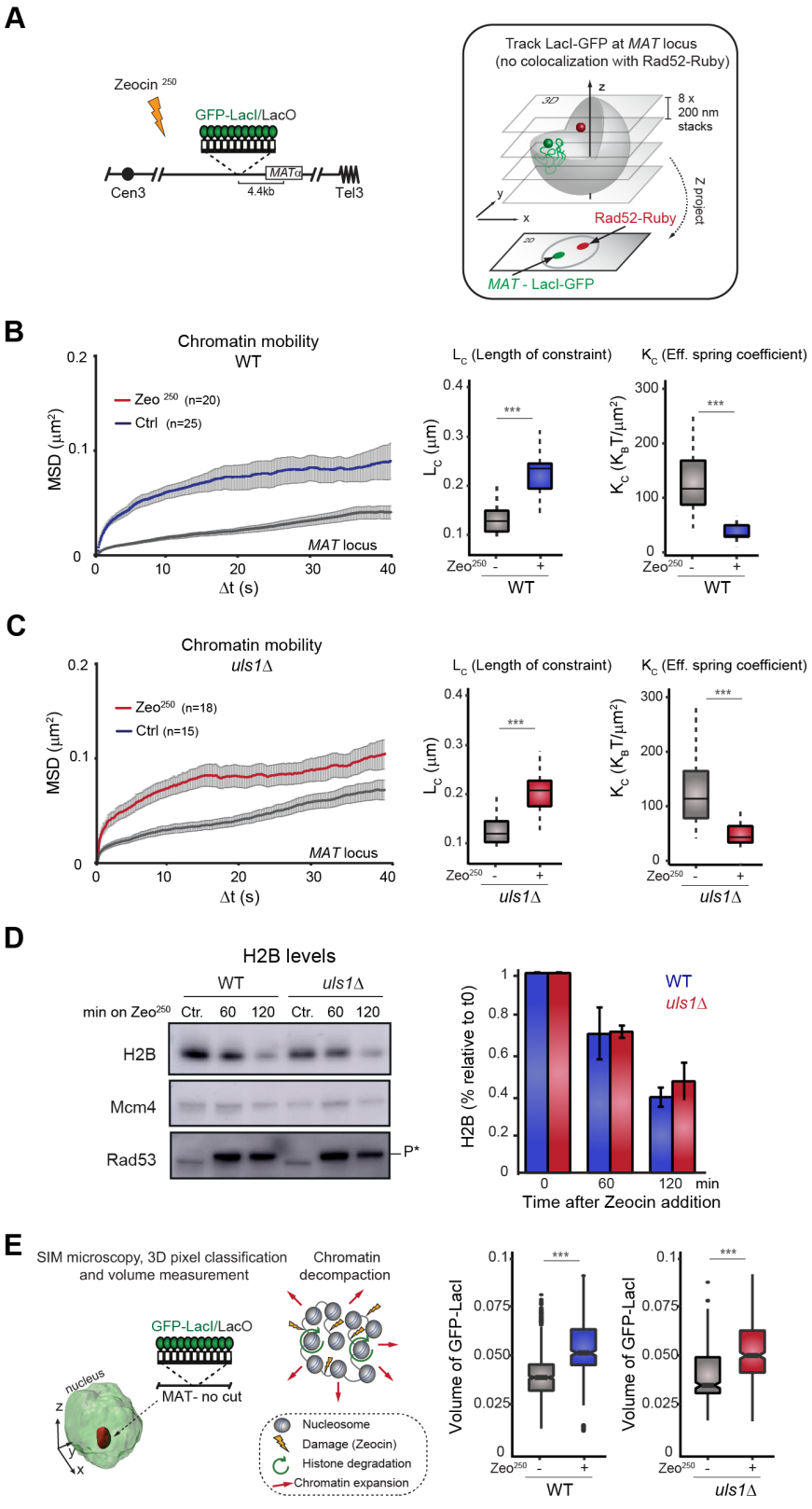

<u>Figure 6:</u> A single DSB at *MAT* triggers ectopic locus movement, enabling efficient DSB repair in *uls1Δ* cells.

A) Experimental set-up for high-speed imaging of an undamaged *MET10* locus through LacI-GFP after galacatose-induction of HO endonuclease, which creates a single DSB at the *MAT* locus.

B) MSD analysis (Δt= 80ms) of the *MET10* locus 4 h after DSB induction in GA-10706 (WT; n^{DSB}=18, n^{noDSB}=16) and **C)** in GA10718 (*uls1Δ*) (n^{DSB}=12, n^{noDSB}=20) cells in S phase. Checkpoint activation at this point is shown in Fig. S6C. To the right, box plots of biophysical parameters as Fig. 1B. Statistical analysis were performed as Fig.1B.

D) Quantitation of undamaged locus expansion (*MET10*) in response to a single DSB at *MAT*, was performed as described for Fig. 5E. (STAR methods) The significance of the change in compaction is calculated using t-test ($p<0.05$ *; $p<0.01$ **; $p<0.001$ ***).

E) BIR efficiency determined by CFU Lys+ YPGal/CFU YPGlu in GA-8990 (WT, n=7) and GA-10524 *(uls1Δ*, n=5), as in Fig. 3E. Bar represents mean of biological replica and error bar represents SEM. Welch's t-test scores non-significant difference between WT and *uls1Δ* (P=0.45).

F) Kinetics of BIR product formation quantified in G2-M arrested GA-8990 (WT, n=4) and GA-10524 *(uls1Δ*, n=3), as described in Fig. 3D,F,G. Right panel: representative PCR to detect DSB and BIR product from G2-M arrested cells after HO induction.

Cheblal et al., Figure 6: A single DSB at MAT triggers ectopic locus movement, enabling efficient DSB repair rates in *uls1*Δ cells.

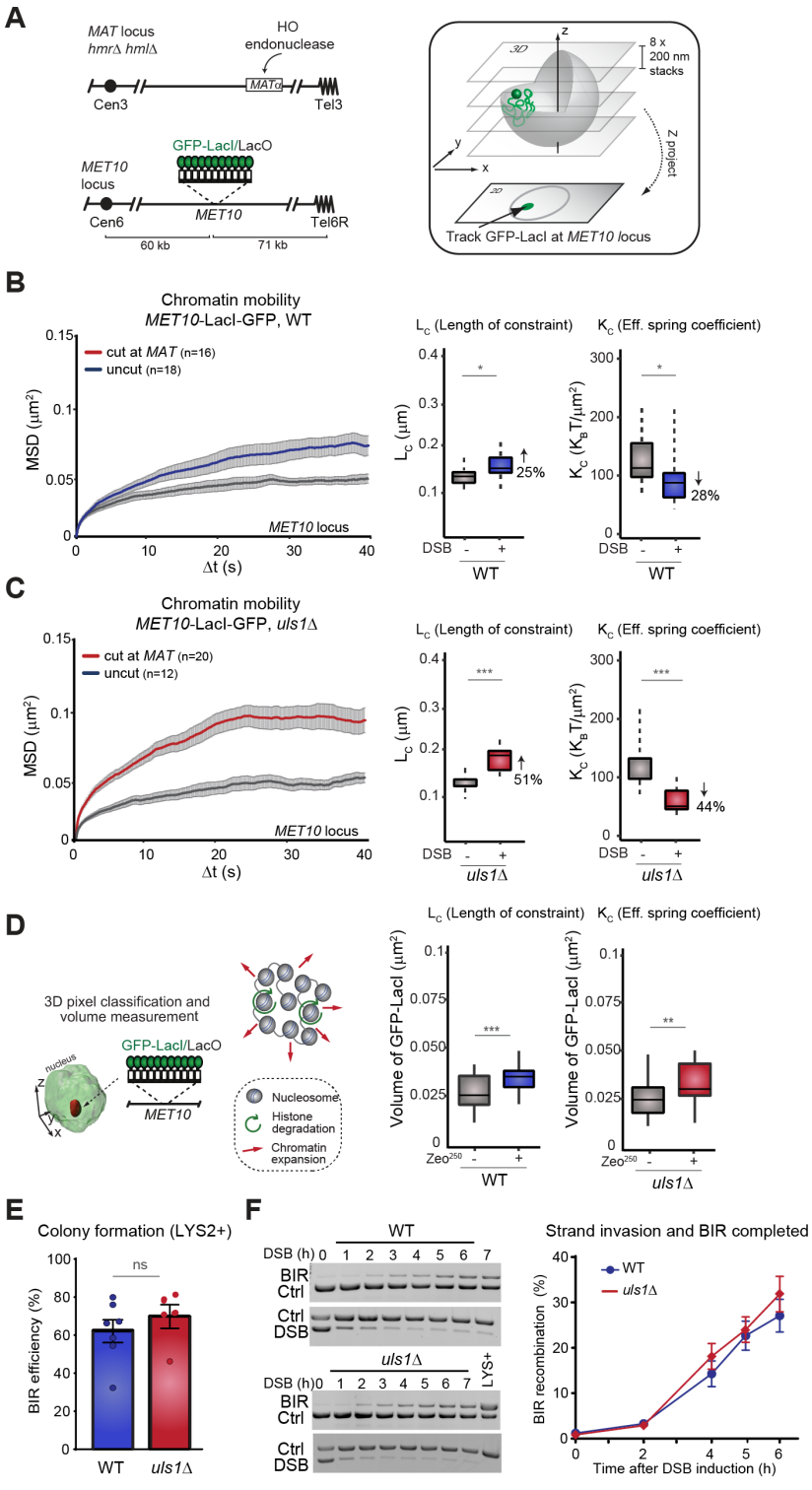

Figure 7: Model of the role of histone loss and enhanced DNA movement in HDR.
The role of chromatin decompaction in HDR mediated repair of a DSB as described in the Discussion. Local break mobility is attenuated by Cohesin and MRX loading which Uls1 normally keeps in check. Chromatin decompaction is due to checkpoint kinase-triggered histone degradation, and histone loss correlates with enhanced chromatin mobility.

Cheblal et al., Figure 7: Model of the role of histone loss and enhanced DNA movement in HDR

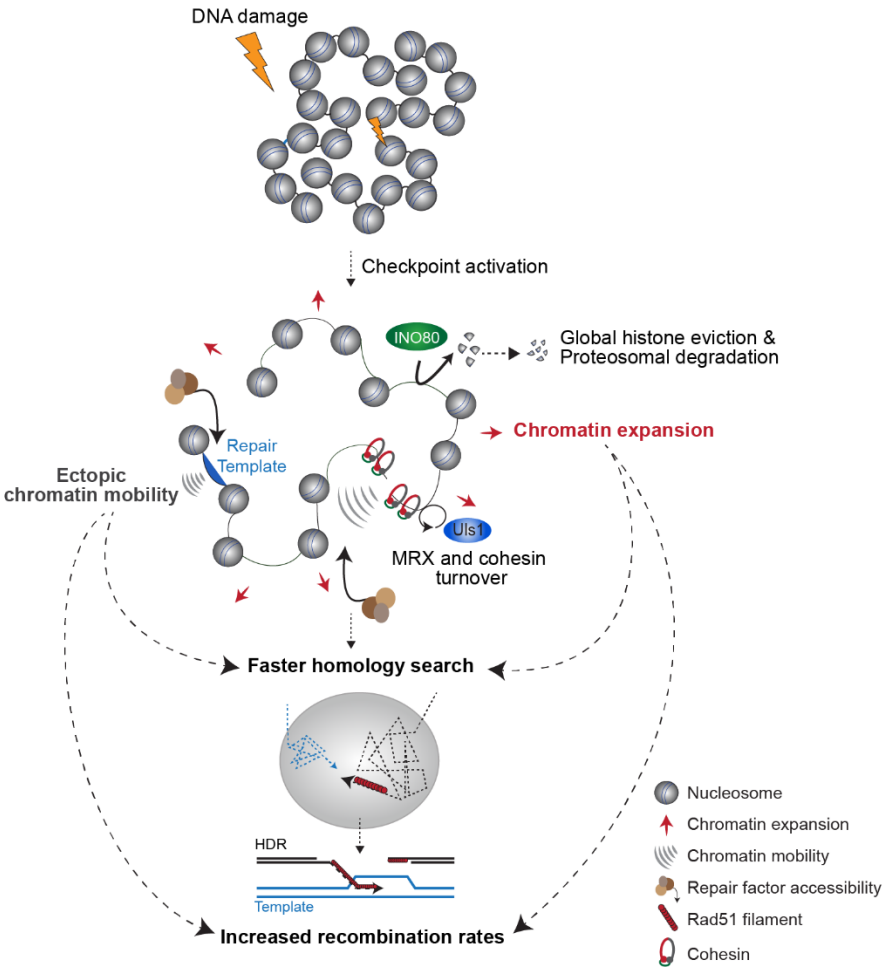

STAR Methods

Resource Availability

Lead Contact

Further information and requests for resources and reagents should be directed to and will be fulfilled by the Lead Contact: Prof. Susan M. Gasser (susan.gasser@fmi.ch).

Materials Availability

All strains used in this study are available by direct request to the lead contact without any further restrictions.

Data and Code Availability

Time-lapse imaging movies raw data are available upon request.

Detailed Methods

Yeast growth conditions and plasmids

Yeast strains were haploid and were derived from the JKM179 or W303 backgrounds. Genotypes of the yeast strains and plasmids are in Supplemental Table 2. Unless stated differently, yeast cells were usually grown in YPAD media at 30˚C until logarithmic growth phase (OD600 = 0.7; 1 × 10^7 cells/ml). Image acquisition was done at 25˚C.

Mtw1 protein was fluorescently tagged with either Ruby2 or ECFP using either pFA6a-link-yomRuby2-Kan (Lee et al., 2013) or pFA6a-link-yECFP-3HA-Kan (Sheff and Thorn, 2004). Correctly tagged Mtw1 clones were identified by colony PCR and visually confirmed by microscopy. For live and fixed cell microscopy, yeast cells were grown overnight to saturation in sterile filtered YPAD medium. The next morning, cultures were inoculated in synthetic complete medium (SCR) and grown until log growth phase. For experiments involving galactose HO cut induction, after reaching log phase, an HO cut is induced by adding 2% galactose for 2h. Cut efficiency of the HO endonuclease at the MAT locus was determined as in (Horigome et al., 2015).

For spot counting and zoning assay experiments, cells were treated with either 250 µg/ml or 500 µg/ml of Zeocin for 2h. Fixation is done using 4% PFA for 1min followed by washing 3x and then resuspending the cells in PBS.

Live cell microscopy

Live cell microscopy was performed using Nikon Eclipse Ti microscope, two EM-CCD Cascade II (Photometrics) cameras, an ASI MS-2000 Z-piezo stage, and a PlanApo x100, NA 1.45 total internal reflection fluorescence microscope, oil objective and Visiview software. Fluorophores were exited at 561 (Ruby2) and 491 (GFP). GFP and Ruby2 fluorescence were acquired simultaneously on separate cameras (Semrock FF01-617/73-25 filter for Ruby2 and Semrock FF02-525/40-25 filter for GFP). Time-lapse series were acquired with 8 optical slices per stack every 80ms for 1min or 1.5s for 5min. Each optical slice received wither a 10ms exposure for the 80ms intervals or 150ms for the 1.5s intervals. Time-lapse image stacks were analyzed as in (Dion et al., 2012), using Spot Tracker 2D ImageJ plugin to extract coordinates of locus position from the movies. By tracking the movement of the interpolated center of the nuclear sphere (based on the pore marker, Nup49-RFP), at the same time as the tagged chromosomal locus, we correct movement frame-by-frame to eliminate nuclear or instrumental drift (Horigome et al., 2015; Klein et al., 2019; Meister et al., 2010) .

Structured illumination microscopy and image analysis.

Structured illumination images were acquired on a Zeiss Elyra S.1 microscope with an Andor iXon 885 EM-CCD camera using an HR diode 488 100-nW solid state laser, a BP 525-580 + LP 750 filter and a PLAN-APOCHROMAT 63×/1.4-NA oil DIC objective lens. Cells were fixed in 4% paraformaldehyde, washed three times in PBS and then attached to a thin 1.5 glass coverslip using concanavalin A. Cells were fully sectioned into 60 slices at 0.1 nm intervals taken at 60ms exposures per slice with five rotations of the illumination grid. Bright-field images of the cells were also acquired with an X-Cite PC 120 EXFO Metal Halide lamp. ZEN Black was used to process the images with the automatic settings and with the “Raw Scale” option selected.

Spot volumes were measured using a custom pipeline developed in KNIME using the Image Processing community nodes (Dietz et al., 2020). In brief, images are read into the workflow with image properties. A quantile filter is used to enhance spots and they are detected using a wavelet based approach (Olivo-Marin, 2002). Spot detections are dilated and eroded to close small holes and a connected component analysis is run to create 3D objects. Volumes are measured in 3D using the Feature Calculator node. A filter is applied to remove spots that have volumes smaller than 10 pixels or greater than 800 pixels.

Microcopy and image analysis of fixed samples

Cells are grown to exponential phase and images are taken on glass slides. Exposure time was 100ms for each of the 21 slices spaced by 200nm. Analysis of locus position was performed with the zoning assay described in (Meister et al., 2010). In the stack where the spot is in focus, the nucleus is divided into three zones of equal area. For each cell, we determine which zone the spot belongs to using the imageJ plugin Pointpicker. Since this measurement is absolute (i.e., the spot is in exactly one of the three zones), there is no error bar for the percentage of cells in the three zones. Statistical relevance is determined by a Chi2 test that compares scored distribution with the predicted random distribution. The cell cycle phase of each cell was determined based on the bud and nuclear morphologies.

Western blot

Western blotting of TCA precipitated proteins separated on a SDS-PAGE gel (Invitrogen) was performed as in (Seeber et al., 2013). Transfer was done using Biorad Turbo blot system onto PVDF membranes. Anti-Mcm2 was purchased from Santa Cruz (#6680). Rad53 protein was detected using a custom-made mouse monoclonal antibody against the FHA2 domain of Rad53 (Seeber et al., 2013)

HiBiT detection system

HiBiT detection was performed as described in technical manual of Nano-Glo HiBiT blotting system (Promega). HiBiT tagged TCA precipitated proteins separated on a SDS-PAGE gel (Invitrogen), transfer proteins from the gel to nitrocellulose membrane

(Invitrogen) using Biorad Turbo blot system. Membrane was incubated in TBST overnight at 4°C to increase the accessibility of the HiBiT tag. 1x Nano-Glo buffer with LgBiT protein 200-fold was added to membrane with TBST and incubated room temperature for 60min with gentle rocking. Nano-Glo Luciferase assay substrate 500-fold added into the membrane containing LgBiT solution and incubated at room temperature for 5min. Signals were detected using chemiluminescence imager with a CCD camera (Amersham, imager 600). Bands were quantified using Image J and HiBiT-HTB2 was normalized to HiBiT-MCM4 loading control.

Chromatin Immunoprecipitation (ChIP)

Chromatin immunoprecipitation (ChIP) ChIP was performed as described in (Marcomini et al., 2018; Seeber et al., 2016) with slight modifications. At each time point about $14x10^8$ cells were collected, crosslinked with 1% formaldehyde for 20min while shaking at room temperature. We then added glycine to a final concentration of 125mM and incubated with shaking for 5min at room temperature. We washed cells twice with ice cold 1xPBS. HA-tagged Scc1 ChIP was performed using 40 µl sheep anti-mouse IgG magnetic beads (Invitrogen) and 6 µg anti-mouse HA antibody (sc-7392, Santa Cruz Biotech), per sample. Cell extracts were incubated with BSA-saturated magnetic beads coupled to anti-HA antibody for overnight at 4 °C. PK-tagged Rad50 ChIP was performed using mouse SV5-PK1 antibody (Acris Antibodies) and cell extracts were incubated with only 2h rotation at 4 °C, given high efficiency of the antibody. DNA was recovered after reversal of crosslinking using the Accuprep DNA extraction kit (Bioneer). Real-time quantitative PCR (Roche, Light cycler 480 II) was used for amplification of the precipitated DNA regions in 384 well format. Taqman probes were used as described in (Seeber et al., 2016). The data for each strain are the average of three independent experiments with quantitative PCR performed in technical triplicates.

BIR plating assay

BIR efficiency determined by Lys+ colony was done as described in (Donnianni and Symington, 2013). Briefly, yeast cells were exponentially cultured at 25°C in YPA- 2% raffinose (YPAR), then plated on YPA-2% glucose (YPAD) or YPA-2% galactose (YPAG)

in triplicate. Colony number was counted after cells were cultured at 25°C for 3-4 days. Cells grown on YPAG were then replica plated onto synthetic complete (SC) medium lacking lysine, and onto YPAD. The percentage of cells repairing by BIR was determined by % colony formation on YPAG over YPAD, then multiplied by the ratio of Lys+/YPAD which was about 0.99 in all cases.

Detection of BIR PCR product and quantification

Cells were exponentially grown in YPA-raffinose (2%) at 25°C, then arrested in G2/M by 15 µg/ml nocodazole 1% DMSO for 2.5h. 2% galactose in final concentration was added to the culture to induce HO endonuclease.1.5 ml of cell culture at indicated time point was taken for DNA preparation and cell pellet was kept at -20°C before DNA isolation. DNA sample was prepared with MasterPure™ Yeast DNA Purification Kit (Lucigen) according to the manufacture protocol. DNA concentration was measured by NanoDrop spectrometer (Thermo Fisher Scientific). PCR reaction was performed at 98°C 30 sec, followed by 25 cycles of 98°C 10 sec denaturation - 72°C 150 sec. annealing & extension in 25 µl reaction consisting of 0.5 µM primers, 1 ng/µl genomic DNA with 12.5 µl of Q5® High-Fidelity 2X Master Mix (New England BioLabs). P1, P2, C1, and C2 primers were used in a reaction for BIR product detection; D1, D2, C1, and C2 primers were used for HO cut detection. After the reaction, PCR samples were mixed with 5 µl of EZ-Vision® One Dye + Loading buffer (VWR Life Science) and run on 1% agarose in 0.5 x TBE. The agarose gel was washed with H_2O for 0.5 h, then DNA was scanned by Typhoon™ FLA 9500 (GE Healthcare Life Sciences). PCR signal was quantified by Quantity One software (Bio-Rad). BIR product (P1-P2) in each reaction was normalized by control band (C1-C2) and mean of two independent BIR PCR reactions from 3 or 4 biological replicates were plotted, as value of Lys+ colony (WT) as 100.

Drop assays

For drop assays, overnight cultures were diluted to a starting density of OD600 = 0.5 and serial 1:10 dilutions were plated on YPAD or the appropriate selective medium containing the indicated concentrations of HU or Zeocin, added freshly to the plates.

Primer extension assay

For the primer-extension assays, we grew three independent cultures of each genotype overnight in YPAD medium (1% yeast extract, 2% peptone, 0.1 g l^{-1} adenine hemisulphate) with 2% glucose. The next day, cells were diluted into YPR (2% raffinose) medium and were grown one day and overnight.

We arrested the cells using final 15 µg/ml of nocodazole and 1% DMSO for 2.5 h, once the culture had reached OD=0.6. Then we added galactose at a concentration of 2% still in the presence of nocodazole. The results were derived from three to six independent samples for each genotype taken every 20 min for up to 6h. To quantify the results we used a qPCR approach with PowerUp SYBER Green qPCR master mix from ThermoFisher. We used primers SG-5624 and SG-1300, and normalized each sample to ARS605 amplified with SG-2953 and SG-2954. Using this approach, we could obtain a direct measure of the percentage of primer-extension products, compared with ARS605.

Resection assay

Resection assay was performed as described in (Marcomini et al., 2018). Cells were grown in YPLG medium and treated with 3% galactose. 10 ml samples were taken at time points 0, 90min and 180min, DNA was extracted by phenol/chloroform method and final DNA was resuspended in 50µl water. 4µg DNA was digested with 10 units *Alu*I (37°C, 14h, NEB Cut Smart buffer). Real-time quantitative PCR (Roche, Light cycler 480 II) was used for DNA amplification. SYBR green based real time PCR (Thermo Fisher Scientific, Cat. No. A25741) 1.6 µl of the digested or the undigested sample was used for a 10µl reaction. A 2-step PCR (95 °C for 15s, 60°C for 40s, 45 cycles) was carried out and Ct values were used for quantitation. Loci were normalized to the qPCR signal at the undamaged *SMC2* locus. The amount of ssDNA was normalized to cut efficiency.

Flow cytometry

For FACS, cultures were grown as for Western blotting. A 1 ml sample was taken for each time-point and was spun down and fixed in 70% ethanol and stored at 4°C. When ready for analysis samples were sedimented and resuspended in 50 mM Tris-HCl pH 7.5 + 200

µg/ml RNase A and digested for 2 h at 37 °C. Samples were then sedimented and resuspended in 50 mM Na-Citrate pH 7.0 + 10 µg/ml PI. Samples were stained overnight at 4 °C. The following morning the samples were briefly sonicated and diluted in more Na-Citrate + PI. Samples were measured on a Becton Dickinson FACS Calibur and at least 10 000 cells were measured.

Cut efficiencies

The HO-dependent cutting efficiency was from cultures treated with galactose as above. DNA was isolated from strains immediately before and at 40, 60, 120 and 240 min after galactose addition.

qPCR using TaqMan probe TQ-28 (5′-CCTGGTTTTGGTTTTGTAGAGTGGTTGACGA-3′) which is specific for the *MAT* locus amplified with SG-2285 and SG-2286, was normalized to the *SMC2* locus amplified with SG-525 and SG-526 and detected using TQ-3 (5′-CGACGCGAATCCATCTTCCCAAATAATT-3′).

Imaging parameters are not responsible for the different results

A recent study in diploid budding yeast show that chromosome dynamics depend on the time interval of imaging used (Mine-Hattab et al., 2017). Because we use an optimized 80ms interval that had been shown to be highly sensitive to changes in locus mobility (Amitai et al., 2017; Shukron et al., 2019), while others have used 1.5s intervals (Strecker et al., 2016), we repeated our analysis of the DSB at *MAT* using 1.5s imaging intervals. Consistent with theoretical considerations, arguing that dynamic changes can occur that cannot be detected with long interval imaging (Amitai et al., 2017; Mine-Hattab et al., 2017; Shukron et al., 2019), we failed to detect an increase in the dynamics of the *MAT* locus even when analyzing S phase and G1 cells separately in WT and *cep3-S575A* cells (Figure S7). Strecker et al. show that *cep3-S575A* impairs DSB induced chromatin mobility in an averaged asynchronous cell population. By FACS we found that the cell-cycle profile of *cep3-S575A* cells before and after DSB formation is not equal to the WT (Fig S3C). While this unequal cell cycle distribution may cause a difference of DSB mobility analysis, when we chose specifically S- and G1-phase cells to analyse, we also found no difference in DSB mobility in *cep3-S575A* and wild-type cells. Thus, we conclude

that Cep3 phosphorylation on Ser575 is not required for DSB increased mobility. As shown in previous studies (Seeber et al., 2013), *arp8Δ* cells showed sensitivity to DNA damage, while *cep3-S575A* cells were not sensitive to either Zeocin or hydroxyurea (Fig. 2D).

Statistical Analysis

All chromatin mobility data (spot tracking) are pooled from at least three independent experiments. Statistical analyses testing the significance of the biophysical parameters derived from the imaging data were performed with Matlab using the Kolmogorov–Smirnov test ($p<0.05$ *; $p<0.01$ **; $p<0.001$ ***) as in (Amitai et al., 2017). Kinetochore detachment and declustering events were tested using a Student T-test ($p<0.05$ *; $p<0.01$ **; $p<0.001$ ***). BIR plating assay significance was tested using Welch's t-test. (See Table 3 for all p values).

REFERENCES

Adam, S., Dabin, J., Chevallier, O., Leroy, O., Baldeyron, C., Corpet, A., Lomonte, P., Renaud, O., Almouzni, G., and Polo, S.E. (2016). Real-Time Tracking of Parental Histones Reveals Their Contribution to Chromatin Integrity Following DNA Damage. Mol Cell *64*, 65-78.

Agmon, N., Liefshitz, B., Zimmer, C., Fabre, E., and Kupiec, M. (2013). Effect of nuclear architecture on the efficiency of double-strand break repair. Nature cell biology *15*, 694-699.

Amitai, A., Seeber, A., Gasser, S.M., and Holcman, D. (2017). Visualization of Chromatin Decompaction and Break Site Extrusion as Predicted by Statistical Polymer Modeling of Single-Locus Trajectories. Cell reports *18*, 1200-1214.

Aylon, Y., Liefshitz, B., and Kupiec, M. (2004). The CDK regulates repair of double-strand breaks by homologous recombination during the cell cycle. The EMBO journal *23*, 4868-4875.

Barzel, A., and Kupiec, M. (2008). Finding a match: how do homologous sequences get together for recombination? Nat Rev Genet *9*, 27-37.

Batte, A., Brocas, C., Bordelet, H., Hocher, A., Ruault, M., Adjiri, A., Taddei, A., and Dubrana, K. (2017). Recombination at subtelomeres is regulated by physical distance, double-strand break resection and chromatin status. The EMBO journal *36*, 2609-2625.

Bermudez-Lopez, M., and Aragon, L. (2017). Detection of Cohesin SUMOylation In Vivo. Methods in molecular biology *1515*, 55-64.

Bruhl, J., Trautwein, J., Schafer, A., Linne, U., and Bouazoune, K. (2019). The DNA repair protein SHPRH is a nucleosome-stimulated ATPase and a nucleosome-E3 ubiquitin ligase. Epigenetics Chromatin *12*, 52.

Bystricky, K., Laroche, T., van Houwe, G., Blaszczyk, M., and Gasser, S.M. (2005). Chromosome looping in yeast telomere pairing and coordinated movement reflect anchoring efficiency and territorial organization. The Journal of cell biology *168*, 375-387.

Caridi, P.C., Delabaere, L., Zapotoczny, G., and Chiolo, I. (2017). And yet, it moves: nuclear and chromatin dynamics of a heterochromatic double-strand break. Philos Trans R Soc Lond B Biol Sci *372*.

Chen, Y.J., Chuang, Y.C., Chuang, C.N., Cheng, Y.H., Chang, C.R., Leng, C.H., and Wang, T.F. (2016). S. cerevisiae Mre11 recruits conjugated SUMO moieties to facilitate the assembly and function of the Mre11-Rad50-Xrs2 complex. Nucleic Acids Res *44*, 2199-2213.

Chiolo, I., Minoda, A., Colmenares, S.U., Polyzos, A., Costes, S.V., and Karpen, G.H. (2011). Double-strand breaks in heterochromatin move outside of a dynamic HP1a domain to complete recombinational repair. Cell *144*, 732-744.

Chung, D.K., Chan, J.N., Strecker, J., Zhang, W., Ebrahimi-Ardebili, S., Lu, T., Abraham, K.J., Durocher, D., and Mekhail, K. (2015). Perinuclear tethers license telomeric DSBs for a broad kinesin- and NPC-dependent DNA repair process. Nat Commun *6*, 7742.

Cremona, C.A., Sarangi, P., Yang, Y., Hang, L.E., Rahman, S., and Zhao, X. (2012). Extensive DNA damage-induced sumoylation contributes to replication and repair and acts in addition to the mec1 checkpoint. Mol Cell *45*, 422-432.

Dietz, C., Rueden, C.T., Helfrich, S., Dobson, E.T.A., Horn, M., Eglinger, J., Evans, E.L., McLean, D.T., Novitskaya, T., Ricke, W.A.*, et al.* (2020). Integration of the ImageJ Ecosystem in KNIME Analytics Platform. Frontiers in Computer Science *2*.

Dimitrova, N., Chen, Y.C., Spector, D.L., and de Lange, T. (2008). 53BP1 promotes non-homologous end joining of telomeres by increasing chromatin mobility. Nature *456*, 524-528.

Dion, V., Kalck, V., Horigome, C., Towbin, B.D., and Gasser, S.M. (2012). Increased mobility of double-strand breaks requires Mec1, Rad9 and the homologous recombination machinery. Nature cell biology *14*, 502-509.

Dion, V., Kalck, V., Seeber, A., Schleker, T., and Gasser, S.M. (2013). Cohesin and the nucleolus constrain the mobility of spontaneous repair foci. EMBO reports *14*, 984-991.

Donnianni, R.A., and Symington, L.S. (2013). Break-induced replication occurs by conservative DNA synthesis. Proceedings of the National Academy of Sciences of the United States of America *110*, 13475-13480.
Duan, Z., Andronescu, M., Schutz, K., McIlwain, S., Kim, Y.J., Lee, C., Shendure, J., Fields, S., Blau, C.A., and Noble, W.S. (2010). A three-dimensional model of the yeast genome. Nature *465*, 363-367.
Garcia, V., Phelps, S.E., Gray, S., and Neale, M.J. (2011). Bidirectional resection of DNA double-strand breaks by Mre11 and Exo1. Nature *479*, 241-244.
Gehlen, L.R., Gasser, S.M., and Dion, V. (2011). How broken DNA finds its template for repair: a computational approach. Progress of Theoretical Physics Supplement *191*, 20129.
Haber, J.E. (2018). DNA Repair: The Search for Homology. Bioessays *40*, e1700229.
Haber, J.E., Leung, W.Y., Borts, R.H., and Lichten, M. (1991). The frequency of meiotic recombination in yeast is independent of the number and position of homologous donor sequences: implications for chromosome pairing. Proceedings of the National Academy of Sciences of the United States of America *88*, 1120-1124.
Hauer, M.H., Seeber, A., Singh, V., Thierry, R., Sack, R., Amitai, A., Kryzhanovska, M., Eglinger, J., Holcman, D., Owen-Hughes, T.*, et al.* (2017). Histone degradation in response to DNA damage enhances chromatin dynamics and recombination rates. Nat Struct Mol Biol *24*, 99-107.
Herbert, S., Brion, A., Arbona, J.M., Lelek, M., Veillet, A., Lelandais, B., Parmar, J., Fernandez, F.G., Almayrac, E., Khalil, Y.*, et al.* (2017). Chromatin stiffening underlies enhanced locus mobility after DNA damage in budding yeast. The EMBO journal *36*, 2595-2608.
Heun, P., Laroche, T., Shimada, K., Furrer, P., and Gasser, S.M. (2001). Chromosome dynamics in the yeast interphase nucleus. Science *294*, 2181-2186.
Horigome, C., Dion, V., Seeber, A., Gehlen, L.R., and Gasser, S.M. (2015). Visualizing the spatiotemporal dynamics of DNA damage in budding yeast. Methods in molecular biology *1292*, 77-96.
Ira, G., Pellicioli, A., Balijja, A., Wang, X., Fiorani, S., Carotenuto, W., Liberi, G., Bressan, D., Wan, L., Hollingsworth, N.M.*, et al.* (2004). DNA end resection, homologous recombination and DNA damage checkpoint activation require CDK1. Nature *431*, 1011-1017.
Jain, S., Sugawara, N., and Haber, J.E. (2016). Role of Double-Strand Break End-Tethering during Gene Conversion in Saccharomyces cerevisiae. PLoS Genet *12*, e1005976.
Janssen, A., Breuer, G.A., Brinkman, E.K., van der Meulen, A.I., Borden, S.V., van Steensel, B., Bindra, R.S., LaRocque, J.R., and Karpen, G.H. (2016). A single double-strand break system reveals repair dynamics and mechanisms in heterochromatin and euchromatin. Genes Dev *30*, 1645-1657.
Klein, H.L., Bacinskaja, G., Che, J., Cheblal, A., Elango, R., Epshtein, A., Fitzgerald, D.M., Gomez-Gonzalez, B., Khan, S.R., Kumar, S.*, et al.* (2019). Guidelines for DNA recombination and repair studies: Cellular assays of DNA repair pathways. Microb Cell *6*, 1-64.
Krawczyk, P.M., Borovski, T., Stap, J., Cijsouw, T., ten Cate, R., Medema, J.P., Kanaar, R., Franken, N.A., and Aten, J.A. (2012). Chromatin mobility is increased at sites of DNA double-strand breaks. Journal of cell science *125*, 2127-2133.
Lawrimore, J., Barry, T.M., Barry, R.M., York, A.C., Friedman, B., Cook, D.M., Akialis, K., Tyler, J., Vasquez, P., Yeh, E.*, et al.* (2017). Microtubule dynamics drive enhanced chromatin motion and mobilize telomeres in response to DNA damage. Molecular biology of the cell *28*, 1701-1711.
Lee, C.S., Wang, R.W., Chang, H.H., Capurso, D., Segal, M.R., and Haber, J.E. (2016). Chromosome position determines the success of double-strand break repair. Proceedings of the National Academy of Sciences of the United States of America *113*, E146-154.
Lee, S., Lim, W.A., and Thorn, K.S. (2013). Improved blue, green, and red fluorescent protein tagging vectors for S. cerevisiae. PLoS One *8*, e67902.

Lengsfeld, B.M., Rattray, A.J., Bhaskara, V., Ghirlando, R., and Paull, T.T. (2007). Sae2 is an endonuclease that processes hairpin DNA cooperatively with the Mre11/Rad50/Xrs2 complex. Mol Cell *28*, 638-651.
Lescasse, R., Pobiega, S., Callebaut, I., and Marcand, S. (2013). End-joining inhibition at telomeres requires the translocase and polySUMO-dependent ubiquitin ligase Uls1. The EMBO journal *32*, 805-815.
Lichten, M., and Haber, J.E. (1989). Position effects in ectopic and allelic mitotic recombination in Saccharomyces cerevisiae. Genetics *123*, 261-268.
Lieber, M.R. (2010). The mechanism of double-strand DNA break repair by the nonhomologous DNA end-joining pathway. Annu Rev Biochem *79*, 181-211.
Lisby, M., Barlow, J.H., Burgess, R.C., and Rothstein, R. (2004). Choreography of the DNA damage response: spatiotemporal relationships among checkpoint and repair proteins. Cell *118*, 699-713.
Lottersberger, F., Karssemeijer, R.A., Dimitrova, N., and de Lange, T. (2015). 53BP1 and the LINC Complex Promote Microtubule-Dependent DSB Mobility and DNA Repair. Cell *163*, 880-893.
Marcomini, I., Shimada, K., Delgoshaie, N., Yamamoto, I., Seeber, A., Cheblal, A., Horigome, C., Naumann, U., and Gasser, S.M. (2018). Asymmetric Processing of DNA Ends at a Double-Strand Break Leads to Unconstrained Dynamics and Ectopic Translocation. Cell reports *24*, 2614-2628 e2614.
Marnef, A., and Legube, G. (2017). Organizing DNA repair in the nucleus: DSBs hit the road. Curr Opin Cell Biol *46*, 1-8.
Meister, P., Gehlen, L.R., Varela, E., Kalck, V., and Gasser, S.M. (2010). Visualizing yeast chromosomes and nuclear architecture. Methods in enzymology *470*, 535-567.
Mine-Hattab, J., Recamier, V., Izeddin, I., Rothstein, R., and Darzacq, X. (2017). Multi-scale tracking reveals scale-dependent chromatin dynamics after DNA damage. Molecular biology of the cell.
Mine-Hattab, J., and Rothstein, R. (2012). Increased chromosome mobility facilitates homology search during recombination. Nature cell biology *14*, 510-517.
Mine-Hattab, J., and Rothstein, R. (2013). DNA in motion during double-strand break repair. Trends in cell biology *23*, 529-536.
Neumann, F.R., Dion, V., Gehlen, L.R., Tsai-Pflugfelder, M., Schmid, R., Taddei, A., and Gasser, S.M. (2012). Targeted INO80 enhances subnuclear chromatin movement and ectopic homologous recombination. Genes Dev *26*, 369-383.
Olivo-Marin, J.C. (2002). Extraction of spots in biological images using multiscale products. Pattern Recogn *35*, 1989-1996.
Onn, I., Heidinger-Pauli, J.M., Guacci, V., Unal, E., and Koshland, D.E. (2008). Sister chromatid cohesion: a simple concept with a complex reality. Annu Rev Cell Dev Biol *24*, 105-129.
Oshidari, R., Mekhail, K., and Seeber, A. (2019). Mobility and Repair of Damaged DNA: Random or Directed? Trends in cell biology.
Piazza, A., Shah, S.S., Wright, W.D., Gore, S.K., Koszul, R., and Heyer, W.D. (2019). Dynamic Processing of Displacement Loops during Recombinational DNA Repair. Mol Cell *73*, 1255-1266 e1254.
Pinsky, B.A., Kung, C., Shokat, K.M., and Biggins, S. (2006). The Ipl1-Aurora protein kinase activates the spindle checkpoint by creating unattached kinetochores. Nat Cell Biol *8*, 78-83.
Qu, Y., Gharbi, N., Yuan, X., Olsen, J.R., Blicher, P., Dalhus, B., Brokstad, K.A., Lin, B., Oyan, A.M., Zhang, W.*, et al.* (2016). Axitinib blocks Wnt/beta-catenin signaling and directs asymmetric cell division in cancer. Proceedings of the National Academy of Sciences of the United States of America *113*, 9339-9344.

Renkawitz, J., Lademann, C.A., and Jentsch, S. (2014). Mechanisms and principles of homology search during recombination. Nat Rev Mol Cell Biol *15*, 369-383.
Roukos, V., Voss, T.C., Schmidt, C.K., Lee, S., Wangsa, D., and Misteli, T. (2013). Spatial dynamics of chromosome translocations in living cells. Science *341*, 660-664.
Ryu, T., Spatola, B., Delabaere, L., Bowlin, K., Hopp, H., Kunitake, R., Karpen, G.H., and Chiolo, I. (2015). Heterochromatic breaks move to the nuclear periphery to continue recombinational repair. Nature cell biology *17*, 1401-1411.
Saad, H., Gallardo, F., Dalvai, M., Tanguy-le-Gac, N., Lane, D., and Bystricky, K. (2014). DNA dynamics during early double-strand break processing revealed by non-intrusive imaging of living cells. PLoS Genet *10*, e1004187.
Sage, D., Neumann, F.R., Hediger, F., Gasser, S.M., and Unser, M. (2005). Automatic tracking of individual fluorescence particles: application to the study of chromosome dynamics. IEEE transactions on image processing : a publication of the IEEE Signal Processing Society *14*, 1372-1383.
Schrank, B.R., Aparicio, T., Li, Y., Chang, W., Chait, B.T., Gundersen, G.G., Gottesman, M.E., and Gautier, J. (2018). Nuclear ARP2/3 drives DNA break clustering for homology-directed repair. Nature *559*, 61-66.
Seeber, A., Dion, V., and Gasser, S.M. (2013). Checkpoint kinases and the INO80 nucleosome remodeling complex enhance global chromatin mobility in response to DNA damage. Genes Dev *27*, 1999-2008.
Seeber, A., Hauer, M.H., and Gasser, S.M. (2018). Chromosome Dynamics in Response to DNA Damage. Annu Rev Genet *52*, 295-319.
Seeber, A., Hegnauer, A.M., Hustedt, N., Deshpande, I., Poli, J., Eglinger, J., Pasero, P., Gut, H., Shinohara, M., Hopfner, K.P*., et al.* (2016). RPA Mediates Recruitment of MRX to Forks and Double-Strand Breaks to Hold Sister Chromatids Together. Mol Cell *64*, 951-966.
Sheff, M.A., and Thorn, K.S. (2004). Optimized cassettes for fluorescent protein tagging in Saccharomyces cerevisiae. Yeast *21*, 661-670.
Shukron, O., Seeber, A., Amitai, A., and Holcman, D. (2019). Advances Using Single-Particle Trajectories to Reconstruct Chromatin Organization and Dynamics. Trends Genet *35*, 685-705.
Stephens, A.D., Haase, J., Vicci, L., Taylor, R.M., 2nd, and Bloom, K. (2011). Cohesin, condensin, and the intramolecular centromere loop together generate the mitotic chromatin spring. J Cell Biol *193*, 1167-1180.
Strecker, J., Gupta, G.D., Zhang, W., Bashkurov, M., Landry, M.C., Pelletier, L., and Durocher, D. (2016). DNA damage signalling targets the kinetochore to promote chromatin mobility. Nature cell biology *18*, 281-290.
Taddei, A., and Gasser, S.M. (2012). Structure and function in the budding yeast nucleus. Genetics *192*, 107-129.
Tsouroula, K., Furst, A., Rogier, M., Heyer, V., Maglott-Roth, A., Ferrand, A., Reina-San-Martin, B., and Soutoglou, E. (2016). Temporal and Spatial Uncoupling of DNA Double Strand Break Repair Pathways within Mammalian Heterochromatin. Mol Cell *63*, 293-305.
Unal, E., Arbel-Eden, A., Sattler, U., Shroff, R., Lichten, M., Haber, J.E., and Koshland, D. (2004). DNA damage response pathway uses histone modification to assemble a double-strand break-specific cohesin domain. Mol Cell *16*, 991-1002.
Unal, E., Heidinger-Pauli, J.M., and Koshland, D. (2007). DNA double-strand breaks trigger genome-wide sister-chromatid cohesion through Eco1 (Ctf7). Science *317*, 245-248.
Unk, I., Hajdu, I., Blastyak, A., and Haracska, L. (2010). Role of yeast Rad5 and its human orthologs, HLTF and SHPRH in DNA damage tolerance. DNA Repair (Amst) *9*, 257-267.
van Attikum, H., Fritsch, O., and Gasser, S.M. (2007). Distinct roles for SWR1 and INO80 chromatin remodeling complexes at chromosomal double-strand breaks. The EMBO journal *26*, 4113-4125.

Verdaasdonk, J.S., Vasquez, P.A., Barry, R.M., Barry, T., Goodwin, S., Forest, M.G., and Bloom, K. (2013). Centromere tethering confines chromosome domains. Mol Cell *52*, 819-831.
Wang, R.W., Lee, C.S., and Haber, J.E. (2017). Position effects influencing intrachromosomal repair of a double-strand break in budding yeast. PLoS One *12*, e0180994.
Weber, S.A., Gerton, J.L., Polancic, J.E., DeRisi, J.L., Koshland, D., and Megee, P.C. (2004). The kinetochore is an enhancer of pericentric cohesin binding. PLoS Biol *2*, E260.
Zheng, S., Li, D., Lu, Z., Liu, G., Wang, M., Xing, P., Wang, M., Dong, Y., Wang, X., Li, J.*, et al.* (2018). Bre1-dependent H2B ubiquitination promotes homologous recombination by stimulating histone eviction at DNA breaks. Nucleic Acids Res *46*, 11326-11339.
Zierhut, C., and Diffley, J.F. (2008). Break dosage, cell cycle stage and DNA replication influence DNA double strand break response. The EMBO journal *27*, 1875-1885.

SUPPLEMENTAL INFORMATION

Figure S1. Related to Figure 1: Scc1-AID degradation and checkpoint activation

A) Experimental layout for detection of Scc1-AID-degron degradation by addition of IAA (left, for panel B) and for monitoring Rad53 phosphorylation following galactose-induced expression of the HO endonuclease, which induces a single DSB at *MAT* coincident with the induction of *scc1-degron* degradation on IAA (right).

B) Western blot showing Scc1-AID degradation at 30, 60 or 90 min on IAA, using the anti-mini-AID-tag monoclonal antibody from MBL (M214-3).

C) Western blot showing Rad53 phosphorylation, indicative of checkpoint activation, at 0, 4 and 5 hours after the addition of galactose to induce expression of the HO endonuclease, which induces a single DSB at *MAT* in GA-8862 (WT), GA-10231 (*scc1-degron)* and GA-9242 (*rad50*Δ) strains. P* indicates phosphorylation dependent upshift of Rad53.

D) Experimental layout for monitoring the dynamics of a single DSB induced at *MAT* by the galactose-inducible HO endonuclease coincident with the degradation (or not) of Scc1-degron. Degradation is triggered by the addition of IAA. Scheme is relevant for Figure 4, panel D.

Figure S1. Related to Figure 1: Scc1-AID degradation and checkpoint activation

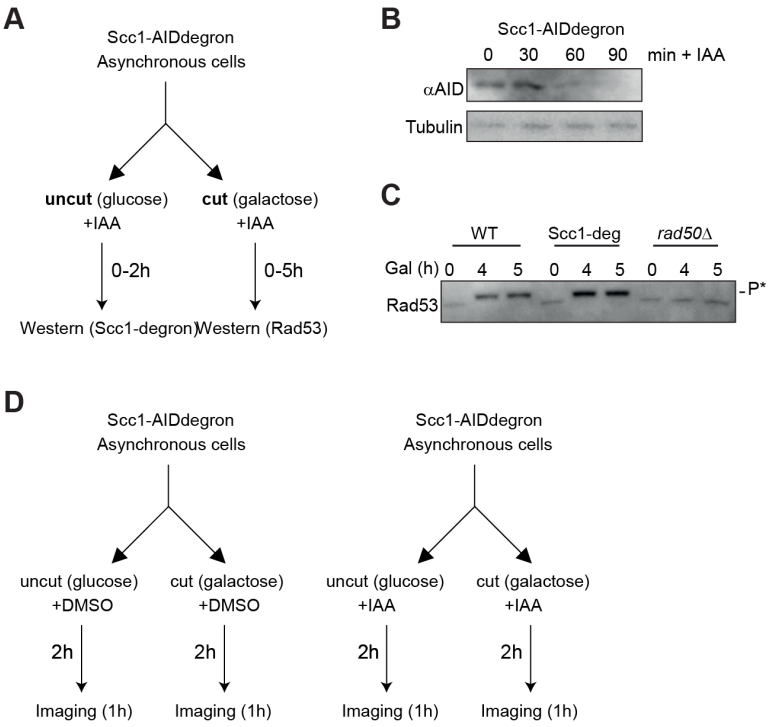

Figure S2. Related to Figure 1: Changes in DNA end-resection rates do not correlate with DSB-induced chromatin mobility

A) Scheme showing the resection assay that monitors ssDNA at proximal (-0.6kb and -4.2kb) and at distal (+0.7kb and +4.5kb) *Alu1* sites surrounding the HO cut site at *MAT,* following 0, 90, and 180 min of HO induction on galactose. Results are normalized to an *Alu1*-free region in *SMC2*. At least 3 biological replicates, amplified in triplicate, are presented as mean values ± SEM.

B) Resection assay in wild-type (WT; GA-8862) as described in a. Results are normalized to an *Alu1*-free region in *SMC2*. At least 3 biological replicates, amplified in triplicate, are presented as mean values ± SEM.

C) Resection assay as described in A and B performed in a *rad50*Δ strain (GA-9242) and **D)** in a *ku70*Δ strain (GA-1954).

E) Calculation and plotting of the MSD analysis based on the time-lapse imaging of a *lacO*-tagged *MAT* locus with and without induced DSB, using the Δt= 80ms imaging scheme. The experiment was performed in the following strains and movie numbers: GA-9948 (WT) (n^{DSB}= 18, n^{noDSB}=16) and GA-9242 (*rad50Δ)* (n^{DSB}=18, n^{noDSB}=17). All cells were in S phase. The dotted horizontal line shows the maximal level of the plateau for the WT strain without DSB (WT uncut).

F) As E, except that MSD analysis (Δt= 80ms) of the *MAT* locus was performed on GA-9948 (WT) (n^{DSB}= 18, n^{noDSB}=16) and GA-1954 (*ku70Δ)* (n^{DSB}=17, n^{noDSB}=17) cells in S phase, with and without DSB.

G) Lc (length of constraint) and Kc (effective spring co-efficient) values for the movies analysed in panel E.

H) Lc (length of constraint) and Kc (effective spring co-efficient) values for the movies analysed in panel F.

For Lc / Kc calculation see (Amitai et al. 2017).

Figure S2. Related to Figure 1: DNA end resection rates do not correlate strictly with DSB-induced chromatin mobility.

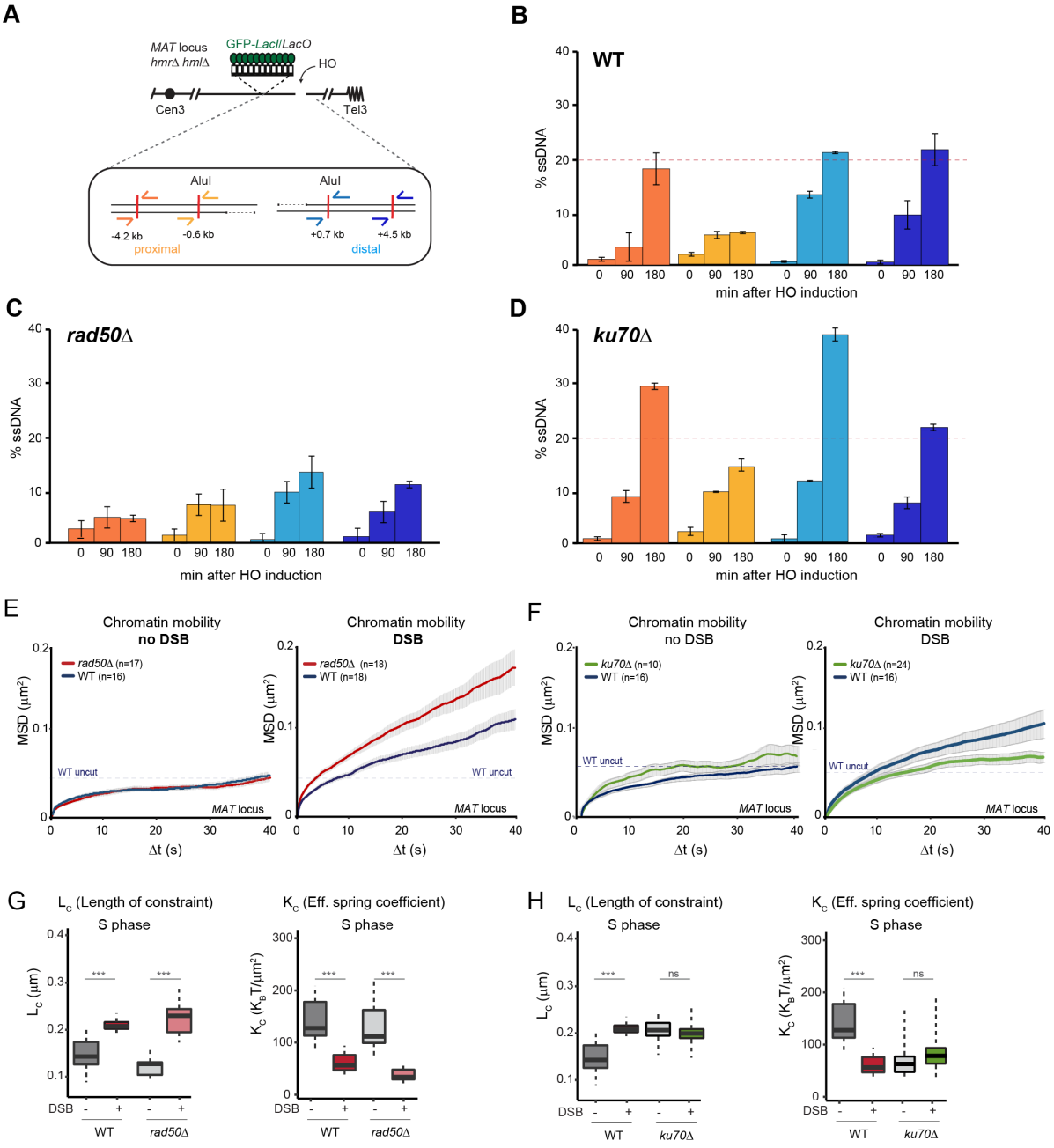

<u>Figure S3. Related to Figure 2:</u> Loss of centromere clustering in *ndc80-1* and loss of the Cep3 phosphoacceptor site does not alter checkpoint induction nor cell cycle distribution

A) Representative images of MTW1-GFP in the *ndc80-1* (GA-10165) temperature sensitive mutant (wild-type at 30°C and mutant at 37°C). Inactivation of Ndc80 triggers kinetochore declustering in S and G2 phase cells. This is a positive control for the absence of declustering observed in *cep3-S575A.*

B) Rad53 phosphorylation after Zeocin treatment (1 h on 250 or 500µg/ml) monitored by Western blot in a wild-type (GA9764) and *cep3-S575A* (GA9767) cells. Mcm2 is used as a loading control (see STAR Methods for details).

C) Flow cytometry analysis of cell-cycle stages in a wild-type (GA9764) and *cep3-S575A* (GA9767) cells before and 2 hours of DSB induction on galactose.

Figure S3. Related to Figure 2: Loss of centromere clustering in *ndc80-1* and loss of the Cep3 phospho-acceptor site does not alter checkpoint induction nor cell cycle distribution

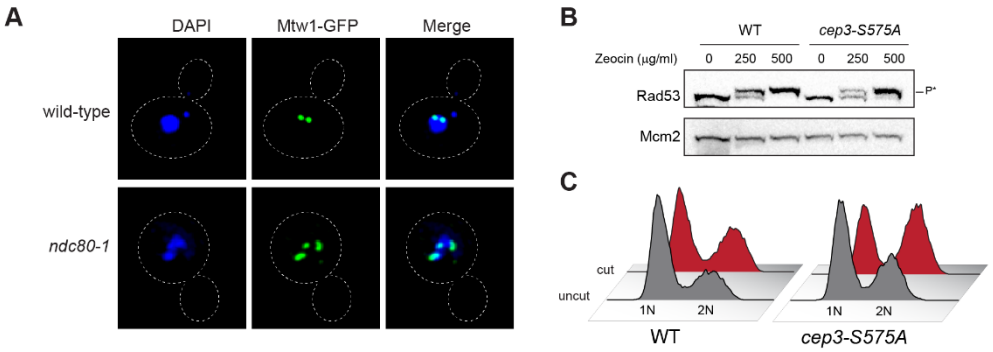

<u>Figure S4. Related to Figure 3</u>: Strand invasion kinetics are delayed in INO80-deficient cells (*arp8Δ*)

A) Scheme of the recombination event monitored by qPCR following galactose induced HO-cleavage at *MAT* on Chr III, and recombination with an ectopic copy of an uncleavable HO cut site otherwise homologous to *MAT,* inserted on Chr V. Primer sequences are designed such that only recombined sequence can be detected.

B) Quantitation of primer extension intermediates in G2/M arrested cells (arrested by 15μg/ml Nocodazole for 2.5h, as in (Dion et al., 2012) according to Koshland laboratory protocol) after DSB induction in GA-7203 (WT) and GA-9946 (*arp8Δ*). The PCR product can only be formed if productive strand invasion and repair has been completed between ChrIII and ChrV, see arrows in a. The corresponding reporter construct was toxic when combined with *nhp6ΔΔ* (data not shown).

Figure S4. Related to Figure 3: Strand invasion kinetics are delayed in INO80-C deficient cells.

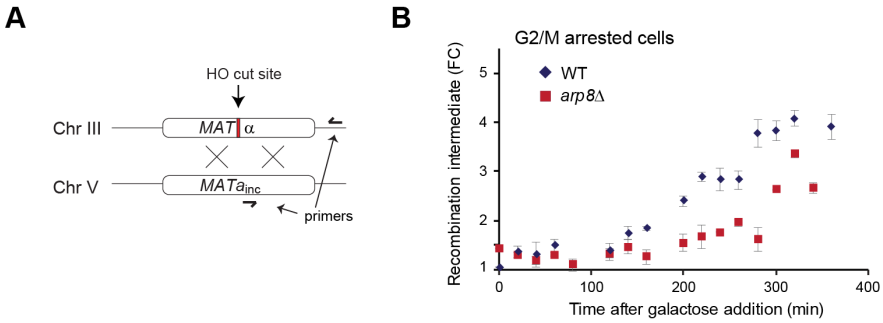

Figure S5. Related to Figure 4: Increased MRX loading in *uls1Δ* cells increases Scc1 levels at a DSB, without extensively affecting DNA end resection.

A) Scheme showing the resection assay that monitors ssDNA at proximal (-0.7kb) and at distal (+0.7) *Alu1* sites in WT (GA-8862), *uls1*Δ (GA-10436) and *Scc1*-degron (GA-10231) strains following 0, 90, and 180 min of HO induction. Results were normalized to an *Alu1*-free region in *SMC2*. At least 2 biological replicates, amplified in triplicate, are presented as mean values ± SEM. In the Scc1-deg strain, Scc1-AIDdegron has been degraded during induction of the DSB as described in Supplemental Figure S1D.

B) Schematic of the *MAT* locus on Chr III, in a strain lacking *HML* and *HMR,* to ensure that there is no intrachromosomal recombination. Probes used for monitoring Chromatin immunoprecipitation (ChIP) are indicated in red. Scc1-3HA ChIP was performed before (0 min) or after (60, 90 min) DSB induction at *MAT* by HO endonuclease, using two qPCR primers at 0.6kb (left) or 4.5kb (right) from the DSB in GA-9194 (WT) and GA-9242 (*rad50Δ*) cells. See STAR Methods for details, including the relevant anti-HA antibody.

C) As B, except that ChIP is for Rad50-PK before (0 min) or after (90, 180 min) DSB induction using indicated probes at 0.6kb (left) or 4.5kb (right) of the HO cut site in GA-9519 (WT) and GA-10643 (*uls1Δ*). See STAR Methods for details, including the relevant anti-PK antibody.

Figure S5. Related to Figure 4: Increased MRX loading in *uls1*Δ cells increases Scc1 levels at a DSB, without extensively affecting DNA end-resection.

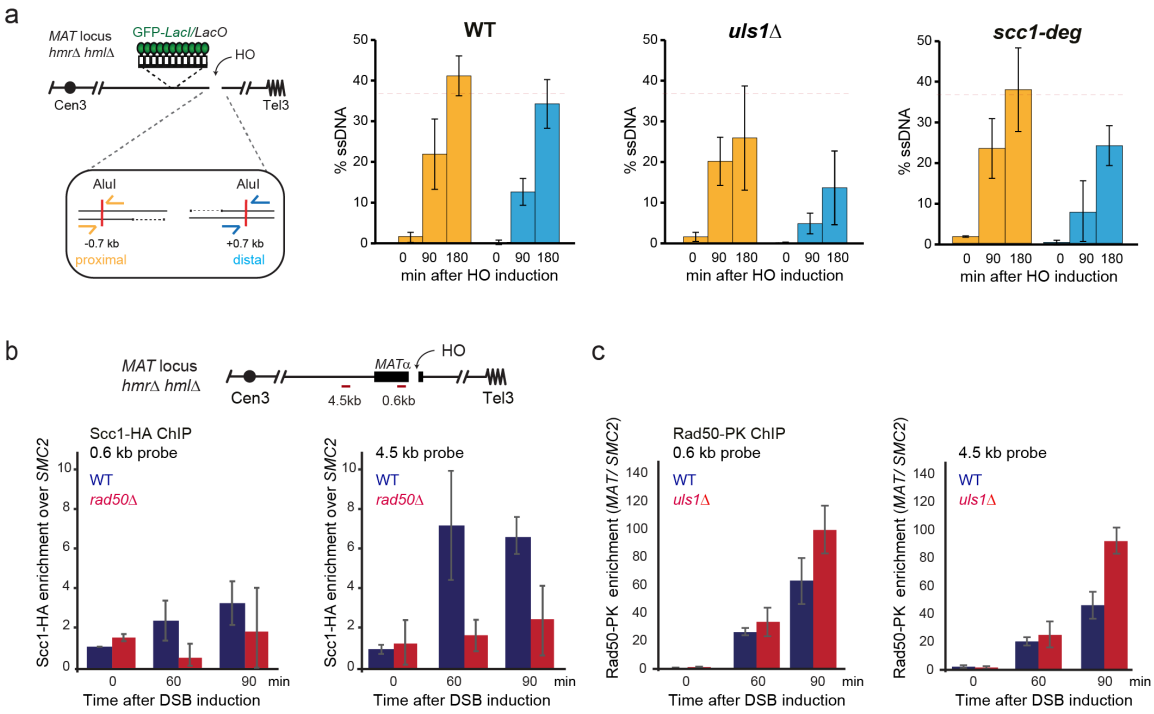

<u>Figure S6. Related to Figure 5 and 6:</u> The *uls1*∆ mutant is proficient in DNA damage checkpoint and survival on Zeocin.

A) Western blot for Rad53 to monitor checkpoint activation through the upshift of the Rad53 band. In strains lacking either Arp8 or Uls1, checkpoint activation by 500 µg/ml Zeocin for 1h is intact. Strains used are GA-8990 (WT), GA-10455 (*arp8Δ*), and GA-10524 (*uls1Δ*), and they were treated with (+) or without (-) 500 µg/ml Zeocin.

B) Ten-fold serial dilutions of WT, *uls1Δ,* and *arp8Δ* cells (same strains as in A) grown on YPAD plates with or without 30 µg/ml of Zeocin for 2 days at 30°C. The *arp8*∆ cells are sensitive to Zeocin while *uls1Δ* cells are not.

C) Rad53 phosphorylation 0, 4 and 5 hours after galactose induction of the HO endonuclease which creates a single DSB at *MAT*. Checkpoint activation is monitored by Western blot in WT and *uls1Δ* cells. P* indicates phosphorylation dependent upshift of Rad53.

Figure S6. Related to Figure 5 and 6: *uls1*Δ is proficient in DNA damage checkpoint and survival

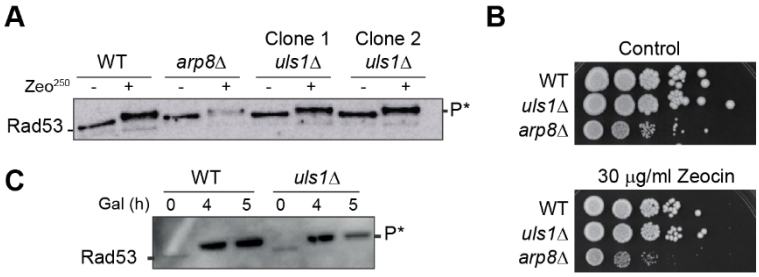

<u>Figure S7. Related to STAR methods:</u> 1.5 sec interval imaging in WT and *cep3-S575A*

(A-B) Calculation and plotting of the MSD analysis based on the time-lapse imaging of a *lacO*-tagged *MAT* locus without induced DSB **(A)** and after DSB induction **(B),** using Δt= 1.5s imaging scheme. The experiment was performed in the following strains and movie numbers: GA-9764 (WT) (n^{DSB}= 48, n^{noDSB}=30) and GA-9767 (*cep3-S575A)* (n^{DSB}=22, n^{noDSB}=30). All cells were in S phase.

Figure S7. Related to STAR Methods: 1.5sec interval imaging in WT and *cep3-S575A*

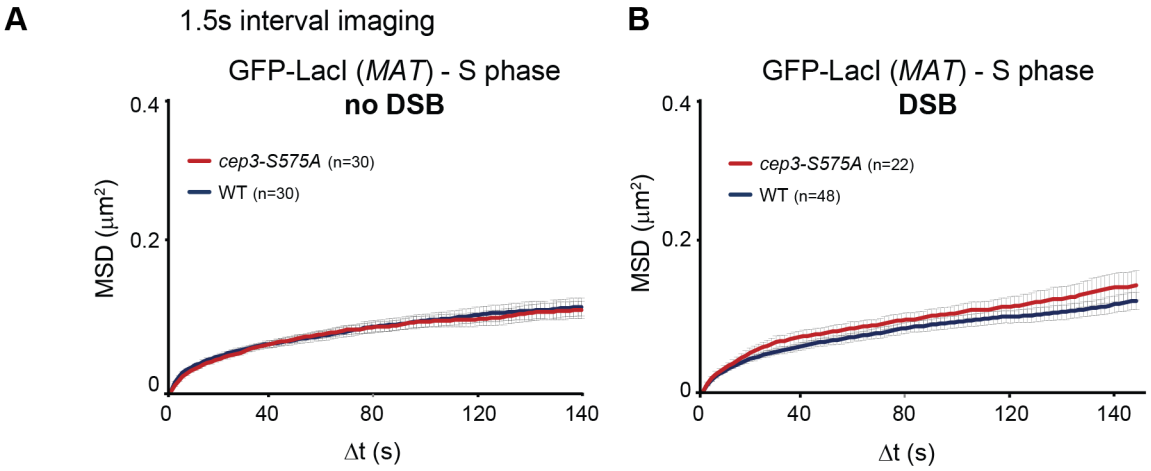

Supplemental Table 1. Related to Figure 1, 2, 3, 4 and 6 : Cleavage efficiency and Rc values

strain/condition	nb movies	Rc (mean +/- SD)	cut efficiency (+/- SD)
wt S phase uncut	25	0.28 +/- 0.01	0
wt S phase cut	28	0.37 +/-0.02	0.81 +/- 0.01
wt G1 phase uncut	26	0.38 +/-0.01	0
wt G1 phase cut	41	0.38 +/-0.02	0.81 +/- 0.01
wt G2 uncut	19	0.25 +/-0.01	0
wt S phase uncut	16	0.24 +/- 0.01	0
wt S phase cut	18	0.37 +/-0.02	0.89 +/- 0.02
scc1 deg S phase uncut	18	0.37 +/- 0.01	0
scc1 deg S phase cut	18	0.61 +/-0.03	0.80 +/-0.03
rad50 S phase uncut	17	0.24 +/- 0.01	0
rad50 S phase cut	18	0.47 +/- 0.02	0.82 +/- 0.04
Scc1 CHIP wt	xxx	xxx	0.89 +/- 0.02
Scc1 CHIP *rad50*	xxx	xxx	0.84 +/- 0.004
cep3-S575A S phase uncut	86	0.30 +/- 0.009	0
cep3-S575A S phase cut	154	0.38 +/- 0.01	0.78 +/- 0.03
cep3-S575A G1 phase uncut	27	0.32 +/- 0.01	0
cep3-S575A G1 phase cut	22	0.37 +/- 0.02	0.78 +/- 0.03
arp8 S phase uncut	19	0.23 +/-0.01	0
arp8 S phase cut	19	0.22 +/- 0.01	0.60 +/- 0.09
arp8 uncut strand invasion	xxx	xxx	0
arp8 cut strand invasion	xxx	xxx	0.80 +/- 0.03
wt uncut strand invasion	xxx	xxx	0
wt cut strand invasion	xxx	xxx	0.93 +/- 0.002
uls1 S phase uncut	15	0.30 +/-0.02	0
uls1 S phase cut	17	0.25 +/- 0.02	0.82 +/- 0.02
rad50 CHIP wt	xxx	xxx	0.91 +/-0.02
rad50 CHIP *uls1*	xxx	xxx	0.86 +/- 0.02
wt - zeo Fig.5	25	0.28 +/- 0.01	xxxx
wt + zeo Fig.5	15	0.42 +/- 0.03	xxxx
uls1 - zeo Fig.5	15	0.30 +/-0.02	xxxx
uls1 + zeo Fig.5	18	0.37 +/-0.02	xxxx
wt uncut Fig.6	18	0.23+/- 0.009	0
wt cut Fig.6	16	0.29 +/- 0.01	0.87 +/- 0.02
uls1 uncut Fig.6	12	0.23 +/- 0.009	0
uls1 cut Fig.6	20	0.33 +/- 0.01	0.88 +/- 0.03

Cheblal et al. Supplemental Table 2. Related to STAR methods: Strains used in this study.

Strain number	Strain background	Genotype	Origin
GA 1081	JKM179	*hml::ADE1 hmr::ADE1 ade3::GALHO*	Jim Haber's laboratory
GA 7203	JKM179	*hml::ADE1 hmr::ADE1 ade3::GALHO MATinc-URA3::TRP1 ade1 leu2-3,112 lys5 trp1::hisG ura3-52*	Jim Haber's laboratory
GA8862	JKM179	*hml::ADE1 hmr::ADE1 ade3::GALHO CFP-NUP49 GFP-LacI::LEU2 MAT::LacO repeats ::TRP1 Rad52-Ruby2::kan ade1 leu2-3,112 lys5 trp1::hisG ura3-52*	Published in Amitai, Seeber *et al.* 2017 Cell Reports
GA 8921	JKM179	GA 9948 with *arp8::natMX4*	This study
GA 8990	W303	*MATa-inc, lys2::natMX4 AVT2::lys-HOcs::kanMX6 (Ch V about 30kb left arm) COS9::TRP1-ys2 (ChXI 15kb) ade3::GAL-HO URA3::TK BAR1::LEU2 ade2-1 trp1-1 his3-11,15 ura3-1 leu2-3,112*	Published in Donniani *et al.* 2013, PNAS original name LSY2743-1.1
GA 8991	W303	*MATa-inc, lys2::natMX4 AVT2::lys-HOcs::kanMX6 ade3::GAL-HO URA3::TK BAR1::LEU2 (no donor) ade2-1 trp1-1 his3-11,15 ura3-1 leu2-3,112*	Published in Donniani *et al.* 2013, PNAS original name LSY2751-1.6
GA 9070	W303	*GA 8990 with pol32::hphMX4*	This study
GA 9194	JKM179	*GA 8862 with SCC1-3HA-URA3*	This study
GA 9242	JKM179	*GA 9194 with rad50::natMX4*	This study
GA 9519	JKM179	*hml::ADE1 hmr::ADE1 ade3::GALHO CFP-NUP49 GFP-LacI::LEU2 MAT::LacO repeats ::TRP1 RAD50-PK9-kan*	Published in Marcomini et al. 2018 Cell report
GA 9764	JKM179	*hml::ADE1 hmr::ADE1, ura3::CUP1-GFP-LacI-URA3 NUP49-mCherry-hphMX, ARS313-LacO repeats-TRP1 ade3::GAL-HO ade1 leu2-3,112 lys5 trp1::hisG ura3-52*	Published in Strecker *et al.* 2016, NCB original name #3165
GA 9767	JKM179	*hml::ADE1, hmr::ADE1, ura3::CUP1-GFP-LacI-URA3 NUP49-mCherry-hphMX, ARS313-LacO repeats-TRP1 ade3::GAL-HO, cep3-S575A ade1 leu2-3,112 lys5 trp1::hisG ura3-52*	Published in Strecker *et al.* 2016, NCB original name #3941
GA 9905	JKM179	*GA 9764 with MTW1-ECFP-kanMX*	This study
GA 9906	JKM179	*GA 9767 with MTW1-ECFP-kanMX*	This study
GA 9946	JKM179	*GA 7203 arp8::natMX4*	This study
GA 9948	JKM179	*hml::ADE1 hmr::ADE1 ade3::GALHO CFP-NUP49 GFP-LacI::LEU2 MAT::LacO repeats ::TRP1 Rad52-Ruby2::kan ade1 leu2-3,112 lys5 trp1::hisG ura3-52*	Published in Marcomini *et al.* 2018, Cell report
GA 10165	W303	*MATa ura3-1:TUB1-CFP:URA3 leu2,3-112 his3-11 trp1-1 ade2-1 can1-100 bar1□ MTW1-3GFP:HIS3 ndc80-1*	Published in Pinsky *et al.* 2005, NCB original name SBY4341
GA 10175	W303	*HTB2-HiBiT MCM4-HiBiT ade2-1 trp1-1 his3-11 his3-15 ura3-1 leu2-3 leu2-112*	This study
GA 10231	JKM179	*GA 8862 with scc1-3xmini-degron:: natNT OsTIR1-9Myc-URA3*	This study
GA 10316	W303	*GA 8990 nhp6aΔ nhp6bΔ by CRISPR-Cas9*	This study
GA 10436	JKM179	*GA 9948 uls1::natMX4*	This study
GA 10455	W303	*GA 8990 arp8Δ by CRISPR-Cas9*	This study
GA 10524	W303	*GA 8990 uls1::hph*	This study
GA 10643	JKM179	*GA 10643 with uls1::hph*	This study
GA 10677	JKM179	*GA 9194 with uls1::natMX4*	This study
GA 10676	W303	*GA 10175 with uls1::natMX4*	This study
GA 10706	JKM179	*GA 1081 with MET10::LacO repeats GFP-LacI-URA3*	This study
GA 10718	JKM179	*GA 10706 with uls1::natMX4*	This study
GA 4467	JKM179	*GA 1081 ris1-13myc:KanMX6*	This study
GA 1954	JKM179	*hml::ADE1 hmr::ADE1 ade3::GALHO ku70::URA3 NUP49-GFP(no more URA3) GFP-Lacrep(::LEU2) MAT::LacI*	Gasser laboratory

Supplemental Table 3. Related to Figure 1, 2, 3, 4, 5 and 6: Stastistical Analysis

Kc and Lc values extracted from imaging and tracking data

Statistical test used : Kolmogorov-Smirnov

p<0.05 *

p<0.01 **

p<0.001 ***

Kc (Eff. Spring Coefficient)			**Lc (Length of constraint)**		
Comparison	p value		Comparison	p value	
WT G1 vs S	0.0004	***	WT G1 vs S	0.0004	***
WT G1 vs G2	0.0004	***	WT G1 vs G2	0.0008	***
WT S uncut vs cut	0.012	*	WT S uncut vs cut	0.023	*
WT G1 uncut vs cut	0.63	ns	WT G1 uncut vs cut	0.6	ns
cep3-S575A S uncut vs cut	0.00023	***	*cep3-S575A* S uncut vs cut	0.00018	***
S uncut (WT vs *cep3-S575A)*	0.0033	**	S uncut (WT vs *cep3-S575A)*	0.015	**
S cut (WT vs *cep3-S575A)*	0.083	ns	S cut (WT vs *cep3-S575A)*	0.41	ns
arp8 S uncut vs cut	0.64	ns	*arp8* S uncut vs cut	0.63	ns
scc1 nodegron uncut vs cut	1.23E-06	***	scc1 nodegron uncut vs cut	2.3E-06	***
scc1 degron uncut vs cut	2.9E-06	***	scc1 degron uncut vs cut	2.9E-06	***
wt uncut vs cut	1.8E-06	***	wt uncut vs cut	1.8E-06	***
uls1 uncut vs cut	0.6	ns	*uls1* uncut vs cut	0.6	ns
S uncut Scc1 (nodegron vs degron)	9.07E-10	***	S uncut Scc1 (nodegron vs degr	9.07E-10	***
S cut Scc1 (nodegron vs degron)	1.08E-05	***	S cut Scc1 (nodegron vs degron)	1.08E-05	***
nhp6 ΔΔ (0 vs 300 μg/ml Zeocin)	0.983372	ns	*nhp6 ΔΔ* (0 vs 300 μg/ml Zeocin)	0.983372	ns
WT (0 vs 250 μg/ml Zeocin)	0.000127		WT (0 vs 250 μg/ml Zeocin)	0.000127	***
uls1 (0 vs 250 μg/ml Zeocin)	0.007909		*uls1* (0 vs 250 μg/ml Zeocin)	0.000471	***
WT (uncut vs cut) Fig.6B	0.03	*	WT (uncut vs cut) Fig.6B	0.03	*
uls1 (uncut vs cut) Fig.6C	0.001	***	*uls1* (uncut vs cut) Fig.6C	0.001	***

a (anomalous exponenent)		
Comparison	p value	
WT S vs G2	0.01	**
WT G1 vs G2	0.0004	***
WT S uncut vs cut	0.9	ns
cep3-S575A S uncut vs cut	0.4	ns
arp8 S uncut vs cut	0.6	ns
nhp6 ΔΔ (0 vs 300 μg/ml Zeocin)	0.019	*

Distances pore -MTW1 foci			**Spot Volume - Expansion**		
Statistical test used : t-test			Statistical test used : t-test		
p<0.05 *			p<0.05 *		
p<0.01 **			p<0.01 **		
p<0.001 ***			p<0.001 ***		
Comparison	p value		Comparison	p value	
WT vs Nocodazole	2.41E-06	***	WT (0 vs 250 μg/ml Zeocin) Fig.5	3.77E-41	***
WT (0 vs 250 mg/ml Zeocin)	0.15	ns	*uls1* (0 vs 250 μg/ml Zeocin) Fig.	9.29E-37	***
WT (0 vs 500 mg/ml Zeocin)	0.43	ns	WT (uncut vs cut) Fig.6D	0.004	***
cep3-S575A (0 vs 250 μg/ml Zeocin)	0.003	down	*uls1* (uncut vs cut) Fig.6D	0.01	**
cep3-S575A (0 vs 500 μg/ml Zeocin)	0.94	ns			

Supplemental Table 4. Related to Figure 3, 4 and 6 : Primer information

BIR assay PCR primers

Name	Sequence
P1 (SG-9902):	GACCATATCCACCAGTGAGCCCGC
P2 (SG-9903):	GGGTGTCTTGAAAGCCGGCGCAAC
C1 (SG-9900):	GGGCCAGGTCAACCCAACATCTACC
C2 (SG-9901):	CGCTCGGTTTCGATCCGAGGACATC
D1 (SG-9898):	CCAACGATAAAGGCCTTTGCCGCGG
D2 (SG-9899):	GGGGATCGCAGTGGTGAGTAACC
P1 (SG-9902):	GACCATATCCACCAGTGAGCCCGC
P2 (SG-9903):	GGGTGTCTTGAAAGCCGGCGCAAC

Real Time PCR primers

Name	Sequence	Target
SG-525	AATTGGATTTGGCTAAGCGTAATC	*SMC2*
SG-526	CTCCAATGTCCCTCAAAATTTCTT	
SG 8450	AAGGGCAAGTTCTCCACAGA	*ISB5*
SG8451	CAGCCACCAGTTCATCATTG	
SG-2285	AATATGGGACTACTTCGCGCAACA	HOcs (*MAT*)
SG-2286	CGTCACCACGTACTTCAGCATAA	
SG-8444	CCCAAACAAAACCCAGACAT	-0.6kb from HOcs
SG-8445	TGCTGGATTTAAACTCATCTGTG	
SG 10854	GTAGTAGTGAGTTGAGATGTTG	-0.7kb from HOcs
SG 10855	CACAGATGAGTTTAAATCCAGC	
SG-8440	CTCTCCCTTGGTGTTTCCAA	+0.7kb from HOcs
SG-8441	GAAAAGATTGGCCGTCAAAA	
SG-8448	CAATGCCTTCCTTCTCCAAA	-4.2kb from HOcs
SG-8449	ACCTGAGCGACGAGAAATTG	
SG-8459	TGCGATGAAGTCAACGAATTA	+4.5kb from HOcs
SG-8460	GAGCACTTTTACCGGCAGTT	
SG 9385	TCGAAGCCTGCTTTCAAAAT	- 0.6 kb from HOcs
SG 9386	TCGAGAGGAAGGAACAGGAA	
SG 7704	GTCGATCGCCGTTCTAAACA	- 1.6 kb from HOcs
SG 7705	GGCCCAACTAGAAGCCATAC	
SG 1883	AACTGGCAAAGGTCTATGTAAAGATTTA	- 4.5 kb from HOcs
SG 1884	AATGGATGAAGATGATGACGTTGAC	

CHAPTER IV: UBIQUITIN AND THE SMALL UBIQUITIN-RELATED MODIFIER (SUMO) ROLE IN DNA REPAIR

Summary

In this fourth Chapter, I will discuss the roles of two post-translational modifications (PTMs) in the regulation of DNA repair pathway choice in budding yeast. This concerns the covalent attachment of Ubiquitin or the small ubiquitin-related modifier protein (SUMO) to lysine residues in response to DNA damage. Several laboratories have studied how sumoylation regulates the processing of DNA damage and this posttranslational modification was proven to be essential in the repair of telomeric breaks, double-strand breaks as well as collapsed forks.

Here I review research that has revealed how sumoylation regulates and coordinate DNA repair processes in the nuclear space. More specifically, I also describe how a tight interplay between these two modifications is essential to maintain genomic integrity.

Mechanism of Ubiquitination and SUMOylation

Ubiquitination was originally discovered as a means to target modified substrates to the proteasome machinery and thereby regulate protein turnover. Since then, several studies have shown that it also regulates protein activity without targeting the modified protein for degradation. Ubiquitin is a small protein made of 76 amino acid residues that is attached through its C-terminal glycine residue to a lysine in the target protein. The ubiquitin protein can be conjugated to the target protein as a monomer or as a polymeric chain that results from the repetitive addition of Ubiquitin. There are also different linkages for ubiquitin chains, for example, Ubiquitin chains that are linked through their Lys-K48 has been shown to target the modified protein to the proteasome, while Lys 63-linked chains tend to regulate protein-protein interactions.

There are several ubiquitin-like proteins (UBLs) that similarly modify their substrate through a highly conserved cascade of enzymatic reactions mediated by E1, E2 and E3 ligases (add scheme). One particular UBL, the small ubiquitin-related modifier (SUMO) has been shown to regulate several cellular mechanisms including the DNA damage response. In contrast to vertebrates, which have two types of SUMO: SUMO-1 and the highly related proteins SUMO-2 and SUMO-3 (SUMO2/3), that functions redundantly, the budding yeast has a single SUMO protein called Smt3. Like Ubiquitin, SUMO residues can be conjugated as a monomer or as a polymeric chain to the target protein. While the role of SUMOylation in general has been extensively studied, however, the function of specific polySUMO chains remains to be further characterized.

In addition to their distinct roles and pathways of modification, there is a clear crosstalk between SUMO and Ubiquitin. First, there exist SUMO-targeted Ubiquitin ligases (STUbLs), which are ubiquitin E3 ligases that can specifically target and bind sumoylated proteins through a SUMO-interacting motif (SIM), catalyzing the ubiquitination of the sumoylated substrates. There are two STUbLs in yeast, Uls1 and Uls2 (also called Slx5/Slx8 complex) and three in mammalian cells (SHPRH, RNF111 and RNF4). Intriguingly, sumoylation and STUbLs are often involved in DNA repair pathways.

The role of SUMO in DNA repair and subnuclear localization.

The role of SUMO in DNA DSB repair

As discussed in the Introduction, it was shown that subnuclear positioning influences DNA repair. Here we will discuss some major findings that implicate the SUMO machinery in this process. When imaging the behavior of a GFP-tagged *MAT* locus in *S. cerevisiae*, the Gasser laboratory observed that an induced persistent DSB shifts to the nuclear periphery, more specifically either to the nuclear pore complex (NPC) or to the inner nuclear membrane SUN domain protein Mps3 (Horigome et al., 2014; Nagai et al., 2008).

Interestingly, Nagai *et al.* observed an enrichment of the SUMO-targeted Ubiquitin ligase (STUBL) complex Slx5/8 at the *MAT* locus after DSB induction. Moreover, they showed that Nup84, an NPC component, and Slx5/8 physically interact, suggesting that Slx5/8 might target the induced DSB to the NPC (Nagai et al., 2008). Intriguingly, in Slx5/8 deficient mutants, they reported an increase in DNA recombination foci as well as in gross chromosomal rearrangement. This observation suggested that Slx5/8 target DSB to the NPC to prevent inappropriate genomic rearrangements. Interestingly, Sxl5/8 has multiple SUMO-interacting motifs (SIMs) and its ubiquitination activity is stimulated by polySUMO chains (Mullen and Brill, 2008).

Later, the Gasser laboratory showed that DSB relocation to the NPC is dependent on the SUMO-targeted Ubiquitin ligase (STUBL) complex Slx5/8 (Horigome et al., 2016). They further reported that the targeting of a DSB to the NPC depends on the SUMO E3 ligase Mms21 in complex with SMC5/6, which deposits mono SUMO on the DNA repair protein Rad52. Moreover, they showed that the E3 SUMO ligase Siz2 subsequently creates a polySUMO chain on the targets proteins that is recognized by Slx5/8. More specifically, the authors showed that a lexA-Slx5 fusion was able to relocate a locus to the nuclear pore in G1 cells in the absence of damage, suggesting that Slx5 is sufficient for DSB localization to the NPC. Consistent with the previous observations (Nagai et al., 2008), Horigome *et al.* showed that DSB relocation to the NPC enabled appropriate repair by NHEJ or BIR.

On the other hand, a second mechanism is functional in S-phase cells whereby DSB are localized to the inner nuclear membrane protein Mps3. This was shown to be mediated by the SMC5/6 in complex

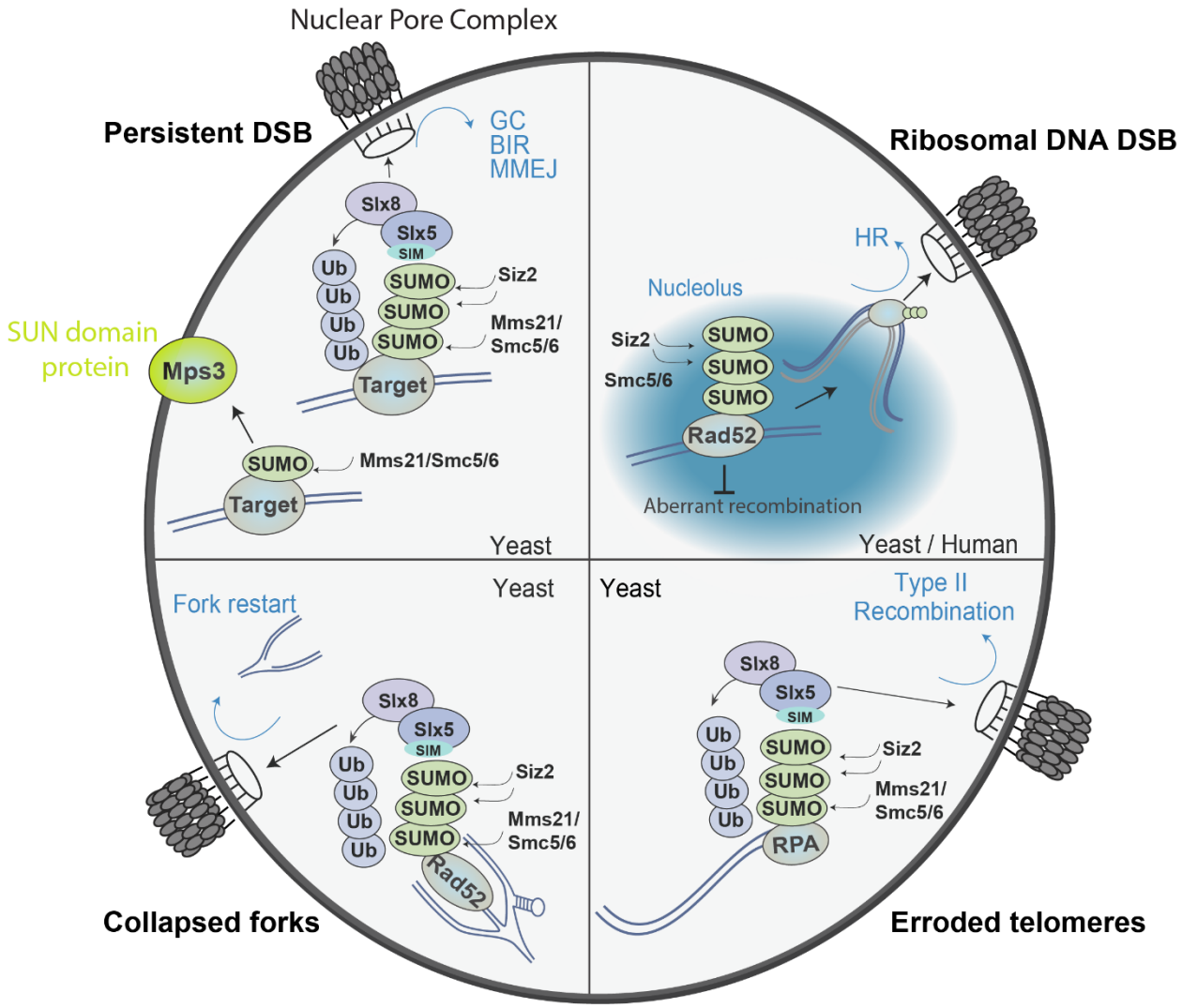

<u>Figure 4:</u> SUMO implication in DNA repair and spatial positioning

The extent of SUMO chain deposition affects spatial sequestration of a canonical DSB, rDNA DSB, collapsed forks and eroded telomeres. SUMO-mediated relocation to the nuclear pore complex affects DNA repair pathway choice.

with Mms21 that deposit a monoSUMO residue on a target protein at the break independently of Slx5/8 **(Figure 4).**

The role of SUMO in rDNA

This mechanism was further extended to DSB in the ribosomal DNA (rDNA). The Lisby laboratory, have observed that DSB in the rDNA relocate to the nucleolar periphery (Torres-Rosell et al., 2007). This nucleolar extrusion is dependent on Rad52 sumoylation and SMC5/6 activity. Mutations that suppresses these activities, led to a loss of Rad52 foci relocation, and of rDNA hyper-recombination and excision of extrachromosomal rDNA circle. This work suggested that sumoylation is a key player in nucleolar dynamics, more specifically in allowing break to repair outside of repetitive DNA. However, Horigome *et al.* showed that DSB relocation to the NPC was independent of Rad52 (Horigome et al., 2014). Taken together these observations suggest that it may be the extent of sumoylation rather than the specific substrate that is critical for site specific relocation to the nuclear or nucleolar periphery **(Figure 4).**

Interestingly, a recent study showed that replication-dependent damage in the rDNA associates with the NPC in a DNA damage checkpoint kinase Tel1 dependent manner. Moreover, they suggested that this relocation is due to replication fork block and subsequent DSB formation. This relocation was shown to prevent improper recombination repair that could induce repeat instability in the rDNA (Horigome et al., 2019).

The role of SUMO in the repair of replication fork collapse

These observations have been shown to be relevant as well for collapsed replication forks (Nagai et al., 2008). Triplet CAG repeat sequences interfere with replication and DNA repair machinery leading to repeat instability that arises in S phase thanks to an inappropriate recombination event. In a recent study the Freudenreich laboratory have shown that expanded CAG repeats relocalize to the NPC in a Slx5/8 dependent manner. They also observed Rad52 sumoylation and ubiquitination and its subsequent degradation by the ubiquitin proteasome system. This degradation then enables fork restart and decreases aberrant recombination (Su et al., 2015). A recent follow up of Su *et al.* showed that the relocalization of stalled forks induced by CAG repeats to the NPC depends on the Mms21 SUMO ligase activity in complex with Smc5/6, as shown in Horigome *et al.* 2016 for canonical DSBs (Whalen and Freudenreich, 2020). Moreover, they confirmed that that RPA, Rad52 and Rad59 are all

targets of sumoylation, which in turn mediate the relocation of damage to the NPC, where Rad51 binding enables fork restart through unequal strand invasion **(Figure 4).**

The role of SUMO at telomeres

Interestingly, this relocation appears to happen at telomeres as well. In budding yeast the inactivation of telomerase causes telomere erosion and induces telomere relocation to the NPC. In a recent study, Churikov *et al.* reported a mechanism similar to that discussed above. They found that Siz2-dependent sumoylation of RPA at eroded telomeres triggers telomere relocation to the NPC through Slx5/8. Similar to Whalen *et al.,* the authors speculate that the targeting to the nuclear pore is a way to desumoylate eroded telomeres (through the degradation of sumoylated proteins in a STUbL dependent manner), giving the telomere another chance for repair (Churikov et al., 2016) **(Figure 4).**

Subsequent work from the Gasser laboratory investigated the behavior of an internal DSB that is flanked on one side by telomeric-like TG repeats (Marcomini et al., 2018). In this study, we showed that, in contrast to a canonical DSB where the relocation to the pore was shown to be Slx5/8 dependent, the TG-flanked DSB relocation was dependent on another yeast STUbL, Uls1. We propose that the already reported recognition of poly-sumoylated Rap1 by Uls1 (Lescasse et al., 2013) may lead to the ubiquitination and degradation of Rap1 at telomeres. This may happen at internal TG repeats when they are found near a DSB **(Figure 5)** or other targets may be degraded, such as Cohesin or MRX. Indeed, in the Marcomini *et al.* study we observed a loss of MRX binding on the TG-side of the DSB. It had been already shown that Mre11, one component of the MRX complex, is sumoylated (Cremona et al., 2012). The absence of MRX made the TG-flanked DSB increase its dynamic movement, and was counteracted by Uls1 deletion. This observation suggested that the loss of Uls1 might restore MRX binding at the TG-flanked DSB (Cheblal, in press). We speculate that the Uls1 STUbL ubiquitinates poly-sumoylated MRX (Mre11) at certain breaks, and targets it for degradation. In line with this hypothesis, Marcomini *et al.* showed an increase in the rate of imprecise NHEJ over translocations in Uls1-deficient cells, probably reflecting MRX accumulation at the DSB and suppression of DSB movement (Cheblal, in press; Marcomini et al., 2018)**(Figure 5).**

The role of SUMO in chromatin motion

How translocation of damage to the NPC occurs is still unclear. A recent work in *Drosophila melanogaster* suggested a model in which heterochromatic DSBs induce the formation of nuclear actin filaments that connects repair sites to the nuclear periphery (Caridi et al., 2017). This relocation was shown to

happen through a directed motion in Smc5/6- associated myosin dependent manner. This work suggest that the SUMO modifying system might play a critical role in the way chromatin moves in the nucleoplasm. Given that directed motion has not been observed in yeast, and that the radius of constraint of a damaged site in yeast encompasses 47% of the nuclear volume, it is easy to imaging that in yeast there is no need for actin fibers or directed motion, for DSBs to "collide" productively with the NPC and be further processed. Sumoylation clearly would be one means to tether damage once a spontaneous collision occurs.

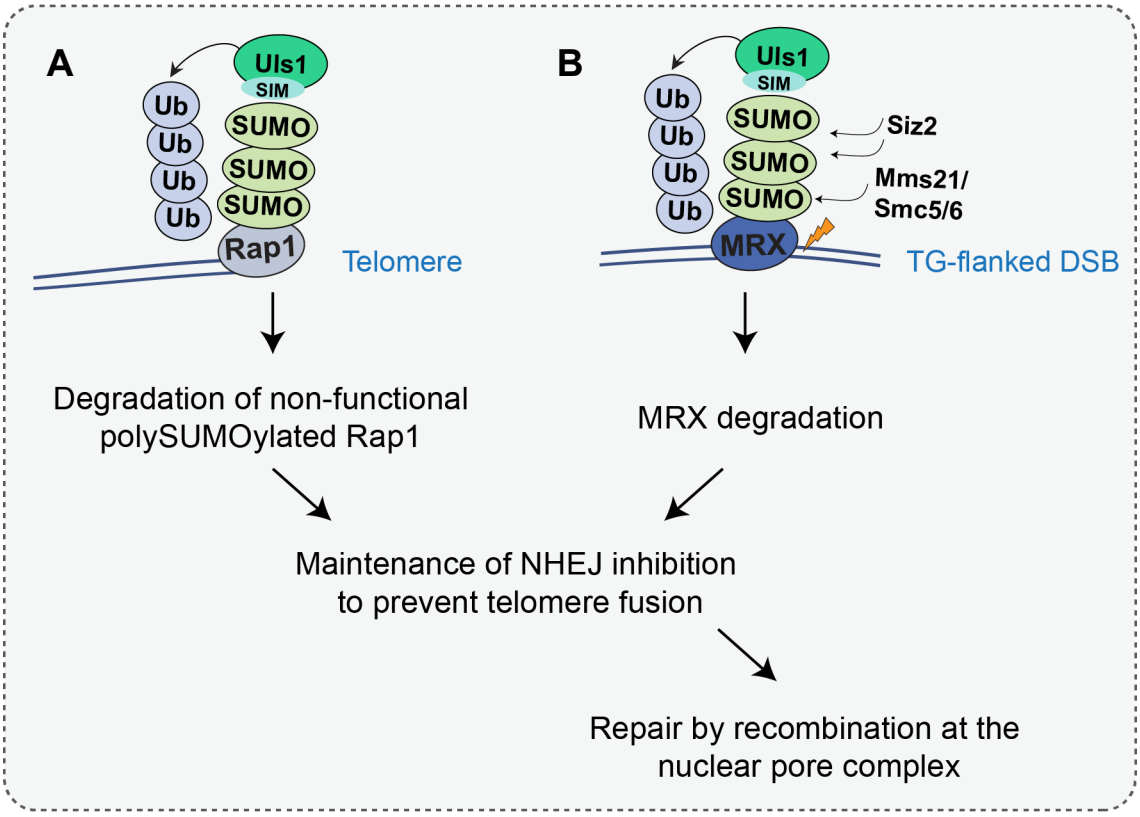

<u>Figure 5:</u> Proposed model of the regulation of telomere maintenance by the STUbL Uls1

(A) Inhibition of NHEJ at telomeres is crucial to prevent telomere fusion, this is ensured by Rap1. The accumulation of non-functional poly-SUMOylated Rap1 at telomeres is cleared by Uls1 to ensure the continuous efficiency of NHEJ inhibition (Lescasse et al., 2013). **(B)** At a TG-flanked DSB, Uls1 ubiquitinates poly-SUMOylated MRX and targets it for degradation. MRX clearance from the break inhibit NHEJ and enable repair by recombination at the nuclear pore complex (Marcomini et al., 2018).

REFERENCES

Caridi, P.C., Delabaere, L., Zapotoczny, G., and Chiolo, I. (2017). And yet, it moves: nuclear and chromatin dynamics of a heterochromatic double-strand break. Philos Trans R Soc Lond B Biol Sci *372*.

Churikov, D., Charifi, F., Eckert-Boulet, N., Silva, S., Simon, M.N., Lisby, M., and Geli, V. (2016). SUMO-Dependent Relocalization of Eroded Telomeres to Nuclear Pore Complexes Controls Telomere Recombination. Cell reports *15*, 1242-1253.

Horigome, C., Bustard, D.E., Marcomini, I., Delgoshaie, N., Tsai-Pflugfelder, M., Cobb, J.A., and Gasser, S.M. (2016). PolySUMOylation by Siz2 and Mms21 triggers relocation of DNA breaks to nuclear pores through the Slx5/Slx8 STUbL. Genes Dev *30*, 931-945.

Horigome, C., Oma, Y., Konishi, T., Schmid, R., Marcomini, I., Hauer, M.H., Dion, V., Harata, M., and Gasser, S.M. (2014). SWR1 and INO80 chromatin remodelers contribute to DNA double-strand break perinuclear anchorage site choice. Mol Cell *55*, 626-639.

Horigome, C., Unozawa, E., Ooki, T., and Kobayashi, T. (2019). Ribosomal RNA gene repeats associate with the nuclear pore complex for maintenance after DNA damage. PLoS Genet *15*, e1008103.

Lescasse, R., Pobiega, S., Callebaut, I., and Marcand, S. (2013). End-joining inhibition at telomeres requires the translocase and polySUMO-dependent ubiquitin ligase Uls1. The EMBO journal *32*, 805-815.

Marcomini, I., Shimada, K., Delgoshaie, N., Yamamoto, I., Seeber, A., Cheblal, A., Horigome, C., Naumann, U., and Gasser, S.M. (2018). Asymmetric Processing of DNA Ends at a Double-Strand Break Leads to Unconstrained Dynamics and Ectopic Translocation. Cell reports *24*, 2614-2628 e2614.

Mullen, J.R., and Brill, S.J. (2008). Activation of the Slx5-Slx8 ubiquitin ligase by poly-small ubiquitin-like modifier conjugates. J Biol Chem *283*, 19912-19921.

Nagai, S., Dubrana, K., Tsai-Pflugfelder, M., Davidson, M.B., Roberts, T.M., Brown, G.W., Varela, E., Hediger, F., Gasser, S.M., and Krogan, N.J. (2008). Functional targeting of DNA damage to a nuclear pore-associated SUMO-dependent ubiquitin ligase. Science *322*, 597-602.

Su, X.A., Dion, V., Gasser, S.M., and Freudenreich, C.H. (2015). Regulation of recombination at yeast nuclear pores controls repair and triplet repeat stability. Genes Dev *29*, 1006-1017.

Torres-Rosell, J., Sunjevaric, I., De Piccoli, G., Sacher, M., Eckert-Boulet, N., Reid, R., Jentsch, S., Rothstein, R., Aragon, L., and Lisby, M. (2007). The Smc5-Smc6 complex and SUMO modification of Rad52 regulates recombinational repair at the ribosomal gene locus. Nature cell biology *9*, 923-931.

Whalen, J.M., and Freudenreich, C.H. (2020). Location, Location, Location: The Role of Nuclear Positioning in the Repair of Collapsed Forks and Protection of Genome Stability. Genes (Basel) *11*.

CHAPTER V: ASYMMETRIC PROCESSING OF DNA DSB ENDS LEAD TO UNCONSTRAINED DYNAMICS AND ECTOPIC TRANSLOCATION

Isabella Marcomini, Kenji Shimada, Neda Delgoshaie, Io Yamamoto, Andrew Seeber, **Anaïs Cheblal**, Chihiro Horigome, Ulrike Naumann, and Susan M. Gasser

Asymmetric Processing of DNA Ends at a Double-Strand Break Leads to Unconstrained Dynamics and Ectopic Translocation. Cell Reports, 2018. DOI: 10.1016/j.celrep.2018.07.102

Summary

Multiple pathways regulate the repair of double-strand breaks (DSBs) to suppress potentially dangerous ectopic recombination. Both sequence and chromatin context are thought to influence pathway choice between non-homologous end-joining (NHEJ) and homology-driven recombination. To test the effect of repetitive sequences on break processing, we have inserted TG-rich repeats on one side of an inducible DSB at the budding yeast MAT locus on chromosome III.

Five clustered Rap1 sites within a break-proximal TG repeat are sufficient to block Mre11-Rad50-Xrs2 recruitment, impair resection, and favor elongation by telomerase. The two sides of the break lose end-to-end tethering and show enhanced, uncoordinated movement. Only the TG-free side is resected and shifts to the nuclear periphery. In contrast to persistent DSBs without TG repeats that are repaired by imprecise NHEJ, nearly all survivors of repeat-proximal DSBs repair the break by a homology-driven, non-reciprocal translocation from ChrIII-R to ChrVII-L. This suppression of imprecise NHEJ at TG-repeat-flanked DSBs requires the Uls1 translocase activity.

My contribution to this manuscript was to analyze chromatin dynamics at a TG-flanked DSB in Uls1-deficient cells as compared to wild-type conditions.

Article

Cell Reports

Asymmetric Processing of DNA Ends at a Double-Strand Break Leads to Unconstrained Dynamics and Ectopic Translocation

Graphical Abstract

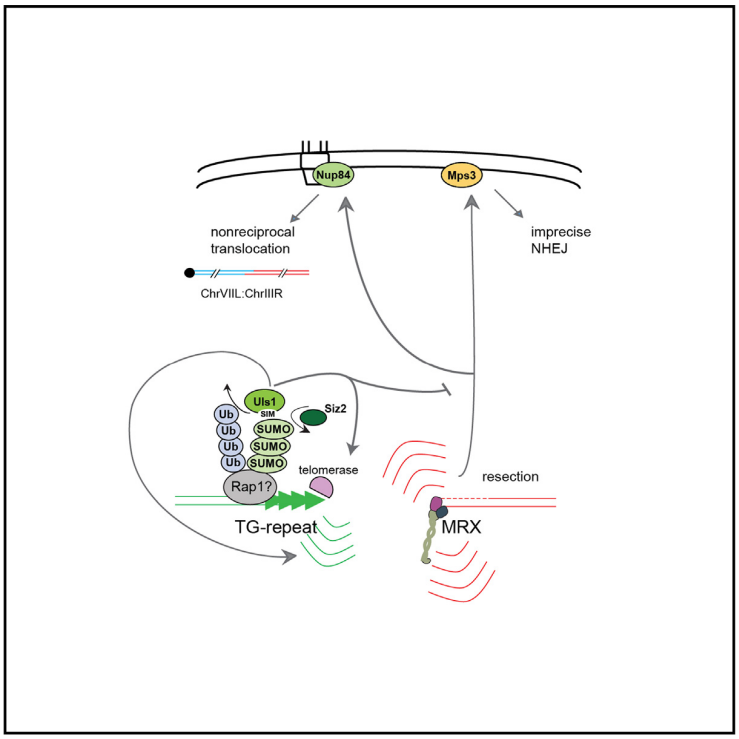

Authors

Isabella Marcomini, Kenji Shimada, Neda Delgoshaie, ..., Chihiro Horigome, Ulrike Naumann, Susan M. Gasser

Correspondence

susan.gasser@fmi.ch

In Brief

Marcomini et al. show that the presence ofinterstitial telomeric repeat sequences near a double-strand break alters the outcome of repair. A TG-flanked break loads MRX asymmetrically, supports resection only on one side, and allows uncoordinated movement of the break ends. The resected TG-free end invades homology on another chromosome driving a unidirectional translocation event.

Highlights

- TG repeats near an internal break impair MRX binding and end resection
- Asymmetric MRX binding leads to enhanced end mobility
- TG repeats near an internal break promote repair by ectopic recombination
- The STUbL Uls1, not Slx5/Slx8, downregulates imprecise NHEJ at TG repeats

Marcomini et al., 2018, Cell Reports 24, 2614–2628
September 4, 2018
https://doi.org/10.1016/j.celrep.2018.07.102

OPEN ACCESS
CellPress

Cell Reports
Article

Asymmetric Processing of DNA Ends at a Double-Strand Break Leads to Unconstrained Dynamics and Ectopic Translocation

Isabella Marcomini, [1,2] Kenji Shimada, [1,5] Neda Delgoshaie, [1,5] Io Yamamoto, [1] Andrew Seeber, [1] Anais Cheblal, [1,2] Chihiro Horigome, [1,4] Ulrike Naumann, [3] and Susan M. Gasser [1,2,6,*]

[1]Friedrich Miescher Institute for Biomedical Research, Maulbeerstrasse 66, 4058 Basel, Switzerland
[2]University of Basel, Faculty of Natural Sciences, 4056 Basel, Switzerland
[3]Novartis Institutes of Biomedical Research, 4002 Basel, Switzerland
[4]Present address: Institute of Quantitative Biology, University of Tokyo, Bunkyo-ku, Tokyo 113-0032, Japan
[5]These authors contributed equally
[6]Lead Contact
*Correspondence: susan.gasser@fmi.ch
https://doi.org/10.1016/j.celrep.2018.07.102

SUMMARY

Multiple pathways regulate the repair of double-strand breaks (DSBs) to suppress potentially dangerous ectopic recombination. Both sequence and chromatin context are thought to influence pathway choice between non-homologous end-joining (NHEJ) and homology-driven recombination. To test the effect of repetitive sequences on break processing, we have inserted TG-rich repeats on one side of an inducible DSB at the budding yeast MAT locus on chromosome III. Five clustered Rap1 sites within a break-proximal TG repeat are sufficient to block Mre11-Rad50-Xrs2 recruitment, impair resection, and favor elongation by telomerase. The two sides of the break lose end-to-end tethering and show enhanced, uncoordinated movement. Only the TG-free side is resected and shifts to the nuclear periphery. In contrast to persistent DSBs without TG repeats that are repaired by imprecise NHEJ, nearly all survivors of repeat-proximal DSBs repair the break by a homology-driven, non-reciprocal translocation from ChrIII-R to ChrVII-L. This suppression ofimprecise NHEJ at TG-repeat-flanked DSBs requires the Uls1 translocase activity.

INTRODUCTION

Eukaryotic genomes are riddled with repeat sequences. Simple sequence repeats include mini-, micro-, and centromeric satellites, as well as telomeric repeats. Complex repeats include protein-encoding RNA and DNA transposons. Collectively, repeats comprise up to 70% of the human genome (Padeken et al., 2015). While the functions served by repeats are unclear, it is unequivocally established that they are a source of genomic instability (Kim and Mirkin, 2013; Leffak, 2017). Replication-induced insertions, deletions, and breaks are enhanced at repeats, and spontaneous breaks within repeat elements compromise genome integrity, as they are prone to inappropriate translocations (Aksenova et al., 2013). In mammals, such events can lead to loss of heterozygosity, which in the case of oncogenes or tumor suppressor genes contributes to oncogenic transformation.

To suppress the risk of nonreciprocal or unequal crossovers, the repair of double-strand breaks (DSBs) in repetitive DNA is accompanied by the relocation of the repeat-flanked DSB away from the repetitive sequence domain prior to resection and the loading of Rad51 (Amaral et al., 2017). Only then can single-strand invasion and homologous recombination (HR) occur. This was shown for budding yeast, where breaks in the repetitive rDNA shift from the nucleolus prior to repair by HR (Torres-Rosell et al., 2007), and for breaks that occur within centromeric heterochromatin of both Drosophila (Chiolo et al., 2011) and mouse cells (Tsouroula et al., 2016). In both yeast and flies, this relocation has been shown to depend on sumoylation of break-associated factors (Horigome et al., 2016; Amaral et al., 2017). In budding yeast, poly-sumoylation is implicated in the relocation ofirreparable DSBs to the nuclear pore complex, which favors alternative recombination-mediated repair pathways like break-induced replication (BIR) (Horigome et al., 2016). Satellite-embedded breaks in Drosophila similarly relocate to nuclear pores, although repair outcomes were not monitored (reviewed in Amaral et al., 2017).

Telomeric repeats pose a special case as they normally demarcate a natural DNA end that must be protected from both non-homologous end joining (NHEJ) and HR, in order to prevent chromosomal end-to-end fusions. In most eukaryotes, telomeres contain tandem TG-rich repeats. In budding yeast, the irregular $(TG_{1\text{-}3})_n$ repeat covers 300 to 600 bp, while the mammalian terminal TTAGGG repeat can extend hundreds of kilobases (Palm and de Lange, 2008). These sequences are bound by sequence-specific DNA binding proteins and their ligands, forming the telosome. The telosome protects the eukaryotic genome from erosion during genomic replication, mediates short telomere elongation in S phase by nucleating

telomerase-mediated repeat extension, and prevents the recognition of chromosome ends as breaks. All three actions attenuate DNA damage checkpoint activation that would arrest the cell cycle to promote recombination-mediated repair (Symington and Gautier, 2011).

In contrast to telomeric ends, proteins recruited to internal DSBs process the ends for repair and trigger a checkpoint response. In budding yeast, DSBs are initially sensed by both yKu and the Mre11-Rad50-Xrs2 (MRX) complex (Mre11, Rad50, Nbs1 in mammals); MRX in turn recruits Tel1 kinase (ATM). If end ligation is not immediate, MRX makes a single-strand nick distal to the break, to initiate short-range resection (Cannavo and Cejka, 2014). The single-stranded DNA (ssDNA) is then extended by a second set of partially redundant enzymes, namely, Exo1, Dna2, and Sgs1 (Nicolette et al., 2010). Resection is more efficient in S phase than in G1 phase, and robust resection favors repair by HR over NHEJ, as long as a homologous template is available (Symington and Gautier, 2011). The Ku70/80 heterodimer competes for MRX and favors NHEJ (Langerak et al., 2011), which can either be precise or imprecise. Precise NHEJ entails error-free religation, while imprecise NHEJ occurs after limited resection or trimming and leads to short deletions (Sfeir and Symington, 2015). Independent of the repair pathway, the two sides of a break must be held together. This is achieved in part by MRX, which can be recruited to breaks by the single-strand DNA binding factor, replication protein A (Seeber et al., 2016).

It is noteworthy that short yeast telomeres in telomerase-deficient strains and internal HO endonuclease-induced DSBs that lack homologous donors behave similarly with respect to nuclear organization: both shift to the nuclear envelope (NE) (Nagai et al., 2008). Short telomeres bound by recombination proteins accumulate at nuclear pores (Khadaroo et al., 2009), as do difficult-to-repair DSBs. Both depend on sumoylation and the SUMO-targeted ubiquitin ligase (STUbL) Slx5/Slx8 (Horigome et al., 2016; Churikov et al., 2016). Slx5/Slx8 is also required to maintain telomere length by asymmetric strand invasion and elongation, called ALT (alternative lengthening of telomeres) or BIR (Azam et al., 2006). Differentiating internal DSBs from short telomeres is the fact that short telomeres present a free end, while at DSBs two ends are held together.

There are many sumoylated proteins found at DSBs, including Htz1, Ku, RPA, Rad51, and Rad52 (Cremona et al., 2012; Kaloc-say et al., 2009), while at short telomeres, Rap1 is also sumoylated (Lescasse et al., 2013). The binding of SUMO-targeted ubiquitin ligase subunit Slx5 to both poly-SUMO chains and to Nup84 are needed for the localization of telomeres (Churikov et al., 2016) and DSBs (Horigome et al., 2016) to nuclear pores for BIR or ALT, and the impaired relocation and damage survival phenotypes of slx5 or slx8 strains are epistatic with nup84Δ (Nagai et al., 2008). This mechanism is conserved, as homologs of the SUMO E3 ligase Siz2 and Slx5/Slx8 are similarly implicated in the sequestration of heterochromatic DSBs to nuclear pore complexes in Drosophila (Amaral et al., 2017).

Here, we sought to understand how a repetitive TG-rich sequence alters the processing and repair of an internal DSB in budding yeast. We added a telomeric TG-rich sequence to the centromere-proximal side of the natural HO endonuclease cleavage site at the MAT locus on ChrIII. Only the TG-rich side of the break showed no MRX recruitment nor end resection, which allowed the two ends to separate and acquire very high levels oflocal movement. The non-repetitive, distal side of the break was efficiently resected and then bound by Mps3 at the nuclear envelope, whereas the TG-rich side resisted resection and was elongated by telomerase. Imprecise NHEJ was suppressed by the TG sequence and the surviving yeast colonies underwent homology-dependent, nonreciprocal translocation of the distal arm of ChrIIIR to ChrVIIL. This required a putative SUMO-targeted ubiquitin ligase, Uls1. In the absence of Uls1 there is no increased movement despite normal end resection, and ablation of the Uls1-associated translocase activity increased imprecise NHEJ efficiency. Thus, the presence of Rap1-binding TG repeats near breaks alters MRX recruitment and end-to-end tethering, and impairs imprecise NHEJ, favoring nonreciprocal translocations. The latter event resembles genome rearrangements observed in human cancers.

RESULTS

TG Repeats Affect Nuclear Envelope Interactions of a Persistent DSB

The budding yeast genome has relatively little interstitial repeat sequence and lacks centromeric satellite arrays. The introduction ofinternal repeats leads to replication fork stalling and both the expansion and reduction of the initial repeat (Kim and Mirkin, 2013; Leffak, 2017). Inserts of 120 bp of (TGTGTGGG)$_{15}$ can lead to gross chromosomal rearrangements, translocations, and acentric minichromosomes (Aksenova et al., 2013), yet how internal repeats influence break processing was never determined. To examine this, we inserted telomeric repeats on the centromeric side of the HO endonuclease cleavage site at the MAT locus on yeast chromosome III (Figure 1A), such that the G-rich strain is oriented 5^{0} to 3^{0} and would create a TG-rich overhang if resected.

The induction of Gal1p:HO by galactose led to rapid cleavage at the HO cut site with efficiencies that were comparable with or without inserted repeats (Figure 1B). We note that the presence of 250 bp of TG (Tg250), unlike 80 bp (Tg80), tethers the intact MAT locus at the nuclear envelope prior to cleavage (Figures 1C and S1), likely reflecting Sir4 binding and SIR-mediated transcriptional repression (Gartenberg et al., 2004).

We examined whether the short Tg80 insert would affect the efficiency of DSB relocation to the nuclear envelope by tracking LacI-GFP after Gal1p:HO induction. After 100 min of continuous HO induction, the lacO-tagged Tg0 and Tg80 constructs had both shifted significantly toward the Nup49-CFP tagged nuclear rim. However, the kinetics of relocation differed: at time points of 40 and 70 min, the Tg80 DSB was not enriched at the nuclear envelope, unlike the Tg0 break (Figure 1D). The Tg250 locus, on the other hand, was peripheral prior to cleavage and remained there after HO induction (Figure S1).

There are at least two characterized sites of damage binding at the nuclear envelope, the nuclear pore complex and the SUN domain protein Mps3 (Horigome et al., 2014). Persistent breaks in G1- and S-phase cells shift to nuclear pores, while resected ends in cells lacking a homologous template bind Mps3 in S or G2 phase (Horigome et al., 2014). We therefore examined

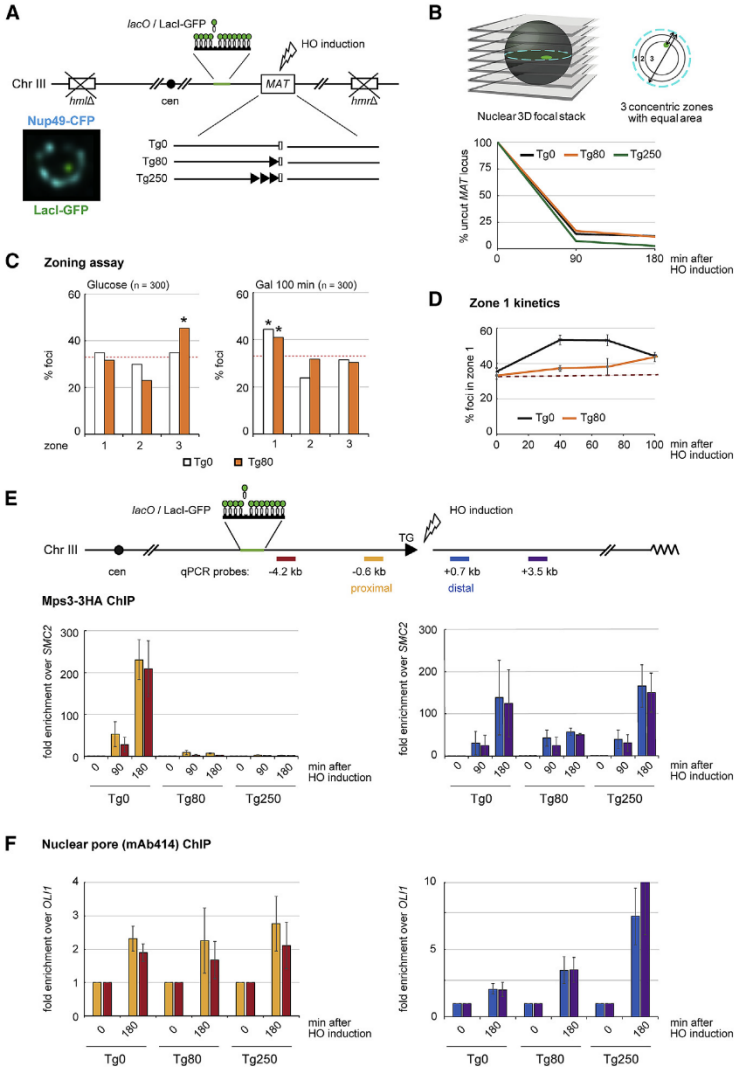

Figure 1. Telomeric Repeats at a Persistent DSB Affect Relocalization Timing and Anchorage Site

(A) TG-flanked DSB constructs with 80 or 250 bp of $(TG_{1\text{-}3})_n$ (Gilson et al., 1993) as shown at the MAT locus (ChrIII) with 256 lacO repeats at 4.6 kb. HML and HMR loci are deleted, and CFP-Nup49, LacI-GFP, and Gal1p::HO-expressing constructs are integrated. A single-plane confocal image with Nup49 and MAT signals is shown at left.

(B) Zoning assay used in (C): the ratio oflocus distance to nuclear envelope divided by the nuclear diameter is determined in the focal plane in which the LacI-GFP spot is brightest. Ratios are binned into three equal concentric zones of equal surface. HO cleavage efficiency at 90 and 180 min of HO induction monitored by qPCR in GA-8860 (Tg0), GA-8119 (Tg80), and GA-8502 (Tg250). HO-cut site Ct values were normalized to an amplicon in SMC2 and were further normalized to the ratio at time point 0. Experiments were done in triplicate, and error bars are not shown as SD < 5%.

(C) Zoning assay for GFP-tagged MAT locus as in (B), on glucose (left) or 100 min after HO induction on galactose (right) in Tg0 (GA-8861, white) and Tg80 (GA-8119, orange) strains. n = nuclei scored. Red dotted line indicates a random distribution, or 33% in each zone. *significantly non-random distribution using c^2 test versus random (degree offreedom, 2; confidence limit, 95%).

(D) Percentage of GFP-tagged foci in zone 1 after HO induction in Tg0 (GA-8861) and Tg80 (GA-8119). Error bars, mean values of three independent experiments ± SEM. n = 80 for each strain and experiment; red dotted line, random.

(E) ChIP of HA-tagged Mps3 in Tg0 (GA-8306), Tg80 (GA-8633), and Tg250 (GA-8845) at 0, 90, and 180 min after HO induction. The four qPCR probes (color-coded) are shown relative to the DSB.

(F) Nuclear pore ChIP using Mab414 in Tg0 (GA-8860), Tg80 (GA-8119), and Tg250 (GA-8502) at 0 and 180 min after HO induction is quantified using qPCR probes; (E) and (F) each show data from two biological replicates, amplified in triplicate and presented as mean values ± SEM.

whether the presence of Tg80 or Tg250 near a DSB alters perinuclear anchorage site. Using chromatin immunoprecipitation (ChIP) for nuclear pores and Mps3, we scored for interaction on either side of the break (Figure 1 E). The Tg0 DSB interacted with Mps3 on both sides at 90 and 180 min after HO induction, while the Tg80-flanked break bound Mps3 exclusively on the non-TG side (Figure 1 E). The same was observed for the cleaved Tg250 construct (Figure 1 E). Thus, the presence of TG repeats led to asymmetric Mps3 binding, with the TG-containing end failing to bind Mps3. Low-level interaction with nuclear pores was detected in all constructs for both break sides (Figure 1 F).

Resection and MRX Binding Are Blocked by TG Repeats at an Internal HO-Induced DSB

Given that the interaction of a DSB with Mps3 requires end resection (Horigome et al., 2014), we hypothesized that the TG-rich inserts might impair resection at the HO cut site. We therefore monitored the amount of exposed ssDNA following HO endonuclease induction at either 90 or 180 min, using a restriction enzyme-based method (Zierhut and Diffley, 2008). Because Alu1 only cleaves dsDNA, the generation of ssDNA by end resection will block cleavage at its cognate sites near a resected DSB. By monitoring amplification efficiency at Alu1 consenses, we could score the extent and efficiency of resection

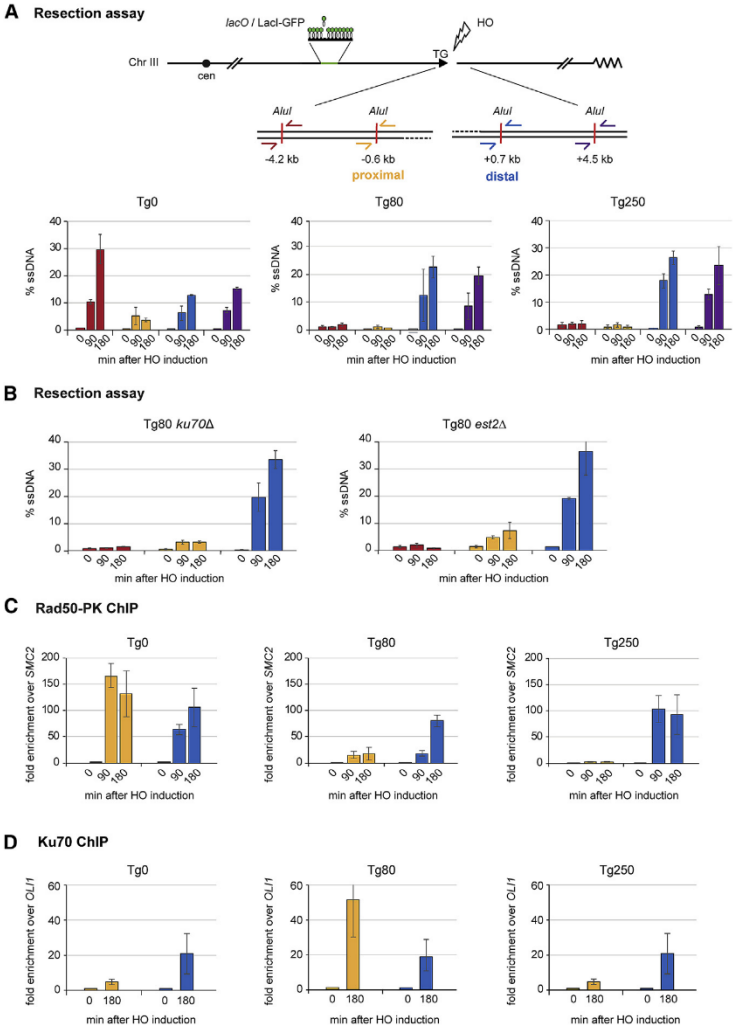

Figure 2. TG Repeats at a DSB Impose a Strong Block to 5′-End Resection and Inhibit MRX Binding

(A) A resection assay monitors ssDNA at indicated Alu1 sites in Tg0 (GA-8861), Tg80 (GA-8119), and Tg250 (GA-8502) strains, following 0, 90, and 180 min of HO induction. Results were normalized to an Alu1-free region in SMC2 . Two biological replicates, amplified in triplicate, are presented as mean values ± SEM.

(B) Absence of either yKu70 (Tg80 ku70D; GA-9553) or telomerase (Tg80 est2 D; GA-9005) does not release the resection block on the TG side of the DSB. Resection from two biological replicates, amplified in triplicate and presented as mean values ± SEM.

(C) Anti-PK ChIP of MRX subunit Rad50-PK in Tg0 (GA-9519), Tg80 (GA-9549), and Tg250 (GA-9521) at the indicated times after HO induction.

(D) ChIP as in (C), but for Ku70 in Tg0 (GA-8861), Tg80 (GA-8119), and Tg250 (GA-8502) strains, 0 and 180 min after HO induction. Fold enrichments over the mitochondrial locus OLI1 were normalized to levels at time 0. (C) and (D) are three experiments shown as mean ± SEM.

around the break, which was proportional to the intensity of the Alu1-spanning qPCR bands (Figure 2 A).

In the Tg0 strain, we detected nearly equal resection on both sides of the break after 90 min on galactose (Figure 2 A), with the centromere-proximal side showing more extensive resection by 180 min. In contrast, in the strains bearing a Tg80 or Tg250 insert, little or no resection was scored on the TG-containing side of the break, even after 180 min, although resection proceeded efficiently on the distal side of the same break (Figure 2 A). We hypothesized that yKu or telomerase might bind and block the Tg80 repeats, given that Tg80 in a subtelomeric location is recognized as short telomere in need of elongation (Negrini et al., 2007). However, the resection block was not alleviated by deletion of yKu nor of the catalytic subunit of telomerase, Est2 (Figure 2 B). There was limited improvement in resection on the Tg80 side of the break upon overexpression of Exo1, which drives the extended resection at DSBs (Figure S2).

The 5′-end resection is generally initiated by the MRX complex and requires the ATPase activity of Rad50 (Deshpande et al., 2014). Therefore, we monitored the recruitment of MRX to the DSB by performing ChIP for a fully complementing PK-tagged Rad50 (Seeber et al., 2016). As expected, we find Rad50 recruited equally to both sides of the break in the Tg0 strain, enabling MRX to bridge the DNA ends and initiate resection on both sides (Figure 2 C, left graph). In contrast, in strains carrying either the Tg80 or Tg250 insert, we observe strongly reduced Rad50 binding on the TG side of the break, while its recruitment to the distal side was readily detected, at levels equivalent to the Tg0 strain (Figure 2 C). Previous studies suggested that natural short telomeres have a reduced complement of Rap1-Rif1-Rif2, which allows more MRX recruitment (Shore and Bianchi, 2009). This appears not to occur at a Tg80-proximal DSB at MAT , where the TG repeats block MRX binding, leading to an asymmetrical processing of the two sides of the break.

Although Ku does not affect resection, it might influence MRX association. Therefore, we monitored the presence of yKu on either the TG-rich or the distal side of Tg80- or Tg250-flanked HO cuts by ChIP-qPCR. As presented in Figure 2 D, in Tg0, Tg80, and Tg250-bearing strains, yKu70 showed equal enrichment by ChIP at 180 min on the distal side of the break. yKu70 levels were equal between Tg0 and Tg250 on the TG-rich side

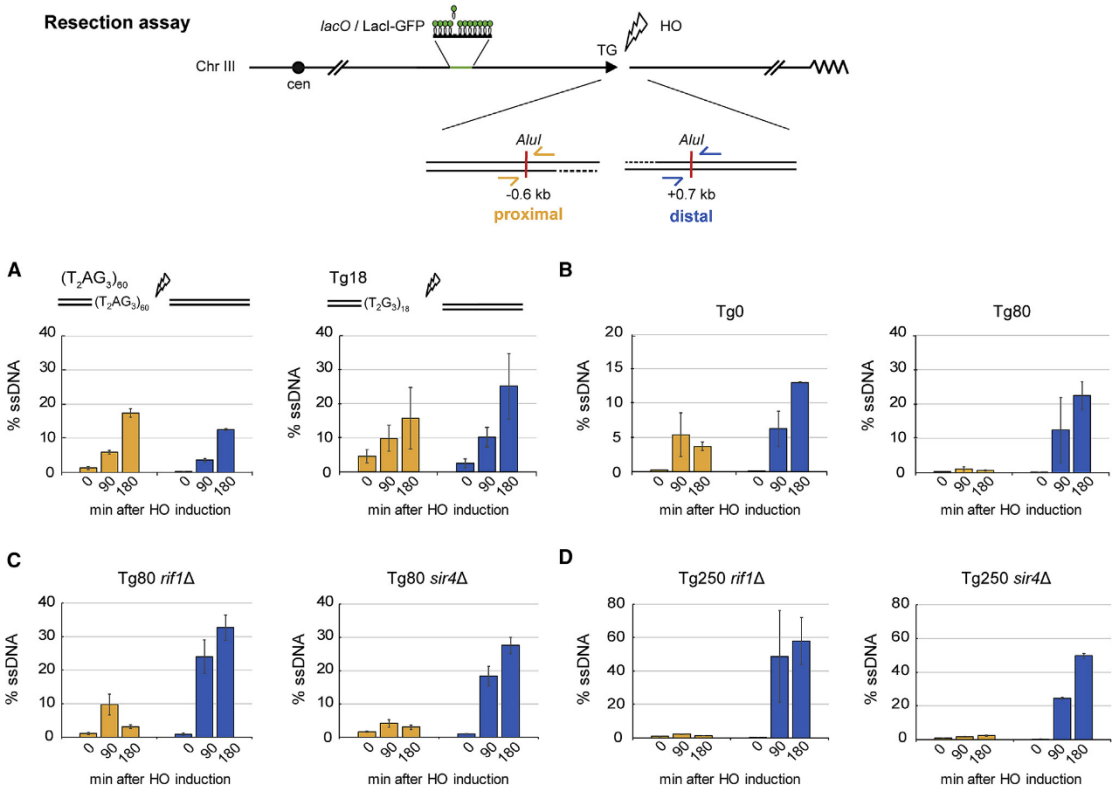

Figure 3. TG Resection Block Requires Multiple Rap1 Motifs but Not Major Rap1 Ligands

(A) Resection assay as Figure 2A after HO induction, using color-coded probes. Strain ($T_2AG_3)_{60}$ (GA-9823) contains human TTAGGG repeats that cannot bind Rap1, while Tg18 (GA-9824) harbors one Rap1 consensus. Two biological replicates, amplified in triplicate, are presented (mean values ± SEM).

(B–D) Resection assay at the DSB in Tg0 and Tg80 strains as in Figure 2A, in isogenic Tg80 and Tg250 strains (B); Tg80 rif1D (GA-9449), Tg80 sir4D (GA-9158) in (C); Tg250 rif1D (GA-8596) and Tg250 sir4D (GA-8587) in (D). Loss of Rif1 partially relieved the TG-resection block in Tg80 but not Tg250. Loss of Sir4 had no effect in either background. Data of GA-8596 and GA-8587 are mean values of three technical replicates ± SEM; data of GA-9449 and GA-9158 are mean values of three biological replicates ± SEM.

but were strikingly enriched in Tg80 (Figure 2D). This latter may reflect Ku's role in telomerase recruitment (Bertuch and Lundblad, 2003), because Tg80, but not Tg250, triggers elongation (Ribeyre and Shore, 2012).

Sequence and Length of TG Repeats Control the Resection Block at TG-Flanked DSBs

The asymmetric binding of MRX at the Tg80 DSB is a likely cause of the differential processing of the two DNA ends, yet why should MRX bind asymmetrically? To ask whether it stems from the repetitive nature of the Tg80 DNA or the binding of Rap1, the $(TG_{1\text{-}3})_n$ ligand, we replaced the yeast repeat with 60 bp of human telomeric repeat and monitored end resection. The human $(TTAGGG)_n$ repeat is known to recruit telomerase for elongation in yeast, although Rap1 does not bind it with significant affinity (Brevet et al., 2003; Ribaud et al., 2012). Using the Alu1-amplicon method, we found that the human repeat allowed efficient resection on both sides (Figure 3A), unlike the Tg80 insert (Figure 3B), arguing that Rap1 binding, rather than a G-quartet forming sequence, blocks end resection. Consistently, the Tg250 insert with 14 Rap1 binding sites (Gilson et al., 1993), was an even more effective barrier to resection and MRX binding than Tg80, while a single high-affinity Rap1 consensus (Tg18) functioned like Tg0 (Figures 3A and 3B).

A previous study inserted a similar Tg80-flanked HO cleavage site in a telomere-proximal region and found that the C terminus of Rap1 inhibits MRX binding to the break in a Rif1-dependent manner (Hirano et al., 2009). A second Rap1C ligand, Sir4, competes for Rif1 binding (Moretti et al., 1994; Wotton and Shore, 1997) and is recruited to DSBs (Martin et al., 1999). Therefore, we tested the effect of either Rif1 or Sir4 deletion on Tg80 resection. While the loss of Rif1 slightly improved resection on the Tg80 side at 90 min, this impact did not persist at 180 min and was not detectable at the Tg250-flanked break. Loss of Sir4

also showed no significant increase in resection (Figures 3 C and 3D), and neither Tg80 nor Tg250 flanked sites showed any resection at the distal probe at −4.2 kb in these mutants (data not shown). Given that the HO cleavage was equally efficient in all strains (Figure S3) and that resection on the non-TG side occurred, we conclude that the asymmetric resection pattern at the Tg80 DSB reflects the binding of Rap1, but not Rif1 or Sir4.

Rap1 is encoded by an essential gene in yeast, and it plays a major role in controlling the transcription of growth-regulatory genes. Because telomeres become dramatically extended upon loss of the Rap1 C-terminal domain, we next tried to monitor DSB resection at Tg80 either in a rap1 DC background or after depletion of a degron-tagged Rap1 protein. However, galactose-induced transcription of Gal1p:HO was compromised under both conditions, obviating this approach (data not shown). We cannot exclude that Rap1's affinity for $(TG_{1\text{-}3})_n$ itselfimpairs resection, although we note that Tbf1 binds the TTAGGG repeat with similar avidity without blocking resection.

The TG-Rich and Non-TG Sides of the DSB Separate, Allowing Increased Break Movement

Recent work has shown that the binding of MRX to short ssDNA stretches at DSBs through the N-terminal OB fold of RPA1 contributes to holding the two break ends together (Seeber et al., 2016). Given that MRX is missing from the proximal side of the break in the Tg80 strain, we next asked whether the association of the two ends is affected by the Tg80 insert. We tracked the proximal TG-containing side of the break through the binding of LacI-GFP to the lacO array, and of the distal non-TG side through Rad52-Ruby2, which binds after cleavage and resection (Dion et al., 2012; Lisby et al., 2004). Visible Rad52 foci assemble within 1 hr after HO induction (Miyazaki et al., 2004).

To estimate the impact of TG-repeats on end tethering, we first quantified the level of Rad52 and LacI-GFP colocalization at 135 min after cut induction. Whereas 55% of the green and the red signals coincide in the Tg0 cells bearing both LacI-GFP and Rad52-Ruby2 foci, only 14% offoci showed coincidence in Tg80 cells and 70% were fully separated (Figure 4 A). This striking loss of tethering of Rad52 and LacI-GFP tagged sides is consistent with the observed asymmetry in MRX binding to only one side of the break in the Tg80 strain (Figure 2 D) and contrasts with break behavior at normal HO cut sites (Tg0), where 97% of the ends remained together (Seeber et al., 2016).

The induction of a persistent DSB increases local chromatin movement (Dion et al., 2012; Mine´-Hattab and Rothstein, 2012), even though the ends remain linked through a protein bridge. Our ability to visualize the two sides of the same break by fluorescence microscopy (LacI-GFP on the TG-side and Rad52-Ruby2 on the resected side) allowed us to monitor their dynamics independently using through-focal three-dimensional (3D) stacks acquired at 80-ms intervals on a total internal fluorescence (TIRF) microscope (Figure 4 B). From the single-particle tracking (SPT) data taken at 2 hr after HO induction, we extracted characteristic statistical parameters of movement of either end, and calculated the extent of nuclear volume explored by either focus using mean square displacement (MSD) curves. From the plateau of constrained diffusive movement of multiple SPTs, we estimated the radius of the maximal volume of particle movement, or Rc, before and after HO cut induction (Figure 4 C). As expected, prior to DSB induction, the LacI-GFP foci had similar subdiffusive movement in both Tg0 and Tg80 strains, and the Rad52-Ruby2 marker was not present (Figure 4 C, left, uncut). Upon cut induction, movement of the LacI-tagged focus increased more significantly at the Tg80 DSB than at the Tg0 break (R_c = 0.41 mm^2 versus 0.37; Figures 4 C and 4D; Figure S4 for SEs). Moreover, the Rad52-tagged distal side of the break had extremely robust movement in Tg80 cells, with Rc and diffusion constant (Dc) values much larger than those of the Rad52 focus in Tg0. As expected, the Tg0 Rad52-Ruby2 and LacI- lacO foci coincided and moved coordinately (R_c = 0.34 versus 0.37; Figure 4 D), in contrast to the uncoordinated movement observed at the Tg80 break.

Statistical parameters from time-lapse imaging (Amitai et al., 2017) confirm that the movement of the resected Rad52-bound side has thrice the diffusion coefficient and one-half the spring constant (K_c) in the Tg80 background (Figure 4 D). A particularly informative parameter of SPTs is the anomalous exponent (a), which indicates whether movement is directed, diffusive, or subdiffusive in character (Amitai et al., 2017). Intriguingly, the change in a is significantly different on the two sides of the Tg80 break, but not of the Tg0 break; a increases from 0.409 to 0.479 on the Tg80 side, while it decreases to 0.328 on the resected distal end (Figure 4 D). Thus, the resected end not only moves more, but in a more diffusive manner. This coincides with the loading of Rad51, which is proposed to form a damage-induced stiffening of the ssDNA distal to DSB site (Mine´-Hattab and Rothstein, 2012). This asymmetrical behavior of the two DNA ends in the Tg80 strain underscores the fact that the break ends are not tethered and are differentially processed for repair (Figure 4 E). Given that increased chromatin mobility is thought to favor homology-dependent repair (Dion et al., 2012; Mine´-Hattab and Rothstein, 2012), the increased mobility of the non-TG side at the Tg80 break suggests that it may be engaging in early steps of HR.

Telomeric Repeats Near a Persistent DSB Inhibit Imprecise End Joining but Allow Alternative Repair

Haploid colony survival in face of persistent HO endonuclease expression requires a repair event that eliminates the HO consensus but retains the distal arm of ChrIII, which bears many essential genes. Given that the test strain lacks the homologous mating type loci that provide donor sequences for repair (Figure 5 A), no intrachromosomal gene conversion events can occur. Thus, in a wild-type background, most survivors of continuous HO endonuclease expression repair the cut site by imprecise NHEJ, generating survivors with mutated cleavage consenses that resist HO endonuclease cleavage.

As shown in Figure 5 B, the introduction of TG repeats on one side of the break reduced the frequency of colony formation on galactose by 76% (Tg80*), in comparison to the survivor frequency at the native MAT (Tg0, wild-type [WT] MAT). Since survivor colony number was very low, we provided 300 bp of homology to the 3^0 of MNT2 , a non-essential gene located in the left subtelomeric region of ChrVII, to the distal side of the HO consensus. Addition of this sequence restored the survival frequency of TG-flanked DSBs to a level roughly equivalent to the

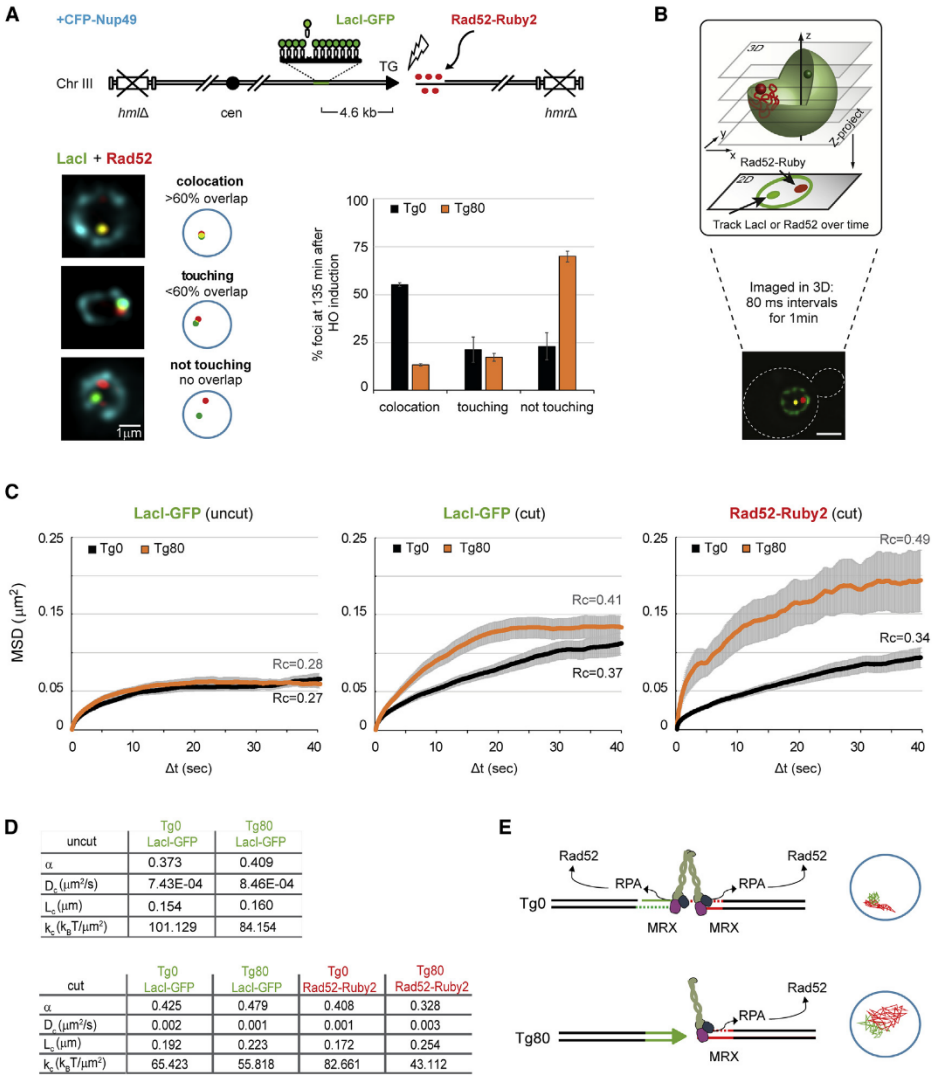

uncut	Tg0 LacI-GFP	Tg80 LacI-GFP
α	0.373	0.409
D_c (μm²/s)	7.43E-04	8.46E-04
L_c (μm)	0.154	0.160
k_c (k_BT/μm²)	101.129	84.154

cut	Tg0 LacI-GFP	Tg80 LacI-GFP	Tg0 Rad52-Ruby2	Tg80 Rad52-Ruby2
α	0.425	0.479	0.408	0.328
D_c (μm²/s)	0.002	0.001	0.001	0.003
L_c (μm)	0.192	0.223	0.172	0.254
k_c (k_BT/μm²)	65.423	55.818	82.661	43.112

Figure 4. Break Ends at TG-Flanked DSBs Separate and Move in an Uncoordinated Fashion

(A) System used to visualize Rad52-Ruby2 on one side of the resected HO-induced non-TG break side, while the TG side was visualized by LacI-GFP. Criter ia for juxtaposition offoci are shown. Percentage of colocalization of LacI-GFP and Rad52-Ruby2 foci in Tg0 (GA-9948) and Tg80 (GA-9912) are quantified at 1 35 min after HO induction. Cleavage efficiency is >95%. n = 80 cells per strain per experiment; mean values of three independent experiments ± SEM are shown.

(B) Scheme of LacI-GFP and Rad52-Ruby2 locus tracking by TIRF microscopy acquired at 80-ms time intervals for 1 min, starting 2 hr after HO induction.

(C) MSD analysis based on SPTs of LacI-GFP and Rad52-Ruby2 using Tg0 (GA-9948, black) and Tg80 (GA-9913, orange) strains, with and without HO cut. SPTs per strain and conditions are as follows: Tg0 uncut, 20; Tg0 Rad52-Ruby2, 23; Tg80 uncut, 23; Tg0 LacI-GFP, 25; Tg80 Rad52-Ruby2, 24; and Tg80 LacI-GFP , 24. Rc, radii of constrained movement (mm), are indicated above each averaged track.

(D) Statistical biophysical parameters (Amitai et al., 2017) determined from single-particle trajectories as in (C). Numbers are means of at least 20 trajectories. a, anomalous exponent; D $_c$, diffusion coefficient; k $_c$, effective spring constant; L $_c$, length of constraint (Amitai et al., 2017).

(E) In the absence of TG repeats, ends are held together by the MRX complex, which leads to end resection, RPA, Rad51, and Rad52 binding. In Tg80, MRX bind s only the non-TG side. Ends separate, moving without constraint.

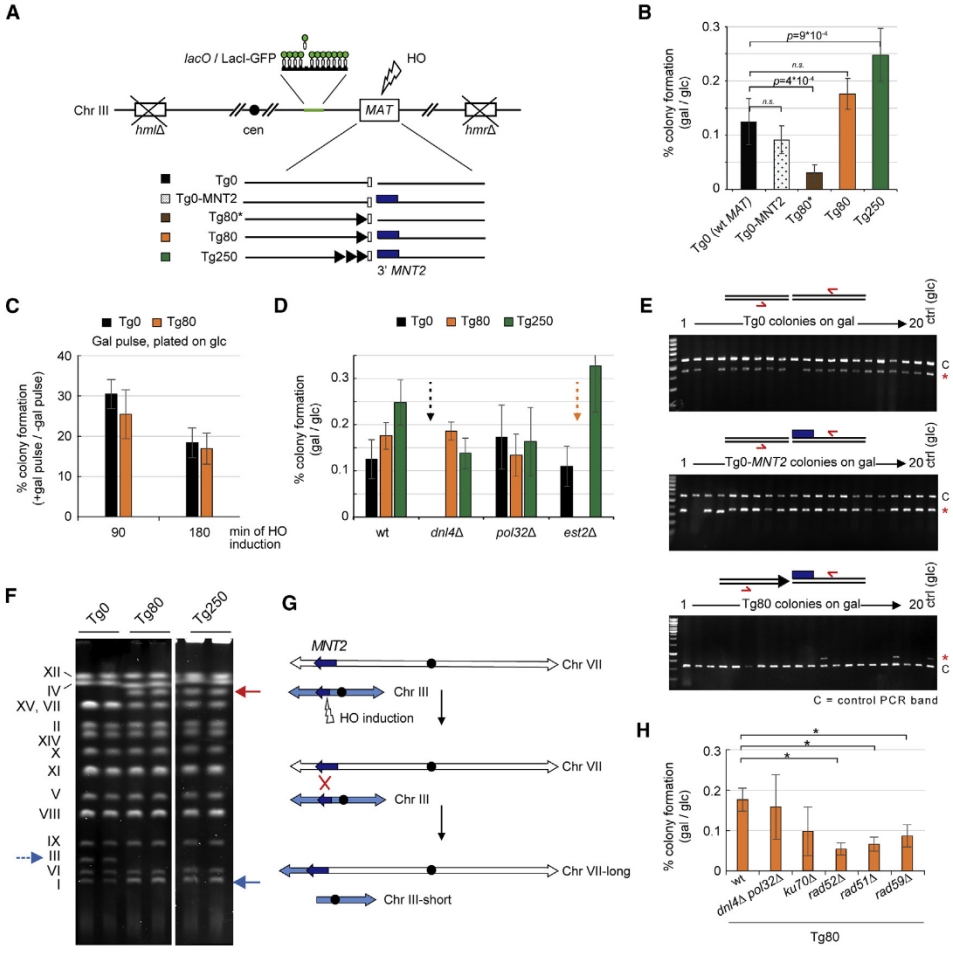

Figure 5. Telomeric-Like Repeats Flanking a Persistent DSB Determine Repair Outcome

(A) Scheme of TG-flanked DSB constructs at the MAT locus (Figure 1 A): blue box, 300-bp MNT2 homology relative to the HO cut site.

(B) Colony formation on galactose (HO on, DSB cut) normalized to colony growth on glucose (HO off, DSB uncut) in GA-8861 (Tg0), GA-10085 (Tg0-MNT2), GA-9918 (Tg80*), GA-8119 (Tg80), and GA-8502 (Tg250). Colony growth on galactose requires mutation of HO consensus. Mean ratios offour or more experiments ± SD are shown; p values from a t test with 95% confidence interval between Tg0 and test constructs. n.s., nonsignificant ($p > 0.05$).

(C) Cultures of Tg0 and Tg80 were grown in 3% galactose for 90 or 180 min and then plated on glucose; colony outgrowth mostly represents precise end joini ng. Percentage of colony formation rate after the galactose pulse is normalized to colony formation rate on glucose without galactose. Mean ± SD of three independent experiments is presented.

(D) As (B) for the indicated Tg0, Tg80, and Tg250 strains with indicated mutations. Arrows mark no growth on galactose (Tg0 dnl4D; Tg80 est2 D) based on three independent experiments (mean ± SD).

(E) For each construct, genomes from 20 colonies grown on galactose were used in parallel PCRs across the HO cut site (red asterisk), and within SMC2 (labeled C). Pooled PCR products were resolved on agarose gels. Uncut control from the same strain (on glucose; uncut) is indicated.

(F) CHEF gel analysis of two of ten independent galactose-grown colonies of Tg0, Tg80, and Tg250 survivors on galactose. For each strain, all ten karyo types resembled the two shown. Dotted blue arrow, ChrIII; solid blue arrow, ChrI signal; red arrow, new band in Tg80 and Tg250 survivors.

(G) Scheme for the MNT2 -mediated nonreciprocal translocation from ChrIIIR to subtelomeric ChrVIIL.

(H) As (B) in indicated mutants. Each column represents the mean offour independent experiments ± SD. *Statistical significance with a p value < 0.001 (t test with 95% confidence interval, wild-type versus mutant).

Tg0 strain, while the presence of Tg250 instead of Tg80 at the DSB further increased survivor frequency (Figure 5B).

To see whether the presence of Tg80 affects rates of precise end joining, we first checked whether Tg80 inhibits NHEJ generally. For precise or imprecise end-joining reactions to occur, unblocked 3 ^{0}OH and 5 ^{0}PO$_{4}$ groups are needed together with DNA ligase 4 (Dnl4), resulting in end-to-end ligation and an intact ChrIII (Boulton and Jackson, 1996; Matsuzaki et al., 2008). Ligation following limited resection generates a mutated HO consensus, which prevents the continuous cleavage-ligation cycle that provokes cell-cycle arrest. To score NHEJ events in the presence of Tg80, we placed cells on galactose to induce the HO endonuclease for a limited time (90 or 180 min), and then plated the cells on glucose to repress HO endonuclease expression. This allows cells in which the DSB is repaired by precise NHEJ to grow, as well as those repaired by imprecise end joining. Intriguingly, we scored statistically equivalent rates of colony outgrowth in Tg0 and Tg80 strains under these conditions (Figure 5C). Given that cleavage was equally efficient (Figure S5A), we argue that Tg80 per se does not inhibit precise NHEJ.

As mentioned above, Gal1p:HO strains that survive on galactose generally undergo imprecise NHEJ, and thus survivor rates drop upon ablation of DNA ligase 4 (*dnl4Δ*). For the Tg0 strain on galactose, this is indeed the case (Figure 5D). However, the Tg80 and Tg250 survivor colonies on galactose were insensitive to the loss of DNA ligase 4 (Figure 5D). We further tested the deletion of *POL32*, which encodes the regulatory subunit of DNA polymerase δ required for BIR (Lydeard et al., 2007). Neither altered the rate of survivor formation, arguing that neither NHEJ nor BIR mediates the repair in Tg80 DSB survivors.

We next tested directly for end-to-end re-ligation events in the galactose-grown survivors of Tg80 and Tg0 strains. Using colony PCR with primers that span the HO cut site, we scored for the regeneration of an intact *MAT* fragment, which arises from either precise or imprecise NHEJ (Figure 5E). As an internal control for PCR efficiency, we amplified the *SMC2* gene on ChrVI, and the PCR products were pooled for analysis by agarose gel electrophoresis. As shown for 20 randomly chosen Tg80 survivors (from 80 tested per strain), 18 had no PCR product from primers that span the HO consensus (Figure 5E). This argues for a repair event that does not restore an intact ChrIII (Figure 5E). In contrast, nearly all Tg0 and Tg0-HO-MNT2 survivors of continuous HO induction restored a contiguous *MAT* locus, as expected for repair by imprecise NHEJ (Figure 5E). We ruled out the possibility of cleavage site deletion by performing PCR on DNA isolated from the strain prior to galactose exposure (ctrl glc). These results argue that the Tg80 insert profoundly alters DSB repair of a persistent HO cut, possibly by suppressing imprecise NHEJ.

We checked the karyotypes of the survivors by pulsed-field gel electrophoresis (clamped homogeneous electric fields [CHEFs]) to examine karyotype after Gal1p:HO-induced cleavage. Genomic DNA from galactose-growth survivors for Tg0, Tg80, and Tg250 strains (ten each) was analyzed, and representative CHEF gels are shown (Figure 5F). Tg0 survivor karyotypes were identical to the reference genome, while all Tg80 and Tg250 survivors shared exactly the same changes: an additional chromosomal band appears above the doublet of ChrVII and ChrXV (~1.1 Mb), and loss of ChrIII at 320 kb (Figure 5G). None of these changes was detected in cells that were grown continuously on glucose (Figure S5B).

We determined the precise chromosome rearrangements by performing whole Pacific Biosciences (PacBio) genome sequencing on three Tg80 and three Tg250 galactose survivors. In all those analyzed, the distal 100 kb of ChrIII had been translocated to the native *MNT2* gene in the left subtelomere of ChrVII. The recombination restored the intact *MNT2* reading frame precisely, indicating that strand invasion must have been initiated by the 300 bp of *MNT2* homology inserted at *MAT* (Figure 5G, PacBio data in Figure S5C). This explains the upshift of ChrVII to a slower migrating band, and the loss of full-length ChrIII. Loss of the ChrIII sequences distal to *MAT* results in a chromosome the size of ChrI (230 kb), explaining the increase in intensity of a band at 220 kb. No other recurrent variations were detected in the six colonies sequenced.

We examined the repair pathway/factors needed for this nonreciprocal translocation event in Tg80, by testing for survivors in strains lacking genes involved in HR, and in the *dnl4Δ pol32Δ* double mutant, which ablate NHEJ and BIR, respectively. The rate of Tg80 survivors in the *pol32Δ dnl4Δ* double mutant was like wild-type, but we found a significant reduction of survivors in strains lacking Rad51 and Rad52 (Figure 5H). Deletion of yKu or Rad59 had more minor effects (Figure 5H). In conclusion, the presence of TG repeats at a DSB blocked imprecise NHEJ and drove repair toward ectopic recombination, generating a nonreciprocal chromosomal translocation (Figure 5G).

Telomerase Elongates the Tg80 Side of the DSB

The stability of ChrIII in the TG-DSB survivors requires that the TG-flanked end is stabilized or capped. While Tg250 is sufficient to serve as a telomere, Tg80 has been previously shown to be "critically short" and seed telomerase-mediated elongation. In the absence of telomerase (*est2Δ*), we no longer recovered survivors in the Tg80 background, while both the Tg0 and Tg250 yielded normal colony outgrowth (Figure 5D). To confirm that the right arm of ChrIII is elongated by de novo telomere extension at the Tg80-flanked cut, we performed telomere-specific PCR to monitor terminal TG-repeat length on DNA extracted from cells at specific time points after HO induction (Förstemann et al., 2000). Without telomere elongation, a single stable band is amplified, as shown in the left-hand gel for the Tg0 DSB (Figures S5D and S5E). The population of fragments larger than the expected PCR band in the Tg80 strain was absent upon mutation of the catalytic telomerase subunit, Est2 (Figure S5D), confirming that the Tg80 end is a substrate for telomerase.

Previous work argued that the activation of telomerase in S-phase cells leads to a release of telomeres from Mps3, their perinuclear anchorage site (Schober et al., 2009), which was restored only after telomere elongation (Ferreira et al., 2011). We therefore tested whether telomerase binding was responsible for the delayed relocation of the Tg80 end to the nuclear envelope (Figure 1). Upon deletion of the telomerase catalytic subunit Est2, the Tg80 side of the DSB shifted more rapidly to zone 1 (Figure S5F), confirming that telomerase action delayed Tg80 binding at the nuclear envelope (Ferreira et al., 2011).

Sumoylation and the Translocase Uls1 Affect Nuclear Envelope Relocation of the Tg80 DSBs and Repair Outcome

The Tg80 break localization data argue that the TG insert initially prevents both resection and Mps3 binding (Figures 1B and 1C), while the TG-free side of the break showed strong association with Mps3, much like normal S-phase resected DSBs that lack an intact sister for repair (Horigome et al., 2014). Earlier work has implicated sumoylation and the poly-SUMO targeted ubiquitin ligase Slx5/Slx8 (a SUMO-targeted ubiquitin ligase enzyme) in the shift of damage to the Nup84 complex at pores, while monosumoylation was implicated in Mps3 binding (Horigome et al., 2016). The importance of SUMO recognition by SUMO-targeted ubiquitin ligase enzymes extends to the human homolog RNF4 in the relocation of damage to PML bodies for repair (Prudden et al., 2007), as well as to DSB relocation to nuclear pores in Drosophila (Amaral et al., 2017).

We therefore tested the role of the SUMO E3 ligase Siz2 and the Slx5/Slx8 SUMO-targeted ubiquitin ligase on the relocation of the Tg80 DSBs (Horigome et al., 2016). Surprisingly, the loss of Slx5/Slx8 had no effect, while the loss of the SUMO E3 ligase Siz2 completely impaired relocation to the nuclear envelope (Figure 6B). This suggests that sumoylation, but not the Slx5/Slx8 SUMO-targeted ubiquitin ligase, mediates Tg80 end relocation. We therefore examined the second putative SUMO-targeted ubiquitin ligase in yeast, Uls1 (or Ris1, Figure 6A), which in addition to harboring SUMO-interacting motifs (SIMs) and the ubiquitin E3 ligase RING finger, has a SNF2 DNA-dependent ATPase domain. Uls1 has been reported to be recruited to short telomeres in yeast, potentially recognizing sumoylated Rap1 (Lescasse et al., 2013). Indeed, deletion of the ULS1 gene completely blocked relocation of the Tg80-proximal side of the DSB at MAT (Figure 6B).

Next, we examined whether Uls1 plays a role in the relocation of normal DSBs to either Mps3 or nuclear pores, by monitoring DSB association with Mps3 by ChIP in the uls1D strain, and by performing DSB colocation with clustered pores (Horigome et al., 2014). This assay makes use of a well-characterized pore-clustering strain (nup133DN) as previously reported (Horigome et al., 2014), in which we monitor colocation of the GFP-tagged break with the CFP-Nup49 tagged pore cluster. Figure 6C shows the percentage of cells in which the DSB was in contact with the Nup49-CFP pore cluster at the indicated times after HO induction. In the Tg0 strain, interaction increased from a background level of 20% to roughly 40% after HO cut induction. For Tg0, the increase required Slx5/Slx8 and the E3 SUMO ligase Siz2 (Horigome et al., 2016), but not Uls1 (Figure 6C). In contrast, for the Tg80 DSB, both uls1D and siz2D reduced DSB association with the periphery, while slx8D did not (Figure 6B). This suggests a unique role for the Uls1 ubiquitin ligase at breaks harboring telomeric repeats, consistent with the reported ability of Uls1 to bind sumoylated Rap1 at telomeres (Lescasse et al., 2013).

Because uls1D and siz2D reduce pore relocation, we next asked whether these mutants influence the pathway of repair at the Tg80-flanked DSB. We scored for NHEJ in survivor colonies grown on galactose by monitoring for a PCR band across the cleavage consensus. While the overall rate of survivor colony formation on galactose is roughly equal in all Tg80 strains (Figure S6B), the frequency ofimprecise NHEJ over ectopic recombination events increased 10-fold in either the uls1D or siz2D Tg80 strain (from 5% to 55%), but not in slx8D (Figure 6D), correlating reduced relocation with enhanced NHEJ. Although previous studies reported a role for Rif1 in facilitating NHEJ at normal DSBs (Mattarocci et al., 2017), we scored only a slight increase in NHEJ in rif1D, while sir4D mutants enhanced NHEJ much like the mutants uls1D and siz2D (Figure 6D). Rif1 may play a minor role in suppressing NHEJ at Tg80-flanked breaks, probably acting only at early-stage processing. In contrast, the 10-fold increase ofimprecise NHEJ observed in the Tg80 uls1D and sir4D mutants suggests that Uls1 and Sir4 strongly inhibit NHEJ at Tg80 DSBs in wild-type strains. We examined whether this might be due to altered resection, yet loss of these factors had no effect on 5′-end resection at Tg80 breaks (Figures 3C and 6E). Importantly, in the case of Uls1, the suppression of NHEJ required its translocase activity (Figure S6C).

The increased chromatin movement observed at DSBs correlates with increased rates of recombination (Hauer et al., 2017; Dion et al., 2012), as enhanced diffusive movement is thought to enhance the efficiency of homology search. The Swi2/Snf2-like domain at the Uls1 C terminus could mediate chromatin remodeling and enhance movement; thus, we monitored break-induced chromatin movement at the Tg80 DSB in the absence of Uls1. MSD analysis of LacI-GFP (TG side) and Rad52-Ruby2 (non-TG side) foci was performed (as Figure 4D). ULS1 deletion slightly reduced the basal subdiffusive chromatin movement even before HO induction (Figure 6F, left panel) and strongly reduced DSB movement on both sides of the HO-induced break in the Tg80 strain (Figure 6F, dotted lines). Moreover, the level of Rad52 foci in uls1D cells was reduced. Both of these observations correlate with the elevated rate of NHEJ repair in uls1D cells (Figure 6D). Thus more NHEJ correlates with less movement, and both were favored by uls1D.

In wild-type backgrounds, the TG-rich side of the Tg80 DSB failed to bind Mps3, and this coincided with reduced imprecise NHEJ. Consistent with earlier work, this argues that Mps3-mediated sequestration of resected breaks favors imprecise NHEJ over ectopic recombination. To see whether deletion of the Mps3 nucleoplasmic domain (mps3DN) reduces NHEJ, we monitored end joining by qPCR across the cut site in a strain with efficient NHEJ, that is, the Tg18 strain (Figure S6D). Indeed, imprecise end-joining repair of the Tg18-proximal break dropped by 50% in mps3DN cells compared to cells bearing intact Mps3 (Figure S6D). This confirms that DSB association with Mps3 protects from ectopic recombination after resection, and in some cases favors imprecise NHEJ.

Taken together, our results argue that poly-sumoylation and Uls1 binding at a TG-flanked DSB protect the end from NHEJ, while helping load telomerase (Figure 7). The binding of a resected DSB to Mps3 favors imprecise NHEJ, as long as the ends are held together, which is not the case at the Tg80-flanked break. At these, Uls1 counters NHEJ by antagonizing end-to-end tethering and increasing chromatin movement. This in turn enhances the homology search and the observed nonreciprocal translocation.

DISCUSSION

Interstitial telomeric sequences (ITSs) are present in many organisms and are recognized as markers of chromosome fragile

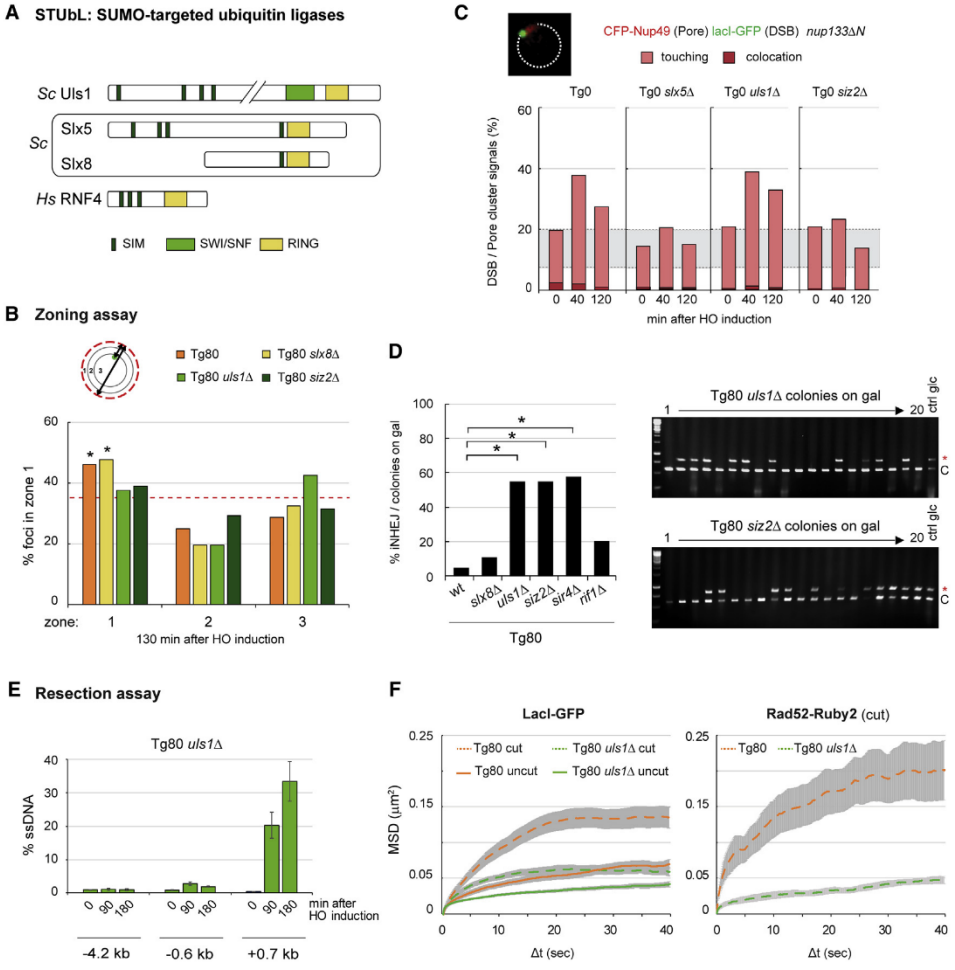

Figure 6. Siz2 and Uls1 Control Relocation of the TG Side at the Tg80 DSB and Suppress NHEJ

(A) Scheme of major yeast SUMO-dependent ubiquitin ligases (STUbLs) and RNF4 in man. Uls1 contains a SNF2-like ATPase as well as SUMO-interacting mot ifs (SIMs) and RING finger ubiquitin ligase domain.

(B) Zoning assay (Figure 1 B) for DSB distribution at 130 min after galactose-induced HO expression. Strains used were Tg80 (GA-8119), Tg80 slx8 D (GA-10050), Tg80 ul s1 D (GA-9855), and Tg80 siz2 D (GA-9794). Mean values of three independent experiments ± SEM are shown. *Non-random distribution in zone 1 (c^2 test of random versus experimental distribution; degree offreedom, 2; confidence limit, 95%), p = 0.048.

(C) Co-localization of MAT with the pore cluster in nup133 DN background, in wild-type (GA-7314), slx5 D (GA-7969), ul s1 D (GA-8475), and siz2 D (GA-7970) strains at specific times after HO induction. Pink and red colors indicate adjacency and colocalization, respectively (Horigome et al., 2016). Gray, random distribution zone based on theoretical tests.

(D) Indicated genes were deleted in the Tg80 strain (wild-type, GA-8119) generating GA-10050, GA-9855, GA-9794, GA-9158, and GA-9449. Graph presen ts the percentage of colonies repaired by imprecise NHEJ out of all survivors on galactose, as scored by qPCR across the HO cut site (Figure 1 C). n = 60 per strain. *Statistical significance with a p value < 10^{-4} in a c^2 test of wild-type and mutant with 95% confidence interval. Example gels showing 20 colonies ofindicated strains are shown.

(E) Loss of Uls1 does not release the resection block on the TG side of the DSB in Tg80. Resection scored by ssDNA AluI assay (Figure 2 A) with Tg80 ul s1 D (GA-9555). Probe distance from the HO consensus is shown. Three biological replicates, assayed in triplicate, are presented as mean values ± SEM.

(F) MSD analysis based on single-particle trajectories of LacI-GFP and Rad52-Ruby2 in Tg80 (GA-9913, orange) and Tg80 uls1 D (GA-10435, green), with and without HO induction (cut versus uncut). Tg80 control data are from Figure 4 C. Videos analyzed per strain are as follows: Tg80 lacI-GFP uncut, 23; Tg80 Rad52-Ruby2, 28; Tg80 lacI-GFP cut, 28; Tg80 ul s1 D LacI-GFP uncut, 43; Tg80 ul s1 D Rad52-Ruby2 cut, 25; Tg80 ul s1 D LacI-GFP cut, 9. Rad52 foci in the Tg80 ul s1 D are rare due to elevated rates of NHEJ.

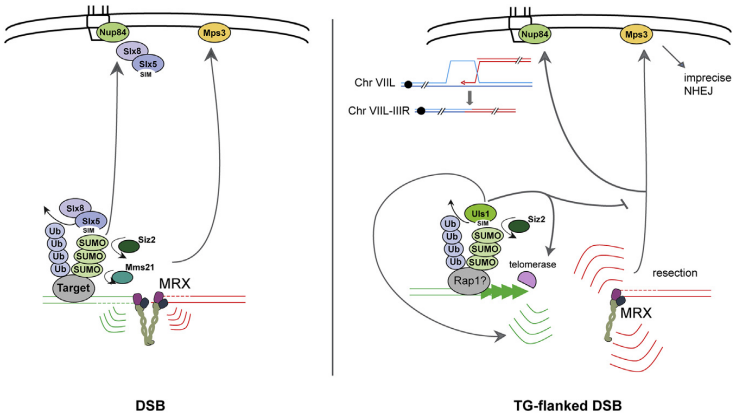

Figure 7. Model for the Effect of TG-Rich Repeats on DSB Repair

MRX binds and helps tether the ends of a Tg0 DSB together (Seeber et al., 2016). On the TG-rich side of a TG-flanked DSB, MRX binding is reduced, allowing the two ends to separate. Tg80 seeds telomerase, and once elongated, the end moves to the nuclear envelope, while the TG-free side, lacking end-to-end tethering, moves freely, favoring homology-driven ectopic recombination. The processing of Tg0 and Tg80 ends requires the translocase activity of Uls1 and sumoylation by the SUMO E3 ligase Siz2. Siz2 and Uls1 antagonize NHEJ.

sites (Ruiz-Herrera et al., 2009), hot spots for replication fork stalling, repeat expansion, deletion events (Aksenova et al., 2013), and nonreciprocal chromosomal rearrangements. It has been unclear whether ITSs influence the repair pathway or only generate more damage. By inserting a short stretch of yeast telomeric repeats next to a controlled HO cleavage site at the MAT locus, 80 bp of a TG-rich repeat was shown sufficient to significantly alter DSB repair outcome. Five Rap1 binding sites blocked resection of the TG-rich side of the break, allowing separation of the two break ends and enabling distinct repair mechanisms to act. MRX binding was reduced only on the repeat-containing side, while the opposite side was resected normally for HR and Rad52-mediated Rad51 loading. The distal side of the break shows dramatically increased subnuclear movement, which correlates with a nonreciprocal ectopic recombination event or chromosomal translocation. All survivor colonies of persistent HO endonuclease expression underwent the ChrIII-ChrVII translocation, while without the TG-rich insert, almost all undergo repair by imprecise NHEJ (Figure 5). This is striking because asymmetric chromosomal translocation at repeats is a frequent form of genomic instability in cancer cells. Mechanisms that suppress their occurrence are unknown.

We propose that the absence of MRX, which holds DSB ends together at TG-free DSBs (Seeber et al., 2016), and the ensuing increase in DSB movement, both attenuate NHEJ and enable the distal side of the break to engage in homology search. We note that loss of the translocase activity of the SUMO-targeted ubiquitin ligase, Uls1, or silencing factor Sir4, increase the rate ofimprecise NHEJ over translocation (Figure 6 and S6 C), but does not increase end resection on the TG-rich side of the break (Figures 3 C and S5 A). Thus, the resection-initiating role of MRX may not be the definitive parameter in repair pathway choice. Instead, MRX may influence repair outcome by recruiting Sae2 or Tel1, or it may simply hold the two sides of the break together, reducing their uncoordinated mobility (Seeber et al., 2016). We cannot exclude a role for the MNT2 homology present at MAT in the enhanced end movement, yet the MNT2 insert did not have a significant effect on repair outcome in the Tg0 strain (Figure 5 B). Thus, it is not sufficient to promote end movement. Rather, we argue that the asymmetrical binding of MRX coupled with the telomerase-seeding capacity of $(TG_{1\text{-}3})_n$ suppress imprecise NHEJ and promote ectopic HR.

Importantly, the nature of the repeat sequence present at the DSB can influence the pathway of repair. TTAGGG can seed telomerase, yet it does not significantly increase ectopic HR when it flanks the HO-induced break. Moreover, a single Rap1 binding site fails to have the same effect as a cluster of 5. We cannot attribute the repair outcome to the Rap1 ligand, Rif1, given that rif1D only slightly enhances imprecise NHEJ at the Tg80 break (Figure 6 D). Stronger effects on repair were seen upon ablation of either the SUMO E3 ligase, Siz2, or the SUMO binding ATPase, Uls1. Both factors significantly suppress imprecise NHEJ (Figure 6). The recognition of poly-sumolyated Rap1 by Uls1 (Lescasse et al., 2013) may lead to the ubiquitination and degradation of Rap1 or other sumoylated targets at break sites . We note that the loss of Uls1 also reduces the exaggerate d movement of the untethered ends, suggesting that its loss may restore MRX binding to the Tg80 end.

While the Siz2 SUMO ligase acts at both Tg0 and Tg80 DSBs, the effect of Uls1 appears to be specific for Tg80-adjacent breaks. At TG-free DSBs, it was shown that poly-sumoylation recruits the SUMO-targeted ubiquitin ligase Slx5/Slx8, which then mediates relocation of the DSB to nuclear pores (Horigome et al., 2016). This does not require Uls1 (Figure 6 C). The opposite is true for the shift of Tg80 to pores: repeat-flanked damage depends on Uls1 and not on Slx5/Slx8 (Figure 6 B). Uls1 has, in addition to SUMO binding motifs and a E3-like Ring finger, a unique ATP-dependent translocase activity, which is required to impair NHEJ at the Tg80 end (Figure S6 C).

Besides these break-binding factors, we find that nuclear envelope binding sites influence repair outcome. The loss of the nucleoplasmic domain of the yeast Mps3 protein (mps3 DN) led to increased spontaneous sister chromatid exchange (Horigome et al., 2014) and less imprecise NHEJ (Figure S6 A). In contrast, DSB-pore interaction favored ectopic recombination pathways, BIR, and other nonreciprocal homology-driven events (Chung et al., 2015; Horigome et al., 2014).

Telomeric Identity and DNA Repair Outcome

This work sheds new light on how cells safeguard telomeres: the $(TG_{1\text{-}3})_n$ sequence inhibits imprecise end joining in yeast, in a length-dependent manner. This explains why TG repeats are primarily found at telomeres; the largest internal $(TG_{1\text{-}3})_n$ stretch in budding yeast is <34 bp (Mangahas et al., 2001). From an evolutionary perspective, ITSs of $(TG_{1\text{-}3})_n$ repeats R 80 bp would be destabilizing, inducing translocations at spontaneous DSBs. Whereas other researchers have invoked folded G-structures as an intrinsic means to block NHEJ and/or recombination at telomeres (Moriyama et al., 2017), the effect we see does not stem solely from TG richness. Human and yeast telomere repeats are similarly TG-rich, yet did not have the same impact. Intriguingly, an earlier study still saw MRX bound to a subtelomeric TG-flanked DSB, although end resection was reduced (Ribeyre and Shore, 2012). These authors did not score repair pathway choice, however, since all survivors simply lost the distal part of the chromosome, a nonlethal event in their strain. Because the ChrIII sequences distal to MAT are essential, our internal TG-flanked DSB more closely reflects ITS-associated breaks in mammalian cells.

In the human genome, short ITSs have been correlated with jumping translocations, a rare case of cytological aberrations in which a fragment of donor chromosome is translocated onto more than one recipient chromosome. This kind of nonreciprocal translocation is frequent in Prader-Willi syndrome and hematological malignancies (Miller et al., 2015; Rivera et al., 1990; Vermeesch et al., 1997). Previous work also reported several kinds of chromosome rearrangements favored by internal telomeric sequences in yeast (Aksenova et al., 2013). While fork stalling was suggested to drive these rearrangements, they may stem from TG-specific factors that favor ectopic recombination over end joining, by competing with MRX and preventing end-to-end tethering. We show in yeast that this correlates with an asymmetrical processing of DNA ends and nonreciprocal translocation events. We propose that asymmetrical end processing may be the critical feature that drives recombination-dependent, nonreciprocal translocations at a TG-flanked DSB. In our system, this required the activity of the SNF2-ATPase containing putative SUMO-targeted ubiquitin ligase, Uls1, which disfavors imprecise NHEJ. We speculate that, in mammals, the repair of repeat-flanked DSBs may be influenced by ATRX, a mammalian AAA+ translocase (Lovejoy et al., 2012), which suppresses repeat-induced translocations at ITSs.

STAR + METHODS

Detailed methods are provided in the online version of this paper and include the following:

- KEY RESOURCES TABLE
- CONTACT FOR REAGENT AND RESOURCE SHARING
- EXPERIMENTAL MODEL AND SUBJECT DETAILS
  - Yeast Strains and Construction
- METHOD DETAILS
  - DNA Extraction for PCR
  - Fluorescence Microscopy
  - DSB Survival Assay by Colony Formation
  - Pulsed-Field Gel Electrophoresis (PFGE)
  - Telomerase PCR at a Double Strand Break
  - Chromatin Immunoprecipitation (ChIP)
  - Resection Assay
  - SMRTbell Library Construction for Sequencing
  - PacBio RSII Sequencing
- QUANTIFICATION AND STATISTICAL ANALYSIS
- DATA AND SOFTWARE AVAILABILITY

SUPPLEMENTAL INFORMATION

Supplemental Information includes six figures and three tables and can be found with this article online at https://doi.org/10.1016/j.celrep.2018.07.102.

ACKNOWLEDGMENTS

We thank H. Ferreira for the Uls1 plasmids, J.E. Haber for yeast strains, and D. Shore for constructs and these three and J. Lingner (EPFL) for helpful advice. We thank E. Oakeley for supervising the PacBio sequencing, J. Eglinger, S. Bourke, and L. Gelman for advanced imaging, and M. Tsai-Pflugfelder for experimental support. I.M. was supported by the Swiss National Science Foundation NCCR Frontiers in Genetics PhD program, C.H. by a Marie Curie International Fellowship, and the Gasser laboratory by the Novartis Research Foundation and Swiss National Science Foundation Research Grant 310030B_156936 awarded to S.M.G.

AUTHOR CONTRIBUTIONS

I.M. performed experiments, interpreted results, and prepared figures and text. K.S. and N.D. performed experiments, interpreted results, and edited figures and text. A.S., A.C., I.Y., and C.H. performed experiments, interpreted results, and made figures. U.N. performed deep sequencing. S.M.G. supervised, interpreted results, and helped write the paper.

DECLARATION OF INTERESTS

The authors declare no competing interests.

Received: March 24, 2018
Revised: June 7, 2018
Accepted: July 27, 2018
Published: September 4, 2018

REFERENCES

Aksenova, A.Y., Greenwell, P.W., Dominska, M., Shishkin, A.A., Kim, J.C., Petes, T.D., and Mirkin, S.M. (2013). Genome rearrangements caused by interstitial telomeric sequences in yeast. Proc. Natl. Acad. Sci. USA 110, 19866–19871.

Amaral, N., Ryu, T., Li, X., and Chiolo, I. (2017). Nuclear dynamics of heterochromatin repair. Trends Genet. 33, 86–100.

Amitai, A., Seeber, A., Gasser, S.M., and Holcman, D. (2017). Visualization of chromatin decompaction and break site extrusion as predicted by statistical polymer modeling of single-locus trajectories. Cell Rep. 18, 1200–1214.

Azam, M., Lee, J.Y., Abraham, V., Chanoux, R., Schoenly, K.A., and Johnson, F.B. (2006). Evidence that the S. cerevisiae Sgs1 protein facilitates recombinational repair of telomeres during senescence. Nucleic Acids Res. 34, 506–516.

Bertuch, A.A., and Lundblad, V. (2003). The Ku heterodimer performs separable activities at double-strand breaks and chromosome termini. Mol. Cell. Biol. 23, 8202–8215.

Boulton, S.J., and Jackson, S.P. (1996). Identification of a Saccharomyces cerevisiae Ku80 homologue: roles in DNA double strand break rejoining and in telomeric maintenance. Nucleic Acids Res. 24, 4639–4648.

Brevet, V., Berthiau, A.S., Civitelli, L., Donini, P., Schramke, V., Ge´li, V., Ascenzioni, F., and Gilson, E. (2003). The number of vertebrate repeats can be

regulated at yeast telomeres by Rap1-independent mechanisms. EMBO J. 22, 1697–1706 .

Cannavo, E., and Cejka, P. (2014). Sae2 promotes dsDNA endonuclease activity within Mre11-Rad50-Xrs2 to resect DNA breaks. Nature 514, 122–125 .

Chiolo, I., Minoda, A., Colmenares, S.U., Polyzos, A., Costes, S.V., and Karpen, G.H. (2011). Double-strand breaks in heterochromatin move outside of a dynamic HP1a domain to complete recombinational repair. Cell 144, 732–744 .

Chung, D.K., Chan, J.N., Strecker, J., Zhang, W., Ebrahimi-Ardebili, S., Lu, T., Abraham, K.J., Durocher, D., and Mekhail, K. (2015). Perinuclear tethers license telomeric DSBs for a broad kinesin- and NPC-dependent DNA repair process. Nat. Commun. 6, 7742 .

Churikov, D., Charifi, F., Eckert-Boulet, N., Silva, S., Simon, M.N., Lisby, M., and Ge´li, V. (2016). SUMO-dependent relocalization of eroded telomeres to nuclear pore complexes controls telomere recombination. Cell Rep. 15, 1242–1253 .

Cremona, C.A., Sarangi, P., Yang, Y., Hang, L.E., Rahman, S., and Zhao, X. (2012). Extensive DNA damage-induced sumoylation contributes to replication and repair and acts in addition to the mec1 checkpoint. Mol. Cell 45, 422–432 .

Deshpande, R.A., Williams, G.J., Limbo, O., Williams, R.S., Kuhnlein, J., Lee, J.H., Classen, S., Guenther, G., Russell, P., Tainer, J.A., and Paull, T.T. (2014). ATP-driven Rad50 conformations regulate DNA tethering, end resection, and ATM checkpoint signaling. EMBO J. 33, 482–500 .

Dion, V., Kalck, V., Horigome, C., Towbin, B.D., and Gasser, S.M. (2012). Increased mobility of double-strand breaks requires Mec1, Rad9 and the homologous recombination machinery. Nat. Cell Biol. 14, 502–509 .

Ferreira, H.C., Luke, B., Schober, H., Kalck, V., Lingner, J., and Gasser, S.M. (2011). The PIAS homologue Siz2 regulates perinuclear telomere position and telomerase activity in budding yeast. Nat. Cell Biol. 13, 867–874 .

Förstemann, K., Ho¨ss, M., and Lingner, J. (2000). Telomerase-dependent repeat divergence at the 3 ^{0} ends of yeast telomeres. Nucleic Acids Res. 28, 2690–2694 .

Gartenberg, M.R., Neumann, F.R., Laroche, T., Blaszczyk, M., and Gasser, S.M. (2004). Sir-mediated repression can occur independently of chromosomal and subnuclear contexts. Cell 119, 955–967 .

Gilson, E., Roberge, M., Giraldo, R., Rhodes, D., and Gasser, S.M. (1993). Distortion of the DNA double helix by RAP1 at silencers and multiple telomeric binding sites. J. Mol. Biol. 231, 293–310 .

Hage, A.E., and Houseley, J. (2013). Resolution of budding yeast chromosomes using pulsed-field gel electrophoresis. Methods Mol. Biol. 1054, 195–207 .

Hauer, M.H., Seeber, A., Singh, V., Thierry, R., Sack, R., Amitai, A., Kryzhanovska, M., Eglinger, J., Holcman, D., Owen-Hughes, T., and Gasser, S.M. (2017). Histone degradation in response to DNA damage enhances chromatin dynamics and recombination rates. Nat. Struct. Mol. Biol. 24, 99–107 .

Hirano, Y., Fukunaga, K., and Sugimoto, K. (2009). Rif1 and rif2 inhibit localization of tel1 to DNA ends. Mol. Cell 33, 312–322 .

Horigome, C., Oma, Y., Konishi, T., Schmid, R., Marcomini, I., Hauer, M.H., Dion, V., Harata, M., and Gasser, S.M. (2014). SWR1 and INO80 chromatin remodelers contribute to DNA double-strand break perinuclear anchorage site choice. Mol. Cell 55, 626–639 .

Horigome, C., Bustard, D.E., Marcomini, I., Delgoshaie, N., Tsai-Pflugfelder, M., Cobb, J.A., and Gasser, S.M. (2016). PolySUMOylation by Siz2 and Mms21 triggers relocation of DNA breaks to nuclear pores through the Slx5/Slx8 STUbL. Genes Dev. 30, 931–945 .

Kalocsay, M., Hiller, N.J., and Jentsch, S. (2009). Chromosome-wide Rad51 spreading and SUMO-H2A.Z-dependent chromosome fixation in response to a persistent DNA double-strand break. Mol. Cell 33, 335–343 .

Khadaroo, B., Teixeira, M.T., Luciano, P., Eckert-Boulet, N., Germann, S.M., Simon, M.N., Gallina, I., Abdallah, P., Gilson, E., Ge´li, V., and Lisby, M. (2009). The DNA damage response at eroded telomeres and tethering to the nuclear pore complex. Nat. Cell Biol. 11, 980–987 .

Kim, J.C., and Mirkin, S.M. (2013). The balancing act of DNA repeat expansions. Curr. Opin. Genet. Dev. 23, 280–288 .

Langerak, P., Mejia-Ramirez, E., Limbo, O., and Russell, P. (2011). Release of Ku and MRN from DNA ends by Mre11 nuclease activity and Ctp1 is required for homologous recombination repair of double-strand breaks. PLoS Genet. 7, e1002271 .

Lee, S.E., Bressan, D.A., Petrini, J.H., and Haber, J.E. (2003). Complementation between N-terminal S. cerevisiae mre11 alleles in DNA repair and telomere length maintenance. DNA Repair 1, 27–40 .

Leffak, M. (2017). Break-induced replication links microsatellite expansion to complex genome rearrangements. BioEssays 39, 1700025 .

Lescasse, R., Pobiega, S., Callebaut, I., and Marcand, S. (2013). End-joining inhibition at telomeres requires the translocase and polySUMO-dependent ubiquitin ligase Uls1. EMBO J. 32, 805–815 .

Lisby, M., Barlow, J.H., Burgess, R.C., and Rothstein, R. (2004). Choreography of the DNA damage response: spatiotemporal relationships among checkpoint and repair proteins. Cell 118, 699–713 .

Lovejoy, C.A., Li, W., Reisenweber, S., Thongthip, S., Bruno, J., de Lange, T., De, S., Petrini, J.H., Sung, P.A., Jasin, M., et al.; ALT Starr Cancer Consortium (2012). Loss of ATRX, genome instability, and an altered DNA damage response are hallmarks of the alternative lengthening of telomeres pathway. PLoS Genet. 8, e1002772 .

Lydeard, J.R., Jain, S., Yamaguchi, M., and Haber, J.E. (2007). Break-induced replication and telomerase-independent telomere maintenance require Pol32. Nature 448, 820–823 .

Mangahas, J.L., Alexander, M.K., Sandell, L.L., and Zakian, V.A. (2001). Repair of chromosome ends after telomere loss in Saccharomyces . Mol. Biol. Cell 12, 4078–4089 .

Martin, S.G., Laroche, T., Suka, N., Grunstein, M., and Gasser, S.M. (1999). Relocalization of telomeric Ku and SIR proteins in response to DNA strand breaks in yeast. Cell 97, 621–633 .

Matsuzaki, K., Shinohara, A., and Shinohara, M. (2008). Forkhead-associated domain of yeast Xrs2, a homolog of human Nbs1, promotes nonhomologous end joining through interaction with a ligase IV partner protein, Lif1. Genetics 179, 213–225 .

Mattarocci, S., Reinert, J.K., Bunker, R.D., Fontana, G.A., Shi, T., Klein, D., Cavadini, S., Faty, M., Shyian, M., Hafner, L., et al. (2017). Rif1 maintains telomeres and mediates DNA repair by encasing DNA ends. Nat. Struct. Mol. Biol. 24, 588–595 .

Meister, P., Gehlen, L.R., Varela, E., Kalck, V., and Gasser, S.M. (2010). Visualizing yeast chromosomes and nuclear architecture. Methods Enzymol. 470, 535–567 .

Miller, C.R., Stephens, D., Ruppert, A.S., Racke, F., McFaddin, A., Breidenbach, H., Lin, H.J., Waller, K., Bannerman, T., Jones, J.A., et al. (2015). Jumping translocations, a novel finding in chronic lymphocytic leukaemia. Br. J. Haematol. 170, 200–207 .

Miné-Hattab, J., and Rothstein, R. (2012). Increased chromosome mobility facilitates homology search during recombination. Nat. Cell Biol. 14, 510–517 .

Miyazaki, T., Bressan, D.A., Shinohara, M., Haber, J.E., and Shinohara, A. (2004). In vivo assembly and disassembly of Rad51 and Rad52 complexes during double-strand break repair. EMBO J. 23, 939–949 .

Moretti, P., Freeman, K., Coodly, L., and Shore, D. (1994). Evidence that a complex of SIR proteins interacts with the silencer and telomere-binding protein RAP1. Genes Dev. 8, 2257–2269 .

Moriyama, K., Lai, M.S., and Masai, H. (2017). Interaction of Rif1 protein with G-quadruplex in control of chromosome transactions. Adv. Exp. Med. Biol. 1042, 287–310 .

Nagai, S., Dubrana, K., Tsai-Pflugfelder, M., Davidson, M.B., Roberts, T.M., Brown, G.W., Varela, E., Hediger, F., Gasser, S.M., and Krogan, N.J. (2008). Functional targeting of DNA damage to a nuclear pore-associated SUMO-dependent ubiquitin ligase. Science 322, 597–602 .

Negrini, S., Ribaud, V., Bianchi, A., and Shore, D. (2007). DNA breaks are masked by multiple Rap1 binding in yeast: implications for telomere capping and telomerase regulation. Genes Dev. 21, 292–302.

Nicolette, M.L., Lee, K., Guo, Z., Rani, M., Chow, J.M., Lee, S.E., and Paull, T.T. (2010). Mre11-Rad50-Xrs2 and Sae2 promote 5′ strand resection of DNA double-strand breaks. Nat. Struct. Mol. Biol. 17, 1478–1485.

Padeken, J., Zeller, P., and Gasser, S.M. (2015). Repeat DNA in genome organization and stability. Curr. Opin. Genet. Dev. 31, 12–19.

Palm, W., and de Lange, T. (2008). How shelterin protects mammalian telomeres. Annu. Rev. Genet. 42, 301–334.

Prudden, J., Pebernard, S., Raffa, G., Slavin, D.A., Perry, J.J., Tainer, J.A., McGowan, C.H., and Boddy, M.N. (2007). SUMO-targeted ubiquitin ligases in genome stability. EMBO J. 26, 4089–4101.

Ribaud, V., Ribeyre, C., Damay, P., and Shore, D. (2012). DNA-end capping by the budding yeast transcription factor and subtelomeric binding protein Tbf1. EMBO J. 31, 138–149.

Ribeyre, C., and Shore, D. (2012). Anticheckpoint pathways at telomeres in yeast. Nat. Struct. Mol. Biol. 19, 307–313.

Rivera, H., Zuffardi, O., and Gargantini, L. (1990). Nonreciprocal and jumping translocations of 15q1—qter in Prader-Willi syndrome. Am. J. Med. Genet. 37, 311–317.

Ruiz-Herrera, A., Nergadze, S.G., Santagostino, M., and Giulotto, E. (2009). Telomeric repeats far from the ends: mechanisms of origin and role in evolution. Cytogenet. Genome Res. 122, 219–228.

Sage, D., Neumann, F.R., Hediger, F., Gasser, S.M., and Unser, M. (2005). Automatic tracking ofindividual fluorescence particles: application to the study of chromosome dynamics. IEEE Trans. Image Process. 14, 1372–1383.

Schober, H., Ferreira, H., Kalck, V., Gehlen, L.R., and Gasser, S.M. (2009). Yeast telomerase and the SUN domain protein Mps3 anchor telomeres and repress subtelomeric recombination. Genes Dev. 23, 928–938.

Seeber, A., Hegnauer, A.M., Hustedt, N., Deshpande, I., Poli, J., Eglinger, J., Pasero, P., Gut, H., Shinohara, M., Hopfner, K.P., et al. (2016). RPA mediates recruitment of MRX to forks and double-strand breaks to hold sister chromatids together. Mol. Cell 64, 951–966.

Sfeir, A., and Symington, L.S. (2015). Microhomology-mediated end joining: a back-up survival mechanism or dedicated pathway? Trends Biochem. Sci. 40, 701–714.

Shore, D., and Bianchi, A. (2009). Telomere length regulation: coupling DNA end processing to feedback regulation of telomerase. EMBO J. 28, 2309–2322.

Storici, F., and Resnick, M.A. (2006). The delitto perfetto approach to in vivo site-directed mutagenesis and chromosome rearrangements with synthetic oligonucleotides in yeast. Methods Enzymol. 409, 329–345.

Symington, L.S., and Gautier, J. (2011). Double-strand break end resection and repair pathway choice. Annu. Rev. Genet. 45, 247–271.

Torres-Rosell, J., Sunjevaric, I., De Piccoli, G., Sacher, M., Eckert-Boulet, N., Reid, R., Jentsch, S., Rothstein, R., Aragón, L., and Lisby, M. (2007). The Smc5-Smc6 complex and SUMO modification of Rad52 regulates recombinational repair at the ribosomal gene locus. Nat. Cell Biol. 9, 923–931.

Tsouroula, K., Furst, A., Rogier, M., Heyer, V., Maglott-Roth, A., Ferrand, A., Reina-San-Martin, B., and Soutoglou, E. (2016). Temporal and spatial uncoupling of DNA double strand break repair pathways within mammalian heterochromatin. Mol. Cell 63, 293–305.

Vermeesch, J.R., Petit, P., Speleman, F., Devriendt, K., Fryns, J.P., and Marynen, P. (1997). Interstitial telomeric sequences at the junction site of a jumping translocation. Hum. Genet. 99, 735–737.

Wotton, D., and Shore, D. (1997). A novel Rap1p-interacting factor, Rif2p, cooperates with Rif1p to regulate telomere length in Saccharomyces cerevisiae. Genes Dev. 11, 748–760.

Zierhut, C., and Diffley, J.F. (2008). Break dosage, cell cycle stage and DNA replication influence DNA double strand break response. EMBO J. 27, 1875–1885.

STAR + METHODS

KEY RESOURCES TABLE

REAGENT or RESOURCE	SOURCE	IDENTIFIER
Antibodies		
Mab414 nuclear pore antibody	abcam	Mab414, ab24609
Sheep anti-mouse IgG magnetic beads	Invitrogen	11031
Anti-HA antibody	Santa Cruz Biotech	F-7, sc-7392
Anti-PK antibody	Acris Antibodies	SV5-PK1, SM1691
Sheep anti-rabbit IgG Dynabeads	Invitrogen	11203D
anti-yKu70 rabbit polyclonal antibody	A. E. Tomkinson	anti-Hdf1
Critical Commercial Assays		
SMRTbell Template Prep Kit	Pacific Biosciences	100-259-100
PippinHT	Sage Science	HTP0001
protease inhibitors (cOmplete EDTA-free)	Roche	04693159001
AccuPrep DNA extraction kit	Bioneer	K-3034
MagBead-binding One Cell Per Well	Pacific Biosciences	100-267-800-03
Binding Kit P6 v2	Pacific Biosciences	100-372-700
DNA Sequencing Kit 4.0	Pacific Biosciences	100-364-600
Deposited Data		
Pacific Biosciences sequencing datasets	NCBI Bioproject database	Submission ID SUB4312748, under Bioproject ID PRJNA482327
Experimental Models: Organisms/Strains		
Budding yeast: see Table S1	Susan Gasser, FMI	Table S1
Oligonucleotides		
Primer lists: see Tables S2 and S3	different suppliers, this paper	Tables S2 and S3
Recombinant DNA		
Plasmid expressing wild-type ULS1	HFP269, H. Ferreira, St. Andrews University	p416-FLAG-ULS1
Plasmid expressing translocase mutant uls1-K975A	HFP282, H. Ferreira, St. Andrews University	p416-FLAG-uls1-K975A
Plasmid containing EXO1	Lee et al., 2003	pJH1772
Plasmid containing Ruby2 fluorophore	Addgene	pFA6a-link-yomRuby2-Kan
Plasmid containing TG80-HO-3 ^{9}MNT2	Ribeyre and Shore, 2012	pIM35
Plasmid containing (TTAGGG)60-HO-3^{9}MNT2	Ribaud et al., 2012	pVR4
Plasmid 3571 containing TG250-HO-3^{9}MNT2	This paper	pUC57-TG250
Plasmid 3892 containing TG18-HO-3 ^{9}MNT2	This paper	pUC57-TG18
Software and Algorithms		
SPT analysis and biophysical parameter extraction	S. Gasser, Amitai et al., 2017	NA
Spot tracker ImageJ (FIJI) plug-in	S. Gasser, Sage et al., 2005	NA
PointPicker	S. Gasser, Meister et al., 2010	NA

CONTACT FOR REAGENT AND RESOURCE SHARING

All reagents and resources can be obtained by contacting Susan M. Gasser, at the Friedrich Miescher Institute for Biomedical Research, Maulbeerstr. 66, 4058 Basel, Switzerland; Susan.gasser@fmi.ch

EXPERIMENTAL MODEL AND SUBJECT DETAILS

Yeast Strains and Construction

All strains were derived from JKM179 and are listed in Table S1. Strain GA-8119 (TG80-HO-3 ^{0}MNT2 construct at MAT) and strain GA-9823 ((TTAGGG)60-HO-3 ^{0}MNT2 construct at MAT) were constructed by delitto perfetto (Storici and Resnick, 2006), followed by insertion of the TG-HO-3 ^{0}MNT2 PCR fragment obtained from plasmid pIM35 (Ribeyre and Shore, 2012) and pVR4 (Ribaud et al., 2012) respectively, using primers SG-6571 and SG-6572. Strain GA-9918 was constructed by subsequent deletion of the 3^{0} MNT2 fragment present in GA-8119. The strains GA-8502 and GA-9824 were constructed the same as GA-8119, except that the PCR products containing TG250-HO-3 ^{0}MNT2 orTG18-HO-3 ^{0}MNT2 were amplified from plasmids 3571 (pUC57-TG250) and 3892 (pUC57-TG18), respectively (available upon request). These constructs differ from TG80-HO-3 ^{0}MNT2 only by the presence of either 250 bp or 18 bp of TG repeats, instead of 80. The Ruby2 fluorophore plasmid used to create GA-9912 and GA-9948 was obtained from Addgene. For all live microscopy and localization assays, SC medium was used instead of YP. For DSB localization assays, 1ml of cells was harvested at each time point, fixed in 4% paraformaldehyde (final concentration) for 5 min and washed three times with PBS before microscopy.

METHOD DETAILS

The primers used in this work are listed in Tables S2 and S3. The plasmid containing EXO1 in Figure 2C is pJH1772 (Lee et al., 2003). The plasmid expressing wild-type ULS1 (p416-FLAG-ULS1) and translocase mutant uls1-K975A (p416-FLAG-uls1-K975A) were cloned into pRS416 from HFP269 and HFP282 (gifts from Dr. H. Ferreira), respectively.

DNA Extraction for PCR

Unless otherwise specified, DNA for PCR and quantitative PCR was extracted by spinning down 1ml of cells and resuspending them in 200 ml DNA isolation buffer (2% v/v Triton X-100, 1% w/v SDS, 100 mM NaCl, 10 mM Tris-HCl pH 8, 1 mM EDTA). Cell lysis was performed by addition of 200 ml zirconia/silica beads and 200 ml phenol:chloroform:isoamylalcohol (25:24:1), followed by vortexing for 5 min at room temperature. 200 ml TE buffer pH 8 was added to each sample, and samples were centrifuged for 5 min at 16,000 g. DNA was precipitated by addition of 1 ml 100% ethanol and 50 ml of 3 M sodium acetate to the aqueous phase. Samples were incubated at −70°C for 40 min, then centrifuged for 10 min at 16,000 g. The pellet was washed once in 70% ethanol, dried and resuspended in 100 ml sterile water for use in PCR reactions.

Fluorescence Microscopy

Images for assessment of DSB localization by performing zoning or colocalization measurements were captured on a Metamorph-driven Spinning-disk confocal system based on an Olympus IX81 microscope, Yokogawa CSU-X1 scan head, EM- CCD Cascade II (Photometrics) camera and an ASI MS-2000 Z-piezo stage. We used a PlanApo 3 100, NA 1.45 total internal reflection fluorescence microscope oil objective.

Live microscopy was done at 25 °C on a Nikon Eclipse Ti microscope, two EM-CCD Cascade II (Photometrics) cameras, an ASI MS-2000 Z-piezo stage and a PlanApo x100, NA 1.45 total internal reflection fluorescence microscope oil objective and Visiview software. Fluorophores were excited at 561 nm (for Ruby2) and at 491 nm (for GFP), and emitted fluorescence was acquired simultaneously on separate cameras (Semrock FF01-617/73-25 filter for mCherry/ Ruby2 and Semrock FF02-525/40-25 filter for GFP). Time-lapse series were streamed taking 8 optical slices per stack every 80 ms for 60 s with 10 ms exposure times per slice respectively with laser powers set to ~7%–12% for either laser line. Gain was set to 800.

DSB Survival Assay by Colony Formation

Cultures were grown in YPLGg medium (2% glycerol lactate, 0.05% glucose) at 30 °C overnight to late log phase (1 3 10^{7} cells/ml). For colony formation assays (e.g., Figure 5), cells were counted and diluted as follows: for each strain, 10 and 100 cells were plated on two YPAD (Yeast extract, bactopeptone, adenine, and 2% dextrose (glucose)) plates, while 10,000, 20,000 and 50,000 cells were plated on YPGal (2% galactose instead of dextrose) plates and incubated at 30 °C. Survivor colonies were counted after 4 days at 30°C. In Figure S6C, cells were grown in synthetic LGg-uracil medium, and survivors were obtained on synthetic-2% galactose-uracil medium after 5 days at 30 °C. Total survivor numbers were calculated by normalizing colony number on YPGal to colony number on YPD. For the experiment in Figure 5C: in late log phase, HO cut was induced by addition of 2% galactose in liquid cultures. Before induction (time 0'), cells were counted and diluted. For each culture, 10 or 100 cells were plated in duplicate on YPAD plates. At 90 and 180 min after cut induction, 250 and 500 cells for each strain were plated in duplicate on YPAD plates, respectively. Plates were incubated at 30 °C. Survivor colonies were counted after 3 days ofincubation, and the total survivor numbers were determined at each time point by normalizing number of colonies from that time point to number of colonies at time 0 (before HO induction).

Pulsed-Field Gel Electrophoresis (PFGE)

PFGE was performed as previously described (Hage and Houseley, 2013). Yeast genomic DNA was prepared in an agarose plug as described in the instruction manual of the Pulsed Field Electrophoresis System (Bio-Rad, CHEF-DR II) with the following

modifications. Cultures were grown in YPLGg overnight to log phase. About 5x10 ^{5} cells were harvested and washed in ice-cold 0.05 M EDTA pH 8.0 and pelleted. Cell pellets were resuspended in Zymolyase buffer (50 mM Na-PO4 [pH 7.0], 50 mM EDTA, 1 mM dithiothreitol [DTT]) and embedded in a 2% agarose plug (Cleancut agarose, Biorad): 50 µl agarose was mixed with 50 µl of cells. Genomic DNA was prepared by treating the plug with 0.4 mg/ml Zymolyase (20T, Seikagaku) in Zymolyase buffer at 37 °C for 1 h, followed by 1 mg/ml proteinase K digestion in 10 mM Tris-HCl (pH 7.5), 50 mM EDTA, 1% sodium N-lauroylsarcosinate at 50°C or 30 °C for 15–20 h. After 4 washes in 20 mM Tris-50 mM EDTA pH 8.0, plugs were loaded in 0.8% agarose/0.5 3 Tris-Borate-EDTA (TBE) on the CHEF-DR II (Bio-Rad) and chromosomal DNA was migrated at 14 °C, 6V/cm, 60 s switch time for 15 h, then 90 s for 9 h. The gel was stained for 1 h at room temperature with RedSafe (Fisher Scientific), destained for 2 h and imaged on c400 Imaging System (Azure Biosystems).

Telomerase PCR at a Double Strand Break

Telomerase PCR was performed as previously described (Förstemann et al., 2000). DNA was extracted from 1.5 ml of culture collected at each time point indicated (Figure S5 D). A starting amount of 150 ng/ µl of DNA was used in each C-tailing reaction: first, DNA was diluted in CutSmart buffer (NEB) to a final volume of 8 µl and denatured at 96 °C for 10 min on a PCR block. Once samples cooled down to 37 °C, 1 µl of tailing mix was quickly added to each reaction: the tailing mix contained 1 U of terminal transferase (NEB), 0.1 mM dCTP and 1x CutSmart buffer. The tailing reaction was performed using the following program: 37 °C for 30 min, 65°C for 10 min and 95 °C for 5 min. Immediately afterward, telomerase PCR was started by addition of 30 µl PCR mix to each tube. The PCR mix contained 0.5 mM fresh dNTPs, 0.75 µM G18 primer (SG-7613), 2.5 U ExTaq polymerase (Takara), 0.75 µM forward primer (SG-2659 for Tg0, SG-6611 for Tg80), 4 µl 10X telomerase PCR buffer. 10X PCR buffer containing 50% glycerol, 670 mM Tris-HCl (pH 8.8), 160 mM (NH4)2SO4, 0.1% Tween-20, 0.74% HCl. The telomerase PCR program was as follows: 95 °C 3 min, [95 °C for 30 s, 62 °C for 20 s, 72 °C for 20 s] for 35 cycles, and 72 °C for 5 min. PCR products were separated on a 2.5% agarose gel (10 µl PCR product with 2 µl 6x loading dye) and imaged with Azure c400 Imaging Systems. The control band was obtained in a standard PCR reaction using the same DNA, and primers SG-525 and SG-526 for the SMC2 gene.

Chromatin Immunoprecipitation (ChIP)

ChIP using the Mab414 nuclear pore antibody (Abcam) was performed as previously described (Horigome et al., 2014) with slight modifications. At each time point about 15x10 ^{8} cells were sampled, crosslinked with 1% formaldehyde for 20 min while rotating at rt, then washed twice in ice cold 1x PBS. 40 µl of sheep anti-mouse IgG magnetic beads (Invitrogen) per sample were washed twice in 500 µl PBS, 5 mg/ml bovine serum albumin (BSA, A-4503 Sigma Aldrich), and blocked in the same solution for 30 min while rotating at 4°C. Beads were washed with 500 µl PBS, and 1 µg nuclear pore antibody (mAB414) per sample was added to the beads followed by 4 h incubation while rotating at 4 °C. After incubation, antibody-coupled beads were washed twice in 1 ml lysis buffer (50 mM HEPES-KOH pH 7.5, 140 mM NaCl, 1 mM EDTA, 1% Triton X-100, 0.1% sodium deoxycholate) and then added to cell lysates, which were prepared as follows. Cell pellets were resuspended in 600 µl lysis buffer and lysed by addition of 200 µl zirconia-silica beads and bead beating in a bead beater (Fastprep-24 5G, MP Biomedicals) for 1 min at 6.5 m s-1 for 3 times. Lysates were recovered from beads by centrifugation at 2000 g for 10 min at 4 °C. The pellet fraction containing cross-linked chromatin was then resuspended in 1 mL oflysis buffer and sonicated on a (Bioruptor) for 20 cycles (30 s on, 30 s off). Samples were centrifuged at 7000 g for 2 min and the supernatant containing released chromatin proteins was recovered: 50 µl of the supernatant was collected as input and stored at −20°C until the crosslinking reversal step, and the rest was added to antibody-coupled beads and incubated on a rotating wheel at 4 °C overnight (about 16 h). The next day, beads were washed 3 times 5 min in lysis buffer, and once in wash buffer (10 mM Tris-HCl pH 8.0, 250 mM LiCl, 0.5% Nonidet P40 (Igepal), 0.5% sodium deoxycholate, 1 mM EDTA) for 10 min, and lastly once in Tris-EDTA (TE) pH 8.0 for 1 min. All washes were done on a rotating wheel at 4 °C. DNA was eluted from beads in 100 µl 1% SDS-TE by incubation at 65 °C for 10 min, and repeated once (200 µl total elute). 200 µl 1% SDS-TE was also added to input samples, and crosslinking was reversed for all samples by an overnight incubation at 65 °C.

ChIP with anti-yKu70 rabbit polyclonal antibody was performed as follows. Briefly, after sonication 1 µl primary antibody anti-yKu70 (kind gift of Dr. A. E. Tomkinson) was added directly to each lysate and samples were incubated for 10 h at 4 °C. 40 µl M-280 sheep anti-rabbit IgG Dynabeads (Invitrogen) were added to each sample followed by 2h incubation while rotating at 4 °C for to capture Ab-bound species. Bead washes, elution and crosslink reversal were performed as for pore ChIP. HA-tagged Mps3 ChIP was performed similarly as pore ChIP using 50 µl sheep anti-mouse IgG magnetic beads (Invitrogen) and 6 µg anti-HA antibody (sc-7392, Santa Cruz Biotech), per sample. Slight modifications were made in the washing steps, after overnight incubation of antibody-coupled beads with lysates: samples were washed 3 times in lysis buffer for 10 min at 4 °C, once with high salt buffer (1% Triton X-100, 0.1% sodium deoxycholate, 1 mM EDTA pH 8.0, 10 mM Tris-HCL pH8.0, 0.5 M NaCl) for 5 min, two washes in standard wash buffer for 10 min on rotation, and one wash in Tris-EDTA (TE) pH 8.0 for 1 min. Elution and decrosslinking were performed as for pore ChIP.

ChIP for PK-tagged Rad50 was done as described (Seeber et al., 2016) and with the same procedure as pore ChIP, except that immunoprecipitation required only 2 h rotation at 4 °C, given the high efficiency of the antibody. 1 µl of SV5-PK1 antibody (Acris Antibodies) was used per sample. All ChIP buffers contained protease inhibitors (cOmplete EDTA-free, Roche). In all ChIP experiments, DNA was recovered after reversal of crosslinking using the AccuPrep DNA extraction kit (Bioneer), and DNA was eluted in

20% kit elution buffer (diluted with deionized water). This DNA was analyzed by quantitative PCR on StepOnePlus machine (Applied Biosystem) using Taqman or SYBR green detection methods. Primers were used at 0.3 mM concentration, probes at 0.04 mM.

Resection Assay

For this technique, it is important to use a robust DNA extraction method that produces very clean DNA. For each time point, 6 3 10^7 cells grown at 30 °C to late log phase were harvested and washed once in cold phosphate-buffered saline (PBS). Cells were resuspended in 500 ml buffer L (50 mM Tris-HCl pH 8.0, 7 mM b-mercaptoethanol, 150 mM NaCl, 1 mM EDTA, 1% v/v SDS), transferred to cryotubes with 300 ml zirconia silica beads and 500 ml phenol: chloroform:isoamylalcohol (PCI) 25:24:1. Samples were vortexed for 2 min, beat in a cell lyser (Fastprep-24 5G, MP Biomedicals) for 90 s at 6.5 m s-1, placed on ice for 2 min and centrifuged at 16,000 g for 5 min. The top aqueous layer was isolated, and 500 ml PCI was added to it. Samples were vortexed for 2 min, centrifuged for 5 min at 16,000 g. The aqueous layer was isolated and 1 ml ethanol was added to it. DNA was precipitated at −70°C for 40 min. Samples were centrifuged at 4 °C for 10 min at 16,000 g. The pellet was dried briefly, then resuspended in 300 ml TE buffer + 15 mg RNase A (BioBasic) and incubated at 37 °C for 2 h. DNA was precipitated by addition of 600 ml isopropanol and 0.15 mM NaCl. Samples were centrifuged at 4 °C for 10 min at 16,000 g. The pellet was washed once in 70% ethanol and dried, then resuspended in TE pH 8.0. The amount of DNA isolated was quantified by Nanodrop measurement and all samples were diluted to a 200 ng/ ml for the resection assay, which was carried out as previously described (Zierhut and Diffley, 2008). The only exception was that Alu1 (NEB) was used as the restriction enzyme. For each sample, a mock digestion and an Alu1 digestion were set up in 25 ml overnight at 37 °C with 3 mg DNA per sample. Digestions were diluted 1:10 in sterile water and used directly in quantitative PCR. DNA was analyzed by quantitative PCR with StepOnePlus machine (Applied Biosystem) and SYBR green detection method. For each time point, Ct values were normalized to those obtained from the mock sample, and then further normalized to values obtained from an amplicon in SMC2 control gene.

SMRTbell Library Construction for Sequencing

The amount of 20 mg of genomic DNA were needle-sheared with a 26-gauge blunt-end needle (BD), and used as input for SMRTbell library construction using the SMRTbell Template Prep Kit (Pacific Biosciences), following Pacific Biosciences' 20 kb Template Preparation protocol. The final libraries were size-selected on a PippinHT (Sage Science) using the 0.75% 6-10 kb High-Pass 75D method, with a starting size of 9900 bp. The final average library size was about 60,000 bp as judged on an Agilent Genomic DNA ScreenTape (Agilent).

PacBio RSII Sequencing

Each SMRTbell library was sequenced on three to four Pacific Biosciences RSII SMRTcells at loading concentrations ranging from 300 to 450 pM using the MagBead-binding One Cell Per Well workflow, the Binding Kit P6 v2 and DNA Sequencing Kit 4.0 (all Pacific Biosciences). Data was acquired for a duration of 240 min, with Stage Start enabled.

QUANTIFICATION AND STATISTICAL ANALYSIS

Time-lapse image stacks were analyzed as in (Dion et al., 2012) and in (Amitai et al., 2017) using a custom made ImageJ (FIJI) plug-in (Sage et al., 2005), to correct for translational movement and to extract the coordinates oflocus position. Only S phase cells were tracked. The error bars of all mean square displacement (MSD) plots represent the s.e.m. In all microscopy experiments, cut induction was verified by quantitative PCR using primers flanking the cut site. The derivation and extraction of biophysical parameters of the single particle tracking data was performed exactly as described in the supplemental methods of Amitai et al. (2017) . MSD graphs were calculated as described in Hauer et al. (2017) . Three-zone position analysis for LacI- GFP foci was preformed using a through-focus stack of 16-21 0.2 mm steps and was measured by ImageJ (NIH, USA) and software PointPicker (Meister et al., 2010). Standard tests for significance are described in the corresponding figure legends.

For quantification of ChIP results, the absolute enrichment was calculated as follows. For each time point, the signal from a PCR reaction near the DSB was normalized to the signal from the control genomic locus, SMC2 or the mitochondrial gene, OLI1 , in the same sample. For each time point and probe, the normalized IP signal was then normalized to the input signal.

DATA AND SOFTWARE AVAILABILITY

The accession number for the Pacific Biosciences sequencing data sets reported in this paper is NCBI: PRJNA482327.

All sequencing data and software used are available from the lead author, upon request.

Cell Reports, Volume 24

Supplemental Information

Asymmetric Processing of DNA Ends at a Double-Strand Break Leads to Unconstrained Dynamics and Ectopic Translocation

Isabella Marcomini, Kenji Shimada, Neda Delgoshaie, Io Yamamoto, Andrew Seeber, Anais Cheblal, Chihiro Horigome, Ulrike Naumann, and Susan M. Gasser

Supplementary Material

Asymmetric processing of DNA ends at a double-strand break leads to unconstrained dynamics and ectopic translocation

Isabella Marcomini, Kenji Shimada, Neda Delgoshaie, Io Yamamoto, Andrew Seeber, Anais Cheblal, Chihiro Horigome and Susan M. Gasser

Inventory

Marcomini et al. Supplementary tables

Table S1. Strains used in this study (related to Fig. 1-7, S1-4).

Name	Genotype	Source
GA-8861	JKM179: *MAT*α, Δ*ho hml::ADE1 hmr::ADE1 ade3::GALHO ade1- 100 leu2-3, 112 lys5 trp1::hisG ura3-52 CFP-NUP49 GFP-LacI:Leu2 MAT::LacO* repeats*:TRP1*	Horigome et al., 2014
GA-8119	GA8861 TG80-HO-MNT2	This study
GA-8502	GA8861 TG250-HO-MNT2	This study
GA-10085	GA8861 HO-MNT2	This study
GA-9005	GA-8119 *est2::natMX4*	This study
GA-9502	GA-8119 *pol32::natMX4*	This study
GA-9511	GA-8119 *dnl4::natMX4*	This study
GA-8561	GA-8861 *dnl4::natMX4*	This study
GA-9551	GA-8561 *pol32::hphMX4*	This study
GA-9512	GA-8502 *dnl4::natMX4*	This study
GA-9918	GA-8861 TG80-HO	This study
GA-9549	GA-8119 *rad50-9PK-k.i.*	This study
GA-9519	GA-8861 *rad50-9PK-k.i.*	This study
GA-9521	GA-8502 *rad50-9PK-k.i.*	This study
GA-9948	GA-8861 *yom-Ruby2-kanMX6*	This study
GA-9913	GA-8119 *yom-Ruby2-kanMX6*	This study
GA-9449	GA-8119 *rif1::hphMX4*	This study
GA-9158	GA-8119 *sir4::natMX4*	This study
GA-8596	GA-8502 *rif1::hphMX4*	This study
GA-8587	GA-8502 *sir4::natMX4*	This study
GA-9553	GA-8119 y*ku70::natMX4*	This study
GA-9823	GA-8861 (TTAGGG)60-HO-MNT2	This study
GA-9824	GA8861 TG18-HO-MNT2	This study
GA-8306	JKM139: *MAT*a *Δho hml::ADE1 hmr::ADE1 ade3::GALHO ade1-100 leu2-3,112 lys5 trp1::hisG ura3-52 Mps3-3HA*	Horigome et al., 2014
GA-8633	GA8119 *Mps3-3HA*	This study
GA-8845	GA8502 *Mps3-3HA*	This study
GA-10054	GA-9824 *mps3Δ65-145*	This study
GA-8334	GA8119 *nup84::natMX4*	This study
GA-9855	GA8119 *uls1::kanMX6*	This study
GA-10050	GA8119 *slx8::natMX4*	This study
GA-9794	GA-8119 *siz2*::*hphMX4*	This study
GA-10435	GA9913 *uls1*::*natMX4*	This study
GA-7314	GA-8861 *nup133::natMX4* pUN100-*nup133ΔN:kanMX6*	Horigome et al., 2014
GA-7969	GA-7314 *slx5*::*C.a. URA3*	Horigome et al., 2016
GA-8475	GA-7314 *uls1*::*C.a. URA3*	This study
GA-7970	GA-7314 *siz2*::*C.a. URA3*	Horigome et al., 2016

Table S2. PCR Primers used in this study. Related to Fig. 1, 2, 7.

Name	Sequence
SG-7613	CGGGATCCGGGGGGGGGGGGGGGGG
SG-6611	CGCTGGTTTGCATAAAGGTA
SG-2659	CACAGTTTGGCTCCGGTGTA
SG-5771	ACAAAGAATGATGCTAAGAATT
SG-475	GACGACCTT GTAACAGTCC AGACAG
SG-476	TACGTCCTTACCTTCGCATGGAACC
SG-525	AATTGGATTTGGCTAAGCGTAATC
SG-526	CTCCAATGTCCCTCAAAATTTCTT

Table S3. Real-time PCR Primers used in this study. Related to Fig. 3, 5, 6, 7, S1, S2, S4.

Name	Sequence	Target
SG-525	AATTGGATTTGGCTAAGCGTAATC	*SMC2*
SG-526	CTCCAATGTCCCTCAAAATTTCTT	
TQ-3 (probe)	CGACGCGAATCCATCTTCCCAAATAATT	
SG-2918	CAAGAAACCCATCAATTAAAGACCTAGT	*OLI1*
SG2919	ATGAAACCATTAAACAGAATAAACCTGTAG	
SG-6695	GTAGTTGTGTGCCAGAAGGC	HOcs (TG strains)
SG-6696	GGCAGGGGGAATTCTTATACT	
SG-2285	AATATGGGACTACTTCGCGCAACA	HOcs (wt *MAT*)
SG-2286	CGTCACCACGTACTTCAGCATAA	
SG-563	TCAACCATATATAATAACTTAATAGACGACATTC	-0.6kb from HOcs
SG-564	CTAGACGTTTTTCTTTCAGCTTTTTTG	
TQ-2 (probe)	CTTTCAAAATTAAGAACAAAGCATCCAAATCATACAGAA	
SG-2912	TCACGCTTTATAACAATATCAAGTTTACCT	+0.7 kb from HOcs
SG-2913	ATTGGAAACACCAAGGGAGAGA	
TQ-44 (probe)	TCATTACTATTCATCTTCGCCACAAG	
SG-8444	CCCAAACAAAACCCAGACAT	-0.6kb from HOcs
SG-8445	TGCTGGATTTAAACTCATCTGTG	
SG-8440	CTCTCCCTTGGTGTTTCCAA	+0.7kb from HOcs
SG-8441	GAAAAGATTGGCCGTCAAAA	
SG-8448	CAATGCCTTCCTTCTCCAAA	-4.2kb from HOcs
SG-8449	ACCTGAGCGACGAGAAATTG	
SG-8459	TGCGATGAAGTCAACGAATTA	+4.5kb from HOcs
SG-8460	GAGCACTTTTACCGGCAGTT	
SG-7702	CACACAATCACATCCCTCAAAC	+3.5 kb from HOcs
SG-7703	AGAAGAAGAGGAAGGCGAAAG	
TQ-56 (probe)	CCTCAATATTCCGCCTTTCCTCTTCCC	
SG-6761	ACATTAAAAAAGAGAAGAGCCCAAAG	-0.24 kb from HOcs
SG-6762	GCCACATTTCTTTGCAACTTC	
TQ-54 (probe)	AGCACGGGCATTTTTAGAACAGGTTTTTAGAAG	

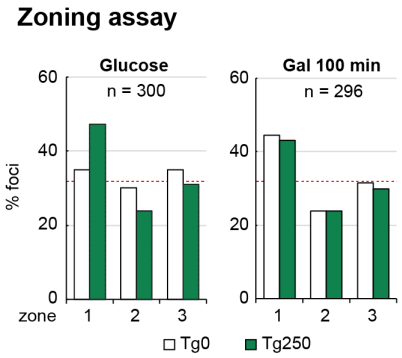

Marcomini et al., Figure S1

Figure S1. Tg250 is at the nuclear periphery before and after HO cleavage.
a) Relates to Figure 1C. Results from scoring the position of the *MAT* locus in the 3 zoning assay in panel 1B, for an exponentially growing culture in glucose (left graph) or 100 min after HO induction on galactose (right graph) in Tg0 (GA-8861, white) and Tg250 (GA-8502, green) strains. n=number of nuclei scored per condition. A random distribution of a locus results in 33% of cells with the locus in each zone, as indicated by the red dotted line. The lacI-GFP focus in Tg250 strains is significantly perinuclear before and after HO cut induction, presumably due to the binding of Sir4.

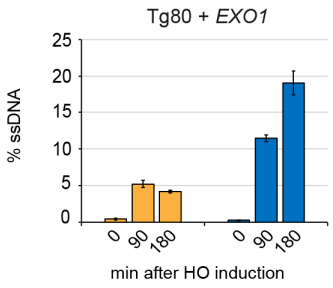

Marcomini et al., Figure S2

Figure S2. Overexpression of Exo1 exonuclease partially rescues the resection block at the TG-flanked end in Tg80 strains. Relates to Figure 2. Quantification of ssDNA generated by 5' end resection as in panel 2A, in a Tg80 strain overexpressing EXO1 from a galactose-inducible 2µ plasmid (pJH1772). Data from 2 biological replicates, amplified in triplicate are presented as mean values +/- s.e.m.

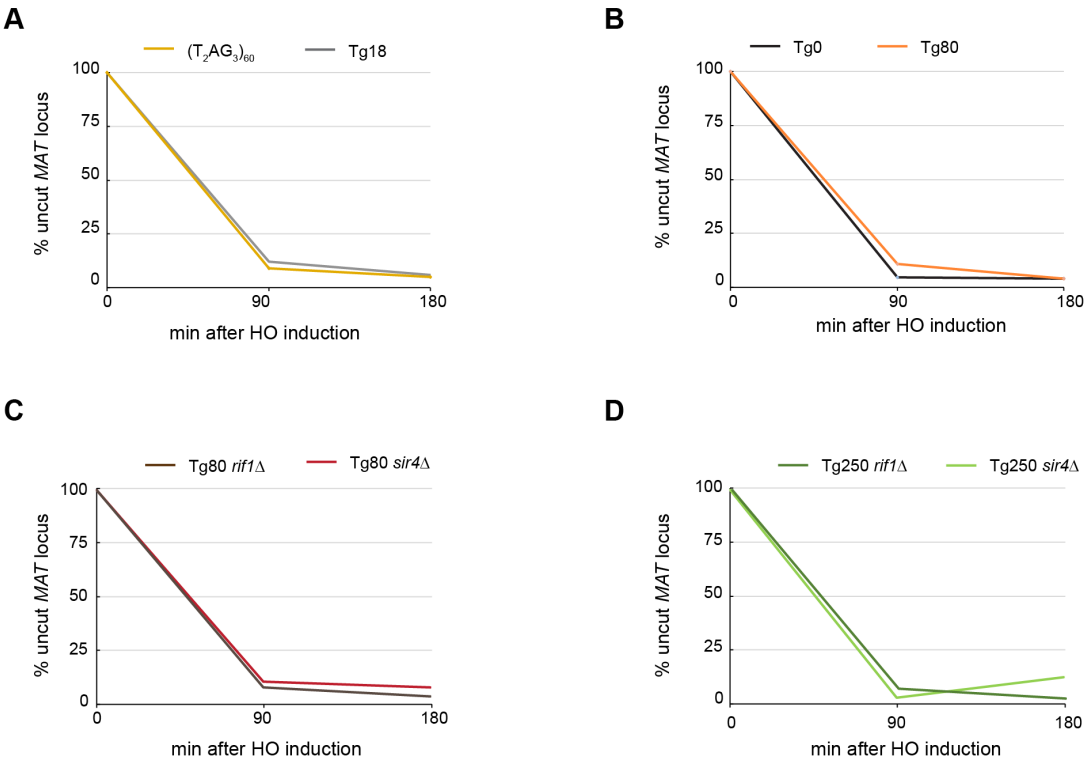

Marcomini et al., Figure S3

Figure S3. HO cleavage efficiency is not affected by TG-rich insertions nor by *rif1* or *sir4* mutation. A) – D) Relates to Figure 3. The *MAT* locus is cut with comparable efficiencies by HO endonuclease upon galactose addition to exponentially growing cultures of GA-9823, GA-9824, GA-8861, GA-8119, GA-9449, GA-9158, GA-8596, GA-8587. DNA samples were collected at 0, 90 and 180 mins after HO induction and were used to quantify the percentage of intact *MAT* locus by qPCR. Ct values of amplicons across the HO cut site were normalized for those obtained by amplification of the control locus *SMC2* at 90 and 180 minutes after galactose addition, and these ratios were further normalized for the ratio obtained at time point 0. Mean of 3 replicates are shown. Standard deviation is not shown, as it was lower than 2% for each strain and time point.

Movement parameters - standard errors of the mean (s.e.m.)

uncut	Tg0 lacI-GFP	Tg80 lacI-GFP
α (μm)	0.036	0.024
D_c ($\mu m^2/s$)	8.28E-03	5.77E-05
L_c (μm)	7.38E-03	5.54E-03
k_c ($k_BT/\mu m^2$)	13.382	5.579

cut	Tg0 lacI-GFP	Tg80 lacI-GFP	Tg0 Rad52-Ruby2	Tg80 Rad52-Ruby2
α (μm)	0.032	0.039	0.039	0.047
D_c ($\mu m^2/s$)	7.6E-04	4.3E-05	1.5E-04	3.7E-04
L_c (μm)	0.010	0.011	0.009	0.020
k_c ($k_BT/\mu m^2$)	6.075	13.053	9.117	4.920

Marcomini et al., Figure S4

Figure S4. Standard deviation values for the biophysical parameters defining DSB end movement. Relates to Figure 4D. Derivation of these values is described in Amitai et al., 2017. See text for details.

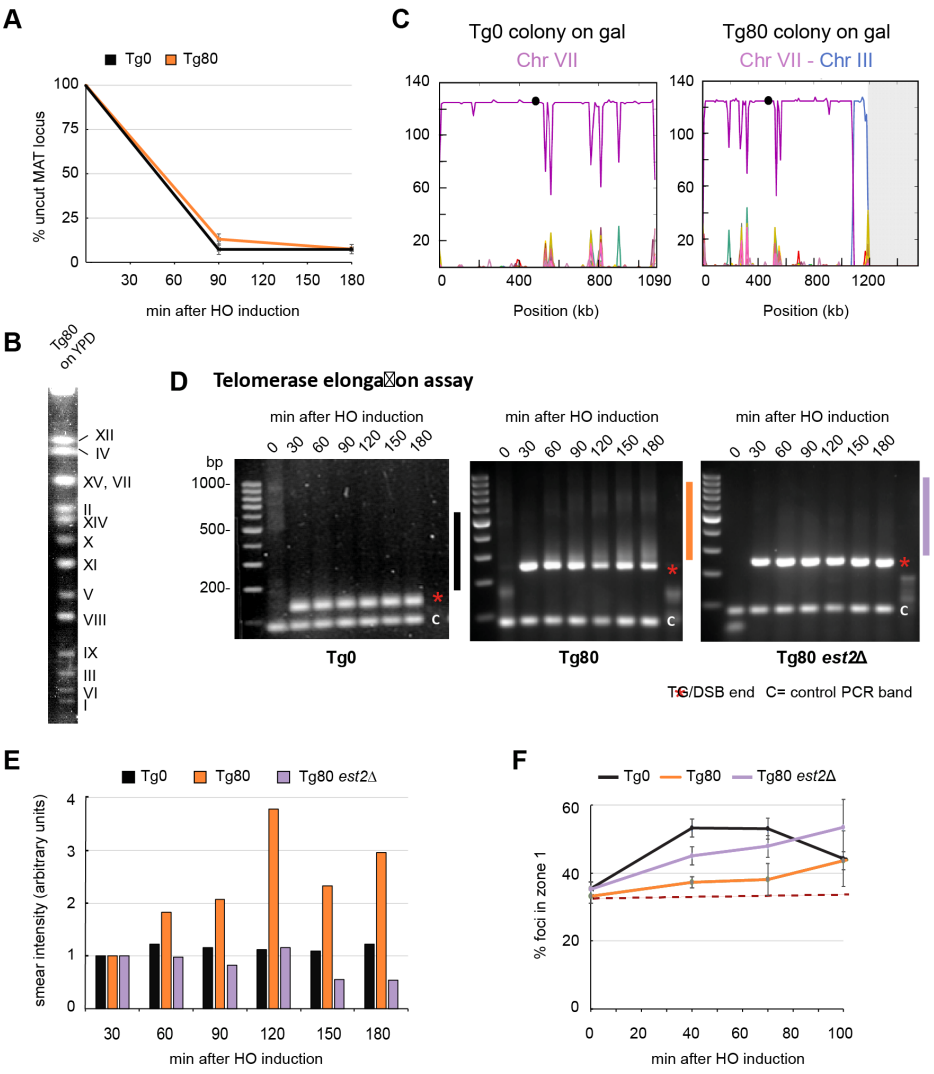

Marcomini et al., Figure S5

Figure S5. Processing of the Tg80 break by telomerase.
A) Relates to Figure 5C. Cut efficiency calculated by qPCR as percentage of intact *MAT* locus in Tg0 (GA-8861) and Tg80 (GA-8119). Ct values from qPCR of cut locus at 90 and 180 minutes HO induction were normalized to a control locus *SMC2*, and were further normalized to the ratio at t=0. Results show the mean of 3 independent experiments, +/- s.d. B) Relates to Figure 5F. CHEF gel of wild-type chromosomal pattern forTg80 (GA-8119) grown always on glucose. C) Relates to Figure 5F,G. Sequencing analysis by PacBio for aTg0 and aTg80 colony grown on galactose, out of 3 analyzed by SMRT sequencing with identical results. This shows homology-mediated ectopic recombination between the non-TG side of the Tg80 DSB on Chr III with the *MNT2* gene on Chr VII-L. D,E) Relates to Figure 5F,G. Telomere PCR at a DSB in Tg0 (GA-8860), Tg80 (GA-8119) and Tg80 *est2Δ (*GA-9005), at indicated time points after HO induction in exponentially growing cultures. Extracted DNA samples was used as template for two PCR reactions: the control amplicon in *SMC2* (marked as C), and the amplified telomeric repeat extension which generates an upward smear of varying sizes (red asterisk plus bar). Shown is a 1.5% agarose gel and stained with RedSafe nucleic acid staining solution (Chembio). The graph in panel E represents the quantification of the smear in arbitrary units for the color-coded indicated zone over back-ground values. F) Relates to Fig. 5 and Fig. 1D. Deletion of telomerase catalytic subunit Est2 rescues the delay in relocation to the nuclear periphery of Tg80. Quantitation of focus number in zone 1 of the nuclear volume as in Fig. 1D at indicated time-points after HO induction in Tg0 (GA-8861), Tg80 (GA-8119) and Tg80 *est2Δ (*GA-9005). Error bars represent mean values of 3 independent experiments, +/- s.e.m. n=80 nuclei for each strain and experiment. The red dotted line indicates a random distribution.

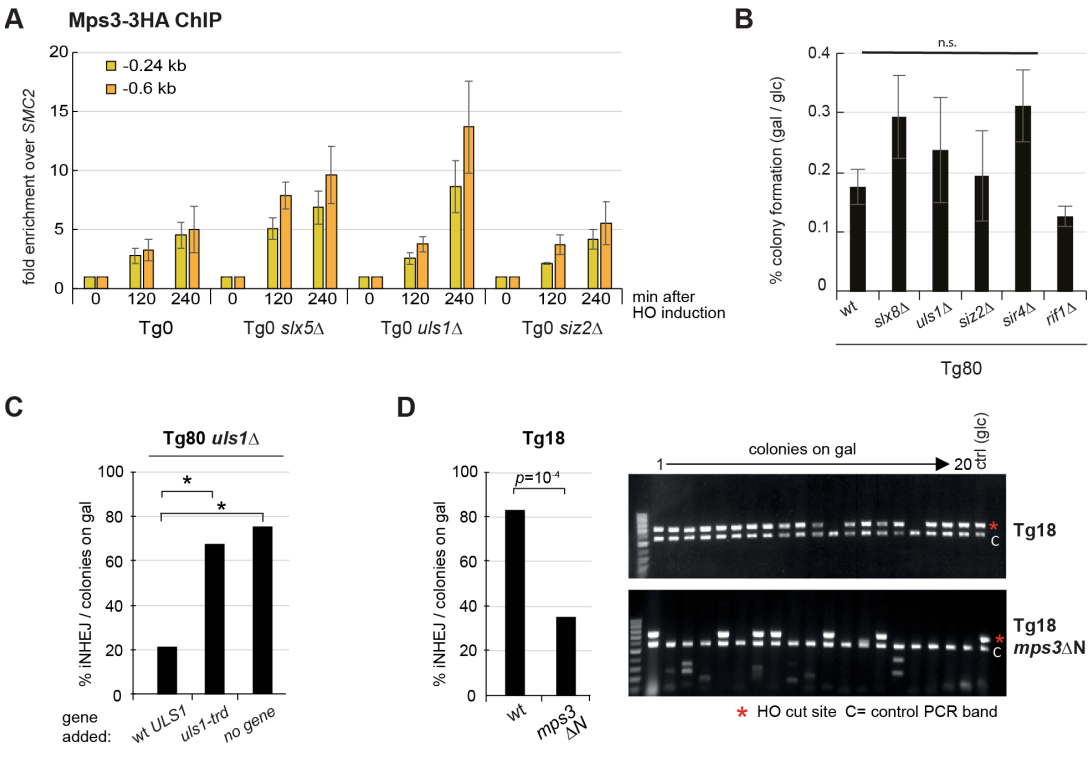

Marcomini et al., Figure S6

Figure S6. DSB-Mps3 anchorage is Siz2 and Uls1 independent and enhances NHEJ over ectopic HR. A) Relates to Figure 6B,C. ChIP for HA-tagged Mps3 monitors *MAT* locus association with Mps3 at indicated time points after HO cut induction on galactose in Tg0 wild-type (GA-8306), *slx5*Δ (GA-8539) and *uls1*Δ (GA-8542) cells. Data from two- (Tg0) or three- (*slx5Δ, uls1Δ, siz2Δ*) independent experiments are presented as mean +/- s.e.m. B) Relates to Figure 6D. The indicated mutants do not compromise overall survival on galactose of a cut at Tg80. Ratio of colonies on galactose normalized to colony numbers on glucose was calculated for the indicated Tg80 mutants. Each column represents the mean of at least three independent experiments, +/- s.d. C) Relates to Figure 6D. The *uls1*Δ strain (GA-9855) was complemented with a plasmid expressing either no *ULS1* (no gene, pRS416), wt *ULS1* (p416-FLAG-ULS1) or translocase-dead *uls1* (p416-uls1-K975A, *uls1-trd*). Survivor colonies after 5 days on galactose from each strain were monitored by PCR for repair by imprecise NHEJ (as in Fig. 6D, n= 40, wt *ULS1*; 40, *uls1-trd*; 37, no gene). Whereas wt *ULS1* reduces imprecise NHEJ events, the translocase deficient *uls1* mutant does not. The asterisk indicates statistical significance with a p value < 10^{-4} in a Chi square test with 95% confidence interval. D) Relates to Fig. 6. The assay for NHEJ pathway efficiency (Fig. 6D) was performed on exponentially growing cultures of Tg18 (GA-9824) and Tg18 *mps3ΔN* (GA-10054). NHEJ is highly efficient in the Tg18 strain which allows us to monitor a drop in mps3ΔN (GA-10054). The graph presents the % of colonies resulting from NHEJ over all galactose-grown survivor colonies (n= 40). The p value is indicated for a Chi square test with 95% confidence interval between wt and mutant. Alongside are examples of agarose gels obtained as in Fig. 6D, from DNA of galactose-grown colonies of Tg18 and Tg18 *mps3ΔN*. 20 colonies grown on galactose were selected and their genomic DNA was used in two PCR reactions to amplify the region encompassing the HO cut site (asterisk), as well as a control region in *SMC2* gene (marked with C). For each colony pooled PCR products were resolved on an agarose gel. The last lane represents a colony of the same strain grown on glucose (uncut).

CHAPTER VI: CONCLUSION AND DISCUSSION

My research contributed to two papers Cheblal *et al.* 2020 and Marcomini *et al.* 2018, which are presented above together with their importance for the field. Here I will discuss an additional paper that I contributed to (Challa et al. under review) which extends these results, and I will highlight future directions of this research.

Conclusion

In this thesis, I have explored how the cellular response to DNA damage, more specifically to DNA DSBs, alters chromatin and in turn repair efficiency. I have optimized multiple techniques including fixed and high-speed live fluorescence imaging to analyze chromatin dynamics and the subnuclear localization of specific loci in response to DNA damage (Chapter 2). This led to the contributions discussed in Chapter 3 – 5.

In my main project, we tackled the long-standing question of whether chromatin mobility enhances homology search during repair by HR in yeast. I have optimized a quantitative repair assay that measures the kinetics of appearance of a strand invasion product during homology directed repair. Unexpectedly, we found that DNA damage-induced nucleosome depletion and ectopic chromatin expansion and movement enhances homology search, independently of local DSB movement (Chapter 3). Moreover, we found that telomeric-like TG-flanked DSBs are processed asymmetrically as compared to canonical DSBs (Chapter 5). Both studies made use of an unusual enzyme Uls1, a SUMO-targeted ubiquitin ligase that regulates protein turnover at breaks.

DNA damage induced histone depletion enhances and homology search

In Chapter 5, we investigated the mechanisms that underlie DNA damage induced chromatin movement and its role in homologous recombination efficiency **(Figure 6).** First we showed that movement of the chromatin fiber is cell-cycle dependent, being lower in S/G2 than in G1, due to the loading of Cohesin which tethers replicated sister chromatids to each other (Dion et al., 2013). This finding highlights the importance of identifying cell cycle stages and triaging data when measuring chromosomal loci dynamics in yeast. Next, we showed that a reduction in nucleosome density, manifest as a lower steady-state pool of histones and decompacted chromatin, occurs in yeast not only in response to global DNA damage such as treatment with Zeocin (Hauer et al., 2017), but also in

response to a single localized DSB (Cheblal, in press). This leads to increased movement not only of the DSB, but also of undamaged sequences, for example, the template for recombination-based repair. By tracking undamaged loci in a nucleus contain a single DSB we observed that chromatin generally becomes become more accessible and explores larger nuclear volumes through random subdiffusive movement triggered by checkpoint activation. This result raised the question how critical the induced ectopic response is for the subsequent DNA repair by recombination.

I asked the question whether nucleosome remodeling upon DNA damage is required for efficient homology-directed repair. Indeed, I observed that INO80-C deficient (*arp8*Δ) cells reduce strand invasion efficiency, coincident with a drop in both DSB and ectopic mobility, suggesting that histone mobilization is crucial for HDR. Similarly, in *nhp6*ΔΔ cells, which show a reduced steady state histone level by 20%, I observed enhanced rates and kinetics of recombination, suggesting that reduced nucleosome density can facilitate the homology search during repair. Nevertheless, under these conditions it was not possible to determine whether the observed enhanced rate of recombination reflected reduced nucleosome occupancy and a resulting expansion of chromatin genome-wide or to an increase in local DSB dynamics.

Luckily, using a yeast strain deficient for a SUMO-binding Ubiquitin ligase called Uls1, I found that one can compromise local DSB movement, but maintain resection, checkpoint activation, histone degradation and chromatin expansion at undamaged sites, in response to a single break. I show that under these conditions, homology-directed strand invasion was not compromised, despite the absence of increased DSB movement. This argues strongly that local DSB mobility is not rate-limiting for repair, as long as ectopic chromatin mobility and expansion is ensured. In unpublished work, Challa et al. we have now used another mutant (*ufd4*Δ) which also reduces histone degradation but specifically compromises ectopic, and not the local DSB movement. This mutation did impair the efficiency of HDR **(Figure 1-2)**. Thus, we propose that local mobility is neither sufficient nor necessary for efficient HDR, while ectopic locus expansion and mobility are.

I was unable to detect centromere release nor declustering in response to DNA damage. Moreover, the loss of the regulatory Cep3 phosphoacceptor site, which was thought to regulate this release (Strecker et al., 2016), did not compromise the damage-enhanced mobility of a DSB at *MAT*. This result helps clarify conflicting information in the literature on whether DNA damage triggers

kinetochore decluttering. I showed that these events cannot be the underlying mechanism that controls DNA damage induced chromatin mobility.

Instead, we propose that general reduction in nucleosome occupancy drives DNA damage-induced chromatin mobility. With a quantitative strand-invasion assay we show that a general increase in undamaged locus movement and not the local increase in DSB movement is rate-limiting for ectopic strand invasion during homology-directed repair in yeast.

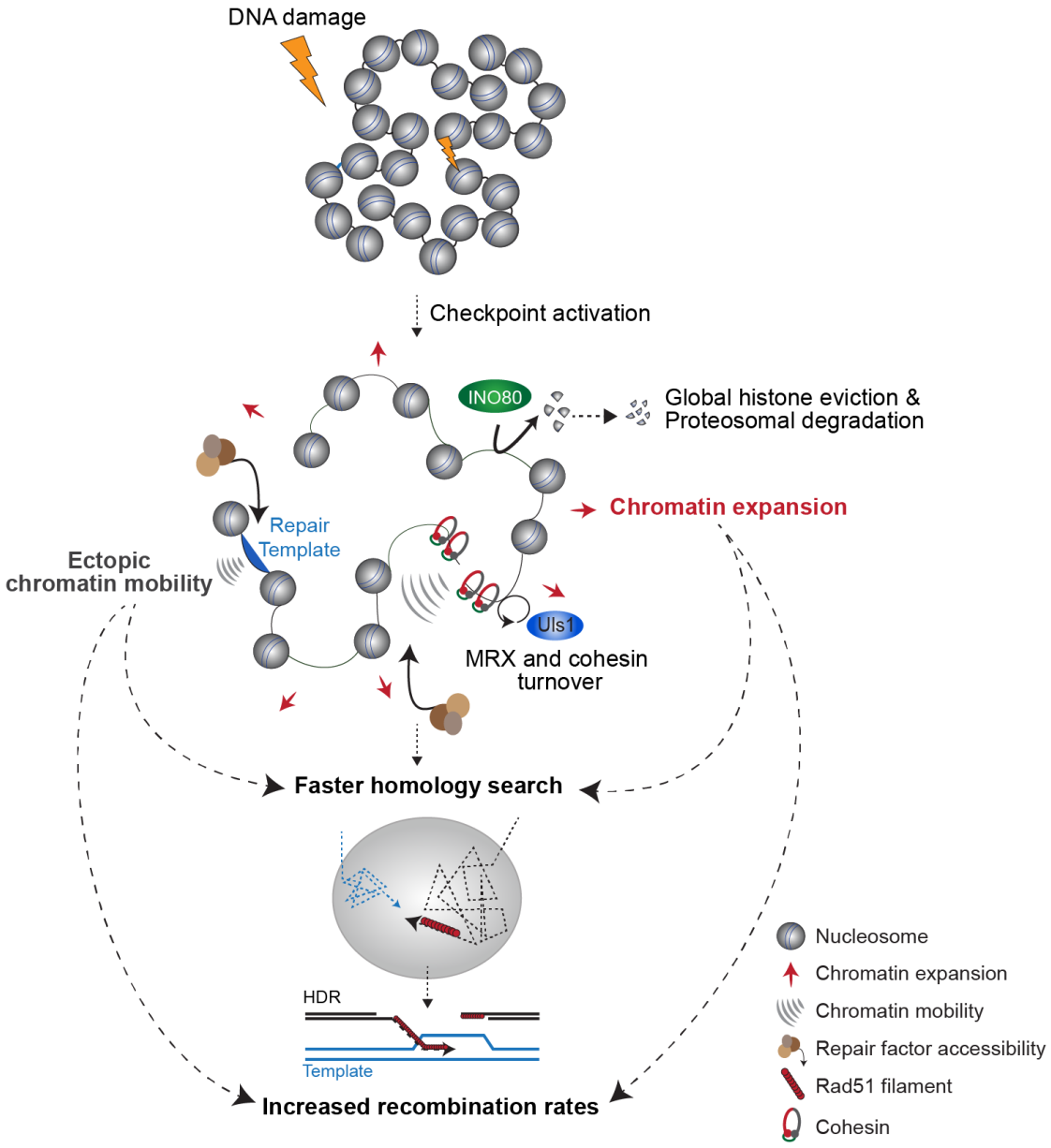

<u>Figure 6:</u> Model of the role of histone loss and enhanced DNA movement in Homology-directed repair (HDR).

DNA damage-induced histone depletion triggers global ectopic chromatin expansion and mobility. Chromatin opening might facilitate accessibility to repair factors or to the repair template and therefore enhancing HDR kinetics.
MRX and Cohesin turnover and mobility at a DSB is regulated by the STUbL Uls1 (Cheblal et al., in press).

Processing of TG-flanked double-strand breaks

In Chapter 3, I contributed to an ongoing effort in the laboratory to answer what defines a telomere and protects it from the DNA repair machinery as compared to a canonical DSB **(Figure 7).** This study used a system developed by Dr. Marcomini in which as short stretch of telomeric repeats (TG) were inserted on one side of a controlled HO cleavage site at the *MAT* locus.

Using this system we showed that on the TG-rich side, MRX binding was reduced and locus dynamics were increased. This resulted in the separation of the two break ends, enabling distinct repair processes to act. Interestingly, the reduced MRX and increased dynamics depended on the translocase activity of the SUMO targeted Ubiquitin ligase Uls1. On the non-TG side, MRX binding and DNA end resection occurred normally. In wild-type cells we observed high locus mobility, which resulted in chromosomal translocations, while in *uls1*Δ cells the mobility was less and NHEJ occurred more efficiently.

We propose that, the absence of MRX on the TG-rich side, which normally holds the broken ends together resulted in an increase in movement that might have allowed homology search to occur and resulted in chromosomal translocation. The loss of Uls1 strongly affect the repair outcome through an increase of imprecise NHEJ, probably by allowing MRX accumulation on the TG-rich side and favoring end-to-end ligation. My main contribution to this manuscript was in analyzing chromatin dynamics of the non-TG end and the TG-rich end comparing wild-type and *uls1*Δ conditions. This contribution was not only important for Marcomini et al., but it also shaped the study describe in Chapter 5. Indeed, I tested the behavior of Uls1-deficient cells in response to canonical DSBs and extended our understanding of how Uls1 regulates local chromatin dynamics.

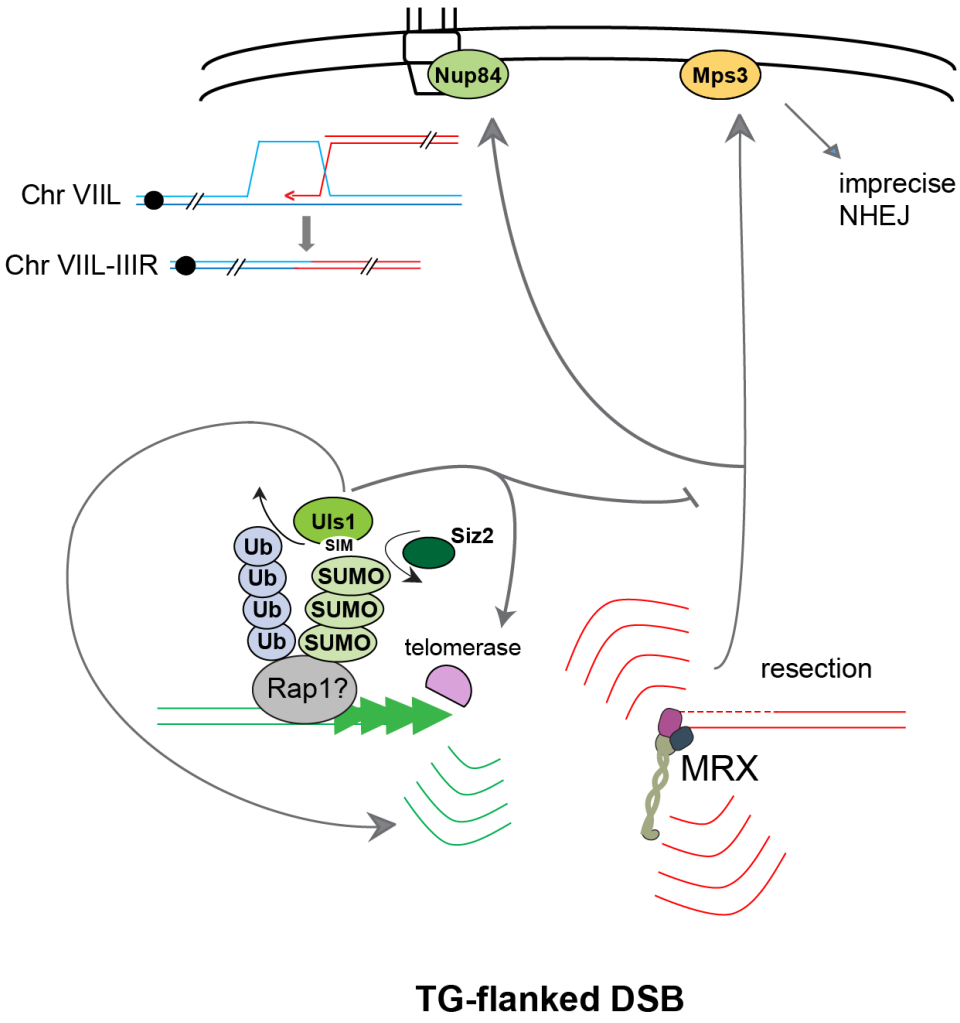

Figure 7: Model for the effect of TG-rich repeats on DSB repair

On the TG-rich side of a TG-flanked DSB, MRX binding is reduced, allowing the two ends to separate.The end moves to the nuclear envelope, while the TG-free side, lacking end-to-end tethering, moves freely, favoring homology-driven ectopic recombination. The processing of Tg0 and Tg80 ends requires the translocase activity of Uls1 and sumoylation by the SUMO E3 ligase Siz2. Siz2 and Uls1 antagonize NHEJ (Marcomini et al., 2018).

Discussion and future prospects

DNA damage induced centromere detachment hypothesis

In Chapter 5, we concluded that the Strecker *et al.* 2016 study, which suggested a release of chromosomal tethers around the centromere as the source of the increase in DSB movement (Strecker et al., 2016), is not reproducible. Moreover, this study suggested that Cep3 phosphorylation by the DNA damage checkpoint kinase Rad53 drives centromere release and heightened chromatin dynamics, which was also irreproducible.

I have attempted to understand why the earlier study failed to see an increase in DSB mobility in this the Cep3 phospho-mutant, and I highlighted various conditions that obscure accurate mobility measurements. First, the authors did not monitor nor select cell cycle stages, and secondly they did not measure the efficiency of cut induction in all their imaging conditions. Omitting either of these parameters can lead to erroneous and irreproducible results, and given that they did neither, we feel that this is a likely source of error.

In addition, we note that capturing time-lapse imaging at a significantly lower frequency (1.5s ms intervals), as they did, can mask one's ability to detect an increase in DSB mobility (Shukron et al., 2019; Strecker et al., 2016). Indeed, when imaging the cleaved *MAT* locus mobility in S phase with 1.5ms intervals, we could not detect significant increase in DSB dynamics, as we could with higher imaging frequency (80ms intervals).

Recently, we have investigated how the chromatome changes in response to Zeocin-induced DNA damage by quantitative mass spectrometry (Challa et al., under review). Interestingly, we observed a significant reduction in the kinetochore complex from the chromatin after DNA damage, including the essential kinetochore protein Cep3. It would be interesting to further test whether kinetochore proteins are lost locally at centromeric DSB for example, potentially understanding their implication in the DNA damage response. Although, Cep3-deficient cells are not sensitive to DNA damage (Cheblal, in press; Strecker et al., 2016) , we do not exclude a potential implication of other spindle assembly checkpoint proteins in DNA repair. Moreover, this global reduction in kinetochore proteins was shown to be independent of the INO80C chromatin remodeler, suggesting that this is not driven by the observed global histone depletion.

DNA damage induced histone depletion and ectopic response

In Chapter 5, we reported that DNA damage induced nucleosome depletion is the major mechanism underlying ectopic chromatin mobility. Hauer et *al.,* showed that the observed nucleosome depletion was driven by an active proteasomal degradation of the main core histones. In a recent study (Challa et al. under review), we have identified the key E3 ubiquitin ligases that targets core histones to degradation upon Zeocin treatment. Intriguingly, most of these ubiquitin ligases seem to both control local DSB dynamic and ectopic movement and expansion, suggesting that they might play a role locally at the DSB where they are recruited. In Cheblal et *al.,* we suggested that local DSB processing and ectopic response might be regulated by distinct processes.

Based on our study of movement and strand invasion in *uls1Δ* cells, we demonstrated that ectopic locus mobility, driven by checkpoint activation is critical for efficient homology directed repair (Cheblal et al., in press). Interestingly, Challa et al., identified a specific E3 Ubiquitin ligase called Ufd4 that is involved in histone degradation, and which controls only the global ectopic response to Zeocin, without affecting the enhanced dynamics at the DSB **(Figure 8A-C).** In line with our previous observations, Ufd4-deficient cells show a delayed homology directed repair rates and kinetics (Challa et al. under review) **(Figure 8D-E).** This observation strengthens a model in which the movement and the accessibility of ectopic sequences, including potential repair templates, are required to enable homology search and efficient repair by HR. The current results do not distinguish between the accessibility of the ectopic sequence, or its dynamic movement. Of course, we do note that the two phenomena are linked through histone loss (Hauer et al., 2017).

Opening chromatin to enable homology directed repair

It was shown that *nhp6⊿⊿* was sufficient to increase the rate of gene targeting and of homology directed strand invasion and repair efficiency (Cheblal et al., in press). We hypothesize that this happens by making chromatin more accessible to both the repair template and to DNA repair proteins, although the search may also be physically faster due to the movement of chromatin generally. We have not strictly shown that chromatin is more accessible in *nhp6*ΔΔ cells. Consistent with this hypothesis, however, Challa et al., observed that the loss of the histone linker H1 (HHO1), resulted in an increase of the DSB dynamics **(Figure 9A-B).** Moreover, it was previously shown that HHO1 is required for chromatin condensation (Thomas, 1999; Vignali and Workman, 1998).

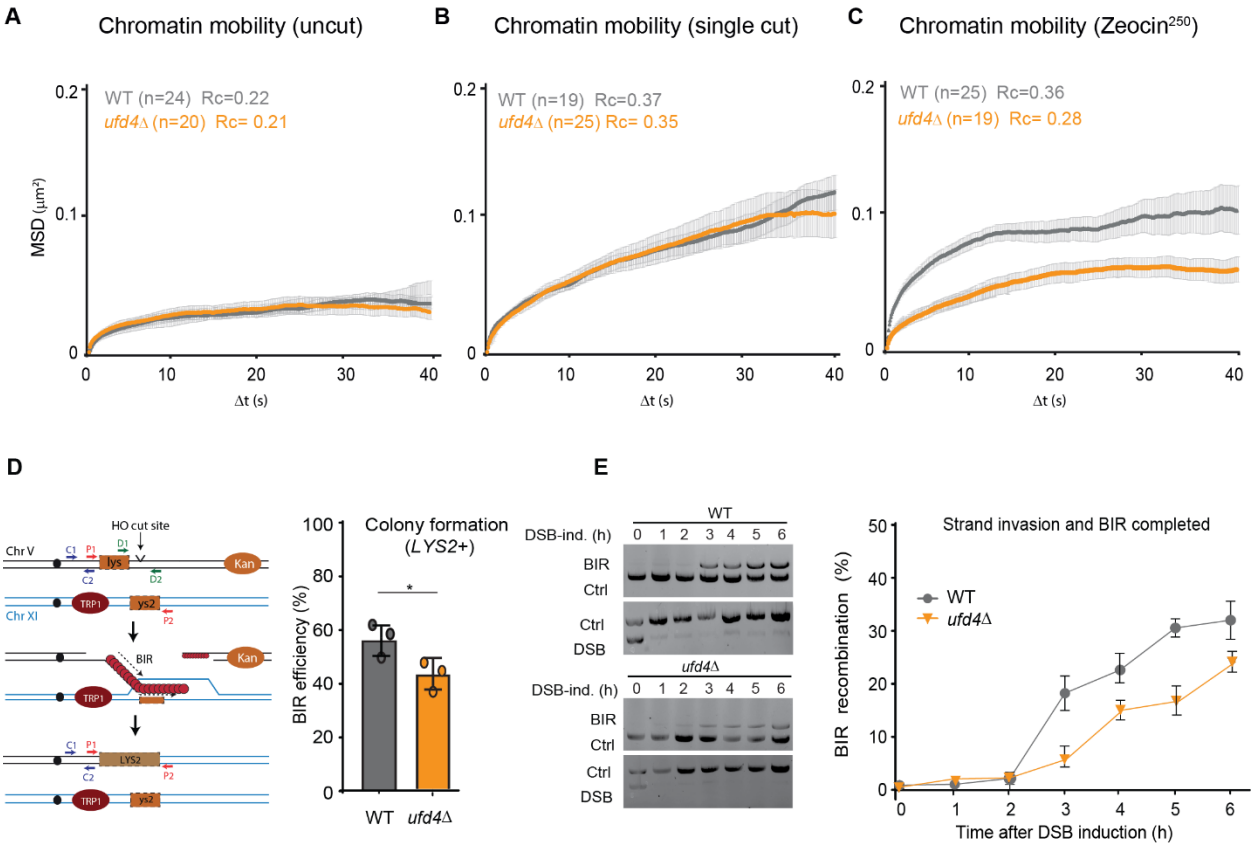

Figure 8: Ufd4 regulates global chromatin dynamics upon DNA damage and is required for an efficient homology-directed repair.

(A-C) MSD trajectories of the MAT locus in WT and *ufd4*Δ without damage (A), after a single HO-cut induction (B) and after Zeocin treatment (C).
(D) Left: Scheme of the BIR assay as described in **Chapter 3.** Right: BIR efficiency scored by *LYS+* colony formation quantified in WT and *ufd4*Δ. **(E)** Left: Representative PCR to detect DSB and BIR product in G2-M arrested cells after HO induction in WT and *ufd4*Δ. Quantification of the kinetics of BIR product formation is shown on the left side. (Challa et al., under review).

We have not yet monitored the accessibility of linker DNA in an *hho1*Δ mutant, although we assume, based on work in mammalian cells (reviewed in (Fyodorov et al., 2018)) that the loss of *Hho1* increases chromatin decompaction and accessibility. Interestingly, Challa et al and others showed an increase in homology directed repair rates and a slight increase in the kinetics of recombination in *HHO1* deficient cells (Downs et al., 2003; Mukherjee et al., 2020)**(Figure 9C-D).** Although, the ectopic response to Zeocin remains to be shown, this result strengthens the idea that the efficiency of homology directed repair can be increased by degrading a linker histone which increase chromatin accessibility and mobility generally **(Figure 9E).**

An obvious question arising from this work is whether chromatin accessibility *per se* increases upon DNA damage, and whether accessibility or movement is critical for enhancing the kinetics of repair by HDR. Hauer et al. showed that nucleosome occupancy decreases upon Zeocin treatment, and chromatin compaction was measured through specific loci expansion analysis. Although we were able to show that locus expansion upon DNA damage strongly correlate with histone degradation, it remains to be shown whether this reflects an increase in global chromatin accessibility to repair factors. It would be of upmost importance to perform an Assay for Transposase-Accessible Chromatin using sequencing (ATAC-seq). If the hypothesis stated above holds true, we expect to see an increase in chromatin accessibility in wild-type cells upon DNA damage, but not in INO80C deficient cells. On the other hand, we expect that *nhp6*⌟Δ will show increased global steady-state chromatin accessibility. Moreover, we expect that Uls1 deletion will not impair global chromatin accessibility, but may reduce accessibility around the DSB. Finally, because Challa *et al.* observed an impaired Zeocin response in *Ufd4*-deficient cells, we expect that we will be able to monitor reduced accessibility genome-wide although perhaps not at the DSB. Analyzing chromatin accessibility in *ufd4*⌟ cells will provide additional information on the role of histone degradation in controlling chromatin accessibility and repair.

One practical outcome of our study is to reinforce the model that a transient reduction in nucleosome density could enhance repair by HR over NHEJ. This will be crucial for CRISPR-mediated gene therapies, which are currently too inefficient to be used clinically. Preliminary evidence suggests that a transient reduction in nucleosome levels in human cultured cells, can increase recombination by 2-3 fold (Koren, S., Hauer, M.H., and S.M.G., personal communication). Combining this with

appropriately upregulated chromatin remodelers, or targeting of the relevant E3 Ubiquitin ligases (Challa et al. under review) may increase the efficiency of cleavage, processing, and resection.

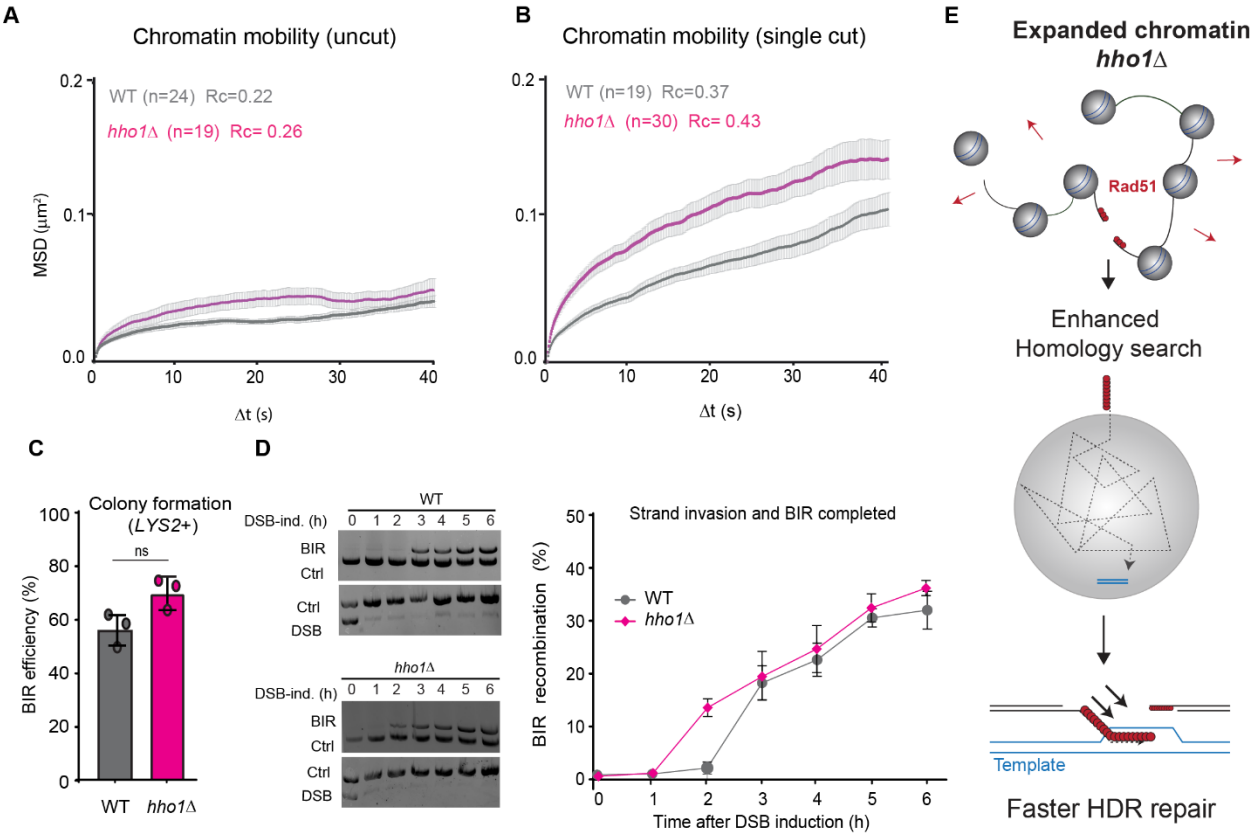

Figure 9: HHO1 deletion enhances DSB dynamics and homology-directed repair.

(A-B) MSD trajectories of the *MAT* locus in WT and *hho1*Δ without damage (A), and after a single HO-cut induction (B).

(C) BIR efficiency scored by *LYS*+ colony formation quantified in WT and *hho1*Δ. **(D)** Left: Representative PCR to detect DSB and BIR product in G2-M arrested cells after HO induction in WT and *hho1*Δ. Quantification of the kinetics of BIR product formation is shown on the left side. (Challa et al., in revision). (E) Model showing how chromatin decompaction in *hho1*Δ influence homology-directed repair kinetics. (Challa et al., under review).

Additionally, we argue in Cheblal et al. that DNA damage induced histone degradation and ectopic movement enhances homology search during HDR. In a system where both the DSB loci and the repair template are artificially tethered to the nuclear periphery and in proximity, the repair efficiency should not be affected by a loss of histone degradation (i.e., would be INO80-C insensitive). However, if DNA repair is impaired in such conditions, this would argue that the processing of the break by INO80 is critical for repair by HR rather than nucleosome depletion and the search for homology.

SUMO targeted Ubiquitin ligase Uls1 role in DNA DSB repair

At DSBs, movement is restricted by the local loading of Cohesin in an MRX-dependent manner (Seeber et al., 2016; Unal et al., 2007). We found that Cohesin and to a lesser extent, MRX, accumulate at an induced DSB in *uls1*Δ strain. This correlates with a failure to increase DSB mobility, even though resection occurs. We propose that Uls1, which mediates a SUMO-dependent protein ubiquitination, controls the levels of Cohesin (Scc1) and MRX (Rad50) at processed breaks, possibly by regulating their turnover.

The removal of these tethering molecules may enable access for the recombination machinery, and/or release the damage from local constraining forces. Although we argue that break mobility is not rate-limiting under the conditions employed here, there may be other sites of damage for which local movement is rate-limiting. We do not exclude that at some sites, for example centromere-proximal breaks, the removal of MRX and Cohesin from sequences surrounding the damage might be crucial to facilitate repair.

We note that Mre11 is a key target of sumoylation, as are subunits of Cohesin following DNA damage (Cremona et al., 2012). It has been shown that MRX helps recruit SUMO ligases, and sumoylation would, in turn, recruit Uls1 through its SIM domains (Chen et al., 2016; Cremona et al., 2012). Uls1 could then trigger a dynamic turnover of Cohesin and MRX, given that the loss of Uls1 led to a steady-state increase of Cohesin and Rad50 at a persistent DSB (Fig). We note that a similar accumulation was reported for MRX at a TG-flanked break (Marcomini et al., 2018).

Uls1 is an unusual member of the STUbL family, in that besides Ubiquitin ligase activity, it contains a SNF2-like helicase domain related to nucleosome remodelers, and multiple SIM motifs. A very close homologue to Uls1, the human E3 Ub ligase SHPRH, was identified as a tumor suppressor that helps prevent genome instability (Bruhl et al., 2019; Qu et al., 2016). It is thought that SHPRH increases

DNA damage tolerance or post-replication repair, which depends on the ubiquitination of PCNA (Unk et al., 2010). We do not know all the relevant targets of Uls1, but our results suggest that turnover of components of the MRX and Cohesin complexes may also be relevant for repair.

The strong effect of Uls1 on chromatin mobility could stem from a lack of Cohesin and MRX turnover at breaks but could also reflect a SIM-mediated crosslinking of SUMOylated proteins to each other. One main perspective of research is to investigate how does Uls1 regulate cohesin and MRX turnover at the break. More specifically, it would be relevant to analyze whether the SUMO targeted ubiquitin ligase activity of Uls1 is required for the control of DSB dynamics and whether sumoylated motifs (including sumoylated MRX and Cohesin) accumulate at a DSB site in the absence of Uls1.

REFERENCES

Adam, S., Dabin, J., Chevallier, O., Leroy, O., Baldeyron, C., Corpet, A., Lomonte, P., Renaud, O., Almouzni, G., and Polo, S.E. (2016). Real-Time Tracking of Parental Histones Reveals Their Contribution to Chromatin Integrity Following DNA Damage. Mol Cell *64*, 65-78.

Agmon, N., Liefshitz, B., Zimmer, C., Fabre, E., and Kupiec, M. (2013). Effect of nuclear architecture on the efficiency of double-strand break repair. Nature cell biology *15*, 694-699.

Amitai, A., Seeber, A., Gasser, S.M., and Holcman, D. (2017). Visualization of Chromatin Decompaction and Break Site Extrusion as Predicted by Statistical Polymer Modeling of Single-Locus Trajectories. Cell reports *18*, 1200-1214.

Aylon, Y., Liefshitz, B., and Kupiec, M. (2004). The CDK regulates repair of double-strand breaks by homologous recombination during the cell cycle. The EMBO journal *23*, 4868-4875.

Bannister, A.J., and Kouzarides, T. (2011). Regulation of chromatin by histone modifications. Cell Res *21*, 381-395.

Barzel, A., and Kupiec, M. (2008). Finding a match: how do homologous sequences get together for recombination? Nat Rev Genet *9*, 27-37.

Batte, A., Brocas, C., Bordelet, H., Hocher, A., Ruault, M., Adjiri, A., Taddei, A., and Dubrana, K. (2017). Recombination at subtelomeres is regulated by physical distance, double-strand break resection and chromatin status. The EMBO journal *36*, 2609-2625.

Berg, H.C. (1993). Random Walks in Biology. Princeton University Press, Princeton, New Jersey.

Bermudez-Lopez, M., and Aragon, L. (2017). Detection of Cohesin SUMOylation In Vivo. Methods in molecular biology *1515*, 55-64.

Bronshtein, I., Kepten, E., Kanter, I., Berezin, S., Lindner, M., Redwood, A.B., Mai, S., Gonzalo, S., Foisner, R., Shav-Tal, Y.*, et al.* (2015). Loss of lamin A function increases chromatin dynamics in the nuclear interior. Nat Commun *6*, 8044.

Bruhl, J., Trautwein, J., Schafer, A., Linne, U., and Bouazoune, K. (2019). The DNA repair protein SHPRH is a nucleosome-stimulated ATPase and a nucleosome-E3 ubiquitin ligase. Epigenetics Chromatin *12*, 52.

Buhler, M., and Gasser, S.M. (2009). Silent chromatin at the middle and ends: lessons from yeasts. The EMBO journal *28*, 2149-2161.

Bystricky, K., Laroche, T., van Houwe, G., Blaszczyk, M., and Gasser, S.M. (2005a). Chromosome looping in yeast telomere pairing and coordinated movement reflect anchoring efficiency and territorial organization. The Journal of cell biology *168*, 375-387.

Bystricky, K., Laroche, T., van Houwe, G., Blaszczyk, M., and Gasser, S.M. (2005b). Chromosome looping in yeast: telomere pairing and coordinated movement reflect anchoring efficiency and territorial organization. J Cell Biol *168*, 375-387.

Cabal, G.G., Genovesio, A., Rodriguez-Navarro, S., Zimmer, C., Gadal, O., Lesne, A., Buc, H., Feuerbach-Fournier, F., Olivo-Marin, J.C., Hurt, E.C.*, et al.* (2006). SAGA interacting factors confine sub-diffusion of transcribed genes to the nuclear envelope. Nature *441*, 770-773.

Caridi, P.C., Delabaere, L., Zapotoczny, G., and Chiolo, I. (2017). And yet, it moves: nuclear and chromatin dynamics of a heterochromatic double-strand break. Philos Trans R Soc Lond B Biol Sci *372*.

Celona, B., Weiner, A., Di Felice, F., Mancuso, F.M., Cesarini, E., Rossi, R.L., Gregory, L., Baban, D., Rossetti, G., Grianti, P.*, et al.* (2011). Substantial histone reduction modulates genomewide nucleosomal occupancy and global transcriptional output. PLoS Biol *9*, e1001086.

Cheblal, A., ; Challa, K,; Seeber, A,; Shimada, K,; Yoshida, H,; Ferreira, HC.; , Amitai, A,; and Gasser, SM. (in press). DNA damage-induced nucleosome depletion enhances homology search independently of local break movement. Molecular Cell.

Chen, H., Levo, M., Barinov, L., Fujioka, M., Jaynes, J.B., and Gregor, T. (2018). Dynamic interplay between enhancer-promoter topology and gene activity. Nat Genet *50*, 1296-1303.
Chen, Y.J., Chuang, Y.C., Chuang, C.N., Cheng, Y.H., Chang, C.R., Leng, C.H., and Wang, T.F. (2016). S. cerevisiae Mre11 recruits conjugated SUMO moieties to facilitate the assembly and function of the Mre11-Rad50-Xrs2 complex. Nucleic Acids Res *44*, 2199-2213.
Chiolo, I., Minoda, A., Colmenares, S.U., Polyzos, A., Costes, S.V., and Karpen, G.H. (2011). Double-strand breaks in heterochromatin move outside of a dynamic HP1a domain to complete recombinational repair. Cell *144*, 732-744.
Cho, N.W., Dilley, R.L., Lampson, M.A., and Greenberg, R.A. (2014). Interchromosomal homology searches drive directional ALT telomere movement and synapsis. Cell *159*, 108-121.
Chung, D.K., Chan, J.N., Strecker, J., Zhang, W., Ebrahimi-Ardebili, S., Lu, T., Abraham, K.J., Durocher, D., and Mekhail, K. (2015). Perinuclear tethers license telomeric DSBs for a broad kinesin- and NPC-dependent DNA repair process. Nat Commun *6*, 7742.
Churikov, D., Charifi, F., Eckert-Boulet, N., Silva, S., Simon, M.N., Lisby, M., and Geli, V. (2016). SUMO-Dependent Relocalization of Eroded Telomeres to Nuclear Pore Complexes Controls Telomere Recombination. Cell reports *15*, 1242-1253.
Conrad, M.N., Lee, C.Y., Chao, G., Shinohara, M., Kosaka, H., Shinohara, A., Conchello, J.A., and Dresser, M.E. (2008). Rapid telomere movement in meiotic prophase is promoted by NDJ1, MPS3, and CSM4 and is modulated by recombination. Cell *133*, 1175-1187.
Cremer, T., and Cremer, C. (2001). Chromosome territories, nuclear architecture and gene regulation in mammalian cells. Nat Rev Genet *2*, 292-301.
Cremona, C.A., Sarangi, P., Yang, Y., Hang, L.E., Rahman, S., and Zhao, X. (2012). Extensive DNA damage-induced sumoylation contributes to replication and repair and acts in addition to the mec1 checkpoint. Mol Cell *45*, 422-432.
Dietz, C., Rueden, C.T., Helfrich, S., Dobson, E.T.A., Horn, M., Eglinger, J., Evans, E.L., McLean, D.T., Novitskaya, T., Ricke, W.A*., et al.* (2020). Integration of the ImageJ Ecosystem in KNIME Analytics Platform. Frontiers in Computer Science *2*.
Dimitrova, N., Chen, Y.C., Spector, D.L., and de Lange, T. (2008). 53BP1 promotes non-homologous end joining of telomeres by increasing chromatin mobility. Nature *456*, 524-528.
Dion, V., and Gasser, S.M. (2013). Chromatin movement in the maintenance of genome stability. Cell *152*, 1355-1364.
Dion, V., Kalck, V., Horigome, C., Towbin, B.D., and Gasser, S.M. (2012). Increased mobility of double-strand breaks requires Mec1, Rad9 and the homologous recombination machinery. Nature cell biology *14*, 502-509.
Dion, V., Kalck, V., Seeber, A., Schleker, T., and Gasser, S.M. (2013). Cohesin and the nucleolus constrain the mobility of spontaneous repair foci. EMBO reports *14*, 984-991.
Dixon, J.R., Selvaraj, S., Yue, F., Kim, A., Li, Y., Shen, Y., Hu, M., Liu, J.S., and Ren, B. (2012). Topological domains in mammalian genomes identified by analysis of chromatin interactions. Nature *485*, 376-380.
Donnianni, R.A., and Symington, L.S. (2013). Break-induced replication occurs by conservative DNA synthesis. Proceedings of the National Academy of Sciences of the United States of America *110*, 13475-13480.
Downs, J.A., Kosmidou, E., Morgan, A., and Jackson, S.P. (2003). Suppression of homologous recombination by the Saccharomyces cerevisiae linker histone. Mol Cell *11*, 1685-1692.
Duan, Z., Andronescu, M., Schutz, K., McIlwain, S., Kim, Y.J., Lee, C., Shendure, J., Fields, S., Blau, C.A., and Noble, W.S. (2010). A three-dimensional model of the yeast genome. Nature *465*, 363-367.
Fabre, E., and Zimmer, C. (2018). From dynamic chromatin architecture to DNA damage repair and back. Nucleus *9*, 161-170.

Fyodorov, D.V., Zhou, B.R., Skoultchi, A.I., and Bai, Y. (2018). Emerging roles of linker histones in regulating chromatin structure and function. Nat Rev Mol Cell Biol *19*, 192-206.
Garcia, V., Phelps, S.E., Gray, S., and Neale, M.J. (2011). Bidirectional resection of DNA double-strand breaks by Mre11 and Exo1. Nature *479*, 241-244.
Gartenberg, M.R., Neumann, F.R., Laroche, T., Blaszczyk, M., and Gasser, S.M. (2004). Sir-mediated repression can occur independently of chromosomal and subnuclear contexts. Cell *119*, 955-967.
Gehlen, L.R., Gasser, S.M., and Dion, V. (2011). How broken DNA finds its template for repair: a computational approach. Progress of Theoretical Physics Supplement *191*, 20129.
Germier, T., Kocanova, S., Walther, N., Bancaud, A., Shaban, H.A., Sellou, H., Politi, A.Z., Ellenberg, J., Gallardo, F., and Bystricky, K. (2017). Real-Time Imaging of a Single Gene Reveals Transcription-Initiated Local Confinement. Biophys J *113*, 1383-1394.
Grewal, S.I., and Jia, S. (2007). Heterochromatin revisited. Nat Rev Genet *8*, 35-46.
Gu, B., Swigut, T., Spencley, A., Bauer, M.R., Chung, M., Meyer, T., and Wysocka, J. (2018). Transcription-coupled changes in nuclear mobility of mammalian cis-regulatory elements. Science *359*, 1050-1055.
Haber, J.E. (2018). DNA Repair: The Search for Homology. Bioessays *40*, e1700229.
Haber, J.E., Leung, W.Y., Borts, R.H., and Lichten, M. (1991). The frequency of meiotic recombination in yeast is independent of the number and position of homologous donor sequences: implications for chromosome pairing. Proceedings of the National Academy of Sciences of the United States of America *88*, 1120-1124.
Harding, S.M., Boiarsky, J.A., and Greenberg, R.A. (2015). ATM Dependent Silencing Links Nucleolar Chromatin Reorganization to DNA Damage Recognition. Cell reports *13*, 251-259.
Hauer, M.H., Seeber, A., Singh, V., Thierry, R., Sack, R., Amitai, A., Kryzhanovska, M., Eglinger, J., Holcman, D., Owen-Hughes, T.*, et al.* (2017). Histone degradation in response to DNA damage enhances chromatin dynamics and recombination rates. Nat Struct Mol Biol *24*, 99-107.
Hediger, F., Neumann, F.R., Van Houwe, G., Dubrana, K., and Gasser, S.M. (2002). Live imaging of telomeres: yKu and Sir proteins define redundant telomere-anchoring pathways in yeast. Curr Biol *12*, 2076-2089.
Herbert, S., Brion, A., Arbona, J.M., Lelek, M., Veillet, A., Lelandais, B., Parmar, J., Fernandez, F.G., Almayrac, E., Khalil, Y.*, et al.* (2017). Chromatin stiffening underlies enhanced locus mobility after DNA damage in budding yeast. The EMBO journal *36*, 2595-2608.
Heun, P., Laroche, T., Shimada, K., Furrer, P., and Gasser, S.M. (2001). Chromosome dynamics in the yeast interphase nucleus. Science *294*, 2181-2186.
Ho, J.W., Jung, Y.L., Liu, T., Alver, B.H., Lee, S., Ikegami, K., Sohn, K.A., Minoda, A., Tolstorukov, M.Y., Appert, A.*, et al.* (2014). Comparative analysis of metazoan chromatin organization. Nature *512*, 449-452.
Horigome, C., Bustard, D.E., Marcomini, I., Delgoshaie, N., Tsai-Pflugfelder, M., Cobb, J.A., and Gasser, S.M. (2016). PolySUMOylation by Siz2 and Mms21 triggers relocation of DNA breaks to nuclear pores through the Slx5/Slx8 STUbL. Genes Dev *30*, 931-945.
Horigome, C., Dion, V., Seeber, A., Gehlen, L.R., and Gasser, S.M. (2015). Visualizing the spatiotemporal dynamics of DNA damage in budding yeast. Methods in molecular biology *1292*, 77-96.
Horigome, C., and Gasser, S.M. (2016). SUMO wrestles breaks to the nuclear ring's edge. Cell Cycle *15*, 3011-3013.
Horigome, C., Oma, Y., Konishi, T., Schmid, R., Marcomini, I., Hauer, M.H., Dion, V., Harata, M., and Gasser, S.M. (2014). SWR1 and INO80 chromatin remodelers contribute to DNA double-strand break perinuclear anchorage site choice. Mol Cell *55*, 626-639.
Horigome, C., Unozawa, E., Ooki, T., and Kobayashi, T. (2019). Ribosomal RNA gene repeats associate with the nuclear pore complex for maintenance after DNA damage. PLoS Genet *15*, e1008103.

Hurst, V., Shimada, K., and Gasser, S.M. (2019). Nuclear Actin and Actin-Binding Proteins in DNA Repair. Trends in cell biology *29*, 462-476.
Ira, G., Pellicioli, A., Balijja, A., Wang, X., Fiorani, S., Carotenuto, W., Liberi, G., Bressan, D., Wan, L., Hollingsworth, N.M.*, et al.* (2004). DNA end resection, homologous recombination and DNA damage checkpoint activation require CDK1. Nature *431*, 1011-1017.
Jain, S., Sugawara, N., and Haber, J.E. (2016). Role of Double-Strand Break End-Tethering during Gene Conversion in Saccharomyces cerevisiae. PLoS Genet *12*, e1005976.
Janssen, A., Breuer, G.A., Brinkman, E.K., van der Meulen, A.I., Borden, S.V., van Steensel, B., Bindra, R.S., LaRocque, J.R., and Karpen, G.H. (2016). A single double-strand break system reveals repair dynamics and mechanisms in heterochromatin and euchromatin. Genes Dev *30*, 1645-1657.
Jin, Q.W., Fuchs, J., and Loidl, J. (2000). Centromere clustering is a major determinant of yeast interphase nuclear organization. Journal of cell science *113 (Pt 11)*, 1903-1912.
Joyner, R.P., Tang, J.H., Helenius, J., Dultz, E., Brune, C., Holt, L.J., Huet, S., Muller, D.J., and Weis, K. (2016). A glucose-starvation response regulates the diffusion of macromolecules. Elife *5*.
Kapoor, P., Chen, M., Winkler, D.D., Luger, K., and Shen, X. (2013). Evidence for monomeric actin function in INO80 chromatin remodeling. Nat Struct Mol Biol *20*, 426-432.
Klein, H.L., Bacinskaja, G., Che, J., Cheblal, A., Elango, R., Epshtein, A., Fitzgerald, D.M., Gomez-Gonzalez, B., Khan, S.R., Kumar, S.*, et al.* (2019). Guidelines for DNA recombination and repair studies: Cellular assays of DNA repair pathways. Microb Cell *6*, 1-64.
Koszul, R., Kim, K.P., Prentiss, M., Kleckner, N., and Kameoka, S. (2008). Meiotic chromosomes move by linkage to dynamic actin cables with transduction of force through the nuclear envelope. Cell *133*, 1188-1201.
Krawczyk, P.M., Borovski, T., Stap, J., Cijsouw, T., ten Cate, R., Medema, J.P., Kanaar, R., Franken, N.A., and Aten, J.A. (2012). Chromatin mobility is increased at sites of DNA double-strand breaks. Journal of cell science *125*, 2127-2133.
Kueng, S., Oppikofer, M., and Gasser, S.M. (2013). SIR proteins and the assembly of silent chromatin in budding yeast. Annu Rev Genet *47*, 275-306.
Lachner, M., O'Carroll, D., Rea, S., Mechtler, K., and Jenuwein, T. (2001). Methylation of histone H3 lysine 9 creates a binding site for HP1 proteins. Nature *410*, 116-120.
Lademann, C.A., Renkawitz, J., Pfander, B., and Jentsch, S. (2017). The INO80 Complex Removes H2A.Z to Promote Presynaptic Filament Formation during Homologous Recombination. Cell reports *19*, 1294-1303.
Lawrimore, J., Barry, T.M., Barry, R.M., York, A.C., Friedman, B., Cook, D.M., Akialis, K., Tyler, J., Vasquez, P., Yeh, E.*, et al.* (2017). Microtubule dynamics drive enhanced chromatin motion and mobilize telomeres in response to DNA damage. Molecular biology of the cell *28*, 1701-1711.
Lee, C.S., Wang, R.W., Chang, H.H., Capurso, D., Segal, M.R., and Haber, J.E. (2016). Chromosome position determines the success of double-strand break repair. Proceedings of the National Academy of Sciences of the United States of America *113*, E146-154.
Lee, S., Lim, W.A., and Thorn, K.S. (2013). Improved blue, green, and red fluorescent protein tagging vectors for S. cerevisiae. PLoS One *8*, e67902.
Lemaitre, C., Grabarz, A., Tsouroula, K., Andronov, L., Furst, A., Pankotai, T., Heyer, V., Rogier, M., Attwood, K.M., Kessler, P.*, et al.* (2014). Nuclear position dictates DNA repair pathway choice. Genes Dev *28*, 2450-2463.
Lengsfeld, B.M., Rattray, A.J., Bhaskara, V., Ghirlando, R., and Paull, T.T. (2007). Sae2 is an endonuclease that processes hairpin DNA cooperatively with the Mre11/Rad50/Xrs2 complex. Mol Cell *28*, 638-651.
Lescasse, R., Pobiega, S., Callebaut, I., and Marcand, S. (2013). End-joining inhibition at telomeres requires the translocase and polySUMO-dependent ubiquitin ligase Uls1. The EMBO journal *32*, 805-815.

Levi, V., and Gratton, E. (2008). Chromatin dynamics during interphase explored by single-particle tracking. Chromosome Res *16*, 439-449.
Lichten, M., and Haber, J.E. (1989). Position effects in ectopic and allelic mitotic recombination in Saccharomyces cerevisiae. Genetics *123*, 261-268.
Lieber, M.R. (2010). The mechanism of double-strand DNA break repair by the nonhomologous DNA end-joining pathway. Annu Rev Biochem *79*, 181-211.
Lisby, M., Barlow, J.H., Burgess, R.C., and Rothstein, R. (2004). Choreography of the DNA damage response: spatiotemporal relationships among checkpoint and repair proteins. Cell *118*, 699-713.
Lisby, M., and Rothstein, R. (2009). Choreography of recombination proteins during the DNA damage response. DNA Repair (Amst) *8*, 1068-1076.
Lottersberger, F., Karssemeijer, R.A., Dimitrova, N., and de Lange, T. (2015). 53BP1 and the LINC Complex Promote Microtubule-Dependent DSB Mobility and DNA Repair. Cell *163*, 880-893.
Maison, C., Bailly, D., Roche, D., Montes de Oca, R., Probst, A.V., Vassias, I., Dingli, F., Lombard, B., Loew, D., Quivy, J.P*., et al.* (2011). SUMOylation promotes de novo targeting of HP1alpha to pericentric heterochromatin. Nat Genet *43*, 220-227.
Marcomini, I., Shimada, K., Delgoshaie, N., Yamamoto, I., Seeber, A., Cheblal, A., Horigome, C., Naumann, U., and Gasser, S.M. (2018). Asymmetric Processing of DNA Ends at a Double-Strand Break Leads to Unconstrained Dynamics and Ectopic Translocation. Cell reports *24*, 2614-2628 e2614.
Marnef, A., and Legube, G. (2017). Organizing DNA repair in the nucleus: DSBs hit the road. Curr Opin Cell Biol *46*, 1-8.
Marshall, W.F., Straight, A., Marko, J.F., Swedlow, J., Dernburg, A., Belmont, A., Murray, A.W., Agard, D.A., and Sedat, J.W. (1997). Interphase chromosomes undergo constrained diffusional motion in living cells. Curr Biol *7*, 930-939.
Martin, R.M., Gorisch, S.M., Leonhardt, H., and Cardoso, M.C. (2007). An unexpected link between energy metabolism, calcium, chromatin condensation and cell cycle. Cell Cycle *6*, 2422-2424.
Mattout, A., Gaidatzis, D., Padeken, J., Schmid, C.D., Aeschimann, F., Kalck, V., and Gasser, S.M. (2020). LSM2-8 and XRN-2 contribute to the silencing of H3K27me3-marked genes through targeted RNA decay. Nature cell biology *22*, 579-590.
Meister, P., Gehlen, L.R., Varela, E., Kalck, V., and Gasser, S.M. (2010). Visualizing yeast chromosomes and nuclear architecture. Methods in enzymology *470*, 535-567.
Miescher, F. (1871). Ueber die chemische Zusammensetzung der Eiterzellen. Hoppe-Seyler's Medicinisch-Chemische Untersuchungen, 441-460.
Mine-Hattab, J., Recamier, V., Izeddin, I., Rothstein, R., and Darzacq, X. (2017). Multi-scale tracking reveals scale-dependent chromatin dynamics after DNA damage. Molecular biology of the cell.
Mine-Hattab, J., and Rothstein, R. (2012). Increased chromosome mobility facilitates homology search during recombination. Nature cell biology *14*, 510-517.
Mine-Hattab, J., and Rothstein, R. (2013). DNA in motion during double-strand break repair. Trends in cell biology *23*, 529-536.
Mukherjee, K., English, N., Meers, C., Kim, H., Jonke, A., Storici, F., and Torres, M. (2020). Systematic analysis of linker histone PTM hotspots reveals phosphorylation sites that modulate homologous recombination and DSB repair. DNA Repair (Amst) *86*, 102763.
Mullen, J.R., and Brill, S.J. (2008). Activation of the Slx5-Slx8 ubiquitin ligase by poly-small ubiquitin-like modifier conjugates. J Biol Chem *283*, 19912-19921.
Nagai, S., Dubrana, K., Tsai-Pflugfelder, M., Davidson, M.B., Roberts, T.M., Brown, G.W., Varela, E., Hediger, F., Gasser, S.M., and Krogan, N.J. (2008). Functional targeting of DNA damage to a nuclear pore-associated SUMO-dependent ubiquitin ligase. Science *322*, 597-602.

Nakada, D., Matsumoto, K., and Sugimoto, K. (2003). ATM-related Tel1 associates with double-strand breaks through an Xrs2-dependent mechanism. Genes Dev *17*, 1957-1962.
Neumann, F.R., Dion, V., Gehlen, L.R., Tsai-Pflugfelder, M., Schmid, R., Taddei, A., and Gasser, S.M. (2012). Targeted INO80 enhances subnuclear chromatin movement and ectopic homologous recombination. Genes Dev *26*, 369-383.
Neumann, F.R.H., F. ; Taddei, A. and Gasser, S.M. (2005). Tracking Individual Chromosomes with Integrated lacO sites and GFP-lacI repressor: Analysing Position and Dynamics of Chromosomal loci in S. cerevisiae. Cell Biology A Laboratory Handbook *2*, 359-367
Olivo-Marin, J.C. (2002). Extraction of spots in biological images using multiscale products. Pattern Recogn *35*, 1989-1996.
Onn, I., Heidinger-Pauli, J.M., Guacci, V., Unal, E., and Koshland, D.E. (2008). Sister chromatid cohesion: a simple concept with a complex reality. Annu Rev Cell Dev Biol *24*, 105-129.
Oshidari, R., Mekhail, K., and Seeber, A. (2019). Mobility and Repair of Damaged DNA: Random or Directed? Trends in cell biology.
Palladino, F., Laroche, T., Gilson, E., Axelrod, A., Pillus, L., and Gasser, S.M. (1993). SIR3 and SIR4 proteins are required for the positioning and integrity of yeast telomeres. Cell *75*, 543-555.
Piazza, A., Shah, S.S., Wright, W.D., Gore, S.K., Koszul, R., and Heyer, W.D. (2019). Dynamic Processing of Displacement Loops during Recombinational DNA Repair. Mol Cell *73*, 1255-1266 e1254.
Pinsky, B.A., Kung, C., Shokat, K.M., and Biggins, S. (2006). The Ipl1-Aurora protein kinase activates the spindle checkpoint by creating unattached kinetochores. Nat Cell Biol *8*, 78-83.
Pliss, A., Malyavantham, K., Bhattacharya, S., Zeitz, M., and Berezney, R. (2009). Chromatin dynamics is correlated with replication timing. Chromosoma *118*, 459-470.
Pombo, A., and Dillon, N. (2015). Three-dimensional genome architecture: players and mechanisms. Nat Rev Mol Cell Biol *16*, 245-257.
Qu, Y., Gharbi, N., Yuan, X., Olsen, J.R., Blicher, P., Dalhus, B., Brokstad, K.A., Lin, B., Oyan, A.M., Zhang, W.*, et al.* (2016). Axitinib blocks Wnt/beta-catenin signaling and directs asymmetric cell division in cancer. Proceedings of the National Academy of Sciences of the United States of America *113*, 9339-9344.
Rabl, C. (1885). Über zelltheilung. Morphologisches Jahrbuch *10*, 214-330.
Renkawitz, J., Lademann, C.A., and Jentsch, S. (2014). Mechanisms and principles of homology search during recombination. Nat Rev Mol Cell Biol *15*, 369-383.
Riddle, N.C., Minoda, A., Kharchenko, P.V., Alekseyenko, A.A., Schwartz, Y.B., Tolstorukov, M.Y., Gorchakov, A.A., Jaffe, J.D., Kennedy, C., Linder-Basso, D.*, et al.* (2011). Plasticity in patterns of histone modifications and chromosomal proteins in Drosophila heterochromatin. Genome Res *21*, 147-163.
Roukos, V., Voss, T.C., Schmidt, C.K., Lee, S., Wangsa, D., and Misteli, T. (2013). Spatial dynamics of chromosome translocations in living cells. Science *341*, 660-664.
Ryu, T., Spatola, B., Delabaere, L., Bowlin, K., Hopp, H., Kunitake, R., Karpen, G.H., and Chiolo, I. (2015). Heterochromatic breaks move to the nuclear periphery to continue recombinational repair. Nature cell biology *17*, 1401-1411.
Saad, H., Gallardo, F., Dalvai, M., Tanguy-le-Gac, N., Lane, D., and Bystricky, K. (2014). DNA dynamics during early double-strand break processing revealed by non-intrusive imaging of living cells. PLoS Genet *10*, e1004187.
Sage, D., Neumann, F.R., Hediger, F., Gasser, S.M., and Unser, M. (2005). Automatic tracking of individual fluorescence particles: application to the study of chromosome dynamics. IEEE transactions on image processing : a publication of the IEEE Signal Processing Society *14*, 1372-1383.
Schober, H., Kalck, V., Vega-Palas, M.A., Van Houwe, G., Sage, D., Unser, M., Gartenberg, M.R., and Gasser, S.M. (2008). Controlled exchange of chromosomal arms reveals principles driving telomere interactions in yeast. Genome Res *18*, 261-271.

Schrank, B.R., Aparicio, T., Li, Y., Chang, W., Chait, B.T., Gundersen, G.G., Gottesman, M.E., and Gautier, J. (2018). Nuclear ARP2/3 drives DNA break clustering for homology-directed repair. Nature *559*, 61-66.
Seeber, A., Dion, V., and Gasser, S.M. (2013). Checkpoint kinases and the INO80 nucleosome remodeling complex enhance global chromatin mobility in response to DNA damage. Genes Dev *27*, 1999-2008.
Seeber, A., Hauer, M.H., and Gasser, S.M. (2018). Chromosome Dynamics in Response to DNA Damage. Annu Rev Genet *52*, 295-319.
Seeber, A., Hegnauer, A.M., Hustedt, N., Deshpande, I., Poli, J., Eglinger, J., Pasero, P., Gut, H., Shinohara, M., Hopfner, K.P*., et al.* (2016). RPA Mediates Recruitment of MRX to Forks and Double-Strand Breaks to Hold Sister Chromatids Together. Mol Cell *64*, 951-966.
Sheff, M.A., and Thorn, K.S. (2004). Optimized cassettes for fluorescent protein tagging in Saccharomyces cerevisiae. Yeast *21*, 661-670.
Shen, X., Mizuguchi, G., Hamiche, A., and Wu, C. (2000). A chromatin remodelling complex involved in transcription and DNA processing. Nature *406*, 541-544.
Shukron, O., Seeber, A., Amitai, A., and Holcman, D. (2019). Advances Using Single-Particle Trajectories to Reconstruct Chromatin Organization and Dynamics. Trends Genet *35*, 685-705.
Smith, M.J., Bryant, E.E., and Rothstein, R. (2018). Increased chromosomal mobility after DNA damage is controlled by interactions between the recombination machinery and the checkpoint. Genes Dev *32*, 1242-1251.
Smurova, K., and De Wulf, P. (2018). Centromere and Pericentromere Transcription: Roles and Regulation ... in Sickness and in Health. Front Genet *9*, 674.
Spichal, M., Brion, A., Herbert, S., Cournac, A., Marbouty, M., Zimmer, C., Koszul, R., and Fabre, E. (2016). Evidence for a dual role of actin in regulating chromosome organization and dynamics in yeast. Journal of cell science *129*, 681-692.
Stephens, A.D., Haase, J., Vicci, L., Taylor, R.M., 2nd, and Bloom, K. (2011). Cohesin, condensin, and the intramolecular centromere loop together generate the mitotic chromatin spring. J Cell Biol *193*, 1167-1180.
Strecker, J., Gupta, G.D., Zhang, W., Bashkurov, M., Landry, M.C., Pelletier, L., and Durocher, D. (2016). DNA damage signalling targets the kinetochore to promote chromatin mobility. Nature cell biology *18*, 281-290.
Su, X.A., Dion, V., Gasser, S.M., and Freudenreich, C.H. (2015). Regulation of recombination at yeast nuclear pores controls repair and triplet repeat stability. Genes Dev *29*, 1006-1017.
Taddei, A., and Gasser, S.M. (2012). Structure and function in the budding yeast nucleus. Genetics *192*, 107-129.
Taddei, A., Hediger, F., Neumann, F.R., and Gasser, S.M. (2004). The function of nuclear architecture: a genetic approach. Annu Rev Genet *38*, 305-345.
Taddei, A., Schober, H., and Gasser, S.M. (2010). The budding yeast nucleus. Cold Spring Harb Perspect Biol *2*, a000612.
Thomas, J.O. (1999). Histone H1: location and role. Curr Opin Cell Biol *11*, 312-317.
Toh, G.W., O'Shaughnessy, A.M., Jimeno, S., Dobbie, I.M., Grenon, M., Maffini, S., O'Rorke, A., and Lowndes, N.F. (2006). Histone H2A phosphorylation and H3 methylation are required for a novel Rad9 DSB repair function following checkpoint activation. DNA Repair (Amst) *5*, 693-703.
Torres-Rosell, J., Sunjevaric, I., De Piccoli, G., Sacher, M., Eckert-Boulet, N., Reid, R., Jentsch, S., Rothstein, R., Aragon, L., and Lisby, M. (2007). The Smc5-Smc6 complex and SUMO modification of Rad52 regulates recombinational repair at the ribosomal gene locus. Nature cell biology *9*, 923-931.
Tsouroula, K., Furst, A., Rogier, M., Heyer, V., Maglott-Roth, A., Ferrand, A., Reina-San-Martin, B., and Soutoglou, E. (2016). Temporal and Spatial Uncoupling of DNA Double Strand Break Repair Pathways within Mammalian Heterochromatin. Mol Cell *63*, 293-305.

Unal, E., Arbel-Eden, A., Sattler, U., Shroff, R., Lichten, M., Haber, J.E., and Koshland, D. (2004). DNA damage response pathway uses histone modification to assemble a double-strand break-specific cohesin domain. Mol Cell *16*, 991-1002.
Unal, E., Heidinger-Pauli, J.M., and Koshland, D. (2007). DNA double-strand breaks trigger genome-wide sister-chromatid cohesion through Eco1 (Ctf7). Science *317*, 245-248.
Unk, I., Hajdu, I., Blastyak, A., and Haracska, L. (2010). Role of yeast Rad5 and its human orthologs, HLTF and SHPRH in DNA damage tolerance. DNA Repair (Amst) *9*, 257-267.
van Attikum, H., Fritsch, O., and Gasser, S.M. (2007). Distinct roles for SWR1 and INO80 chromatin remodeling complexes at chromosomal double-strand breaks. The EMBO journal *26*, 4113-4125.
van Sluis, M., and McStay, B. (2015). A localized nucleolar DNA damage response facilitates recruitment of the homology-directed repair machinery independent of cell cycle stage. Genes Dev *29*, 1151-1163.
Verdaasdonk, J.S., Vasquez, P.A., Barry, R.M., Barry, T., Goodwin, S., Forest, M.G., and Bloom, K. (2013). Centromere tethering confines chromosome domains. Mol Cell *52*, 819-831.
Vignali, M., and Workman, J.L. (1998). Location and function of linker histones. Nat Struct Biol *5*, 1025-1028.
Wang, R.W., Lee, C.S., and Haber, J.E. (2017). Position effects influencing intrachromosomal repair of a double-strand break in budding yeast. PLoS One *12*, e0180994.
Weber, S.A., Gerton, J.L., Polancic, J.E., DeRisi, J.L., Koshland, D., and Megee, P.C. (2004). The kinetochore is an enhancer of pericentric cohesin binding. PLoS Biol *2*, E260.
Weber, S.C., Spakowitz, A.J., and Theriot, J.A. (2010). Bacterial chromosomal loci move subdiffusively through a viscoelastic cytoplasm. Phys Rev Lett *104*, 238102.
Weber, S.C., Spakowitz, A.J., and Theriot, J.A. (2012). Nonthermal ATP-dependent fluctuations contribute to the in vivo motion of chromosomal loci. Proceedings of the National Academy of Sciences of the United States of America *109*, 7338-7343.
Whalen, J.M., and Freudenreich, C.H. (2020). Location, Location, Location: The Role of Nuclear Positioning in the Repair of Collapsed Forks and Protection of Genome Stability. Genes (Basel) *11*.
Wilson, J.H., Leung, W.Y., Bosco, G., Dieu, D., and Haber, J.E. (1994). The frequency of gene targeting in yeast depends on the number of target copies. Proceedings of the National Academy of Sciences of the United States of America *91*, 177-181.
Zheng, S., Li, D., Lu, Z., Liu, G., Wang, M., Xing, P., Wang, M., Dong, Y., Wang, X., Li, J*., et al.* (2018). Bre1-dependent H2B ubiquitination promotes homologous recombination by stimulating histone eviction at DNA breaks. Nucleic Acids Res *46*, 11326-11339.
Zhu, Z., Chung, W.H., Shim, E.Y., Lee, S.E., and Ira, G. (2008). Sgs1 helicase and two nucleases Dna2 and Exo1 resect DNA double-strand break ends. Cell *134*, 981-994.
Zidovska, A., Weitz, D.A., and Mitchison, T.J. (2013). Micron-scale coherence in interphase chromatin dynamics. Proceedings of the National Academy of Sciences of the United States of America *110*, 15555-15560.
Zierhut, C., and Diffley, J.F. (2008). Break dosage, cell cycle stage and DNA replication influence DNA double strand break response. The EMBO journal *27*, 1875-1885.

LIST OF ABBREVIATIONS

BIR: break-induced replication repair

DDC: DNA damage checkpoint

DDR: DNA damage response

DSB: DNA double-strand break

HO: Homothallic switching endonuclease, used to induce a DSB at *MAT*

HMGB1: High mobility group box 1 protein in human

HP1: heterochromatin protein 1

HR: homologous recombination

HDR: homology-directed repair

IR: irradiation

LINC complex: linker of nucleoskeleton and cytoskeleton

MAT: mating type locus in chromosome III in *S.cerevisiae*

MRX: Mre11-Rad50-Xrs2 complex

MSD: mean square displacement

NHEJ: non-homologous end joining

NPC: nuclear pore complex

rDNA: ribosomal DNA

RPA: replication protein A

SMC5/6: cohesin related complex, linked to SUMOylation activity

STUbL: SUMO-targeted ubiquitin ligase

SUMO: Small Ubiquitin-like modifier

CURRICULUM VITAE

○ PERSONAL INFORMATION ○

Anaïs, Thiziri Cheblal

8 rue Victor Coste, F-68300 Saint-Louis, France
+33 (0) 777007847
anais.cheblal@fmi.ch

Date of birth	December 10, 1991
Nationality	French/Algerian
Civil Status	Married, one child

○ SKILLS & TECHNIQUES ○

Genetic manipulations in budding yeast	**Fluorescence live cell microscopy**	**Image processing and analysis of large image datasets**	**Quantitative PCR**	**Mammalian cells cellular assays and transfections**

RESEARCH & WORK EXPERIENCE

October 2016 – now
Basel, Switzerland

PhD student at Friedrich Miescher Institute for Biomedical Research
Group of Prof. Dr. Susan Gasser
Scientific project: *"Chromatin dynamics in Homology-directed DNA repair in S.cerevisiae"*
Major tasks:

- Optimization and performance of quantitative DNA repair assays
- Used high temporal resolution imaging to measure chromosome dynamics in living yeast cells
- Used high resolution structured illumination microscopy to measure chromatin compaction state
- Identified key factors that controls chromosome dynamics in yeast
- Characterized the role of chromatin dynamics and organization in DNA repair efficiency
- Managing a scientific collaboration with NIBR CBT Team of Dr. Dominic Hoepfner as a side project

November 2015 - June 2016
Montreal, Canada

Master student at Cancer Research Institute of Montreal
Group of Dr. Francis Rodier
Scientific project: *"Role of the DNA damage response in Prostate cancer aggressiveness"*
Major tasks:

- Optimization of cellular invasion assay to measure cancer aggressiveness
- Analyzed the role of a DNA repair protein 53BP1 overexpression in cancer progression
- Managing a collaboration between the Institute and Hospital Oncology department under the supervision of Dr Guila Delouya

EDUCATION

2016 – now
Basel, Switzerland
PhD in Molecular Biology and Genetics, *University of Basel*

2014 – 2016
Toulouse, France
Master's degree in Functional and Structural Biology, *University Toulouse Paul Sabatier (3rd/11)*

2011 – 2014
Toulouse, France
Bachelor degree in Biochemistry and Molecular biology, *University Toulouse Paul Sabatier (1st/55)*

CAREER DEVELOPMENT TRAININGS

May 2020 - now — **Essentials of European Regulatory Affairs**, *The Organization for Professionals in Regulatory Affairs (TOPRA)*

May 2020 — **Essentials in Drug Development and Clinical Trials**, *Swiss Tropical and Public Health Institute, Basel*

March 2020 — **Design and Interpretation of Clinical Trials**, *Johns Hopkins University (Coursera)*

February 2020 — **Safety assessment for First-in-Human Clinical Trials**, *University of Basel*

August 2017 — **Croucher Summer course on Advanced Imaging, Single molecule super resolution microscopy,** *University of Hong-Kong*

MENTORING & TEACHING

May 2020 - now	**Novartis Associates Grassroots Mentoring program**, *Basel*
2018	**Tutor of Bachelor Biology students at the University of Basel**, *Basel*

AWARDS & SCHOLARSHIPS

2017	**Best Poster Presentation award,** Friedrich Miescher Institute PhD retreat, *Lisbon, Portugal*
2016	**Canderel Scholarship,** Cancer Institute of Montréal (ICM), *Montreal, Canada*

CONFERENCE TALKS AND POSTERS

2018	**Modelling of chromatin organization,** *Pisa, Italy* ***Talk "Chromatin dynamics upon DNA damage in S. cerevisiae"***
2018	**Mechanisms of Recombination, ABCAM,** *London, UK* ***Poster presentation***
2017	**Protecting the Code , EACR conference,** *Berlin, Germany* ***Poster presentation***
2017	**EMBO at Basel life,** *Basel, Switzerland* ***Poster presentation***
2017	**FMI PhD student retreat,** *Lisbon, Portugal* ***Poster presentation***

SCIENTIFIC PUBLICATIONS

Damage-induced chromatome changes and break movement are controlled by INO80C-dependent Ubiquitin ligase recruitment
Challa K, Schmid C, Kitagawa S, **Cheblal A**, Iesmantavicius V, Seeber A, Amitai A, Seebacher J, Hauer MH, Shimada K and Gasser SM.
Under review

DNA damage-induced histone depletion enhances double-strand break repair independently of local break movement
Cheblal A, Challa K, Seeber A, Shimada K, Yoshida H, Amitai A, and Gasser SM.
Molecular Cell, in press.

Guidelines for DNA Recombination and Repair Studies: Cellular Assays of DNA Repair Pathways
Klein HL , Bačinskaja G, Che J, **Cheblal A** […] Lisby M, Malkova A.
Microbial Cell, 2019 Jan 7;6(1):1-64. doi: 10.15698/mic2019.01.664.

Asymmetric Processing of DNA Ends at a Double-Strand Break Leads to Unconstrained Dynamics and Ectopic Translocation
Marcomini I, Shimada K, Delgoshaie N, Yamamoto I, Seeber A, **Cheblal A**, Horigome C, Naumann U, Gasser SM.
Cell Reports, 2018 Sept 4;24(10):2614-2628.e4. doi: 10.1016/j.celrep.2018.07.102.

COMPUTER LITERACY

Microsoft Office (Powerpoint, Word, Excel)

Adobe Illustrator, Photoshop, Prism - GraphPad

Imaging softwares (ImageJ)

○ LANGUANGES ○

French (fluent, native)

Berbère (fluent, native)

English (spoken and written professional level)

○ REFERENCES ○

Prof. Dr. Susan M Gasser
Group Leader and Director Emeritus

FMI, *Basel, Switzerland*
susan.gasser@fmi.ch
+41 61 697 5025

Dr. Nicolas Mercado
Senior Scientist

Roche, *Basel, Switzerland*
nicolas.mercado@roche.com
+41 79 29 76 912

Prof. Dr. Francis Rodier
Group Leader

CRCHUM, *Montreal, Canada*
rodierf@mac.com
+1 514 890 8000

Acknowledgments

First, I would like to deeply thank **Susan M Gasser** who gave me the incredible opportunity to work within her laboratory. Susan, you were an amazing mentor for me and a daily inspiring women leader. Thank you for always supporting me to push my limits and for always believing in my capacities in many aspects, and transmitting your passion of yeast genetics. Most importantly, I would like to highlight how much your support was very important to me during both my pregnancy and my motherhood and I know not many group leaders would have done the same.

Because I think every young women should have one mentor of each gender, I was lucky enough to meet **Andrew Seeber**. Andrew, you taught me (almost) everything I know about microscopy and chromatin dynamics. You convinced me to get onboard of a very unusual project, it was not always easy, but the outcome we got out of this was worth it! It was always fun working with you and spending days in front of the microscope. You were and still are one of my best mentor!

I would like to thank all my co-authors who deeply supported me during my PhD, more specifically:

Kenji Shimada who was the "Yoda best Genetic Counselor", thank you for answering all my numerous and sometimes very basic yeast genetics questions, I can imagine it was not always restful to sit between me and Daphne! But you always took the time to listen and guide us in any setting, this makes you a real Yoda.

Kiran Challa, you joined the lab in the middle of my PhD, probably when I was not at my best confidence, and you clearly changed the way it was supposed to be! Thanks a lot for all the technical and psychological support, this project would not have been the same without you! I really enjoyed working with you and I am sure you will be successful in everything you intend to do.

I also thank **Assaf Amitai** for always taking the time to analyze my tracking data and open to answer all my questions on biophysics; it was both challenging and rewarding to interact with you.

I also would like to mention my old office colleagues: **Isabella**, it was always fun to talk with you both professionally or personally, sharing my office with three Italians was extremely fun! **Ivana**, it was very reassuring to have another pregnant women with whom I was sharing my uncertainties and doubts, thanks a lot for having supported me during this time of my life. **Gabriele**, you were my external "post-doc" and always full of advice and help, you were a pillar at the beginning of my project, Thank! Finally yet importantly, **Benoit**, it was always fun to work with you and share our difficult and best moments together! You know I would have been lost without your help with statistics!

I cannot forget the two other persons that shared that office with us and whom are not among us today: A special thought to **Franz**, I deeply hope you are in peace.

Michi, I cannot express what I feel in few words, but I really enjoyed working with you. You were an amazing model, and incredibly smart scientist. Thank you for transferring me your deep passion for science and research. Always full of genius ideas and at the same time supportive and full of advice. You are a lost not only to us but to the entire community. We miss you, and I deeply think you rest in peace.

I would like to thank **Veronique Kalck**, who was like my second "Maman" during my PhD. You were always here to listen to my issues and always come with the right advice. I enjoyed our discussions in the lab and our time together at the Gym! You are really the lab "Angel".

To close up the yeasties Chapter, a special thanks to my "PhD sister" **Verena Hurst**. Verena, I have to say that you are one the most interesting person that I met. But in the good sense of it. You are a very passionate person and I really enjoyed interacting with you! I think we both supported each other during our PhDs and I wish you all the best in your future career, that you deserve.

A special thought to **Saho Kitagawa**, an incredibly smart and fun Japanese student. I enjoyed interacting with you and having fun at the Gym!

I also would like to thank the Pol delta project team: **Neda**, thanks a lot for all your scientific an career advices; **Nico**, it was really fun working with you on the screen and thanks a lot for supporting me during your time in the lab and after! You were probably the funniest and non-swiss gasser lab member!

A special thanks to the wormies "Gasser mamas" **Daphne, Micol, Anna, Jennifer:** you were my "must have" in the lab and you made this journey very fun. I am happy that I met you all, you always supported me no matter what, and a deeply thank you for that.

Then the boys, **Stephen**, thanks a lot for your support and advice, **Jan, Colin**, **Peter, Jerome** thanks for always being there to answer my questions.

I would like to thank my committee members Lucas Giorgetti, Primo Schar, Kerstin Bystricky and Vincent Dion that were of a huge support during my PhD.

I thank all FMI facilities: mostly the FAIM, **Laurent, Steve** and **Jan** and the administration (**Gabi**, **Elida**) for making our life easier and always being of a huge help and assistance.

Enfin, je remercie mes parents **Soraya et Chabane** et mon frère **Izem** de m'avoir soutenue durant toutes mes études, de m'avoir encouragé à toujours aller plus haut et à repousser mes limites. Cette thèse n'existerait pas sans eux. Je vous aime !

Aussi, je remercie mon mari **Hakim**, de m'avoir soutenu tous les jours durant ces quatre dernières années et d'avoir rendu encore plus agréable le déroulement de ce doctorat. Plus particulièrement, je te remercie d'avoir fait en sorte que je puisse soutenir ma thèse en tant que maman ! **Emma** et toi, je vous aime !

Enfin, je repense à mes amis scientifiques avec qui tout a commencé à Paul Sab' : **Nico, Pauline, Gautier et Mathilde**. Mathilde, je te remercie pour tout le soutient du monde, je t'ai poussé à faire un doctorat et tu m'as poussé à aller au bout ! Tu as toujours été là pour moi et tu sais combien tu comptes pour moi. Comme on dit : Keep going – no matter what !

Finally, I would like to thank some amazing scientists that triggered my passion for science at the early stages of my studies: Remy Poupot, Thomas and Barbara Lambour, Kerstin Bystricky, Fabrice Dumas, Alain Vercellone, Arnaud Labrousse, Fabien Letisse, Francis Rodier, Nicolas Malaquin.